Characterising Indoor Air Quality in UK Homes:
A Population-Based Approach

Aiden Cameron Heeley-Hill BSc, MSc

Master of Philosophy

University of York

Chemistry

September 2021

Abstract

Indoor air quality is of concern in the public health community given the amount of time people are indoors (~90%) and air pollution more generally is linked to a myriad of health issues. The presence of a variety of VOCs, and the subsequent formation of potentially harmful secondary organic aerosols, are of significant concern. This thesis seeks to elucidate some aspects of this complex area of research. First, observing VOC oxidation in chamber experiments has revealed that a number of SOA intermediates form under a variety of oxidant regimes introduced to the chamber, and that these oxidant regimes greatly impact the rate of decay of the parent compound. Further, differing NO_x regimes can have a notable impact, such as on VOC decay, and particle and SOA intermediate formation. Secondly, a number of VOCs are found indoors, however, VOC concentrations cannot be linked to the frequency of use of products in the majority of instances, though covariance analysis reveals some weak but statistically significant relationships. Total VOC concentrations provided some insight into potential exposure indoors. Finally, the reactive potential and the pseudo-first order reactivity of VOCs indoors and major indoor oxidants were assessed. The reaction of *n*-butane and OH was the reaction with the greatest propensity to form secondary products, and whilst OH was significant in many reactions, the abundance of O_3 means it too is a significant oxidant indoors. An indoor chemistry model was used to estimate a variety of key components of indoor air, such as particulate matter and OH concentrations, as well as a novel secondary product creation metric. These components were also measured during a COVID-19 lockdown period in 2020, a proxy for future, low NO_x scenarios. Together, the elements of this thesis provide a comprehensive analysis to some of the issues surrounding indoor air quality.

List of Contents

List of Tables

List of Figures

Acknowledgments

First and foremost, I'd like to thank my supervisor, Ally, for his continued and unwavering support during my degree, and Pete, acting as my independent panel member, for his additional guidance during my time at WACL.

I'd like to extend thanks to everyone in WACL who supported me through the many elements of my various projects, especially Jimmy, Martyn, Marvin, Kelly, Rachel, Steve, and Stuart. Your help, and patience, in all its guises made the stormy path through all the stages of my work much calmer. My thanks to Rammi, Gordon, Rikki, Yu, and Aristeidis of the University of Manchester, School of Earth, Atmospheric and Environmental Sciences for their warm hospitality during my time in Manchester. I'm grateful to Neil Owen, Caroline Jordan and Greg Adamson of Givaudan who helped make the population-based study possible, and to Stuart Grange and Gemma Hodgson for providing help with data and statistical analyses. Thank you to Nic Carslaw from the University of York, Department of Environment and Geography for providing indoor air model work and subsequent support. Thanks to every teacher and mentor who got me to this point, and whose enthusiasm for their subject matters inspired me to push for more.

Finally, I'd like to thank my family and friends for being there every step of the way, through the ups and downs of the last few years, through every problem and success. Thank you.

Author's Declaration

I declare that this thesis is a presentation of original work, and I am the sole author. This work has not previously been presented for an award at this, or any other, University. All sources are acknowledged as references.

Chapter 3 is based on a peer-reviewed publication, for which I was lead author, and is as detailed below:

Heeley-Hill, A.C., Grange, S.K., Ward, M.W., Lewis, A.C., Owen, N., Jordan, C., Hodgson, G., Adamson, G., 2021. Frequency of use of household products containing VOCs and indoor atmospheric concentrations in homes. *Environmental Science: Processes & Impacts* 23(5) 699–713
DOI: https://doi.org/10.1039/D0EM00504E

In Chapter 5, indoor chemical modelling was performed by Professor Nicola Carslaw, Professor of Indoor Air Chemistry at the Department of Environment and Geography, University of York

1. Introduction

Air quality is one of the primary concerns in the public health community to date. Air pollution has been linked to a myriad of health outcomes, and a report by the Royal College of Physicians [1] concluded that poor air quality can be associated with chronic conditions, such as pulmonary and cardiovascular diseases, as well as diabetes and cancer. Other research links highly-polluted urban areas and an increased risk of dementia [2]. $PM_{2.5}$ more specifically is thought to be a contributor to Parkinson's and Alzheimer's diseases and other dementias, with an increase of 13% in the number of first-time hospital admissions per 5 $\mu g\ m^{-3}$ increase in $PM_{2.5}$ concentration [3]. Effects on reproductive health have begun to be researched, with exposure to air pollutants linked as a driver of decreased fertility in both men and women, low birth weight, prematurity, and neonatal death [4]. In 2020, and in an historically-significant case, a coroner in London ruled that air pollution was a contributor to the death of nine-year-old Ella Kissi-Debrah in 2013 [5]. Acute health effects are also observed in periods of poor air quality, with respiratory inflammation and increased blood pressure outlined in the literature [6, 7] More recently, air pollution has been associated with the proliferation of the SARS-CoV-2 virus and subsequent COVID-19 infections by: negatively impacting immune response, exacerbating chronic illnesses, and increasing the persistence of the virus in the atmosphere [8].

Until recently, research has been focussed on pollution outdoors. This is thought to be because outdoor pollution events are more greatly perceived than those derived from indoor pollution e.g. the very obvious presence of phenomena such as smog [9]. In the UK, The Great Smog of 1952 in London prompted a great deal of scientific research, leading to the introduction of the Clean Air Act 1956 to control pollution more effectively than previous legislation [10]. More widespread interest in indoor air quality was not evident until the late 1970s, when the World Health Organization's (WHO) European

Regional Office released their initial report entitled ‘Health Impacts Related to Indoor Air Quality’ following a conference chaired in the Netherlands in 1979. Subsequent meetings held in Germany, 1982 and Sweden, 1984 again referenced indoor air quality issues [11].

The disability adjusted life years, or DALY, model is a commonly used method to evaluate the number of years of life impacted by disease and can be used to recognise contributing factors of chronic illness and premature mortality in human populations.

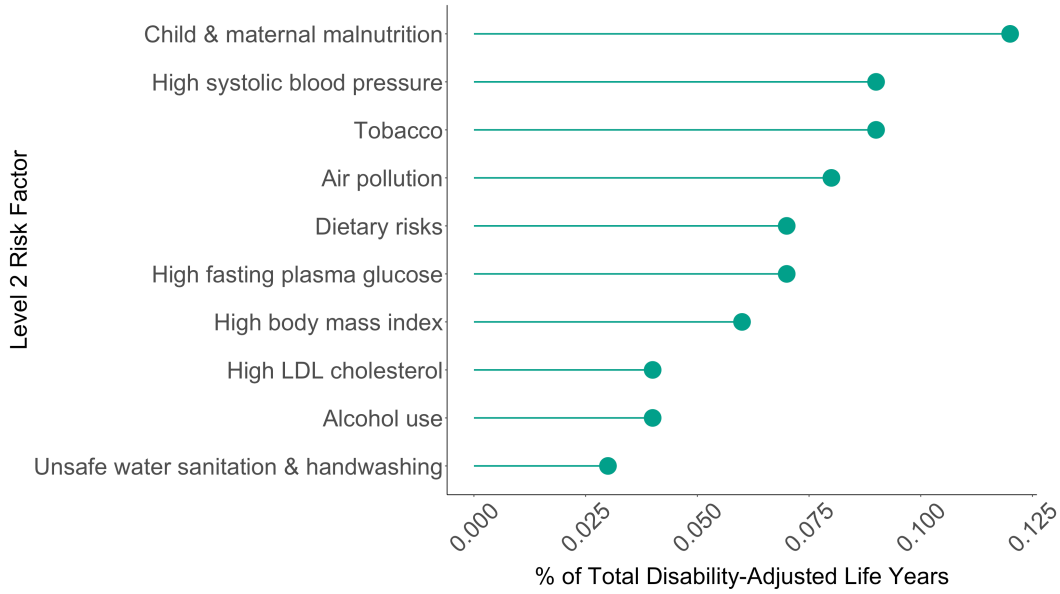

Figure 1.1: The percentage of total global DALYs by Level 2 risk [12]

As detailed in Supplementary Appendix 1 of Gakidou et al. 2017 [13], five risk factor levels are in operation in the Global Burden of Disease study: Level 0 refers to all risk factors. Level 1 refers to the overarching risk factor categories, namely: behavioural, environmental, and occupational; Level 2 details single risks and risk clusters, Level 3 refers to more specific risk factors of Level 2, and Level 4 provides the most detailed risk factors in the study. Using air pollution as an example, Level 3 risk factors are listed as ambient particulate matter pollution and household pollution from solid fuels. Level 4 risk factors for air pollution are not accommodated, but in an

occupational environment, exposure to individual pollutants e.g. benzene and formaldehyde are categorised, and illustrates the detail to which risk levels are defined. Using 2019 data from the Global Health Data Exchange [12], air pollution was ranked 4th amongst level 2 risk factors and accounted for 0.08% of total DALYs (a contribution of over 213 million DALYs). A total of 20, Level 2 risk factors are available from the dataset; Figure 1.1. displays the ten most contributing factors. Each risk factor can be further subdivided into the generic condition it can cause e.g. cardiovascular or respiratory disease, and the attendant DALYs, but this is not considered here.

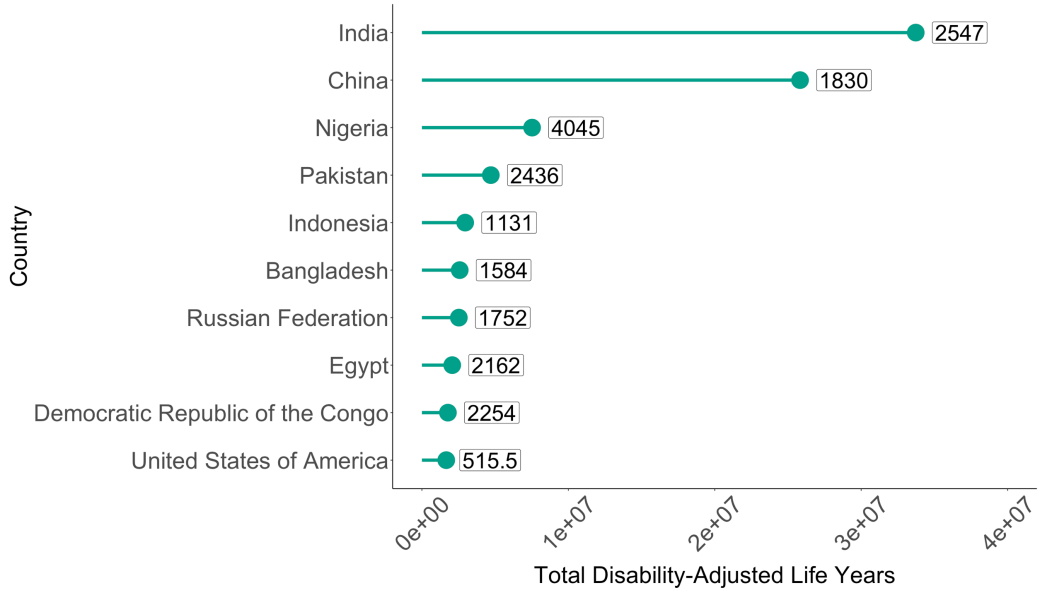

Figure 1.2: The number of DALYs from ambient air pollution, per nation [14]. The number of DALYs per 100,000 population are depicted at the end of each row [15]

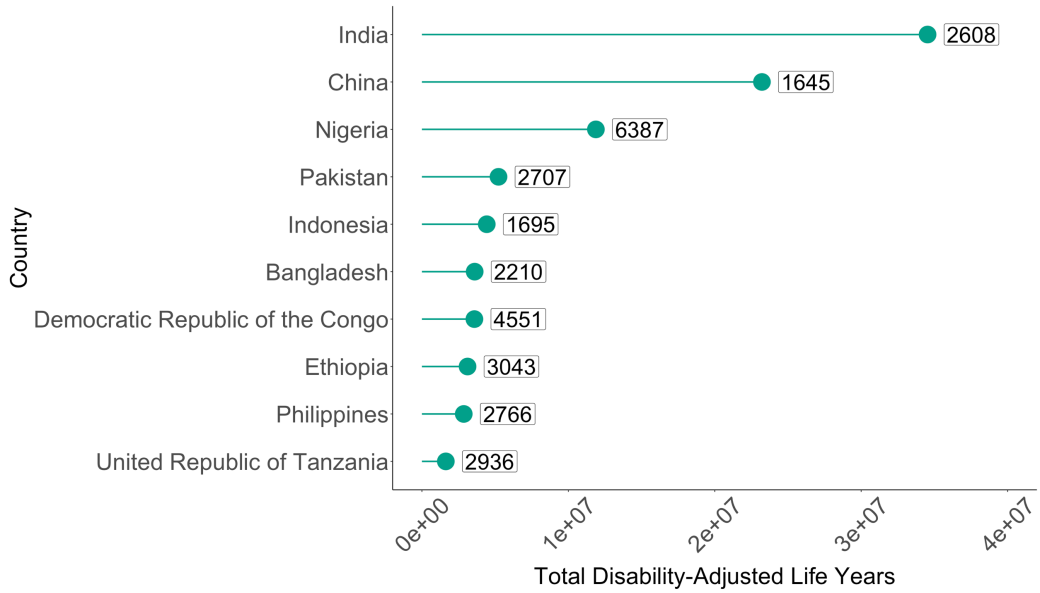

Figure 1.3: The number of DALYs from indoor air pollution, per nation [16]. The number of DALYs per 100,000 population are depicted at the end of each row [17]

The WHO has itself published data on DALYs attributable to household (indoor) and ambient air pollution, with respiratory illness, ischaemic heart disease, stroke, chronic obstructive pulmonary heart disease and cataract formation considered [14, 16]. Indoors, only air pollution directly linked to the combustion of solid fuel used in cooking is considered by the WHO. From the 2016 data used in Figures 1.2 and 1.3, it can be concluded that the burden of poor air quality disproportionately affects developing nations, with DALYs for both indoor and outdoor air pollution in India exceeding 33 million. Indoors, this can largely be attributed to the combustion of solid fuel. Indeed, UN data can attest that in 2017, approximately 61% of the global population had access to clean cooking fuel and technology, and that 840 million people were without electricity [18].

Perhaps one of the most comprehensive indoor air study programmes to date has been the multi-institutional HOMEChem (House Observations of Microbial and Environmental Chemistry) campaign. HOMEChem was

performed in a test house at the University of Texas at Austin and sought to measure the concentrations of gases and aerosols in a typical indoor domestic setting [19]. HOMEChem made observations on ammonia concentrations [20], the impacts of cooking and cleaning [21, 22], and the role of surface chemistry indoors [23].

1.1. Defining Sick-Building Syndrome

The aforementioned meetings of the European Regional Office of the WHO posited a hitherto undiagnosed condition: sick-building syndrome, or SBS [11]. SBS is a condition that causes a general malaise to afflict the occupant, but its cause is multifaceted. The construction of more airtight buildings, as well as the introduction of heating, ventilation, and air-conditioning (HVAC) systems, is thought to have been a catalyst for the increasing number of diagnoses of SBS since the 1970s, with Seppänen and Fisk (2004) [24] observing that in buildings with air-conditioning – as opposed to just natural ventilation – there was a 30–200% increase in the reporting of one or more symptoms associated with SBS. Recently constructed or renovated buildings are a key factor in SBS presentation. More specifically, the presence of volatile organic compounds (VOCs) is one hypothesis behind the phenomenon, though mould and bacterial growth from high humidity, other biological contaminants, endotoxins, ventilation, and psychosocial issues are all contributors posited in the existing literature [9, 25].

SBS, and exposure to pollutants more generally, is of great consequence when one considers the duration of time spent indoors by the modern population. Estimates in the 1980s placed this figure at up to 70% [26], though more recent calculations place this number at closer to 90% [27]. This is evident from a report published by the Office for National Statistics, which states that people spend around seven hours of their day engaged in activities indoors, i.e. watching television, using a computer and listening to the radio [28]. Commuting is also regarded as time spent indoors, with around

67% of working-age people doing so by car, though occupants are subject to generally high pollutant exposures due to the proximity of air inlets to other vehicle exhausts [27, 29, 30]. Nuance in exposure exists even between different commuting methods when private car and bus users are considered: commuters in private cars experienced greatest VOC exposure (e.g. benzene in car = 1.95 ppb; bus = 1.31 ppb), bus users the greatest $PM_{2.5}$ exposure (bus = 39 $\mu g\ m^{-3}$; car = 37.7 $\mu g\ m^{-3}$). [31]. Gym and fitness centre users are also exposed to indoor air pollutants, the effects of which are compounded by the metabolic response to physical exertion [32, 33].

Questionnaires were employed in the latter half of the 20th century in response to an increasing number of people reporting ill-health indoors and to reveal more information regarding property type and age, and whether this information correlated with symptoms of 'sick-building syndrome'. The questionnaires were formally proposed by Andersson and Stridh [34], though first drafts were produced in 1986. These questionnaires, collectively referred to as the MM questionnaires, sought to evaluate people's opinions on air quality in workplaces (MM-WP), residential areas (MM-RA) and schools (MM-S); MM being an acronym for *miljömedicin* in Swedish and translating to *environmental medicine* in English. The United States Environmental Protection Agency (US EPA) developed a large-scale study, named the Building Assessment Survey Evaluation (BASE), which was piloted in 1993, with the full study conducted between 1994 to 1998. This study utilised similar questionnaires [35].

1.2. The Influence of Volatile Organic Compounds

One of the aforementioned concerns of indoor air quality is the presence of volatile organic compounds (VOCs) and has been the focus of many studies. VOCs are organic compounds that are distinguished by their high vapour pressure at room temperature, a range of commonly found VOCs indoors

can be found in Table 1.1. A large number of molecules are evaporated into the gas phase due to their low boiling points [36].

Table 1.1: VOCs commonly found indoors representing a range of vapour pressures, including boiling points and sources

	VP (Pa)	BP (°C)	Sources
Ethane	4.20×10^6	-88.55	Fossil methane gas [37]
Propane	9.53×10^5	-42.05	Fossil methane gas [37]
iso-butane	3.48×10^5	-11.15	Propellant [38]
n-butane	2.43×10^5	-0.15	Propellant [39]
Isoprene	7.33×10^4	33.85	Human breath; biogenic sources [39]
n-pentane	6.85×10^4	36.05	Solvent [40]
Dichloromethane	5.80×10^4	39.85	Solvent [39]
Acetone	3.09×10^4	56.15	Solvent; human breath; biological processes [41, 42]
Benzene	1.26×10^4	80.15	Solvent [43]
Ethanol	7.91×10^3	-88.55	Solvent; human breath biological processes; food [42, 44]
Toluene	3.79×10^3	110.65	Solvent [43]
Ethylbenzene	1.28×10^3	136.15	Solvent [43]
m/p-Xylene	1.14×10^3	139.15	Solvent [43]
α–Pinene	6.33×10^2	156.85	Fragrance [45]
Limonene	2.07×10^2	177.85	Solvent; fragrance [45]
D4 siloxane	1.40×10^2	174.85	Personal care; cleaning products [46]

Vapour pressure values are taken from the US EPA CompTox Chemistry Dashboard wherein data is collated by the US EPA National Center for Computational Toxicology (NCTT) from literature-derived Physical Properties (PHYSPROP) data sets [47, 48]. The data presented here are experimental averages. Boiling point values were taken from the United States Department of Commerce National Institute of Standards and Technology (NIST) Chemistry WebBook [49].

Organic compound volatility can be divided into three categories [50]:

1. Those with a vapour pressure below 10^{-8} Pa. These exist predominantly in the aerosol phase and are not considered volatile under atmospheric conditions

2. Those with a vapour pressure above 1 Pa. These exist predominantly in the gas phase and are considered volatile under atmospheric conditions

3. Those with a vapour pressure between 10^{-8} and 1 Pa. These exist as both gas and aerosols and are considered semi-volatile under atmospheric conditions

As VOCs undergo oxidation, many intermediate species are formed; these are more functionalised than the parent VOC because as oxidation progresses, the number of functions increases [51]. Meaningful gas-particle partitioning from highly functionalised compounds, which usually have lower saturation vapour pressures and/or higher polarities, results in SOA formation [51]. The gas-particle partition is described in an equation that uses the saturated vapour pressure of a compound, see Equation 1.1.

$$P_i = x_i \gamma_i P_i^{vap}$$

Equation 1.1: Gas-particle partition equation as described in Valorso et al. [50] Where P_i is the particle pressure of a given compound, x_i is the mole fraction of the compound, γ_i is the activity coefficient of the compound, and P_i^{vap} is the saturation vapour pressure of the compound [50].

VOCs are ubiquitous in indoor environments, being found in solvents, petroleum-based products, building and furnishing materials, heating and cooking apparatus and tobacco smoke. Surplus VOC concentrations in

building and furnishing materials are outgassed into the environment, exacerbating indoor air pollution over time. It should also be noted that the newer the product, the higher the outgassing rate. These rates are also impacted upon by temperature and humidity [52]. VOC ingress from outside sources has impacts on indoor air pollution [53]. Indeed, the combined concentrations of VOCs in indoor environments, and those infiltrating from outdoors in, often means that indoor concentrations are greater indoors than in an outside environment [27].

A recent study by Su, Mukherjee et al. [54] specifies further the various determinants impacting indoor air quality, such as building ventilation, whether windows are open or not, collectively qualifying the air exchange rate (AER); the house type, years lived in the building and the presence of fireplaces, or lack thereof. More specifically, housing with attached garages saw an increase in the concentration of fossil fuel related VOCs indoors. The authors also refer to personal exposure determinants, such as local emission sources, local weather patterns, personal activities, and household characteristics.

The influence of product usage is a newly developing aspect of indoor air chemistry, as many personal care products contain VOCs that could potentially impact indoor air quality to a significant degree. To fully appreciate these impacts, several factors need to be addressed and quantified, namely: product type uses, their attendant VOCs, and how often are they being used. A number of studies have begun to address such questions with many authors opting for the use of product use questionnaires to determine participant behaviour:

The Air Pollution Exposure Distributions within Adult Urban Populations in Europe (EXPOLIS) study sought to measure a number of different VOCs in typical scenarios, across Europe, in large population groups. Participants were assigned to one of two different groups which then determined the

surveys and diaries they completed amongst a screening survey, a core questionnaire detailing the home and workplace, commutes and socioeconomic information, activity data diary, and exposure questionnaire [55, 56]. The National Human Exposure Assessment Survey (NHEXAS) estimated VOC exposure in large populations across multiple states in the United States [57]. Product usage data specifically was collected by Biesterbos, Dudzina et al. [58] to determine product usage in terms of dose size in Dutch populations. Wu, Bennett et al. [59] recorded product usage amongst Californian residents through telephone interviews and Hart, Walker et al. [60] also conducted product usage information amongst female university students. Product usage studies have been collated into national/regional databases, such as the ExpoFacts database in the European Union that seeks to combine product usage in frequency of use and weight [61]. ExpoFacts contains information on personal care products only. In the United States, the US EPA Exposure Factors Handbook consolidates multiple product usage studies to create a document in which the population usage of a variety of products, from a myriad of studies, is recorded [62].

1.3. Reactive Chemistry

The main constituents of the atmosphere, N_2 and O_2, are photochemically unreactive, therefore, radicals play an important role in removing trace gases [63]. A radical is defined as a molecule that has an unpaired electron [64]. In general terms, radicals are derived from reactions between sunlight and photolabile molecules, and further reaction between radicals and other species in the atmosphere drives chemistry in the troposphere [64]. Radical species, by virtue of being highly reactive, typically have low mixing ratios, often <100 ppt [64]. The hydroxyl (OH) and nitrate (NO_3) radicals, ozone (O_3), and chlorine (Cl) will be considered here. Below (Figure 1.4) is a brief reaction scheme for a VOC in the presence of OH, O_3, or NO_3, and sunlight.

Additional details regarding reaction mechanisms is detailed in subsequent sub-sections.

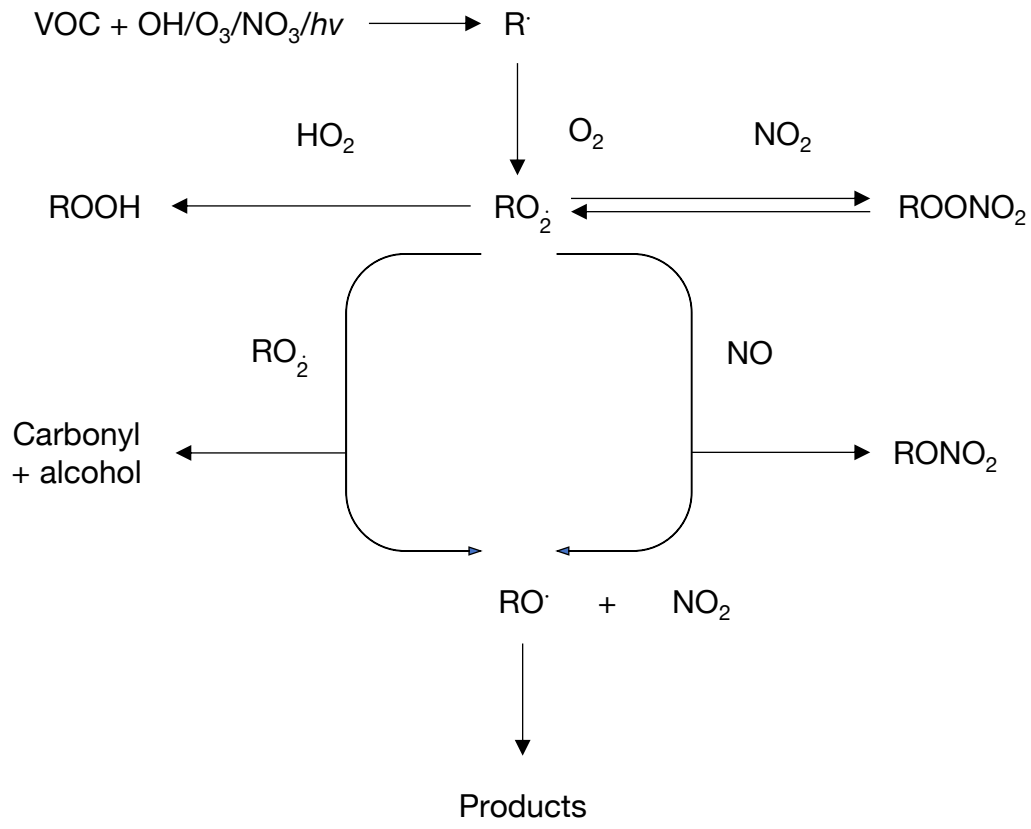

Figure 1.4 Generic VOC oxidation mechanism, where RO_2 = organic peroxy radical, ROOH = hydroperoxide, $ROONO_2$ = peroxynitrate, $RONO_2$ = nitrate ester

Figure 1.4 (adapted from Atkinson and Arey [65]) shows a the oxidation of a generic VOC, via OH, O_3, or NO_3, and sunlight; specific reaction mechanisms for VOCs with each oxidant are described in greater detail in Chapter 5. When reacted with O_2, organic peroxy radicals (RO_2) are formed. Further reaction with HO_2 forms hydroperoxides (ROOH), or reaction with NO_2 forms peroxynitrates ($ROONO_2$). Further interaction amongst organic peroxy radicals forms carbonyls and alcohols, alcoxy radicals (RO), and associated products. Reactions between organic peroxy radicals and nitric

oxide forms nitrate ester ($RONO_2$), alcoxy radicals and associated products [65].

1.3.1. OH formation and reactivity

OH is typically found in low mixing ratios in the atmosphere, less than parts per trillion; and has a lifetime of less than a second [66]. However, because it reacts quickly with most trace gases, its importance in atmospheric chemistry is significant [67]. OH is formed in the atmosphere primarily through the photolysis of O_3 by ultraviolet sunlight in the presence of water vapour (approximately 95% OH in the atmosphere is the result of the photolysis of O_3 and its reaction products), as described by the following reactions in R 1.1 and R 1.2 [68]:

$$O_3 + h\nu \rightarrow O(^1D) + O_2 \qquad \text{(R 1.1)}$$

$$O(^1D) + H_2O \rightarrow 2OH \qquad \text{(R 1.2)}$$

The first reaction generates an excited oxygen atom, which in turn reacts with H_2O to form OH. Further reactions can then lead to the propagation of reaction chains and secondary, or recycled, OH formation [68]. The majority of $O(^1D)$ produced is subject to collisional quenching back to ground-state oxygen atoms by the following reactions in R 1.3 and R 1.4 [64]:

$$O(^1D) + N_2 \rightarrow O(^3P) + N_2 \qquad \text{(R 1.3)}$$

$$O(^1D) + O_2 \rightarrow O(^3P) + O_2 \qquad \text{(R 1.4)}$$

The amount of $O(^1D)$ forming OH is dependent on H_2O concentration in the system [64].

In relatively unpolluted, low NO_x environments, OH primarily reacts with carbon monoxide and methane, producing peroxy radicals e.g. HO_2 via the following reactions in R 1.5 [64]:

$$\begin{aligned} &OH + CO \rightarrow H + CO_2 \\ &H + O_2 + M \rightarrow HO_2 + M \end{aligned} \qquad \text{(R 1.5)}$$

Further, HO_2 can react with ozone, thus leading to greater destruction via a chain sequence that also involves OH production and loss of NO_x through the formation of HNO_3 in R 1.6 [64, 69]:

$$\begin{aligned} &HO_2 + O_3 \rightarrow OH + 2O_2 \\ &OH + O_3 \rightarrow HO_2 + O_2 \\ &OH + NO_2 + M \rightarrow HNO_3 \end{aligned} \qquad \text{(R 1.6)}$$

HNO_3 is in turn converted back to NO_x through in R 1.7 and R 1.8 [70, 71]:

$$HNO_3 + OH \rightarrow H_2O + NO_3 \qquad \text{(R 1.7)}$$

$$HNO_3 + h\nu \rightarrow OH + NO_2 \qquad \text{(R 1.8)}$$

As the formation of peroxides e.g. hydrogen peroxide, can be a significant sink of HO_x, these reactions often result in chain termination [64]. In high NO_x conditions, peroxide forming reactions compete with the peroxy radical catalysed oxidation of NO to NO_2 in R 1.9 [64]:

$$HO_2 + NO \rightarrow OH + NO_2 \qquad \text{(R 1.9)}$$

The photolysis of NO_2 derived from this reaction, and the subsequent reaction of $O(^3P)$ results in the formation of O_3 in R 1.10 [64]:

$$\begin{aligned} &NO_2 + h\nu \rightarrow NO + O(^3P) \\ &O(^3P) + O_2 + M \rightarrow O_3 + M \end{aligned} \qquad \text{(R 1.10)}$$

The presence of HONO can also result in the formation of OH in urban areas through in R 1.11 [64]:

$$HONO + h\nu \rightarrow OH + NO \qquad \text{(R 1.11)}$$

NO_x plays an important role in tropospheric chemistry by affecting the radical budget, particularly with regard to HO_x partitioning, influencing OH and HO_2 concentrations, and the production of O_3 [64]. When OH reacts with CO, CH_4, or O_3, it converts to HO_2, which in turn, converts back to OH when reacted with NO or O_3 [64]. In systems with increasing NO_x concentrations, the HO_2/OH ratio is supressed, leading to increased OH concentrations [64]. These reactions, in this system, are an important secondary source of OH in the atmosphere [64]. With regards to HO_2, and in a system with increasing NO_x, loss through reaction with NO is significant [64]. In this system, the formation of HNO_3 through OH and NO_2, drives the loss of HO_x, causing the loss of OH [64]. These reactions drive a moderately non-linear response of OH to increasing NO_x [64].

In high NO_x-high VOC systems, oxidation is initiated by OH through the following reaction scheme in R 1.12 [72]:

$$\begin{aligned} &OH + RH \rightarrow R + H_2O \\ &R + O_2 + M \rightarrow RO_2 + M \\ &RO_2 + NO \rightarrow RO + NO_2 \\ &RO \rightarrow \text{carbonyl products} + HO_2 \\ &HO_2 + NO \rightarrow OH + NO_2 \end{aligned} \qquad \text{(R 1.12)}$$

Control of ozone in the atmosphere is complicated by these reactions. Reducing VOCs is only effective in reducing O_3 in VOC-sensitive systems (where $N(O_3)$ is proportional to VOC) [72]. Likewise, reducing NO_x will only be effective in NO_x-sensitive systems (where $N(O_3)$ is proportional to NO_x) [64].

Alkenes subjected to ozonolysis can lead to the production of OH in yields of between 7–100%, depending on alkene structure and normally leads to the further production of organic peroxy radicals [64].

1.3.2. O_3 formation and reactivity

O_3 exists in both the troposphere and stratosphere. Stratospheric ozone is known primarily because of its protective role in absorbing UV radiation from the sun, thus preventing it from causing harm to life on Earth. Tropospheric ozone, however, is seen as a pollutant because it can cause harm to living cells [73]. More recently, O_3 has been identified as a significant contributor to crop yield loss, with a 3–16% (US$ 14–16bn) economic loss estimated for 2000 [74].

The main source of O_3 in the troposphere is the reaction of NO_x with VOCs in the presence of sunlight [75], and is outlined in the following reactions in R 1.13 [64]:

$$\begin{aligned} &OH + CO \rightarrow H + CO_2 \\ &H + O_2 + M \rightarrow HO_2 + M \\ &HO_2 + NO \rightarrow OH + NO_2 \\ &NO_2 + h\nu \rightarrow O(^3P) + NO \\ &O(^3P) + O_2 + M \rightarrow O_3 + M \\ &\text{Net: } CO + 2O_2 + h\nu \rightarrow CO_2 + O_3 \end{aligned} \qquad \text{(R 1.13)}$$

However, in low NO_x scenarios, O_3 can both be created and ultimately destroyed by the following reactions in R 1.14 [64]:

$$\begin{aligned} &OH + CO \rightarrow H + CO_2 \\ &H + O_2 + M \rightarrow HO_2 + M \\ &HO_2 + O_3 \rightarrow OH + 2O_2 \\ &\text{Net: } CO + O_3 \rightarrow CO_2 + O_2 \end{aligned} \qquad \text{(R 1.14)}$$

Oxidation of alkenes by O_3 forms a primary ozonide, which subsequently decomposes to a Criegee intermediate and additional carbonyl products [72]. The Criegee intermediate can either then stabilised by an additional compound or undergo further decomposition to products [64]. Compared to the other atmospheric radicals considered here, the reaction of O_3 with alkenes is slow, but can be offset by high concentrations of either O_3 or alkenes [64].

There is also some flux between the stratosphere and troposphere, with stratosphere-troposphere transport estimated to be 1.2 ppb (3.1%) of ozone in the boundary layer, 5.4 ppb (13%) in the lower troposphere, and 22 ppb (34%) in the mid- to upper troposphere [76]. O_3 is found in mixing ratios of between 30–50 ppb and has a lifetime of weeks in the troposphere (mean = 22 days) [75, 77]. O_3 is itself reactive with a number of atmospheric trace gases, and is fundamental in the production of OH, a significant oxidant [78].

1.3.3. NO_3 formation and reactivity

NO_3 forms from the oxidation of NO_2 by O_3, and is most prominent during night time hours due to the rapid photolysis of the nitrate radical in sunlight [79]. The reaction is described below in R 1.15 [80]:

$$NO_2 + O_3 \rightarrow NO_3 + O_2 \qquad \text{(R 1.15)}$$

Another source of NO_3 is through the reaction of N_2O_5 with another molecule, via the following reaction in R 1.16 [64]:

$$N_2O_5 + M \rightarrow NO_3 + NO_2 + M \qquad \text{(R 1.16)}$$

N_2O_5 itself is formed by the reaction of NO_3, NO_2, and another molecule via R 1.17[64]:

$$NO_3 + NO_2 + M \rightarrow N_2O_5 + M \quad \text{(R 1.17)}$$

These reactions mean that N_2O_5 and NO_3 act in a coupled manner, and should be in a steady-state during night-time hours [64, 81]. N_2O_5 can further react with water to form HNO_3 [64]. NO_3 is also short-lived in the atmosphere, persisting for seconds during daylight hours, and has mixing ratio values in the ppt range [82].

As alluded to earlier, NO_3 is rapidly photolysed by daylight through the following reactions in R 1.18 and R 1.19 [64]:

$$NO_3 + h\nu \rightarrow NO + O_2 \quad \text{(R 1.18)}$$

$$NO_3 + h\nu \rightarrow NO_2 + O(^3P) \quad \text{(R 1.19)}$$

It also readily reacts with NO, which has significantly higher concentrations in daytime as compared to night-time via R 1.20 [64]:

$$NO_3 + NO \rightarrow NO_2 + NO_2 \quad \text{(R 1.20)}$$

This potentially implies that in highly polluted systems, NO_3 could become a significant oxidant during daylight hours, especially of monoterpenes such as α-Pinene, p-cresol etc [64].

In alkene chemistry, reactions with NO_3 leads to complex reactions with nitro-oxy substituted organic radicals, which leads, in part, to the regeneration of NO_2 [64]. Depending on the mix of hydrocarbons in the atmosphere, NO_3 can recycle NO_x during the night and impede nitrate aerosol formation [72].

A simplified night-time reaction scheme between NO_3 and a VOC is detailed below, where NO_3 initiates the reaction in R 1.21 [72]:

$$\begin{aligned} &NO_3 + \text{organic compounds} \rightarrow R + \text{products} \\ &R + O_2 + M \rightarrow RO_2 + M \\ &RO_2 + NO_3 \rightarrow RO + NO_2 + O_2 \\ &RO + O_2 \rightarrow R'R''CO + HO_2 \\ &HO_2 + NO_3 \rightarrow OH + NO + O_2 \end{aligned} \qquad \text{(R 1.21)}$$

1.3.4. Cl formation and reactivity

Chlorine is understood to be a potent oxidant in both the troposphere and stratosphere. In the stratosphere, the dissociation of chlorine from chlorofluorocarbons (CFCs) is responsible for the destruction of O_3 in the ozone layer [83]. As such, in tropospheric chemistry, Cl radicals not only have the potential to impact tropospheric ozone concentrations – therefore impacting OH production cycles – but due to competitive reaction times when compared to OH, can oxidise prominent greenhouse gases such as methane and dimethyl sulphide, as well as VOCs [84, 85]. A significant source of chlorine gas in the atmosphere is derived from chloride in sea salt aerosol that form photolytic precursors of Cl by reaction with nitrogen oxides via e.g. R 1.22 and R 1.23 [86, 87]:

$$2NO_2 + NaCl \rightarrow NaNO_3 + NOCl \qquad \text{(R 1.22)}$$

$$N_2O_5 + NaCl \rightarrow ClNO_2 + NaNO_3 \qquad \text{(R 1.23)}$$

The products of both reaction are both rapidly photolysed to Cl.

Tropospheric inorganic chlorine can result from combustion activities, such as in the use of coal and incineration, as well as from biomass burning [85]. Cooling towers and swimming pools are notable sources of localised chlorine emissions [88]. Cl can also be derived from the reaction of OH with HCl (which

is formed from the acidification, by sulphuric or nitric acid, of NaCl aerosols) [87]. Bleach-based cleaning products can lead to chlorine emissions indoors [89].

Fantechi et al. have examined the Cl oxidation of isoprene, 2-methyl-3-buten-2-ol (MBO), and toluene. From isoprene, expected products are OCHCl, HCl, CO, and CO_2; from MBO, the expected products are acetone, OCHCl, HCl, CO, and CO_2; and from toluene, the expected products are benzaldehyde, benzyl chloride, benzal chloride and benzyl alcohol, due to Cl initiating H-abstraction from the $-CH_3$ group to form benzyl radicals [87].

1.3.5. Secondary Organic Aerosols

Following the radical oxidation of VOCs, secondary organic aerosols are formed. SOAs are formed from VOCs via complex reactions of gas-phase oxidation and ageing reactions [90]. The propensity of organic vapours to transfer from the gas to the particle phase is determined largely by its volatility, itself determined by molar mass and composition [90]. SOAs can be derived from both anthropogenic and biogenic VOC emissions, though VOC profiles will obviously vary according to source, for example boreal forests are dominated by monoterpene species [90]. SOA precursors derived from anthropogenic sources are predominantly alkanes (40%), aromatics (20%), and alkenes (10%) [91]. Models estimate that anthropogenic SOA contributes approximately 10 TgC yr to the global annual SOA flux, with biogenic SOA contributing approximately 88 TgC yr annually [91]. Organic aerosols more generally constitute approximately 20–50% of aerosol load globally [91]. In urban areas, secondary organic aerosol constitutes approximately 90% of aerosol load [92].

Further to secondary organic aerosol (SOA) formation is the formation of cloud condensation nuclei (CCN). CCN are small atmospheric particles (between at least 50–100 nm) that form an aerosol substrate upon which

water vapour can condense, and thus develop into cloud droplets [93]. CCNs can be constituted of a number of different atmospheric aerosols, with SOAs formed from VOC oxidation being but one source; the hygroscopicity of different aerosols is the limiting factor of their propensity to form CCNs [94]. As clouds exert significant influence in the Earth's energy budget, an increase in atmospheric SOA concentrations could impact this system notably [93, 95, 96].

1.4. Spatial Variability of Air Pollution and Socio-Economic Determinants

Another aspect to consider is the spatial variability of VOC exposures. As detailed earlier, a study by Macey, Breech et al. [97] examined VOC concentrations in communities near oil and gas extraction sites in the United States. Other studies have been conducted that examine this phenomenon. A study by Sexton, Adgate et al. [98] examined hazardous air pollutants more widely across three suburbs in the Minneapolis/St. Paul Metropolitan area, taking into consideration the socio-economic background of each suburb. Of the 14 out of 15 VOCs measured, two-day average concentrations were highest for personal exposure, intermediate for indoor and lowest for outdoor exposures. The study concluded that outdoor VOC concentrations were lowest in more affluent areas and higher in more economically deprived suburbs. Similarly, a study by Serrano-Trespalacios, Ryan et al. [99], conducted in Mexico, found higher mean concentrations indoors than at outdoor centralised pollutant monitoring sites for most VOCs, with similar conclusions drawn for the difference between outdoor concentrations at home and indoors. In cities with multiple sources of pollution, and with multiple pollutants, Miller, Xu et al. [100] recognise that centralised monitoring stations may not provide an accurate representation of pollutant exposure to individuals.

Air quality indices are an effective way of disseminating daily air pollution information of a specific geographical area to the wider public, though there is a great deal of variation amongst different local governments and the data that are reported [101]. In 1997, the US EPA introduced a colour-coded air quality index that linked pollutant concentrations and associated health effects with a simple colour scheme, with similar indices established in Europe, Asia, and Australia [102]. Miller, Xu et al. [100] developed an air quality index for different areas of Sarnia, Canada. Initially, monitoring sites were chosen to include 25 facilities that are obliged to report pollution data to the Criteria Air Contaminant Emissions Inventory in the National Pollutant Release Inventory. 39 exposure index points were then defined, selected to include at least one monitoring site in, or in close proximity to, a residential census tract. A census tract is defined as an area with a population of between 2,500 and 8,000 within a larger metropolitan area of at least 50,000 [103]. To measure pollutant concentrations, passive samplers were deployed to the 39 exposure index points. 26 VOC species were identified using a gas chromatography/mass selective detector (see VOCs observed in Table 1.2).

Table 1.2: 26 observed VOCs in Miller, Xu et al. (2009) [100]. The subset of ten VOCs in the study are highlighted in bold

Toluene	Trichloroethylene	d-Limonene
m/p-Xylene	1,3,5-Trimethylbenzene	p-Cymene
Hexane	Dichloromethane	1,3-Dichlorobenzene
Benzene	*n*-Decane	1,4-Dichlorobenzene
Ethylbenzene	1,2-Dichloroethane	Hexachloroethane
o-Xylene	Styrene	1,2,4-Trichlorobenzene
1,2,4-Trimethylbenzene	Cumene	
Tetrachloroethylene	α-Pinene	
Naphthalene	1,1,2,2-Tetrachloroethane	
Chloroform	Pentachloroethane	

From this, the ten most commonly found VOCs were selected for further analysis, and a Spearman rank correlation coefficient matrix was developed

to discover correlations between pollutant concentrations and site. The air quality index was developed by assigning a rank to each exposure index point per species. The sum concentration of observed VOCs, total VOC, was used as the determinant. An overall exposure index point ranking was assigned, based on the ranking of each species. Each point was then classified according to a ‘low’, ‘medium’ or ‘high’ concentration.

A more formal spatial analysis can be performed, as evidenced in a review paper by Zhou and Levy [104]. They explain that there is an increasing interest among many public health experts in the spatial extent of impacts from traffic-related emissions. A paper by Chen, Kwong et al. [2] suggests that there is a 7% increase in instances of dementia observed in people who reside within 50 metres of major roads (hazard ratio increase from 1 to 1.07), based on a cohort study conducted in Canada. The study also tried to determine the impacts of heavy traffic on instances of Parkinson’s disease and multiple sclerosis, though no association was noted. Ultimately, it was determined that there are multiple components that construct exposure, such as nitrogen oxides, particulate matter and volatile organic compounds. Zhou and Levy [104] estimated that the spatial extent of impact is around 100–500 m depending on the pollutant, with background concentrations and local weather conditions also influencing result outcome.

Various methods have been employed to perform spatial analysis of pollution extent in previous studies, namely geographical informational systems (GIS). Gorai, Tuluri et al. [105], Theophanides and Anastassopoulou [106], and Tonne, Melly et al. [107] state that the use of GIS is invaluable when it is used in conjunction with models, with particular regard to data management. In traffic-related air pollution studies, GIS analysis involves the generation of buffers around the road. From there, total traffic volume within a defined radius of the roadway is measured, and health outcomes linked to those results. Health outcomes that are strongly related to a particular radius would define the spatial extent of that pollutant [104]. This method can be applied

theoretically to other spatial studies, though the pollution source would be fixed. Other studies measure pollution at pre-defined distances from the source, and account for the concentration differences between the source and background pollution levels. When the difference equilibrates, the presumed extent is defined. Land-use regression models are a popular method, used in tandem with GIS, to estimate pollutant concentrations at pre-defined locations, based on pollutant levels at surrounding sites [104, 108].

A study in the UK by Delgado-Saborit, Aquilina et al. [109] considered personal exposure to VOCs based on geographical determinants, namely location of participant residence and proximity of participant residence to busy roads, whilst also considering exposure to environmental tobacco smoke and if the residence garage was integrated into the property. The study area incorporated urban, semi-urban and rural areas. Results from the study implied that homes were the most influential microenvironment for all compounds, and that there was no clear distinction in personal exposure to VOCs between those who and those who do not reside near main roads. Personal exposure was observed to be higher in urban areas than in semi-urban and rural areas. The results of the impact of residence location within a city is shown to contradict existing studies, suggesting that indoor VOC exposure is approximately equal across urban, semi-urban and rural residences. The authors express that this is due to the greater prevalence of integrated garages in semi-urban and rural residences.

Inequality pertaining to pollution distribution is an issue that is not clearly understood by the scientific community, but Rosofsky, Levy et al. [110] outline that many studies are cross-sectional, as opposed to longitudinal, and therefore limit the scope of the study by not including an historical perspective. The siting of particularly polluting land uses e.g. busy main roads, heavy industry etc. in poorer communities, thereby placing the burden of air pollution on economically deprived populations and ineffectual planning policy are other concerns.

Research into the socio-economic influences of indoor air quality has been conducted in China. As part of a modernisation process, Beijing Municipality has administered a scheme that subsidises the use of electric heat pumps and electricity in the interest of banning coal. A study by Barrington-Leigh, Baumgartner et al. (2019) [111] assessed the impact of this scheme on domestic energy usage and associated expenditure, wellbeing and indoor quality in villages both affected and unaffected by the programme across three districts with different socio-economic backgrounds. The study concluded that high and middle-income areas benefitted from better indoor temperatures, air quality and wellbeing after no longer using coal. Indoor air quality did not improve to the same extent in less affluent areas when compared to wealthier areas. In less affluent areas, on a point scale of 0–10, a decrease in both Satisfaction with Life (SWL) and Satisfaction with Living Conditions (SWC) scores was observed when areas had been converted to electricity from coal power (SWL = -1, SWC = -1.5) in the low-income district. Scores improved when conversion had taken place in the middle-income district (SWL = +0.7, SWC = +1), and there was no observable difference in the high-income district [111].

1.5. A Political and Legislative Perspective

As mentioned previously, the focus of air pollution research, and policy in turn, has been predominantly on outdoor air pollution. Consequently, focus has only shifted to indoor pollution in recent years. Indoor air quality is notoriously difficult to legislate for, with the exception of commercial and industrial premises, as it is determined by the building resident(s), and it is unlikely they would be acquiescent to such prescriptions [112]. Indoor air quality policies can be optimised by addressing four key categories:

1.5.1. Regulatory co-ordination across multiple government agencies

The benefits of regulatory co-ordination have been recognised in economic and immigration policies, as European sovereign states work to integrate with the European Union [113], but this is something yet to be realised in the case of indoor air pollution. Several agencies of the British government have air quality and pollution under their purview, such as the Department for Environment, Food and Rural Affairs (DEFRA) and the Department for Transport, though DEFRA sets most of the regulations. Akin to outdoor air pollution, sources of indoor air pollution are multifaceted, so indoor air quality issues should fall under the purview of multiple agencies. These agencies should work to co-ordinate and optimise these regulations, as recognised more generally by Hallsworth, Parker et al. [114]

1.5.2. Improved building regulations and certification

There is a certain level of trade-off between ventilation and the energy efficiency, with more energy efficient housing being inherently less well-ventilated, or ‘passive’. Conversely, less well-ventilated constructions allow a greater number of outside air pollutants to ingress into the indoor environment. The US EPA suggests that indoor air quality can be improved by limiting pollution at source, increasing air flow through buildings, and by using mechanical air cleaners [115-117].

Certification could contribute to improving construction standards across the industry at the point of construction, and could also be potentially used during periods of building occupancy too. Both the United States Green Building Council through the Leadership in Energy and Environmental Design (LEED) rating and the United Kingdom Building Research Establishment through the Building Research Establishment Environmental Assessment Method (BREEAM) certification provide criteria on achieving

indoor air quality standards, such as on construction materials used and ventilation rates required. However, indoor air quality is one of a number of criteria that need to be fulfilled to achieve certification; the focus of certification is based on building sustainability [118, 119]. There is also some concern regarding uniformity between the two certification systems, but this is not thought to be a significant issue as many criteria are common to both schemes [120]. The International WELL Building Institute through the WELL certification scheme does provide a rating for improved, health-based building design and use. WELL has provision for particulate matter, inorganic compounds (ozone and carbon monoxide), organic compounds (toluene, benzene, and formaldehyde) and total VOC concentrations. Certification is also reassessed every three years, ensuring continued optimal building performance [118].

1.5.3. Working to reduce emissions

A significant issue with establishing a rigorous regulatory framework for indoor air pollution is that it is impractical to police, so the onus is with policy makers to regulate products available for domestic use. Domestic products such as cookers are a common source of indoor air pollutants, especially in developing countries, where access to cleaner burning fuels is limited [121, 122]. As a consequence, residents use firewood, coal or dung as fuel for cooking, creating a burden of greater air pollutant concentrations in more economically deprived areas [123].

Product use data are becoming more numerous, but the steps to identify and mitigate the use of harmful chemicals is more thoroughly understood, such as in the European Chemicals Agency REACH regulation of 2007. An equivalent regulation in the United States is the Toxic Substances Control Act (TSCA). TSCA was introduced in 1976, with an additional Act passed in 2016 which incorporates greater risk evaluation [124].

Where point-source reduction of pollutants isn't feasible, one possible remediation is the deployment of air purifiers; one which has attracted attention recently due to the COVID-19 pandemic. Three approaches to air cleaning have been identified by Collins and Farmer (2021) [125]: i) the removal and degradation of gas-phase pollutants e.g. VOCs, ii) the removal of particulate matter, and iii) the removal of biological particulate matter. One method by which to achieve the removal and degradation of air pollutants is through the use of oxidiser-based air purifiers. In theory, these devices are designed to degrade pollutant to water and carbon dioxide. However, in practise, these purifiers can perturb chemistry indoors by adding ozone, hydroxyl radicals etc. to the atmosphere, therefore forming oxidised VOCs and particulate matter and potentially impacting human health [125, 126]. Filtration-based purifiers, such as the use of HEPA filters are effective in removing particulate matter and have minimal impact on indoor chemistry, but saturated filter media can re-emit semi-volatile compounds to the atmosphere [125].

1.5.4. Education and international collaboration

Auerbach and Flieger [127] recognised the need for public education regarding air pollution more generally, stating that in order for this to be effective, there needs to be open discourse between government bodies and the wider population. A study by Revell [128] identified that local governments are in a prime position to influence public behaviour. However, project outreach programmes, a principal method adopted by councils with which to engage the public, are largely ineffectual by virtue of the fact that easy access to information does not ipso facto drive public concern in environmental issues.

Other countries are equally lacking in indoor air quality policies, though the WHO has implemented a number of guidelines for controlling benzene, carbon monoxide, formaldehyde, naphthalene, nitrogen dioxide, $PM_{2.5}$ and PM_{10}, PAHs, benzo-[*a*]-pyrene, radon, trichloroethylene and

tetrachloroethylene [129]. Finland is one country with structured legislation regarding indoor air quality. The Finnish Health Protection Act was written in 1990, with indoor air quality legislated for in 1995, and a second addendum incorporated in 1997, though this focusses on microbial contamination in municipal buildings and corporate premises. Risk assessment is carried out on the local government level by a health surveillance officer employed by the municipality, usually a veterinarian [130].

The Californian government makes efforts to control indoor air quality through a report published by Shimer, Phillips et al. [131] for the California Environmental Protection Agency. The report focusses on the use of source pollution reduction as a main driver in improving indoor air quality. As such, the California government has produced a list of 800 substances (Proposition 65) that must be reported by the manufacturer should they be contained in commercially available products. Whilst not providing direct legislation for indoor air quality, it does, at least, allow consumers to make an informed decision about the products that they are using [132]. Similarly in the UK, and mandated by the government through the Volatile Organic Compounds in Paints, Varnishes and Vehicle Refinishing Products Regulations 2012 , labels are placed on paints to denote VOC content, with categories ranging from minimal (0–0.29%) to very high (>50%) [133, 134]. In France, since 2013, all construction and decorative materials have had to be labelled with their potential VOC emissions within four categories ‘A+’ to ‘C’, based on the emissions of ten VOCs and total VOCs [135].

Programmes by the United Nations aim to improve air quality to some degree through the Sustainable Development Goals (SDGs). SDGs were implemented to help ensure sustainable development specifically in UN member states. Air pollution is encompassed in several SDGs, particularly: SDG 3 ‘to ensure healthy lives and promote well-being for all at all ages’, SDG 7 ‘to ensure access to affordable, reliable, sustainable, and modern energy for all’, and SDG 11 ‘to make cities and human settlements inclusive,

safe, resilient and sustainable' [136, 137]. Whilst SDGs are not legally binding, UN member states are expected to establish frameworks to achieve these goals, with progress needing to be reported [138].

1.6. Predicted Challenges

As outdoor air infiltrates indoor environments is a source of not only VOCs indoors, but additional oxidants, changes to air pollution profiles in urban areas will subsequently impact indoor air, too. Research by McDonald, de Gouw et al. [139] has concluded that a significant proportion of fossil fuel VOCs in urban areas are now derived from what the authors term volatile chemical products; a category of commercially available products that are used frequently by populations and include personal care products amongst others. Significantly, this proportion is now equivalent to VOCs emitted by the transportation sector. With this in mind, it's clear that policy and legislative interventions need to be drafted that require products to be reformulated to substitute compounds of concern with safer alternatives. These interventions would not only help to reduce the total VOC load of outdoor air in urban areas, but they would also mitigate indoor air pollution, occupant exposure to potentially harmful compounds and subsequent SOA formation.

Climate change presents significant perturbations to air pollution issues. Changes in air circulation and meteorology due to a changing climate could lead to an increase in air stagnation events, wherein ozone and particulate matter could accumulate in greater concentrations in near-surface environments [140]. Extreme heat events are predicted to increase ozone concentrations and thus lead to greater mortality, due to higher temperatures, more sunlight, and greater air stagnation [141-143]. Urban areas are particularly susceptible to increasing temperatures and extreme heat events through the phenomenon of the urban heat island (UHI) effect. UHIs represent urbanised areas that have a higher temperature than the rural areas surrounding them. The synergy between UHIs and heatwaves means

that under climate change – and the attendant increased likelihood of extreme weather events – urban areas will be subject to heat stresses far in excess of the sum of the UHI effect and heatwaves [144]. Given these stressors, it is likely that the UHI effect will exacerbate air pollution in cities through more frequent air stagnation events and increased ozone concentrations.

Alongside urban heat islands, the analogous phenomenon of the urban pollution island (UPI) exists, with a UPI being described as an urban area where pollutant concentrations are higher those of the rural areas thereabouts [145, 146]. UHIs and UPIs are inextricably linked, with the UHI effect driving higher temperatures, causing enhanced ozone concentrations and emission rates of VOCs. The two phenomena also create a positive feedback loop, whereby e.g. higher temperatures lead to the use of air conditioning units, placing greater demand on power plants – releasing more VOCs and contributing to climate change – and venting heat directly into urban areas, leading to the continuation of ever higher temperatures and pollutant concentrations [147, 148].

1.7. Summary of Thesis

This thesis seeks to characterise indoor air quality in domestic environments, both in terms of influences and oxidation mechanisms. Chapter 2 explores the methodologies used in all experiments throughout this thesis, with background knowledge on these techniques provided.

Chapter 3 seeks to understand the decay and oxidation of commonly found VOCs in a controlled chamber environment using a novel instrument method. These experiments investigate different NO_x and oxidant regimes and VOC decay and oxidation. Chapter 3 also explores production of SOA intermediates.

Chapter 4 is a population-scale analysis of indoor air in UK homes. A large population size relative to existing studies and a novel experimental methodology provides a thorough exploration of C_2–C_{10} VOCs indoors. These data are coupled with information from surveys that encompass usage of a variety of products, resident demographics, property type, and age.

Chapter 5 furthers the work performed in Chapter 4 and provides additional analysis on chemical reactivity. OH, O_3, and NO_3 are identified as primary oxidants indoors and the reactive potential and pseudo-first order reactivity is measured for each VOC in all samples obtained in Chapter 4 both dependent and independent of the concentration of the oxidants listed above. Further data were obtained from an indoor chemistry model for NO_x and O_3, OH, and particulate matter concentrations and mixing ratios, as well as for a newly developed secondary product metric.

References

1. Royal College of Physicians. Every breath we take: The lifelong impact of air pollution. Report of a working party [Internet]. London, UK: Royal College of Physicians; 2016. [cited 23.08.2021]. Available from: https://www.rcplondon.ac.uk/file/2912/download.

2. Chen H, Kwong JC, Copes R, Tu K, Villeneuve PJ, van Donkelaar A, Hystad P, Martin RV, Murray BJ, Jessiman B, Wilton AS, Kopp A, Burnett RT. Living near major roads and the incidence of dementia, Parkinson's disease, and multiple sclerosis: A population-based cohort study. Lancet. 2017;389(10070):718–26.

3. Shi L, Wu X, Danesh Yazdi M, Braun D, Abu Awad Y, Wei Y, Liu P, Di Q, Wang Y, Schwartz J, Dominici F, Kioumourtzoglou M-A, Zanobetti A. Long-term effects of $PM_{2.5}$ on neurological disorders in the american medicare population: A longitudinal cohort study. Lancet Planet Health. 2020;4(12):e557–e65.

4. Veras MM, Caldini EG, Dolhnikoff M, Saldiva PHN. Air pollution and effects on reproductive-system functions globally with particular emphasis on the Brazilian population. J Toxicol Environ Health B. 2010;13(1):1–15.

5. Laville S. Air pollution a cause in girl’s death, coroner rules in landmark case. The Guardian. 16.12.2020 [cited 09.02.2022]. Available from: https://www.theguardian.com/environment/2020/dec/16/girls-death-contributed-to-by-air-pollution-coroner-rules-in-landmark-case

6. Hu J, Xue X, Xiao M, Wang W, Gao Y, Kan H, Ge J, Cui Z, Chen R. The acute effects of particulate matter air pollution on ambulatory

blood pressure: A multicenter analysis at the hourly level. Environ Int. 2021;157:1–7.

7. Utell MJ, Frampton MW. Acute health effects of ambient air pollution: The ultrafine particle hypothesis. J Aerosol Med. 2000;13(4):355–9.

8. Bourdrel T, Annesi-Maesano I, Alahmad B, Maesano CN, Bind M-A. The impact of outdoor air pollution on COVID-19: A review of evidence from *in vitro*, animal, and human studies. Eur Respir Rev. 2021;30(159):1–18.

9. Jones AP. Indoor air quality and health. Atmos Environ. 1999;33(28):4535–64.

10. Whittaker A, BéruBé K, Jones T, Maynard R, Richards R. Killer smog of London, 50 years on: Particle properties and oxidative capacity. Sci Total Environ. 2004;334–335:435–45.

11. Stolwijk JAJ. Risk assessment of acute health and comfort effects of indoor air pollution. Ann N Y Acad Sci. 1992;641(1):56–62.

12. Global Burden of Disease Collaborative Network. Global burden of disease study 2019 (gbd 2019) results [Data file]. Institute for Health Metrics and Evaluation (IHME): Seattle, WA, USA; 2020. [cited 30.08.2021]. Available from: http://ghdx.healthdata.org/gbd-results-tool

13. Gakidou E, Afshin A, Abajobir AA, Abate KH, Abbafati C, Abbas KM, Abd-Allah F, Abdulle AM, Abera SF, Aboyans V, Abu-Raddad LJ, Abu-Rmeileh NME, Abyu GY, Adedeji IA, Adetokunboh O, Afarideh M, Agrawal A, Agrawal S, Ahmadieh H, Ahmed MB, Aichour MTE, Aichour AN, Aichour I, Akinyemi RO, Akseer N, Alahdab F, Al-Aly Z, Alam K, Alam N, Alam T, Alasfoor D, Alene KA, Ali K, Alizadeh-

Navaei R, Alkerwi Aa, Alla F, Allebeck P, Al-Raddadi R, Alsharif U, Altirkawi KA, Alvis-Guzman N, Amare AT, Amini E, Ammar W, Amoako YA, Ansari H, Antó JM, Antonio CAT, Anwari P, Arian N, Ärnlöv J, Artaman A, Aryal KK, Asayesh H, Asgedom SW, Atey TM, Avila-Burgos L, Avokpaho EFGA, Awasthi A, Azzopardi P, Bacha U, Badawi A, Balakrishnan K, Ballew SH, Barac A, Barber RM, Barker-Collo SL, Bärnighausen T, Barquera S, Barregard L, Barrero LH, Batis C, Battle KE, Baumgarner BR, Baune BT, Beardsley J, Bedi N, Beghi E, Bell ML, Bennett DA, Bennett JR, Bensenor IM, Berhane A, Berhe DF, Bernabé E, Betsu BD, Beuran M, Beyene AS, Bhansali A, Bhutta ZA, Bicer BK, Bikbov B, Birungi C, Biryukov S, Blosser CD, Boneya DJ, Bou-Orm IR, Brauer M, Breitborde NJK, Brenner H, Brugha TS, Bulto LNB, Butt ZA, Cahuana-Hurtado L, Cárdenas R, Carrero JJ, Castañeda-Orjuela CA, Catalá-López F, Cercy K, Chang H-Y, Charlson FJ, Chimed-Ochir O, Chisumpa VH, Chitheer AA, Christensen H, Christopher DJ, Cirillo M, Cohen AJ, Comfort H, Cooper C, Coresh J, Cornaby L, Cortesi PA, Criqui MH, Crump JA, Dandona L, Dandona R, das Neves J, Davey G, Davitoiu DV, Davletov K, de Courten B, Defo BK, Degenhardt L, Deiparine S, Dellavalle RP, Deribe K, Deshpande A, Dharmaratne SD, Ding EL, Djalalinia S, Do HP, Dokova K, Doku DT, Donkelaar Av, Dorsey ER, Driscoll TR, Dubey M, Duncan BB, Duncan S, Ebrahimi H, El-Khatib ZZ, Enayati A, Endries AY, Ermakov SP, Erskine HE, Eshrati B, Eskandarieh S, Esteghamati A, Estep K, Faraon EJA, Farinha CSeS, Faro A, Farzadfar F, Fay K, Feigin VL, Fereshtehnejad S-M, Fernandes JC, Ferrari AJ, Feyissa TR, Filip I, Fischer F, Fitzmaurice C, Flaxman AD, Foigt N, Foreman KJ, Frostad JJ, Fullman N, Fürst T, Furtado JM, Ganji M, Garcia-Basteiro AL, Gebrehiwot TT, Geleijnse JM, Geleto A, Gemechu BL, Gesesew HA, Gething PW, Ghajar A, Gibney KB, Gill PS, Gillum RF, Giref AZ, Gishu MD, Giussani G, Godwin WW, Gona PN, Goodridge A, Gopalani SV, Goryakin Y, Goulart AC, Graetz N, Gugnani HC, Guo J, Gupta R, Gupta T, Gupta

V, Gutiérrez RA, Hachinski V, Hafezi-Nejad N, Hailu GB, Hamadeh RR, Hamidi S, Hammami M, Handal AJ, Hankey GJ, Hanson SW, Harb HL, Hareri HA, Hassanvand MS, Havmoeller R, Hawley C, Hay SI, Hedayati MT, Hendrie D, Heredia-Pi IB, Hernandez JCM, Hoek HW, Horita N, Hosgood HD, Hostiuc S, Hoy DG, Hsairi M, Hu G, Huang JJ, Huang H, Ibrahim NM, Iburg KM, Ikeda C, Inoue M, Irvine CMS, Jackson MD, Jacobsen KH, Jahanmehr N, Jakovljevic MB, Jauregui A, Javanbakht M, Jeemon P, Johansson LRK, Johnson CO, Jonas JB, Jürisson M, Kabir Z, Kadel R, Kahsay A, Kamal R, Karch A, Karema CK, Kasaeian A, Kassebaum NJ, Kastor A, Katikireddi SV, Kawakami N, Keiyoro PN, Kelbore SG, Kemmer L, Kengne AP, Kesavachandran CN, Khader YS, Khalil IA, Khan EA, Khang Y-H, Khosravi A, Khubchandani J, Kiadaliri AA, Kieling C, Kim JY, Kim YJ, Kim D, Kimokoti RW, Kinfu Y, Kisa A, Kissimova-Skarbek KA, Kivimaki M, Knibbs LD, Knudsen AK, Kopec JA, Kosen S, Koul PA, Koyanagi A, Kravchenko M, Krohn KJ, Kromhout H, Kumar GA, Kutz M, Kyu HH, Lal DK, Lalloo R, Lallukka T, Lan Q, Lansingh VC, Larsson A, Lee PH, Lee A, Leigh J, Leung J, Levi M, Levy TS, Li Y, Li Y, Liang X, Liben ML, Linn S, Liu P, Lodha R, Logroscino G, Looker KJ, Lopez AD, Lorkowski S, Lotufo PA, Lozano R, Lunevicius R, Macarayan ERK, Magdy Abd El Razek H, Magdy Abd El Razek M, Majdan M, Majdzadeh R, Majeed A, Malekzadeh R, Malhotra R, Malta DC, Mamun AA, Manguerra H, Mantovani LG, Mapoma CC, Martin RV, Martinez-Raga J, Martins-Melo FR, Mathur MR, Matsushita K, Matzopoulos R, Mazidi M, McAlinden C, McGrath JJ, Mehata S, Mehndiratta MM, Meier T, Melaku YA, Memiah P, Memish ZA, Mendoza W, Mengesha MM, Mensah GA, Mensink GBM, Mereta ST, Meretoja TJ, Meretoja A, Mezgebe HB, Micha R, Millear A, Miller TR, Minnig S, Mirarefin M, Mirrakhimov EM, Misganaw A, Mishra SR, Mohammad KA, Mohammed KE, Mohammed S, Mohan MBV, Mokdad AH, Monasta L, Montico M, Moradi-Lakeh M, Moraga P, Morawska L, Morrison SD, Mountjoy-Venning C, Mueller UO, Mullany

EC, Muller K, Murthy GVS, Musa KI, Naghavi M, Naheed A, Nangia V, Natarajan G, Negoi RI, Negoi I, Nguyen CT, Nguyen QL, Nguyen TH, Nguyen G, Nguyen M, Nichols E, Ningrum DNA, Nomura M, Nong VM, Norheim OF, Norrving B, Noubiap JJN, Obermeyer CM, Ogbo FA, Oh I-H, Oladimeji O, Olagunju AT, Olagunju TO, Olivares PR, Olsen HE, Olusanya BO, Olusanya JO, Opio JN, Oren E, Ortiz A, Ota E, Owolabi MO, Pa M, Pacella RE, Pana A, Panda BK, Panda-Jonas S, Pandian JD, Papachristou C, Park E-K, Parry CD, Patten SB, Patton GC, Pereira DM, Perico N, Pesudovs K, Petzold M, Phillips MR, Pillay JD, Piradov MA, Pishgar F, Plass D, Pletcher MA, Polinder S, Popova S, Poulton RG, Pourmalek F, Prasad N, Purcell C, Qorbani M, Radfar A, Rafay A, Rahimi-Movaghar A, Rahimi-Movaghar V, Rahman MHU, Rahman MA, Rahman M, Rai RK, Rajsic S, Ram U, Rawaf S, Rehm CD, Rehm J, Reiner RC, Reitsma MB, Remuzzi G, Renzaho AMN, Resnikoff S, Reynales-Shigematsu LM, Rezaei S, Ribeiro AL, Rivera JA, Roba KT, Rojas-Rueda D, Roman Y, Room R, Roshandel G, Roth GA, Rothenbacher D, Rubagotti E, Rushton L, Sadat N, Safdarian M, Safi S, Safiri S, Sahathevan R, Salama J, Salomon JA, Samy AM, Sanabria JR, Sanchez-Niño MD, Sánchez-Pimienta TG, Santomauro D, Santos IS, Santric Milicevic MM, Sartorius B, Satpathy M, Sawhney M, Saxena S, Schmidt MI, Schneider IJC, Schutte AE, Schwebel DC, Schwendicke F, Seedat S, Sepanlou SG, Serdar B, Servan-Mori EE, Shaddick G, Shaheen A, Shahraz S, Shaikh MA, Shamsipour M, Shamsizadeh M, Shariful Islam SM, Sharma J, Sharma R, She J, Shen J, Shi P, Shibuya K, Shields C, Shiferaw MS, Shigematsu M, Shin M-J, Shiri R, Shirkoohi R, Shishani K, Shoman H, Shrime MG, Sigfusdottir ID, Silva DAS, Silva JP, Silveira DGA, Singh JA, Singh V, Sinha DN, Skiadaresi E, Slepak EL, Smith DL, Smith M, Sobaih BHA, Sobngwi E, Soneji S, Sorensen RJD, Sposato LA, Sreeramareddy CT, Srinivasan V, Steel N, Stein DJ, Steiner C, Steinke S, Stokes MA, Strub B, Subart M, Sufiyan MB, Suliankatchi RA, Sur PJ, Swaminathan S, Sykes BL,

Szoeke CEI, Tabarés-Seisdedos R, Tadakamadla SK, Takahashi K, Takala JS, Tandon N, Tanner M, Tarekegn YL, Tavakkoli M, Tegegne TK, Tehrani-Banihashemi A, Terkawi AS, Tesssema B, Thakur JS, Thamsuwan O, Thankappan KR, Theis AM, Thomas ML, Thomson AJ, Thrift AG, Tillmann T, Tobe-Gai R, Tobollik M, Tollanes MC, Tonelli M, Topor-Madry R, Torre A, Tortajada M, Touvier M, Tran BX, Truelsen T, Tuem KB, Tuzcu EM, Tyrovolas S, Ukwaja KN, Uneke CJ, Updike R, Uthman OA, van Boven JFM, Varughese S, Vasankari T, Veerman LJ, Venkateswaran V, Venketasubramanian N, Violante FS, Vladimirov SK, Vlassov VV, Vollset SE, Vos T, Wadilo F, Wakayo T, Wallin MT, Wang Y-P, Weichenthal S, Weiderpass E, Weintraub RG, Weiss DJ, Werdecker A, Westerman R, Whiteford HA, Wiysonge CS, Woldeyes BG, Wolfe CDA, Woodbrook R, Workicho A, Xavier D, Xu G, Yadgir S, Yakob B, Yan LL, Yaseri M, Yimam HH, Yip P, Yonemoto N, Yoon S-J, Yotebieng M, Younis MZ, Zaidi Z, Zaki MES, Zavala-Arciniega L, Zhang X, Zimsen SRM, Zipkin B, Zodpey S, Lim SS, Murray CJL. Global, regional, and national comparative risk assessment of 84 behavioural, environmental and occupational, and metabolic risks or clusters of risks, 1990–2013; 2016: A systematic analysis for the global burden of disease study 2016. Supplementary appendix 1. Lancet. 2017;390(10100):s1–435.

14. World Health Organization. Ambient air pollution attributable dalys [Data file]. The Global Health Observatory: Geneva, Switzerland; 2018. [cited 30.08.2021]. Available from: https://www.who.int/data/gho/data/indicators/indicator-details/GHO/mbd-aap-ambient-air-pollution-attributable-dalys

15. World Health Organization. Ambient air pollution attributable dalys (per 100 000 population) [Data file]. The Global Health Observatory: Geneva, Switzerland; 2018. [cited 02.02.2022]. Available from: https://www.who.int/data/gho/data/indicators/indicator-

details/GHO/ambient-air-pollution-attributable-dalys-(per-100-000-population)

16. World Health Organization. Household air pollution attributable dalys [Data file]. The Global Health Observatory: Geneva, Switzerland; 2018. [cited 30.08.2021]. Available from: https://www.who.int/data/gho/data/indicators/indicator-details/GHO/household-air-pollution-attributable-dalys

17. World Health Organization. Household air pollution attributable dalys (per 100 000 population) [Data file]. The Global Health Observatory: Geneva, Switzerland; 2018. [cited 02.02.2022]. Available from: https://www.who.int/data/gho/data/indicators/indicator-details/GHO/household-air-pollution-attributable-dalys-(per-100-000-population)-

18. Castán Broto V, Kirshner J. Energy access is needed to maintain health during pandemics. Nat Energy. 2020;5(6):419–21.

19. Farmer DK, Vance ME, Abbatt JPD, Abeleira A, Alves MR, Arata C, Boedicker E, Bourne S, Cardoso-Saldaña F, Corsi R, DeCarlo PF, Goldstein AH, Grassian VH, Hildebrandt Ruiz L, Jimenez JL, Kahan TF, Katz EF, Mattila JM, Nazaroff WW, Novoselac A, O'Brien RE, Or VW, Patel S, Sankhyan S, Stevens PS, Tian Y, Wade M, Wang C, Zhou S, Zhou Y. Overview of HOMEchem: House observations of microbial and environmental chemistry. Environ Sci Process Impacts. 2019;21(8):1280–300.

20. Ampollini L, Katz EF, Bourne S, Tian Y, Novoselac A, Goldstein AH, Lucic G, Waring MS, DeCarlo PF. Observations and contributions of real-time indoor ammonia concentrations during homechem. Environ Sci Technol. 2019;53(15):8591–8.

21. Brown WL, Day DA, Stark H, Pagonis D, Krechmer JE, Liu X, Price DJ, Katz EF, DeCarlo PF, Masoud CG, Wang DS, Hildebrandt Ruiz L, Arata C, Lunderberg DM, Goldstein AH, Farmer DK, Vance ME, Jimenez JL. Real-time organic aerosol chemical speciation in the indoor environment using extractive electrospray ionization mass spectrometry. Indoor Air. 2021;31(1):141–55.

22. Mattila JM, Lakey PSJ, Shiraiwa M, Wang C, Abbatt JPD, Arata C, Goldstein AH, Ampollini L, Katz EF, DeCarlo PF, Zhou S, Kahan TF, Cardoso-Saldaña FJ, Ruiz LH, Abeleira A, Boedicker EK, Vance ME, Farmer DK. Multiphase chemistry controls inorganic chlorinated and nitrogenated compounds in indoor air during bleach cleaning. Environ Sci Technol. 2020;54(3):1730–9.

23. Wang C, Collins DB, Arata C, Goldstein AH, Mattila JM, Farmer DK, Ampollini L, DeCarlo PF, Novoselac A, Vance ME, Nazaroff WW, Abbatt JPD. Surface reservoirs dominate dynamic gas-surface partitioning of many indoor air constituents. Sci Adv. 2020;6(8):1–11.

24. Seppänen OA, Fisk WJ. Summary of human responses to ventilation. Indoor Air. 2004;14 Suppl 7:102–18.

25. Redlich CA, Sparer J, Cullen MR. Sick-building syndrome. Lancet. 1997;349(9057):1013–6.

26. Lende RD. Health aspects related to indoor air pollution. Int J Epidemiol. 1980;9(3):195–7.

27. Carslaw N. A new detailed chemical model for indoor air pollution. Atmos Environ. 2007;41(6):1164–79.

28. Seddon C. Lifestyles and social participation [Internet]. Newport, UK: Office for National Statistics; 2011. [cited 25.08.2021]. Available from: https://link.springer.com/content/pdf/10.1057/st.2011.7.pdf.

29. Flint E, Webb E, Cummins S. Change in commute mode and body-mass index: Prospective, longitudinal evidence from UK Biobank. Lancet Public Health. 2016;1(2):e46–e55.

30. Johansson C, Lövenheim B, Schantz P, Wahlgren L, Almström P, Markstedt A, Strömgren M, Forsberg B, Sommar JN. Impacts on air pollution and health by changing commuting from car to bicycle. Sci Total Environ. 2017;584–585:55–63.

31. McNabola A, Broderick BM, Gill LW. Relative exposure to fine particulate matter and vocs between transport microenvironments in Dublin: Personal exposure and uptake. Atmos Environ. 2008;42(26):6496–512.

32. Andrade A, Dominski FH. Indoor air quality of environments used for physical exercise and sports practice: Systematic review. J Environ Manage. 2018;206(Supplement C):577–86.

33. Ramos CA, Wolterbeek HT, Almeida SM. Exposure to indoor air pollutants during physical activity in fitness centers. Build Environ. 2014;82(Supplement C):349–60.

34. Andersson K, Stridh G. NATO/CCMS pilot study on indoor air quality [Internet]. Oslo, Norway: Air Infiltration and Ventilation Centre; 1991. [cited 15.06.2018]. Available from: http://www.inomhusklimatproblem.se/publikations/publikationer/Referens51ny.pdf.

35. Brightman HS, Milton DK, Wypij D, Burge HA, Spengler JD. Evaluating building-related symptoms using the US EPA base study results. Indoor Air. 2008;18(4):335–45.

36. Herrington JS. Rapid determination of TO-15 volatile organic compounds (VOCs) in air [Internet]. Bellefonte, PA: Restek; 2016. [cited 08.05.2018]. Available from: http://www.restek.com/pdfs/EVAN1725B-UNV.pdf.

37. Chang Y-M, Hu W-H, Fang W-B, Chen S-S, Chang C-T, Ching H-W. A study on dynamic volatile organic compound emission characterization of water-based paints. J Air Waste Manage Assoc. 2011;61(1):35–45.

38. Journal of the American College of Toxicology. Final report of the safety assessment of isobutane, isopentane, n-butane, and propane. J Am Coll Toxicol. 1982;1(1):127–42.

39. Salthammer T. Very volatile organic compounds: An understudied class of indoor air pollutants. Indoor Air. 2016;26(1):25–38.

40. Byrne FP, Jin S, Paggiola G, Petchey THM, Clark JH, Farmer TJ, Hunt AJ, Robert McElroy C, Sherwood J. Tools and techniques for solvent selection: Green solvent selection guides. Sustainable Chemical Processes. 2016;4(1):1–24.

41. Vincent G, Marquaire PM, Zahraa O. Abatement of volatile organic compounds using an annular photocatalytic reactor: Study of gaseous acetone. J Photochem Photobiol A: Chem. 2008;197(2):177–89.

42. Galassetti PR, Novak B, Nemet D, Rose-Gottron C, Cooper DM, Meinardi S, Newcomb R, Zaldivar F, Blake DR. Breath ethanol and

acetone as indicators of serum glucose levels: An initial report. Diabetes Technol Ther. 2005;7(1):115–23.

43. Słomińska M, Konieczka P, Namieśnik J. The fate of BTEX compounds in ambient air. Crit Rev Environ Sci Technol. 2014;44(5):455–72.

44. Gorgus E, Hittinger M, Schrenk D. Estimates of ethanol exposure in children from food not labeled as alcohol-containing. J Anal Toxicol. 2016;40(7):537–42.

45. Nazaroff WW, Weschler CJ. Cleaning products and air fresheners: Exposure to primary and secondary air pollutants. Atmos Environ. 2004;38(18):2841–65.

46. Yucuis RA, Stanier CO, Hornbuckle KC. Cyclic siloxanes in air, including identification of high levels in Chicago and distinct diurnal variation. Chemosphere. 2013;92(8):905–10.

47. United States Environmental Protection Agency. CompTox chemicals dashboard [Internet]. 2022 [cited 20.10.2022]. Available from: https://comptox.epa.gov/dashboard/.

48. Williams AJ, Grulke CM, Edwards J, McEachran AD, Mansouri K, Baker NC, Patlewicz G, Shah I, Wambaugh JF, Judson RS, Richard AM. The comptox chemistry dashboard: A community data resource for environmental chemistry. J Cheminform. 2017;9(1):1–27.

49. United States Department of Commerce National Institute of Standards and Technology. NIST chemistry webbook [Internet]. 2022 [cited 20.10.2022]. Available from: https://webbook.nist.gov/chemistry/.

50. Valorso R, Aumont B, Camredon M, Raventos-Duran T, Mouchel-Vallon C, Ng NL, Seinfeld JH, Lee-Taylor J, Madronich S. Explicit modelling of soa formation from α-pinene photooxidation: Sensitivity to vapour pressure estimation. Atmos Chem Phys. 2011;11(14):6895–910.

51. Camredon M, Aumont B, Lee-Taylor J, Madronich S. The SOA/VOC/NO_x system: An explicit model of secondary organic aerosol formation. Atmos Chem Phys. 2007;7(21):5599–610.

52. Spengler JD, Sexton K. Indoor air pollution: A public health perspective. Science. 1983;221(4605):9–17.

53. Kim YM, Harrad S, Harrison RM. Concentrations and sources of VOCs in urban domestic and public microenvironments. Environ Sci Technol. 2001;35(6):997–1004.

54. Su F-C, Mukherjee B, Batterman S. Determinants of personal, indoor and outdoor voc concentrations: An analysis of the RIOPA data. Environ Res. 2013;126:192–203.

55. Edwards RD, Jurvelin J, Saarela K, Jantunen M. VOC concentrations measured in personal samples and residential indoor, outdoor and workplace microenvironments in EXPOLIS-Helsinki, finland. Atmos Environ. 2001;35(27):4531–43.

56. Hänninen OO, Alm S, Katsouyanni K, Künzli N, Maroni M, Nieuwenhuijsen MJ, Saarela K, Srám RJ, Zmirou D, Jantunen MJ. The EXPOLIS study: Implications for exposure research and environmental policy in Europe. J Expo Sci Environ Epidemiol. 2004;14(6):440–56.

57. Gordon SM, Callahan PJ, Nishioka MG, Brinkman MC, O'Rourke MK, Lebowitz MD, Moschandreas DJ. Residential environmental measurements in the national human exposure assessment survey (NHEXAS) pilot study in Arizona: Preliminary results for pesticides and VOCs. J Expo Anal Environ Epidemiol. 1999;9(5):456–70.

58. Biesterbos JW, Dudzina T, Delmaar CJ, Bakker MI, Russel FG, von Goetz N, Scheepers PT, Roeleveld N. Usage patterns of personal care products: Important factors for exposure assessment. Food Chem Toxicol. 2013;55:8–17.

59. Wu X, Bennett DH, Ritz B, Cassady DL, Lee K, Hertz-Picciotto I. Usage pattern of personal care products in California households. Food Chem Toxicol. 2010;48(11):3109–19.

60. Hart LB, Walker J, Beckingham B, Shelley A, Alten Flagg M, Wischusen K, Sundstrom B. A characterization of personal care product use among undergraduate female college students in South Carolina, USA. J Expo Sci Environ Epidemiol. 2020;30(1):97–106.

61. Zenié A, Reina V. Expofacts database [Data file]. European Commission, Joint Research Centre Data Catalogue (JRC): Ispra, Italy; 2007. [cited 06.09.2021]. Available from: http://data.europa.eu/89h/jrc-10114–10001

62. National Centre for Environmental Assessment. Exposure factors handbook: 2011 edition [Internet]. Washington D.C., USA: Office of Research and Development; 2011. [cited 06.09.2021]. Available from: https://ofmpub.epa.gov/eims/eimscomm.getfile?p_download_id=522996.

63. Ehhalt DH. Free radicals in the atmosphere. Free Radic Res Commun. 1987;3(1–5):153–64.

64. Monks PS. Gas-phase radical chemistry in the troposphere. Chem Soc Rev. 2005;34(5):376–95.

65. Atkinson R, Arey J. Atmospheric degradation of volatile organic compounds. Chem Rev. 2003;103(12):4605–38.

66. Li M, Karu E, Brenninkmeijer C, Fischer H, Lelieveld J, Williams J. Tropospheric OH and stratospheric OH and Cl concentrations determined from CH_4, CH_3Cl, and SF_6 measurements. NPJ Clim Atmos Sci. 2018;1(1):1–7.

67. Weschler CJ, Shields HC. Production of the hydroxyl radical in indoor air. Environ Sci Technol. 1996;30(11):3250–8.

68. Lelieveld J, Gromov S, Pozzer A, Taraborrelli D. Global tropospheric hydroxyl distribution, budget and reactivity. Atmos Chem Phys. 2016;16(19):12477–93.

69. Butkovskaya NI, Kukui A, Pouvesle N, Le Bras G. Formation of nitric acid in the gas-phase HO_2 + NO reaction: Effects of temperature and water vapor. J Phys Chem A. 2005;109(29):6509–20.

70. Johnston HS, Chang S-G, Whitten G. Photolysis of nitric acid vapor. J Phys Chem. 1974;78(1):1–7.

71. Poskrebyshev GA, Neta P, Huie RE. Equilibrium constant of the reaction ·OH + HNO_3 ⇆ H_2O + NO_3. In aqueous solution. J Geophys Res Atmos. 2001;106(D5):4995–5004.

72. Carpenter LJ, Fleming ZL, Read KA, Lee JD, Moller SJ, Hopkins JR, Purvis RM, Lewis AC, Müller K, Heinold B, Herrmann H, Fomba KW, van Pinxteren D, Müller C, Tegen I, Wiedensohler A, Müller T, Niedermeier N, Achterberg EP, Patey MD, Kozlova EA, Heimann M,

Heard DE, Plane JMC, Mahajan A, Oetjen H, Ingham T, Stone D, Whalley LK, Evans MJ, Pilling MJ, Leigh RJ, Monks PS, Karunaharan A, Vaughan S, Arnold SR, Tschritter J, Pöhler D, Frieß U, Holla R, Mendes LM, Lopez H, Faria B, Manning AJ, Wallace DWR. Seasonal characteristics of tropical marine boundary layer air measured at the Cape Verde atmospheric observatory. J Atmos Chem. 2010;67(2):87–140.

73. Zhang J, Wei Y, Fang Z. Ozone pollution: A major health hazard worldwide. Front Immunol. 2019;10:1–10.

74. Emberson L. Effects of ozone on agriculture, forests and grasslands. Philos Trans A Math Phys Eng Sci. 2020;378(2183):1–27.

75. Finlayson-Pitts BJ, Pitts JN. Atmospheric chemistry of tropospheric ozone formation: Scientific and regulatory implications. J Air Waste Manag Assoc. 1993;43(8):1091–100.

76. Tarasick DW, Carey-Smith TK, Hocking WK, Moeini O, He H, Liu J, Osman MK, Thompson AM, Johnson BJ, Oltmans SJ, Merrill JT. Quantifying stratosphere-troposphere transport of ozone using balloon-borne ozonesondes, radar windprofilers and trajectory models. Atmos Environ. 2019;198:496–509.

77. Stevenson DS, Dentener FJ, Schultz MG, Ellingsen K, van Noije TPC, Wild O, Zeng G, Amann M, Atherton CS, Bell N, Bergmann DJ, Bey I, Butler T, Cofala J, Collins WJ, Derwent RG, Doherty RM, Drevet J, Eskes HJ, Fiore AM, Gauss M, Hauglustaine DA, Horowitz LW, Isaksen ISA, Krol MC, Lamarque J-F, Lawrence MG, Montanaro V, Müller J-F, Pitari G, Prather MJ, Pyle JA, Rast S, Rodriguez JM, Sanderson MG, Savage NH, Shindell DT, Strahan SE, Sudo K, Szopa S. Multimodel ensemble simulations of present-day and near-future tropospheric ozone. J Geophys Res Atmos. 2006;111(D8):1–23.

78. Ashmore MR, Bell JNB. The role of ozone in global change. Ann Bot. 1991;67:39–48.

79. Ng NL, Brown SS, Archibald AT, Atlas E, Cohen RC, Crowley JN, Day DA, Donahue NM, Fry JL, Fuchs H, Griffin RJ, Guzman MI, Herrmann H, Hodzic A, Iinuma Y, Jimenez JL, Kiendler-Scharr A, Lee BH, Luecken DJ, Mao J, McLaren R, Mutzel A, Osthoff HD, Ouyang B, Picquet-Varrault B, Platt U, Pye HOT, Rudich Y, Schwantes RH, Shiraiwa M, Stutz J, Thornton JA, Tilgner A, Williams BJ, Zaveri RA. Nitrate radicals and biogenic volatile organic compounds: Oxidation, mechanisms, and organic aerosol. Atmos Chem Phys. 2017;17(3):2103–62.

80. Wayne RP, Barnes I, Biggs P, Burrows JP, Canosa-Mas CE, Hjorth J, Le Bras G, Moortgat GK, Perner D, Poulet G, Restelli G, Sidebottom H. The nitrate radical: Physics, chemistry, and the atmosphere. Atmos Environ. 1991;25(1):1–203.

81. Brown SS, Stark H, Ravishankara AR. Applicability of the steady state approximation to the interpretation of atmospheric observations of NO_3 and N_2O_5. J Geophys Res Atmos. 2003;108(D17):1–10.

82. Khan MAH, Cooke MC, Utembe SR, Archibald AT, Derwent RG, Xiao P, Percival CJ, Jenkin ME, Morris WC, Shallcross DE. Global modeling of the nitrate radical (NO_3) for present and pre-industrial scenarios. Atmos Res. 2015;164–165:347–57.

83. Molina MJ, Rowland FS. Stratospheric sink for chlorofluoromethanes: Chlorine atom-catalysed destruction of ozone. Nature. 1974;249(5460):810–2.

84. Baker AK, Sauvage C, Thorenz UR, van Velthoven P, Oram DE, Zahn A, Brenninkmeijer CAM, Williams J. Evidence for strong, widespread

chlorine radical chemistry associated with pollution outflow from continental Asia. Sci Rep. 2016;6(1):1–9.

85. Hossaini R, Chipperfield MP, Saiz-Lopez A, Fernandez R, Monks S, Feng W, Brauer P, von Glasow R. A global model of tropospheric chlorine chemistry: Organic versus inorganic sources and impact on methane oxidation. J Geophys Res Atmos. 2016;121(23):14,271–14,97.

86. Wang X, Jacob DJ, Eastham SD, Sulprizio MP, Zhu L, Chen Q, Alexander B, Sherwen T, Evans MJ, Lee BH, Haskins JD, Lopez-Hilfiker FD, Thornton JA, Huey GL, Liao H. The role of chlorine in global tropospheric chemistry. Atmos Chem Phys. 2019;19(6):3981–4003.

87. Fantechi G, Jensen NR, Saastad O, Hjorth J, Peeters J. Reactions of Cl atoms with selected VOCs: Kinetics, products and mechanisms. J Atmos Chem. 1998;31(3):247–67.

88. Sarwar G, Bhave PV. Modeling the effect of chlorine emissions on ozone levels over the eastern united states. J Appl Meteorol Climatol. 2007;46(7):1009–19.

89. Finewax Z, Pagonis D, Claflin MS, Handschy AV, Brown WL, Jenks O, Nault BA, Day DA, Lerner BM, Jimenez JL, Ziemann PJ, de Gouw JA. Quantification and source characterization of volatile organic compounds from exercising and application of chlorine-based cleaning products in a university athletic center. Indoor Air. 2021;31(5):1323–39.

90. Ylisirniö A, Buchholz A, Mohr C, Li Z, Barreira L, Lambe A, Faiola C, Kari E, Yli-Juuti T, Nizkorodov SA, Worsnop DR, Virtanen A, Schobesberger S. Composition and volatility of secondary organic

aerosol (SOA) formed from oxidation of real tree emissions compared to simplified volatile organic compound (VOC) systems. Atmos Chem Phys. 2020;20(9):5629–44.

91. Srivastava D, Vu TV, Tong S, Shi Z, Harrison RM. Formation of secondary organic aerosols from anthropogenic precursors in laboratory studies. NPJ Clim Atmos Sci. 2022;5(1):1–30.

92. Vivanco MG, Santiago M, Martínez-Tarifa A, Borrás E, Ródenas M, García-Diego C, Sánchez M. SOA formation in a photoreactor from a mixture of organic gases and HONO for different experimental conditions. Atmos Environ. 2011;45(3):708–15.

93. Svensmark H, Enghoff MB, Shaviv NJ, Svensmark J. Increased ionization supports growth of aerosols into cloud condensation nuclei. Nat Commun. 2017;8(1):1–9.

94. Bouzidi H, Fayad L, Coeur C, Houzel N, Petitprez D, Faccinetto A, Wu J, Tomas A, Ondráček J, Schwarz J, Ždímal V, Zuend A. Hygroscopic growth and CCN activity of secondary organic aerosol produced from dark ozonolysis of γ-terpinene. Sci Total Environ. 2022;817:1–16.

95. Liu C, Wang T, Rosenfeld D, Zhu Y, Yue Z, Yu X, Xie X, Li S, Zhuang B, Cheng T, Niu S. Anthropogenic effects on cloud condensation nuclei distribution and rain initiation in east asia. Geophys Res Lett. 2020;47(2):1–10.

96. Tao J, Kuang Y, Ma N, Hong J, Sun Y, Xu W, Zhang Y, He Y, Luo Q, Xie L, Su H, Cheng Y. Secondary aerosol formation alters CCN activity in the North China Plain. Atmos Chem Phys. 2021;21(9):7409–27.

97. Macey GP, Breech R, Chernaik M, Cox C, Larson D, Thomas D, Carpenter DO. Air concentrations of volatile compounds near oil and gas production: A community-based exploratory study. Environ Health. 2014;13(1):1–18.

98. Sexton K, Adgate JL, Ramachandran G, Pratt GC, Mongin SJ, Stock TH, Morandi MT. Comparison of personal, indoor, and outdoor exposures to hazardous air pollutants in three urban communities. Environ Sci Technol. 2004;38(2):423–30.

99. Serrano-Trespalacios PI, Ryan L, Spengler JD. Ambient, indoor and personal exposure relationships of volatile organic compounds in Mexico City metropolitan area. J Expo Anal Environ Epidemiol. 2004;14:S118–S32.

100. Miller L, Xu X, Luginaah I. Spatial variability of volatile organic compound concentrations in Sarnia, Ontario, Canada. J Toxicol Environ Health A. 2009;72(9):610–24.

101. Thom GC, Ott WR. A proposed uniform air pollution index. Atmos Environ. 1976;10(3):261–4.

102. Zhang Y, Bocquet M, Mallet V, Seigneur C, Baklanov A. Real-time air quality forecasting, Part I: History, techniques, and current status. Atmos Environ. 2012;60:632–55.

103. Statistics Canada. Census tract (ct) [Internet]. Ottawa, ON, Canada: Statistics Canada; 2015 [cited 10.01.2018]. Available from: http://www12.statcan.gc.ca/census-recensement/2011/ref/dict/geo013-eng.cfm.

104. Zhou Y, Levy JI. Factors influencing the spatial extent of mobile source air pollution impacts: A meta-analysis. BMC Public Health. 2007;7:1–11.

105. Gorai AK, Tuluri F, Tchounwou PB. A GIS based approach for assessing the association between air pollution and asthma in New York State, USA. Int J Environ Res Public Health. 2014;11(5):4845–69.

106. Theophanides M, Anastassopoulou J. Air pollution simulation and geographical information systems (GIS) applied to Athens International Airport. J Environ Sci Health A Tox Hazard Subst Environ Eng. 2009;44(8):758–66.

107. Tonne C, Melly S, Mittleman M, Coull B, Goldberg R, Schwartz J. A case–control analysis of exposure to traffic and acute myocardial infarction. Environ Health Perspect. 2007;115(1):53–7.

108. Hoek G, Beelen R, de Hoogh K, Vienneau D, Gulliver J, Fischer P, Briggs D. A review of land-use regression models to assess spatial variation of outdoor air pollution. Atmos Environ. 2008;42(33):7561–78.

109. Delgado-Saborit JM, Aquilina NJ, Meddings C, Baker S, Vardoulakis S, Harrison RM. Measurement of personal exposure to volatile organic compounds and particle associated PAH in three uk regions. Environ Sci Technol. 2009;43(12):4582–8.

110. Rosofsky A, Levy JI, Zanobetti A, Janulewicz P, Fabian MP. Temporal trends in air pollution exposure inequality in Massachusetts. Environ Res. 2018;161(Supplement C):76–86.

111. Barrington-Leigh C, Baumgartner J, Carter E, Robinson BE, Tao S, Zhang Y. An evaluation of air quality, home heating and well-being under Beijing's programme to eliminate household coal use. Nat Energy. 2019;4(5):416–23.

112. Harrison PTC. Indoor air quality guidelines. Occup Environ Med. 2002;59(2):73–4.

113. Heims EM. Regulatory co-ordination in the EU: A cross-sector comparison. J Eur Public Policy. 2017;24(8):1116–34.

114. Hallsworth M, Parker S, Rutter J. Policy making in the real world: Evidence and analysis [Internet]. London, UK: Institute for Government; 2011. [cited 15.01.2018]. Available from: https://www.instituteforgovernment.org.uk/sites/default/files/publications/Policy%20making%20in%20the%20real%20world.pdf.

115. Daisey JM, Angell WJ, Apte MG. Indoor air quality, ventilation and health symptoms in schools: An analysis of existing information. Indoor Air. 2003;13(1):53–64.

116. Parliamentary Office of Science and Technology. UK indoor air quality - POSTNOTE 366, November 2010 [Internet]. London, UK: Parliamentary Office of Science and Technology; 2010. [cited 16.09.2021]. Available from: https://researchbriefings.files.parliament.uk/documents/POST-PN-366/POST-PN-366.pdf.

117. United States Environmental Protection Agency. Guide to air cleaners in the home [Internet]. Cincinnati, OH, USA: United States Environmental Protection Agency; 2008. [cited 11.01.2018]. Available from: https://www.nmhealth.org/publication/view/guide/240/.

118. Licina D, Langer S. Indoor air quality investigation before and after relocation to WELL-certified office buildings. Build Environ. 2021;204:1–11.

119. Altomonte S, Saaduoni S, Schiavon S, editors. Occupant satisfaction in LEED and BREEAM-certified office buildings. Proceedings of PLEA 2016 - 36th International Conference on Passive and Low Energy Architecture: Cities, Buildings, People: Towards Regenerative Environments; 2016 10–13 July 2016; Los Angeles, CA, USA. Berkeley, CA, USA: UC Berkeley: Centre for the Built Environment; 2016.

120. Suzer O. Analyzing the compliance and correlation of LEED and BREEAM by conducting a criteria-based comparative analysis and evaluating dual-certified projects. Build Environ. 2019;147:158–70.

121. Kornartit C, Sokhi RS, Burton MA, Ravindra K. Activity pattern and personal exposure to nitrogen dioxide in indoor and outdoor microenvironments. Environ Int. 2010;36(1):36–45.

122. Puzzolo E, Pope D. Clean fuels for cooking in developing countries In: Abraham M.A., editor. Encyclopedia of sustainable technologies. Oxford, UK: Elsevier; 2017. p. 289–97.

123. Watts N, Amann M, Ayeb-Karlsson S, Belesova K, Bouley T, Boykoff M, Byass P, Cai W, Campbell-Lendrum D, Chambers J, Cox PM, Daly M, Dasandi N, Davies M, Depledge M, Depoux A, Dominguez-Salas P, Drummond P, Ekins P, Flahault A, Frumkin H, Georgeson L, Ghanei M, Grace D, Graham H, Grojsman R, Haines A, Hamilton I, Hartinger S, Johnson A, Kelman I, Kiesewetter G, Kniveton D, Liang L, Lott M, Lowe R, Mace G, Odhiambo Sewe M, Maslin M, Mikhaylov S, Milner J, Latifi AM, Moradi-Lakeh M, Morrissey K, Murray K, Neville T, Nilsson M, Oreszczyn T, Owfi F, Pencheon D, Pye S, Rabbaniha

M, Robinson E, Rocklöv J, Schütte S, Shumake-Guillemot J, Steinbach R, Tabatabaei M, Wheeler N, Wilkinson P, Gong P, Montgomery H, Costello A. The Lancet countdown on health and climate change: From 25 years of inaction to a global transformation for public health. Lancet. 2017;1(1):1–50.

124. Borthwick Story J, Schliessner U. An assessment and comparison of new tsca and reach [Internet]. Cleveland, OH, USA: Jones Day; 2017. [cited 18.08.2021]. Available from: https://www.jonesday.com/files/upload/Assessment%20Comparison%20New%20TSCA%20REACH.pdf.

125. Collins DB, Farmer DK. Unintended consequences of air cleaning chemistry. Environ Sci Technol. 2021;55(18):12172–9.

126. Zhong L, Haghighat F. Photocatalytic air cleaners and materials technologies – abilities and limitations. Build Environ. 2015;91:191–203.

127. Auerbach IL, Flieger K. The importance of public education in air pollution control. J Air Pollut Control Assoc. 1967;17(2):102–4.

128. Revell K. Promoting sustainability and pro-environmental behaviour through local government programmes: Examples from London, UK. J Integr Environ Sci. 2013;10(3–4):199–218.

129. World Health Organization. WHO guidelines for indoor air quality: Selected pollutants [Internet]. Copenhagen, Denmark: World Health Organization Regional Office for Europe; 2010. [cited 15.01.2018]. Available from: http://www.euro.who.int/__data/assets/pdf_file/0009/128169/e94535.pdf?ua=1.

130. Husman TM. The Health Protection Act, national guidelines for indoor air quality and development of the national indoor air programs in Finland. Environ Health Perspect. 1999;107 Suppl 3:515–7.

131. Shimer D, Phillips T, Jenkinks P. Report to the California legislature: Indoor air pollution in California [Internet]. Sacramento, CA, USA: California Environmental Protection Agency; 2005. [cited 17.09.2021]. Available from: https://ww2.arb.ca.gov/sites/default/files/classic/research/apr/reports/l3041.pdf.

132. Office for Environmental Health Hazard Assessment. Proposition 65 in plain language [Internet]. Sacramento, CA, USA: California Environmental Protection Agency; 2013 [cited. Available from: https://oehha.ca.gov/proposition-65/general-info/proposition-65-plain-language.

133. Department for Environment Food and Rural Affairs. The Volatile Organic Compounds in Paints, Varnishes and Vehicle Refinishing Products Regulations 2012. 1715. [Internet]. London, UK: Her Majesty's Government UK [cited 08.09.2021]. Available from: https://www.legislation.gov.uk/uksi/2012/1715

134. British Coatings Federation. BCF VOC Globe Scheme [Internet]. Coventry, UK: British Coatings Federation; 2019. [cited 08.09.2021]. Available from: https://www.coatings.org.uk/Media/Download.aspx?MediaId=15569.

135. Mandin C. The indoor air quality observatory (OQAI): A unique project to understand air pollution in our living spaces. Field Actions Sci Rep. 2020;1(21):18–23.

136. Halkos G, Gkampoura E-C. Where do we stand on the 17 Sustainable Development Goals? An overview on progress. Econ Anal Pol. 2021;70:94–122.

137. Rafaj P, Kiesewetter G, Gül T, Schöpp W, Cofala J, Klimont Z, Purohit P, Heyes C, Amann M, Borken-Kleefeld J, Cozzi L. Outlook for clean air in the context of Sustainable Development Goals. Global Environ Change. 2018;53:1–11.

138. Janoušková S, Hák T, Moldan B. Global SDGs assessments: Helping or confusing indicators? Sustainability. 2018;10(5):1–14.

139. McDonald BC, de Gouw JA, Gilman JB, Jathar SH, Akherati A, Cappa CD, Jimenez JL, Lee-Taylor J, Hayes PL, McKeen SA, Cui YY, Kim S-W, Gentner DR, Isaacman-VanWertz G, Goldstein AH, Harley RA, Frost GJ, Roberts JM, Ryerson TB, Trainer M. Volatile chemical products emerging as largest petrochemical source of urban organic emissions. Science. 2018;359(6377):760–4.

140. Horton DE, Harshvardhan, Diffenbaugh NS. Response of air stagnation frequency to anthropogenically enhanced radiative forcing. Environ Res Lett. 2012;7(4):1–15.

141. Hong C, Zhang Q, Zhang Y, Davis SJ, Tong D, Zheng Y, Liu Z, Guan D, He K, Schellnhuber HJ. Impacts of climate change on future air quality and human health in China. Proc Natl Acad Sci U S A. 2019;116(35):17193–200.

142. Schwarz L, Hansen K, Alari A, Ilango SD, Bernal N, Basu R, Gershunov A, Benmarhnia T. Spatial variation in the joint effect of extreme heat events and ozone on respiratory hospitalizations in California. Proc Natl Acad Sci U S A. 2021;118(22):1–9.

143. Nuvolone D, Petri D, Voller F. The effects of ozone on human health. Environ Sci Pollut Res Int. 2018;25(9):8074–88.

144. Li D, Bou-Zeid E. Synergistic interactions between urban heat islands and heat waves: The impact in cities is larger than the sum of its parts. J Appl Meteorol Climatol. 2013;52(9):2051–64.

145. Crutzen PJ. New directions: The growing urban heat and pollution “island” effect—impact on chemistry and climate. Atmos Environ. 2004;38(21):3539–40.

146. Li H, Meier F, Lee X, Chakraborty T, Liu J, Schaap M, Sodoudi S. Interaction between urban heat island and urban pollution island during summer in Berlin. Sci Total Environ. 2018;636:818–28.

147. Ulpiani G. On the linkage between urban heat island and urban pollution island: Three-decade literature review towards a conceptual framework. Sci Total Environ. 2021;751:1–31.

148. Rosenfeld AH, Akbari H, Romm JJ, Pomerantz M. Cool communities: Strategies for heat island mitigation and smog reduction. Energy Build. 1998;28(1):51–62.

2. Methodologies

2.1. Introduction

Gas chromatography (GC) is a well-established methodology in analytical chemistry, ideally suited to the analysis of VOCs due to its ability to resolve isobaric interferences and the relative limitations of other analytical techniques [1-3]. GC systems can be highly parameterised, with oven temperatures able to exceed 400°C and the ability for columns to be changed for the optimised analysis of relevant compounds e.g. through internal diameter, the stationary phase, and the column length [4]. Adaptability in GC systems is evident in the existing literature, with GC being used for sea-borne and air-borne measurements, roadside monitoring, measurements from chamber experiments, and as part of long-term monitoring stations [5-9]. Further adaptations, such as the use of two-dimensional GC, have been used to accurately quantify even the most volatile atmospheric species e.g. isoprene and dimethyl sulphide [10]. GC coupling with temperature controlled injection has also meant that C_4–C_6 hydrocarbons can be measured in the parts per trillion range [11].

Two main methodologies exist for capturing and analysing VOCs in the atmosphere: sorbent tube sampling, and whole air canister sampling; both providing established offline analysis methods. In this thesis, GCs coupled with a mass spectrometer (GC-MS) or a flame ionisation detector (GC-FID) were selected to measure a greater number of, and more volatile, VOCs. Multi-instrument analysis is established in the literature as a method to increase the number of analytes that can be observed [12]. GC-FID offers various operational advantages as a system: FID responds to most organic compounds, it is resistant to minor variations in gas flow, and the response of the detector is predictable due to the rule of equal carbon response [12]. Another consideration is the difficulty of GC-MS to distinguish isomers from

each other, particularly in the event of co-elution [13]. FID is able to distinguish between isomers due to the correlation of carbon response and chemical structure [14]. Here, GC-MS offers an obvious advantage in its ability to identify compounds through the effects of ionisation (see Section 2.2.3) [15]. Limit of detection and quantification (LoD/Q) values tend to be lower in GC-MS systems, whilst GC-FID demonstrates better repeatability (1–9% RSD for GC-FID and 6–26% for GC-MS); this is explained, potentially due to derivatisation instability [12].

Sample collection in stainless steel canisters and attendant analysis using GC-MS is outlined in the USEPA Compendium Method TO-15, wherein a full sampling protocol is detailed [16]. Whole air canister sampling can be divided into active and passive methods. Active sampling uses a pump and mass flow controller to regulate sample, pushing the sample into the canister. Passive sampling draws the air sample into the canister, through a pressure difference, via a flow inlet. Sampling methods can be further subdivided into grab and integrated sampling techniques. Grab sampling involves opening the valve of an evacuated canister and allowing it to fill until it equilibrates with atmospheric pressure. Integrated sampling uses an evacuated canister with a flow restrictor designed to regulate flow over a given duration. Whole air canister sampling was chosen in favour of using sorbent tubes, as sorbent tubes can be limited in the range of VOCs they can detect, as well as the sensitivity of detection [17]. Multiple samples can also be taken from canisters.

Online analysis can be achieved through the use of alternative methods, such as proton transfer reaction mass spectrometry (PTR-MS) and chemical ionisation mass spectrometry (CIMS) [18-20]. Online methodologies provide the benefit of real-time chemical analysis but are often impractical to implement in domestic settings. Offline methods are often simple and inexpensive to implement and are ultimately more scalable to many households than online methods but require experiment periods of greater

length to capture significant quantities of data, typically over hours to days. Utilising canisters with offline laboratory analysis – a combination of gas chromatography-time-of-flight-mass spectrometry (GC-ToF-MS) and GC-FID instrumentation – broadens the range of VOCs that can be detected. A variety of instruments were used across multiple studies, the theories of which are described in Sections 2.2.1 to 2.2.4.

2.2. Principles of Analytical Methodologies

2.2.1. Thermal desorption

A thermal desorption unit (TDU) was used with the GC-ToF-MS, GC-FID and the aircraft GC-MS (herein referred to as AGC-MS) systems. Thermal desorption is used in analytical chemistry to concentrate analytes in a carrier gas prior to analysis via GC. In thermal desorption, sample gas flows onto a sorbent trap, in these experiments utilising Tenax TA, which is held at a low temperature (here, between -30°C and 0°C depending on the instrument used), allowing analytes to adsorb to the sorbent. The trap is subsequently heated to a high temperature (here, 250°C), desorbing the analytes, and flushed with an inert gas to carry the analytes to the GC column. Thermal desorption is a technique based on the principle of decreasing breakthrough volume of a sorbent material in increasing temperatures, thus allowing effective quantitation of analytes in smaller samples of air [21]. This method allows samples with very low analyte concentrations to be analysed effectively by appropriate methodologies [21].

The Markes TT24-7 unit is noted for its use of a two-trap system. Figure 2.1 below illustrates a simplified flow diagram when the TDU is in operation. The traps are inserted into a ceramic heater sleeve contained within the trap housing and cooled by electro-thermally operated Peltier plates. Trap A, on the left, is operating in desorbing mode, where the trap is heated quickly;

Trap B, on the right, in this diagram, is either purging or sampling. The pneumatic module controls the flow of the purging gas, which in the context of the chamber experiments, is helium. Gas flow into the GC is controlled by the heated valves. The flow is mirrored when Trap A is sampling or purging and Trap B is desorbing.

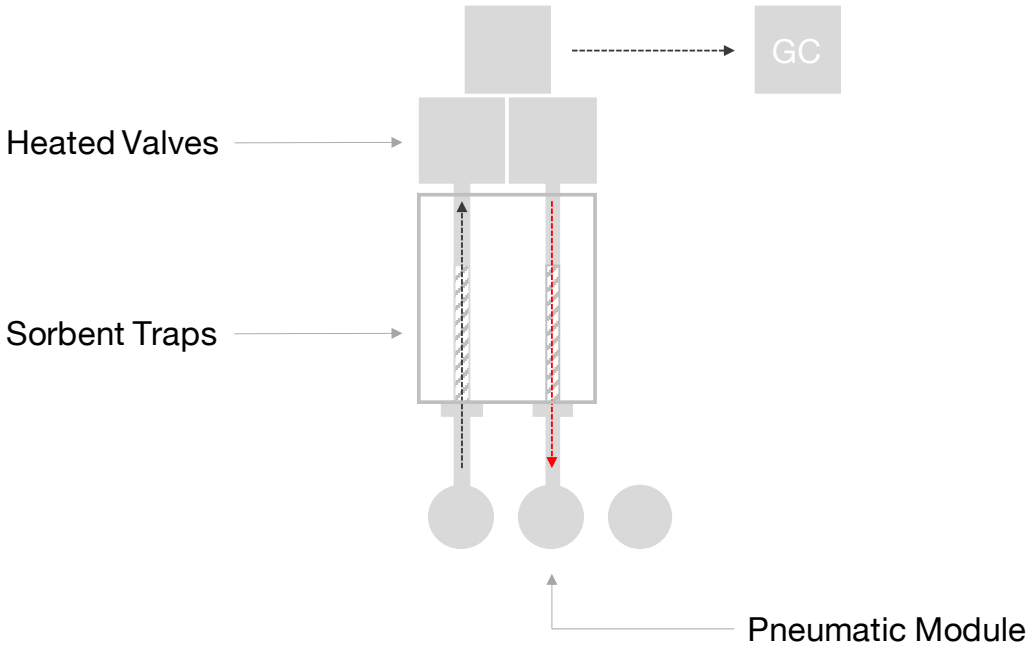

Figure 2.1: Simplified schematic of the Markes TT24-7 thermal desorption unit

2.2.2. Gas chromatography

Gas chromatography is a key analytical method in separating compounds in complex atmospheric samples [22]. The principle of compound separation in gas chromatography is based on the retention time of a given analyte in narrow diameter glass, stainless steel or silica tubing; the GC column [23, 24]. Following thermal desorption, a sample enters the column using an inert carrier gas; the mobile phase. The stationary phase can either be a finely divided material or be a coating on the column wall [23]. The sample passes

through the column with compounds eluting at different times (see Figure 2.2).

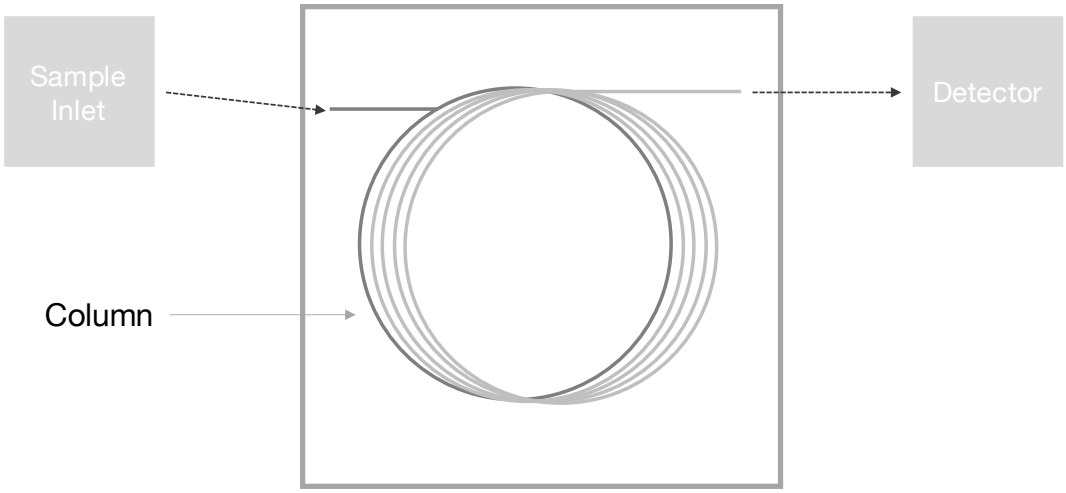

Figure 2.2: Schematic for gas chromatography

The elution time depends upon the analyte's vapour pressure and affinity for the stationary phase [25]. Following elution, the sample enters a detector, which is discussed in 2.2.3 and 2.2.4. Gas chromatographs incorporate an oven with programmable temperature settings which can be optimised to species of interest, this also helps to improve species separation and chromatographic resolution. GCs can be fitted with cryofocussing attachments that use a cryogenic gas to delay entry of a compound into the column, thus improving peak shape, as used in the AGC-MS [26, 27].

During separation, analytes are in equilibrium between the stationary and mobile phases [28]. This equilibrium is governed by a partition coefficient, where C_s = concentration of analyte in the stationary phase and C_m= concentration of the analyte in the mobile phase (see Equation 2.1) [28].

$$K = \frac{C_s}{C_m}$$

Equation 2.1: Partition coefficient for analytes in the stationary and mobile phases

Two different column types were used in the studies detailed in this thesis. In the population and chamber studies, a polysiloxane-coated column was used in GC-MS instrumentation (Restek Rtx-5). For GC-FID instrumentation in the population study, a porous layer open tubular (PLOT) column was used. Polysiloxane columns achieve separation based on vapour pressure, PLOT columns more so by adsorption. Polysiloxane columns are capillary columns coated with polysiloxanes; this improves many aspects of stationary phases in GC columns more generally e.g. efficiency, inertness, and temperature tolerance of the column [29, 30]. A variety of polysiloxanes are often in different proportions depending on polarity required in analysis e.g. 5% diphenyl/95% dimethyl polysiloxane constitutes the Rtx-5 column stationary phase. In PLOT columns, a finely divided sorbent lines the wall of the column and is ideally suited to the analysis of lightweight VOCs and complex mixtures [4]. As analytes pass through the column, they become immobilised by their interactions with the stationary phase [31]. PLOT columns are seen as a hybrid between packed and capillary columns [32]. Despite the differences in column types, partitioning is in strong relation to the analyte's boiling point [23].

2.2.3. Mass spectrometry

Mass spectrometry is often used in tandem with gas chromatography to identify and quantify compounds in complex mixtures [22]. Mass spectrometry further separates analytes from the gas chromatograph based on their mass-to-charge ratio, which is determined by a compound's interaction with electric or magnetic fields generated in the spectrometer [33]. Compounds can then

be identified, and chemical structures derived, using their fragmentation patterns [34]. These results are compared to a library of archived spectra and structures, such as the one provided by the National Institute of Standards and Technology (NIST), and likely comparisons are made by the software based on the information therein [34]. Mass spectrometers operate at low pressures in order to avoid the collisions of ions with the background atmosphere in the chamber [35]. To reach the pressure required for operation and effective analysis, a vacuum pump is needed and is required to operate for an extended period, prior to any analysis, to reach and maintain a stable pressure in the chamber, approximately 0.03 Pa.

Once the sample has eluted from the GC, it enters the ion source of the MS. Here, the compounds in the sample are ionised by electrons from a filament. Formed cations interact with a charged repeller, accelerate into the magnetic field of the mass analyser, and focus onto the detector. Two commonly used mass analysers are quadrupole and time-of-flight analysers, and are detailed in sections 2.2.3.1 and 2.2.3.2.

In mass spectrometry, ionisation is achieved by either ‘hard’ or ‘soft’ techniques [36]. ‘Hard’ ionisation is implemented by such methods as electron impact ionisation, as used in the GC-ToF-MS and AGC-MS, causing a substantial amount of energy to impact the ion thus causing fragmentation [37, 38]. ‘Soft’ ionisation conveys minimal energy to the ion, ergo causing minimal fragmentation [37, 39]. Electron ionisation can be expressed in Equation 2.2 below, where M = a given molecule, e = an electron, M^+ = the resulting ion less an electron [39]:

$$e^- + M \rightarrow 2e^- + M^{+\cdot}$$

Equation 2.2: Electron ionisation

Mass spectrometers can be set to scan in different modes. Selected ion monitoring (SIM) allows the operator to predefine a number of specific masses for analysis in each sample [40]. Full scan analysis allows the operator to set a 'window' of masses to analyse [40]. In samples where the analysis of specific compounds is required, SIM mode is preferable as the analyser spends a longer duration analysing a particular mass, and thus, sensitivity is increased [40]. In samples where unknown compounds need to be identified and quantified, full scan mode is required. As a larger range of masses are analysed, and therefore the analyser spends a lesser duration on each mass, sensitivity can be decreased and the duration of analysis is increased [40]. The selection of scan modes is of concern for quadrupole analysers, but not for other analysers e.g. ToF-MS as these are non-scanning systems [41].

2.2.3.1. Quadrupole mass analysers

Quadrupole analysers (see Figure 2.3) consist of four rods, in parallel pairs, using oscillating electrical fields to destabilise or stabilise ions as they pass through the analyser [41]. A constant DC potential is applied to each rod pair, positive and negative, with alternating radio wave potential superimposed over the DC potential of each pair [41]. The alternating potential has a radio frequency, causing the ion path to spiral through the quadrupole to the detector [42]. A high pass m/z filter exists in one plane and a low pass m/z filter exists in the other [41]. These potentials are typically optimised to allow only one m/z value to pass through the analyser at a time [41]. Ion separation is based on the stability of the ion trajectory through these electrical fields; other ions impact the rods and are neutralised [37].

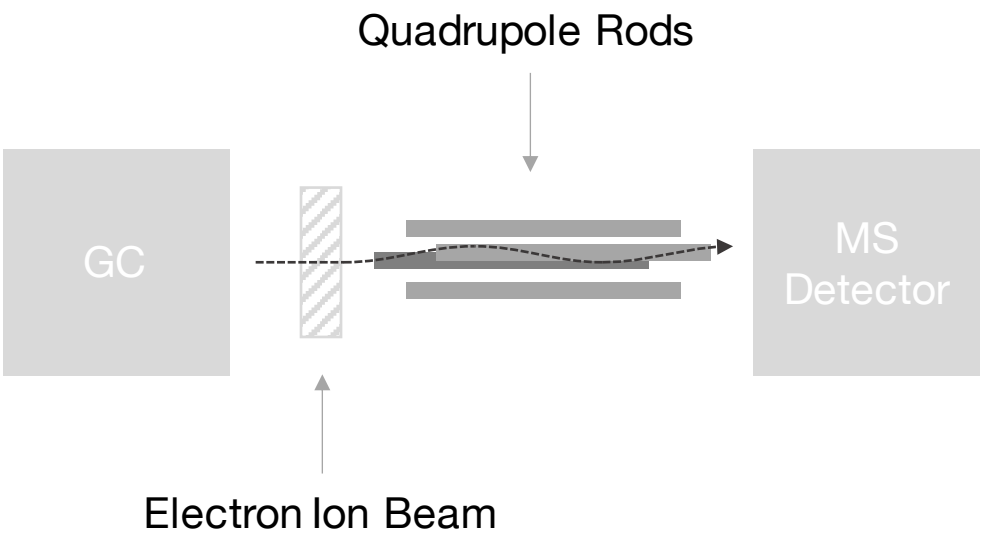

Figure 2.3: Schematic for quadrupole mass spectrometry

2.2.3.2. Time of Flight mass analysers

Time-of-flight analysers (see Figure 2.4) separate analytes based on the length of time it takes the ions to travel through a flight tube to the detector [41]. From the ion source, ions are accelerated to equal kinetic energy – via an electric field — to a flight tube, so separation is based purely on mass, with higher mass ions being slower to reach the detector as determined by the equation ½ mv^2; where m = ion mass and v = ion velocity [41, 43]. Time-of-flight analysers are non-scanning and pulsed systems, so prior to ions entering the flight tube, they accumulate and are released in pulses [41, 44]. Upon release, ions enter the flight tube, and in the instance of a reflectron system, their path is diverted using an ion mirror to the detector [43]. This improves mass resolution and reduces the spread of flight times of ions with identical mass-to-charge ratios [45, 46].

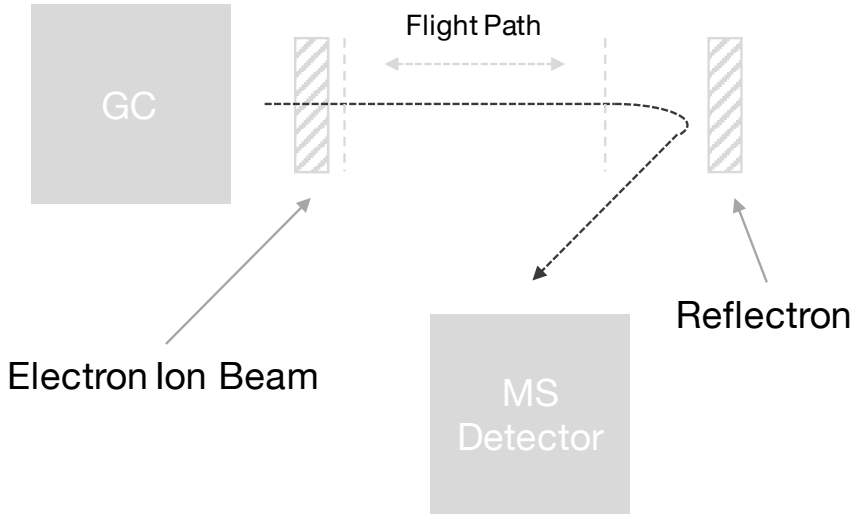

Figure 2.4: Schematic for time-of-flight mass spectrometry

Time-of-flight mass analysers offer some significant advantages over quadrupole analysers; for instance time-of-flight systems deliver faster acquisition rates than quadrupole systems, have an increased dynamic range and can provide reproducible analyses without the use of SIM, the speed of which is often a limiting factor in analysis using quadrupole mass analysers [41]. These facets make time-of-flight analysers suited to the analysis of complex mixtures [41]. Improved sensitivity from the ability to use SIM on quadrupole systems provides advantages in targeted analysis [41]

2.2.4. Flame ionisation detection

Similarly to MS, flame ionisation detection (see Figure 2.5) is a commonly used GC detection method [22]. Flame ionisation detection separates compounds based on ions produced by carbon atoms during combustion using an air-hydrogen flame [47]. When the sample elutes from the GC column, it is combusted in the flame and ions are detected from an electrical charge produced by two electrodes located at the flame nozzle and above the flame [48]. Current is measured when the ions impact the collector plate [48]. The current generated is proportional to the amount and carbon content of the analyte [49].

As mentioned in the Introduction, GC-FID offers several advantages in analysis, such as being responsive to most organic compounds, general systemic stability, and the ability to distinguish isomers of the same compound. One significant drawback, however, is that the sample is combusted, meaning that analysis of the same sample cannot be repeated [48].

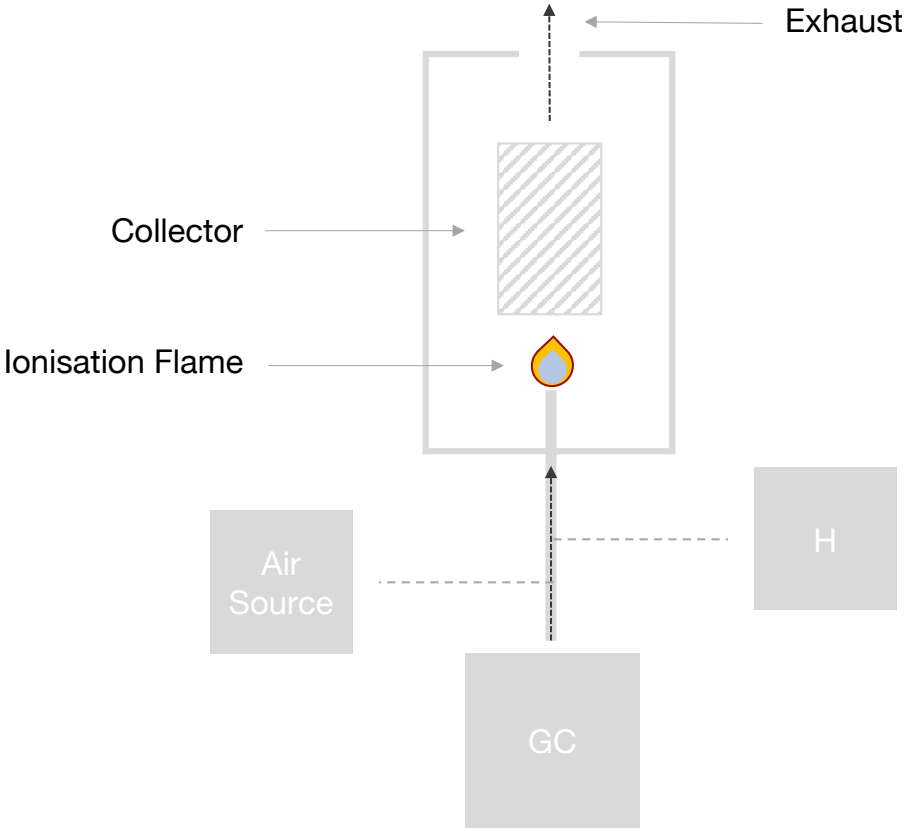

Figure 2.5: Schematic for flame ionisation detection in gas chromatography

2.3. Population Study

2.3.1. Study design

The sample collection methodology for the population study was in accordance with the method outlined in the United States Environmental Protection Agency Compendium Method Toxic Organics 15 methodology

(USEPA TO15). This methodology optimises the collection of VOCs in air within stainless-steel canisters and analysis performed by GC-MS.

This study was designed to be conducted across 9 weeks in winter (February – April 2019) and 10 weeks in summer (July – September 2019). This study utilised 23 stainless steel canisters with restricted flow inlets (Restek, Bellefonte, PA and Entech Instruments, Simi Valley, CA) per week. All canisters had been treated internally with silica to ensure minimal sample contamination by chemical artifacts. Three replicate samples were taken of each household with three randomly selected households also requested to take an outdoor sample per week. This led to a total of 360 indoor and 55 outdoor samples being taken over 19 weeks. A pre-existing and well-characterised panel of participants, provided by Givaudan UK, was used as the study cohort. The cohort consisted of a diverse demographic residing in varied housing stock.

Each canister was given a unique alphanumeric identifier, or 'canister ID' based on the canister serial number, with successive letters appended weekly, for laboratory use, to indicate each canister's rotation e.g. '31138A', '31138B' etc. Prior to a sample being collected, canisters were evacuated from atmospheric to sub-atmospheric pressure (300 Pa) using a high-vacuum rig situated in the laboratory. Before collection by participants, canisters were fitted with a 72-hour flow restrictor. To ensure continuous and uninterrupted sampling, two sets of 23 canisters were prepared and rotated week-to-week for sampling and analysis. Following sample collection in participants' homes, canisters were returned to a centralised hub in Ashford and couriered to the University of York for analysis. Samples were analysed and the canisters prepared within seven days for the proceeding rotation. To prepare the samples for analysis, canisters were pressurised from atmospheric pressure to 179 kPa using highly purified air.

2.3.2. Gas Chromatography-Time-of-Flight-Mass Spectrometer setup and calibration

The GC-ToF-MS comprises several elements: 1) a sample dryer, 2) a Markes Unity thermal desorption unit, 3) an Agilent 7890A gas chromatograph and 4) an ALMSCO time-of-flight mass spectrometer. The sample dryer consists of a Stirling cooler that cools a given sample to -30°C to remove water vapour into a glass cold finger, improving chromatography and reducing potential degradation of the GC column. The thermal desorption unit, as explained in greater detail in 2.2.1, allows for the analysis of low concentrations of VOCs in atmospheric samples via preconcentration prior to analysis. This is achieved by cooling the trap to -20°C whilst trapping a given sample, then rapidly heating it to 250°C to desorb the VOCs into a carrier gas stream. The gas chromatograph was fitted with a non-polar phenyl arylene polymer GC column (length: 50 m, internal diameter: 0.25 mm, film thickness: 0.25 μm), and attached to a time-of-flight mass spectrometer to analyse C_4–C_{12} hydrocarbons. Samples were taken at a volume of 50 mL min^{-1} for 10 minutes, providing a 500 mL sample.

Figure 2.6: Photograph of GC-ToF-MS instrument

The GC-ToF-MS system was calibrated using a high pressure gravimetrically prepared standard gas blended at the Wolfson Atmospheric Chemistry Laboratories, University of York. A list of 39 chemical species was prepared to consider in the analysis and liquid standards procured. Calculations were made for the appropriate volume of liquid standard needed to correspond to parts per billion volume. Liquid standard was injected directly into a modified evacuated Restek 1 L cylinder. At one end, the cylinder was modified with a one directional tap and a 1” Swagelok nut to hold in place a GC septum, into which the syringe needle can be injected and liquid standard transferred with minimal loss of vacuum. The other end was modified with a one directional tap and a length of ¼” stainless steel tubing. Both taps ensure that, depending on configuration, flow through the cylinder flows in one direction through the tubing. Prior to liquid standard injection, the 1 L cylinder was evacuated to sub-atmospheric pressure, refilled with ambient air and evacuated again. This cycle was repeated three times.

The 10 L calibration cylinder was initially evacuated to sub-atmospheric pressure (~300 Pa) in order to aid the transfer of the liquid standard mix to the cylinder. To transfer the liquid standard to the large cylinder, the 1 L cylinder was attached to a high-pressure nitrogen cylinder at one end, and the 10 L cylinder at the other. The small cylinder was initially washed through with a low flow of CP-grade nitrogen for several minutes. The 1 L cylinder was removed from the train and the 10 L cylinder was attached to the nitrogen cylinder directly and diluted to 5 MPa. The 10 L cylinder was vented and refilled again to 5 MPa with nitrogen. This two-stage dilution process ensured that the liquid standard mix was appropriately diluted. The standard mix contained the listed in Table 2.1.

Table 2.1: The 19 compounds contained within the custom calibration gas and their retention times based on the instrumental methodology

Compound	Retention Time (mins)
Acetone	3.3
Isoprene	3.3
Dichloromethane	3.4
2-Methylpentane	3.5
n-hexane	3.6
n-pentane	3.7
Benzene	4.1
Toluene	4.9
Tetrachloroethylene	5.3
Ethylbenzene	6.0
m/p-Xylene	6.1
o-Xylene	6.5
D4 Siloxane	6.9
α-Pinene	7.0
1,3,5-trimethylbenzene	7.6
β-Pinene	7.9
p-Cymene	8.6
Limonene	8.7
γ-Terpinene	10.0

Figure 2.7 displays the chromatogram produced for the above calibration gas mix, based on the GC method outlined in Table 2.2

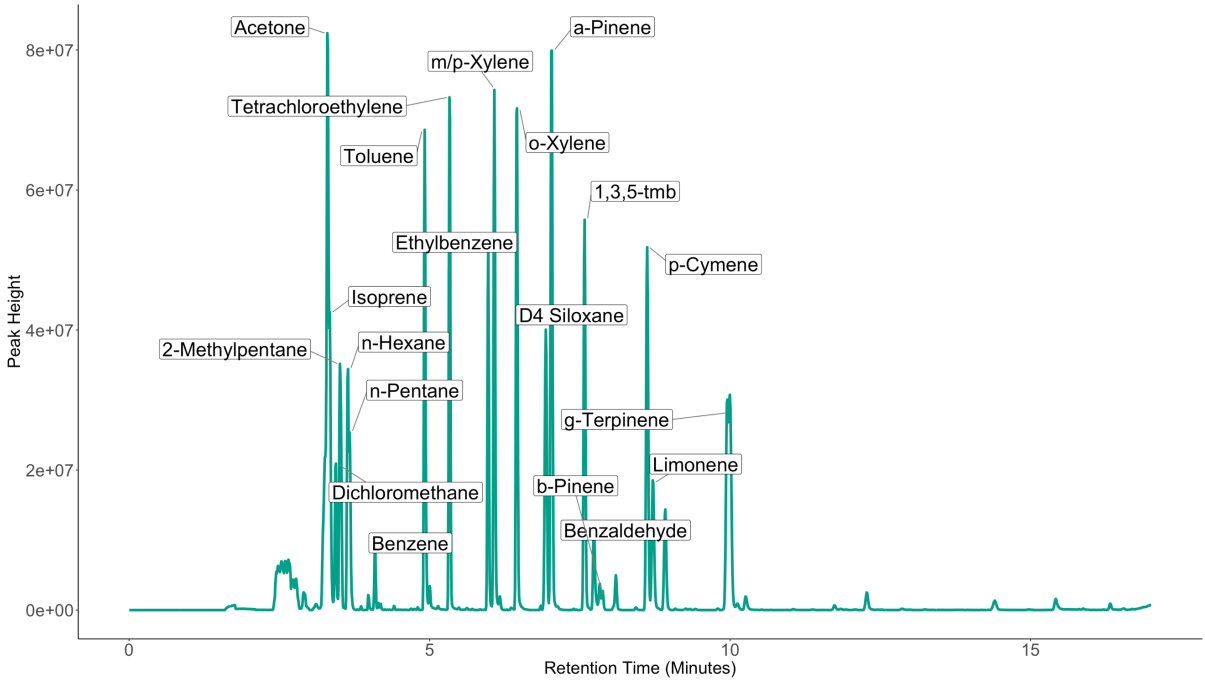

Figure 2.7: GC-ToF-MS signal for the gas calibration mix

Table 2.2: GC-ToF-MS oven programme

	°C/min	Next Temperature (°C)	Hold Time (mins)
Initial	-	40	0
Ramp 1	60	100	0
Ramp 2	10	130	0
Ramp 3	5	150	1
Ramp 4	5	190	0
Ramp 5	35	250	0

Both the aircraft MS and ToFMS were calibrated/tuned using the perfluorotributylamine (PFTBA) calibration mix and automated procedure provided by Agilent and Markes respectively. The aircraft MS was calibrated before each extended calibration period at the chamber. The TOFMS was calibrated at the beginning of each week that experiments took place.

PFTBA is often used because perflourinated compounds in general have minimal mass defects.

2.3.3. Gas Chromatography-Flame Ionisation Detector setup and calibration

The GC-FID comprises several elements: 1) a CIA Advantage-xr autosampler, 2) a Markes Kori-xr water condenser, 3) a Markes Unity-xr thermal desorption unit, 4) an Agilent 7890B gas chromatograph and flame ionisation detector. The Kori-xr provides an alternative method through which to remove water vapour from samples. The system contains an electronically-cooled trap, which is heated between samples to remove excess water, improving chromatography and reducing potential degradation of the GC column. The thermal desorption unit, as explained in greater detail in 2.2.1, allows for the analysis of low concentrations of VOCs in atmospheric samples via preconcentration prior to analysis. This is achieved by cooling the trap to -30°C whilst trapping a given sample, then rapidly heating it to 250°C to desorb the VOCs into a carrier gas stream. The gas chromatograph was fitted with an Na_2SO_4 passivated PLOT column (length: 60 m, internal diameter: 0.53 mm, film thickness = 10 μm). This setup allowed for the analysis of C_2–C_8 hydrocarbons. Samples were taken at a volume of 50 mL min^{-1} for 10 minutes, providing a 500 mL sample.

Figure 2.8: Photograph of GC-FID instrument

The GC-FID system was calibrated using a 4 ppb, 30 component ozone precursor non-methane hydrocarbon standard, provided by the National Physical Laboratory (NPL). The standard gas contained compounds listed in Table 2.3.

Table 2.3: The 26 Compounds contained within the NPL calibration gas and their retention times based on the instrumental methodology

Compound	Retention Time (mins)
Ethane	2.8
Ethene	4.3
Propane	6
Propene	9.2
iso-butane	10.1
n-butane	10.4
Acetylene	11.3
trans-2-butene	12.6
1-butene	12.8
cis-2-butene	13.4
iso-pentane	14
n-pentane	14.4
1,3-butadiene	15.2
trans-2-pentene	15.9
1-pentene	16.5
2-methylpentane	17.7
n-hexane	18.1
Isoprene	18.6
Heptane	21.4
Benzene	22.5
2,2,4-trimethylpentane	23.7
n-octane	25.2
Toluene	27.5
Ethylbenzene	36.2
m/p-xylene	36.8
o-xylene	37.7

Figure 2.9 displays the chromatogram produced for the NPL calibration gas used.

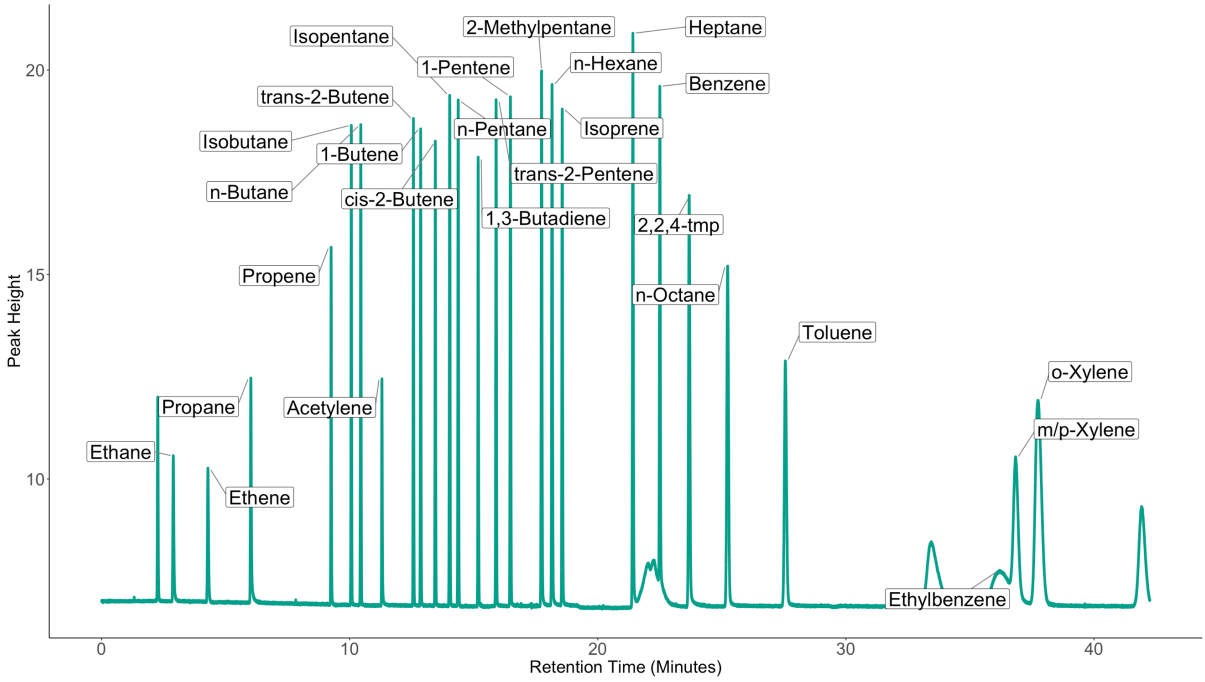

Figure 2.9: GC-FID signal for the NPL gas calibration mix

Table 2.4: GC-FID oven programme

	°C/min	Next Temperature °C	Hold Time (mins)
Initial	-	40	4
Ramp 1	10	110	0
Ramp 2	8	200	20

2.4. University of Manchester Aerosol Chamber Study

The use of aerosol chambers began in the mid-to-late 1900s as a way of modelling chemical components of atmospheric processes in controlled laboratory conditions [50]. As chambers are highly parameterised, with conditions such as relative humidity, light intensity, temperature, and initial

oxidant concentrations being under the operator's control, they are ideal for use in indoor and outdoor air studies. Differing chamber designs mean that experiments can be performed under natural or artificial light. The former taking place in sealed bags surrounded by opaque insulated panels, and the light controlled by arc lamps, such as in the aerosol chamber at the University of Manchester [51]; the latter being conducted under translucent panels to allow the infiltration of natural light, such as in the EUPHORE chamber in Valencia [52]. Figures 2.10 and 2.11 illustrate the University of Manchester Aerosol Chamber.

Figure 2.10: External photograph of the University of Manchester Aerosol Chamber, with the AGC-MS in-situ

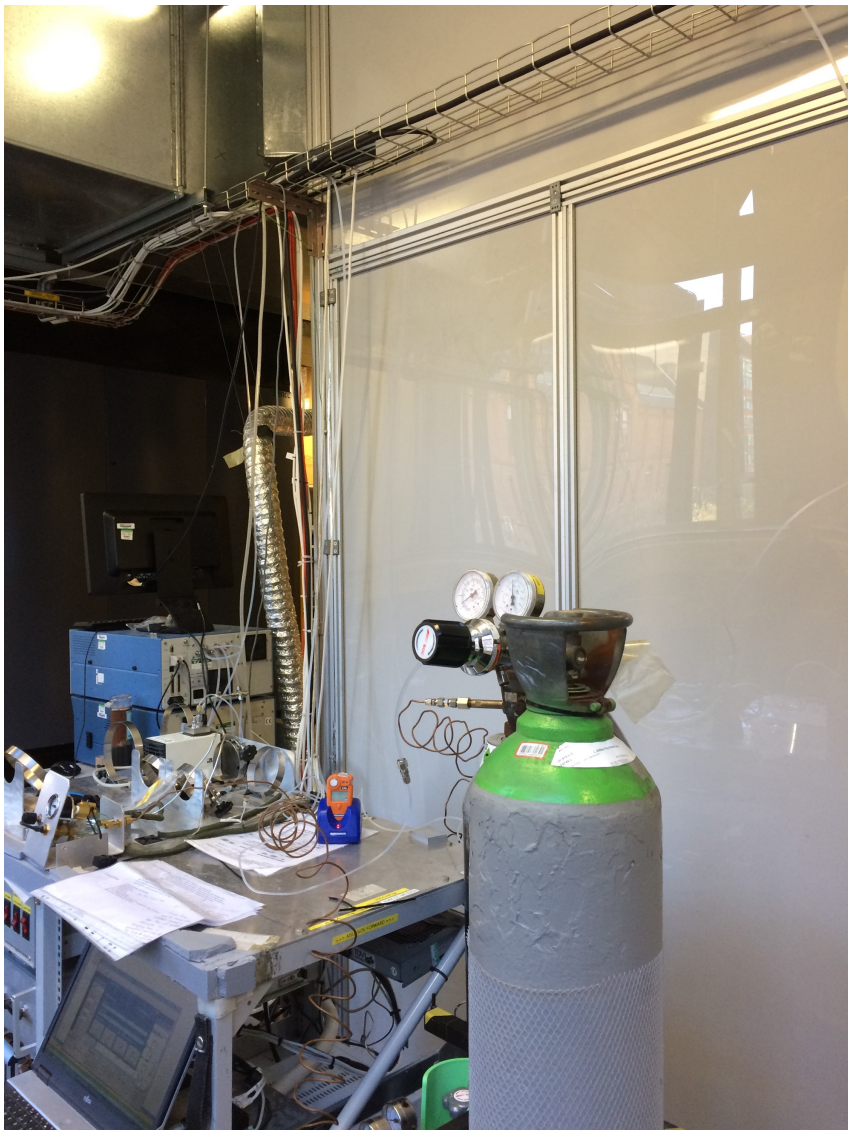

Figure 2.11: Internal photograph of the University of Manchester Aerosol Chamber. The polymer bag is suspended in a moveable frame, surrounded by insulative panels and an array of halogen lights.

2.4.1. Study design

The aerosol chamber experiments were performed at the University of Manchester Aerosol Chamber. The chamber consists of an 18 m^3 fluorinated ethylene propylene Teflon bag measuring 3 x 3 x 2 m [53]. The bag is secured within three rectangular aluminium frames, two of which are free moving [53]. These frames allow the bag to expand and contract according to adjusting sample flows [53]. The chamber enclosure is fitted with two filtered 6 kW Xenon arc lamps and a series of wall-mounted halogen lamps; this is designed to resemble the atmospheric actinic range, which is between 280–420 nm; the chamber has a wavelength range of 290–800 nm [54-56]. The enclosure is lined with reflective plastic sheeting to maximise irradiance, whilst allowing evenness in illumination [56]. VOCs are injected directly into

the chamber by way of a heated glass bulb through which filtered nitrogen flows [53, 56]. NO_x is introduced to the chamber via a cylinder [56].

A variety of experiments were performed to measure 1) VOC decay in different conditions and 2) observable formation of particles and SOA intermediates. α-Pinene, toluene, and 1,3,5-trimethylbenzene were used as parent VOCs at mixing ratios relevant to atmospheric abundance. Decay was observed, along with particle and SOA intermediate formation. Due to the nature of the experiments, median duration was approximately five hours, meaning that only one set of chamber conditions could be tested per day. During these experiments, the VOC and NO_x were injected into the chamber only, wherein OH and O_3 were subsequently generated. Latter experiments involving toluene and 1,3,5-trimethylbenzene used HONO as a source of OH. Particle formation was observed using a Differential Mobility Particle Sizer (DMPS), already in-situ at the facility. The aircraft GC-MS was selected due to its rapid analysis time, as a sample could be collected and analysed every ~10 minutes.

2.4.2. Aircraft Gas Chromatograph-Mass Spectrometer

The AGC-MS is a composite instrument designed for in-situ analysis of airborne atmospheric samples collected in the Facility for Airborne Atmospheric Measurements BAe-146 research aircraft. The AGC-MS is comprised of multiple instruments: 1) A flow control box and sample dryer, 2) a Markes TT24-7 thermal desorption unit, 3) an Agilent 6850 gas chromatograph and 4) an Agilent 5875C mass spectrometer. Parts of the sample drying equipment are commercially available but were assembled in the laboratory as detailed in Minaeian, 2016 [27]. A CP-grade helium cylinder was used to supply the carrier gas and to operate the pneumatic valves for the TDU as laboratory supplies of neither helium nor compressed air were available. The thermal desorption unit, as explained in greater detail in 2.2.1, allows for the analysis of low concentrations of VOCs in atmospheric

samples via preconcentration prior to analysis. This is achieved by cooling the trap to 0°C whilst trapping a given sample, then rapidly heating it to 250°C to desorb the VOCs into a carrier gas stream. The gas chromatograph was fitted with a diphenyl dimethyl polysiloxane column for analysis (length: 10 m, internal diameter: 0.18 mm, film thickness: 0.2 μm). This column is a generic column used for a variety purposes, such as in the analysis of pesticides and drugs, as well as in the analysis of hydrocarbons and semi-volatile compounds. Samples were taken at a volume of 100 mL min^{-1} for 6 minutes, providing a 600 mL sample.

The sample dryer consists of a Stirling cooler designed to maintain the temperature of a glass cold finger at -30°C. This removes water vapour from sample gas prior to analysis; an important measure to both improve chromatography and reduce potential damage to the GC column [57]. The Stirling cooler operates through the continuous compression and expansion of, in this instance, helium gas via a free-moving piston [27, 58]. The heat is transferred to a heat exchanger and subsequently vented [27]. Water vapour is removed from the sample via a glass cold finger encased in an aluminium cover containing a cold head and a thermocouple inserted [27]. The system is encased with an insulative foam block [27].

The TDU is a commercially available instrument with two sampling traps, as constructed by the manufacturer. This allows the sample in one trap to be desorbed and analysed by the GC, whilst simultaneously allowing the collection of another sample in the TDU. An optimised method meant that a sample could be analysed in fast time resolutions (approximately ten minutes including sampling time and the resetting of base parameters prior to a subsequent sample run). For this reason, the AGC-MS was selected as an appropriate instrument for chamber experiments, in which aerosol chemistry reacted rapidly.

Figure 2.12: Photograph of AGC-MS instrument

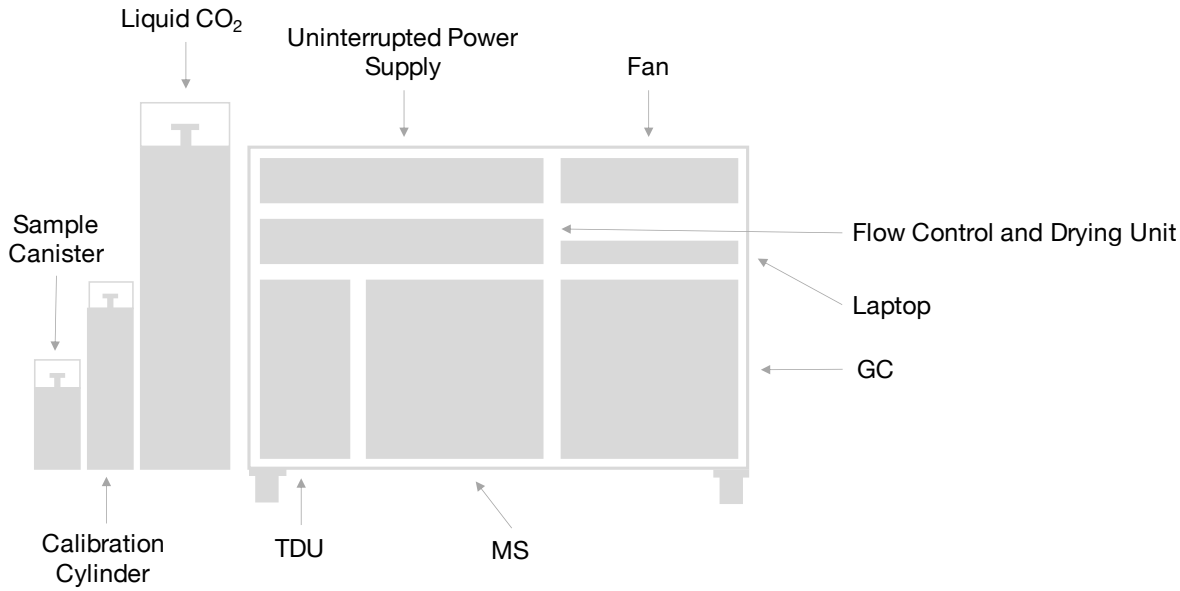

Figure 2.13: Schematic for the AGC-MS instrument

In a typical setup, the sample enters the flow control box and the water vapour is extracted using the Stirling cooler. The dried sample then enters the TDU, where the sample is concentrated before entering the GC, and cryofocussed just before the sample enters the column for detection in the MS. Cryofocussing uses a stainless-steel t-piece through which the GC column is passed. The column entrance is sprayed with liquid CO_2 and thus compounds are slowed down as they are being analysed, and in so doing, improves peak shape. The use of cryogenic refocussing to improve peak shape in gas chromatography is well-recorded in the literature [59, 60]. As conditions in the chamber were at atmospheric pressure, a small pump was used to connect the chamber sample outlet with the GC-MS sample inlet via PTFE tubing, creating a pressure difference between the chamber and the GC-MS.

The AGC-MS was calibrated using a custom blended calibration gas prepared in the same manner as the calibration gas used for the GC-ToF-MS, though containing fewer compounds (see Figure 2.14).

Table 2.5 displays the compounds in the custom calibration gas used for the AGC-MS and their retention time based on the instrument methodology

Compound	Retention Time (mins)
Isoprene	0.6
Benzene	0.8
Toluene	0.7
Ethylbenzene	1.6
m/p-Xylene	1.6
o-Xylene	1.7
α-Pinene	1.9
1,3,5-Trimethylbenzene	2.1
Limonene	2.4

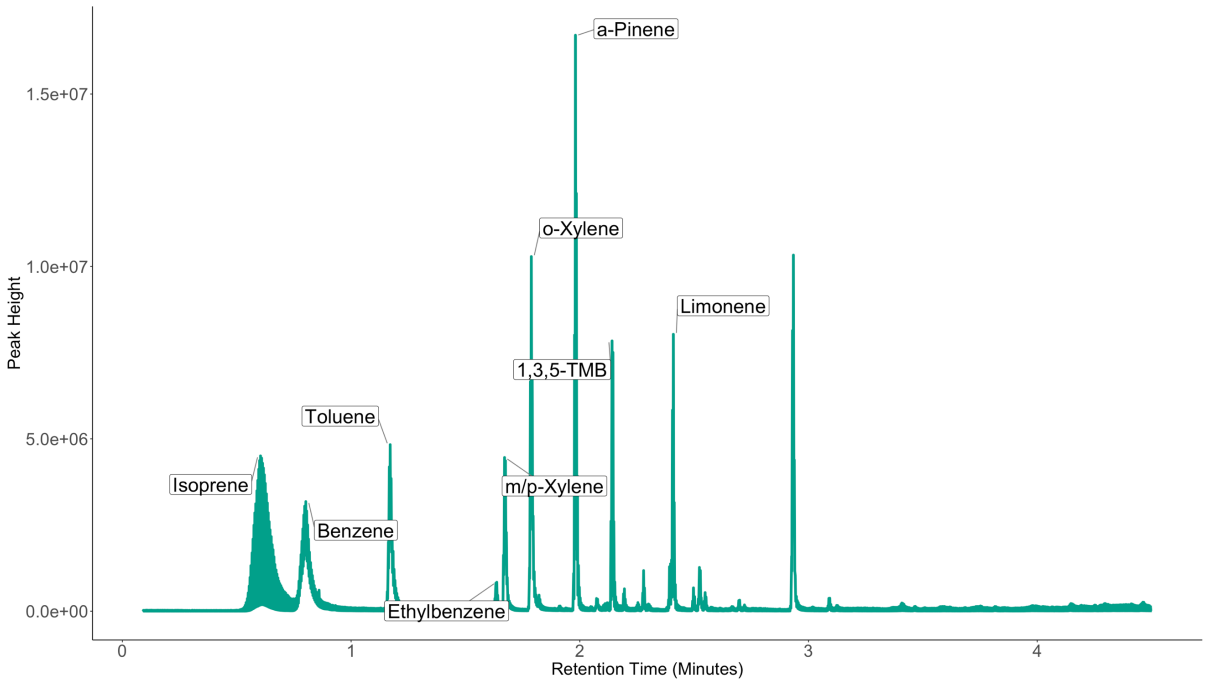

Figure 2.14: AGC-MS signal for the custom blended gas calibration mix for the oven programme outlined in Table 2.6

Table 2.6: AGC-MS oven programme

	°C min	Next Temperature °C	Hold Time (mins)
Initial	-	40	1
Ramp 1	40	180	0

2.4.3. Limits of Detection

The limit of detection (LoD) of an instrument is defined as the lowest detectable concentration of an analyte, discernible from a concentration as defined in limit of blank (LoB) calculations (see Equation 2.3) [61]. It can be calculated using a gas sample containing a known, low concentration of an analyte [61]. Equation 2.4 below can be used to calculate LoD [61]. 1.645 is in reference to the statistical *z* score of a standard normal probability distribution, with 0.90 in centre and 0.05 each in the far left and far right tails of the distribution [62, 63]. The *z* score itself is the number of standard deviations above or below an observation [64].

$$LoB = \bar{x}Blank + 1.645(SD_{blank})$$

Equation 2.3: LoB equation

$$LoD = LoB + 1.645(SD_{low\ concentration\ sample})$$

Equation 2.4: LoD equation

Table 2.7: LoD values for the AGC-MS given in mixing ratios of parts per billion

Compound	Mixing Ratio (ppb)
α-pinene	0.4
o-xylene	0.4
m/p-xylene	0.4
Limonene	1.9
Ethylbenzene	0.4
1,3,5-trimethylbenzene	0.9
Toluene	0.2

Table 2.8: LoD values for the GC-ToF-MS given in mixing ratios of parts per billion

Compound	Mixing Ratio (ppb)
1,3,5-Trimethylbenzene	0.3
2-Methylpentane	0.6
Acetone	0.04
α-Pinene	0.3
Benzene	0.7
β-Pinene	2.2
Dichloromethane	0.3
Ethanol	<0.01
Ethylbenzene	0.6
γ-Terpinene	0.3
n-Hexane	0.2
Isoprene	0.1
Limonene	1.9
m/p-Xylene	0.9
Methanol	0.1
n-pentane	0.7
D4 Siloxane	0.2
o-Xylene	0.6
p-Cymene	0.6
Tetrachloroethylene	0.5

Table 2.9: LoD values for the GC-FID given in mixing ratios of parts per trillion as outlined in Hopkins et al. [65]

Compound	Mixing Ratio (ppt)
Ethane	9
Ethene	7
Propane	2
Propene	2
iso-butane	2
n-butane	2
Acetylene	2
trans-2-butene	2
1-butene	2
cis-2-butene	2
iso-pentane	2
n-pentane	2
1,3-butadiene	2
trans-2-pentene	2
1-pentene	2
2-methylpentane	2
n-hexane	2
Isoprene	2
Heptane	2
Benzene	2
2,2,4-trimethylpentane	2
n-octane	2
Toluene	2
Ethylbenzene	2
m/p-xylene	2
o-xylene	2

2.5. Quantitative Methodology

2.5.1. Gas Chromatography-Time-of-Flight-Mass Spectrometer

During sample analysis on the GC-ToF-MS system, chromatogram and mass spectra data were generated using ALMSCO BenchToFdx and Agilent MSD ChemStation software. Peak integration and peak area calculations were performed using Agilent MassHunter. This software allows the import of raw chromatogram data from BenchTOFdx once they have been processed in groups of files, referred to as batches, by MassHunter translator software. In the MassHunter software, a method can be set up that allows the automatic identification and integration of user-selected compounds for each file batch. In the method, a number of parameters can be constrained to improve automation efficacy, including compound mass-to-charge ratio; m/z (including qualifier ions) and expected retention time (with left and right deltas); see Table 2.10. Both the retention time left and right delta of each compound were set to 0.2 minutes to account for instrument drift in the analysis. The method was parameterised using calibration runs performed at the beginning of each analysis week. MassHunter then analyses imported chromatograms and compares them with the user-defined method, identifying chromatographic peaks that match the parameters of the method. Methods can be individual to each sample file, if necessary, or minor adjustments can be affected manually using various tools available in the software. Once the method has run, key peak identifiers are listed in a table that include file name, peak retention time and peak area. These data can then be exported as a .csv file for further analysis in data analysis software.

Table 2.10: GC-ToF-MS peak integration method parameters used in Agilent MassHunter Quantitative software. The main ion was derived from the NIST Chemistry Webbook [66]. Retention times were identified from the calibration runs detailed in earlier sections in this chapter, with a ± 0.2 minute delta margin provided for retention time

Compound	Main ion (m/z)	Retention Time (mins)
Acetone	43	3.3
Isoprene	67	3.3
Dichloromethane	49	3.4
2-Methylpentane	43	3.5
n-hexane	57	3.6
n-pentane	43	3.7
Benzene	78	4.1
Toluene	91	4.9
Tetrachloroethylene	166	5.3
Ethylbenzene	91	6.0
m/p-Xylene	91	6.1
o-Xylene	91	6.5
D4 Siloxane	91	6.9
α-Pinene	93	7.0
1,3,5-trimethylbenzene	105	7.6
β-Pinene	93	7.9
p-Cymene	119	8.6
Limonene	93	8.7
γ-Terpinene	93	10.0

2.5.2. Gas Chromatography-Flame Ionisation Detector

During sample analysis on the GC-FID, chromatograms were generated using the custom software of the system. After analysis, chromatogram files were transferred to a PC running GC Werks, a peak identification and integration software. GC Werks allows a method to be defined that automatically identifies peaks and calculates peak areas based on mass and retention time; retention times are based on calibration samples (defined in Table 2.3). GC Werks allows individual peak identifiers to be set, referred to

as peak ID windows. Peak ID windows are defined by the predicted retention time, with upper and lower limits of where the peak could fall. Peak ID windows can be further adjusted by manually moving the windows to the point at which the peak is identified by the software, though this can limit the extent to which one method can be applied to multiple chromatograms. Peak areas are then calculated and files can be exported to a .csv format for further analysis in appropriate software.

2.5.3. Aircraft Gas Chromatography-Mass Spectrometer

Sample chromatograms were recorded using Agilent MSD ChemStation software and analysed using MassHunter Qualitative and Quantitative software. Chromatograms for each sample are stored in separate files and peaks can be identified using the mass spectra data and the NIST library stored in the software. Peak areas can be calculated in a number of different ways: either automatically using parameters preset by the software, user defied parameters, or through manual integration. During these experiments, as in the GC-ToF-MS quantitative methodology, a method file was used for each sample batch using the parameters outlined below Table 2.11. Automated integrations were then optimised using manual adjustment.

Table 2.11: AGC-MS peak integration method parameters used in Agilent MassHunter Quantitative software. The main ion was derived from the NIST Chemistry Webbook [66]. Retention times were identified from the calibration runs detailed in earlier sections in this chapter, with a ± 0.2 minute delta margin provided for retention time to

Compounds	Main ion (m/z)	Retention Time (mins)
Isoprene	67	0.6
Benzene	78	0.8
Toluene	91	0.7
Ethylbenzene	91	1.6
m/p-Xylene	91	1.6

o-Xylene	91	1.7
α-Pinene	93	1.9
1,3,5-Trimethylbenzene	105	2.1
Limonene	93	2.4

Following analysis on both the GC-ToF-MS and GC-FID systems, .csv files were exported containing peak area and sample identifier information (i.e. sample analysis date and time). Canister sample information was extracted along with the most relevant and temporally close zero air and calibration samples. Compound peak areas from the most relevant zero air blanks were extracted, and the average deducted from the compound peak areas of each canister and calibration sample in each sample period. The response factor (RF, detailed in Equation 2.5) for each compound was calculated and a parts per billion mixing ratio defined.

$$RF = Peak\ area\ of\ standard\ /\ Concentration\ of\ standard$$

Equation 2.5: Calculating the response factor

Still further calculations were performed to convert ppb to micrograms per cubic metre and molecules per cubic metre concentrations, depending on application required.

References

1. Bartle KD, Myers P. History of gas chromatography. TrAC, Trends Anal Chem. 2002;21(9):547–57.

2. Dewulf J, Van Langenhove H, Wittmann G. Analysis of volatile organic compounds using gas chromatography. TrAC, Trends Anal Chem. 2002;21(9):637–46.

3. Edwards SJ, Lewis AC, Andrews SJ, Lidster RT, Hamilton JF, Rhodes CN. A compact comprehensive two-dimensional gas chromatography (GC×GC) approach for the analysis of biogenic VOCs. Anal Methods. 2013;5(1):141–50.

4. Rahman MM, Abd El-Aty AM, Choi J-H, Shin H-C, Shin SC, Shim J-H. Basic overview on gas chromatography columns. Analytical separation science. Weinheim: Wiley-VCH; 2015. p. 823–34.

5. Aruffo E, Di Carlo P, Dari-Salisburgo C, Biancofiore F, Giammaria F, Busilacchio M, Lee J, Moller S, Hopkins J, Punjabi S, Bauguitte S, O'Sullivan D, Percival C, Le Breton M, Muller J, Jones R, Forster G, Reeves C, Heard D, Walker H, Ingham T, Vaughan S, Stone D. Aircraft observations of the lower troposphere above a megacity: Alkyl nitrate and ozone chemistry. Atmos Environ. 2014;94:479–88.

6. van der Laan S, Neubert REM, Meijer HAJ. A single gas chromatograph for accurate atmospheric mixing ratio measurements of CO_2, CH_4, N_2O, SF_6 and CO. Atmos Meas Tech. 2009;2(2):549–59.

7. Carpenter LJ, Fleming ZL, Read KA, Lee JD, Moller SJ, Hopkins JR, Purvis RM, Lewis AC, Müller K, Heinold B, Herrmann H, Fomba KW, van Pinxteren D, Müller C, Tegen I, Wiedensohler A, Müller T, Niedermeier N, Achterberg EP, Patey MD, Kozlova EA, Heimann M,

Heard DE, Plane JMC, Mahajan A, Oetjen H, Ingham T, Stone D, Whalley LK, Evans MJ, Pilling MJ, Leigh RJ, Monks PS, Karunaharan A, Vaughan S, Arnold SR, Tschritter J, Pöhler D, Frieß U, Holla R, Mendes LM, Lopez H, Faria B, Manning AJ, Wallace DWR. Seasonal characteristics of tropical marine boundary layer air measured at the Cape Verde Atmospheric Observatory. J Atmos Chem. 2010;67(2):87–140.

8. Pankow JF, Luo W, Bender DA, Isabelle LM, Hollingsworth JS, Chen C, Asher WE, Zogorski JS. Concentrations and co-occurrence correlations of 88 volatile organic compounds (VOCs) in the ambient air of 13 semi-rural to urban locations in the United States. Atmos Environ. 2003;37(36):5023–46.

9. Cocker DR, Flagan RC, Seinfeld JH. State-of-the-art chamber facility for studying atmospheric aerosol chemistry. Environ Sci Technol. 2001;35(12):2594–601.

10. Lewis AC, Bartle KD, Rattner L. High-speed isothermal analysis of atmospheric isoprene and dms using on-line two-dimensional gas chromatography. Environ Sci Technol. 1997;31(11):3209–17.

11. McQuaid JB, Lewis AC, Bartle KD, Walton SJ. Sub-ppt atmospheric measurements using PTV-GC-FID and real-time digital signal processing. J High Resolut Chromatogr. 1998;21(3):181–4.

12. Pacchiarotta T, Nevedomskaya E, Carrasco-Pancorbo A, Deelder AM, Mayboroda OA. Evaluation of GC-APCI/MS and GC-FID as a complementary platform. J Biomol Tech. 2010;21(4):205–13.

13. Cochran J, Lorne F, Laura M, Phillip J, Ulrich M. GC/GC-MS. LC GC. 2018;31(3):8–15.

14. Göröcs N, Mudri D, Mátyási J, Balla J. The determination of GC-MS relative molar responses of some n-alkanes and their halogenated analogs. J Chromatogr Sci. 2012;51(2):138–45.

15. Leary PE, Kammrath BW, Lattman KJ, Beals GL. Deploying portable gas chromatography–mass spectrometry (GC-MS) to military users for the identification of toxic chemical agents in theater. Appl Spectrosc. 2019;73(8):841–58.

16. McClenny WA, and Holdren, M. W. Compendium of methods for the determination of toxic organic compounds in ambient air -second edition - Compendium Method TO-15: Determination of volatile organic compounds (VOCs) in air collected in specially-prepared canisters and analyzed by gas chromatography/ mass spectrometry (GC/MS) [Internet]. Cincinnati, OH, USA: United States Environmental Protection Agency; 1999. [cited 27.11.2017]. Available from: https://www3.epa.gov/ttnamti1/files/ambient/airtox/to-15r.pdf.

17. Woolfenden E. Monitoring vocs in air using sorbent tubes followed by thermal desorption-capillary GC analysis: Summary of data and practical guidelines. J Air Waste Manage Assoc. 1997;47(1):20–36.

18. Liu Y, Misztal PK, Xiong J, Tian Y, Arata C, Weber RJ, Nazaroff WW, Goldstein AH. Characterizing sources and emissions of volatile organic compounds in a northern california residence using space- and time-resolved measurements. Indoor Air. 2019;29(4):630–44.

19. Price DJ, Day DA, Pagonis D, Stark H, Algrim LB, Handschy AV, Liu S, Krechmer JE, Miller SL, Hunter JF, de Gouw JA, Ziemann PJ, Jimenez JL. Budgets of organic carbon composition and oxidation in indoor air. Environ Sci Technol. 2019;53(22):13053–63.

20. Schripp T, Etienne S, Fauck C, Fuhrmann F, Märk L, Salthammer T. Application of proton-transfer-reaction-mass-spectrometry for indoor air quality research. Indoor Air. 2014;24(2):178–89.

21. Analytical Methods Committee AN. Thermal desorption Part 1: Introduction and instrumentation. Anal Methods. 2020;12(26):3425–8.

22. Hamilton JF. Using comprehensive two-dimensional gas chromatography to study the atmosphere. J Chromatogr Sci. 2010;48(4):274–82.

23. Majors R, Vickers A, Decker D. The art and science of GC capillary column production. LC GC N Am. 2007;25(7):616–31.

24. Lorenzo M, Pico Y. Chapter 2 - Gas chromatography and mass spectroscopy techniques for the detection of chemical contaminants and residues in foods. In: Schrenk D., Cartus A., editors. Chemical contaminants and residues in food (second edition). Sawston: Woodhead Publishing; 2017. p. 15–50.

25. Mani D, Kalpana MS, Patil DJ, Dayal AM. Chapter 3 - Organic matter in gas shales: Origin, evolution, and characterization. In: Dayal A.M., Mani D., editors. Shale gas. Amsterdam: Elsevier; 2017. p. 25–54.

26. Novaes FJM, Marriott PJ. Cryogenic trapping as a versatile approach for sample handling, enrichment and multidimensional analysis in gas chromatography. J Chromatogr. 2021;1644:1–14.

27. Minaeian J. Development and deployment of an airborne gas chromatography/mass spectrometer to measure tropospheric volatile organic compounds: University of York; 2016.

28. Ettre LS, Welter C, Kolb B. Determination of gas-liquid partition coefficients by automatic equilibrium headspace-gas chromatography utilizing the phase ratio variation method. Chromatographia. 1993;35(1):73–84.

29. Mayer BX, Rauter W, Kählig H, Zöllner P. A trifluoropropyl-containing silphenylene–siloxane terpolymer for high temperature gas chromatography. J Sep Sci. 2003;26(15–16):1436–42.

30. Lee ML, Kuei JC, Adams NW, Tarbet BJ, Nishioka M, Jones BA, Bradshaw JS. Polarizable polysiloxane stationary phases for capillary column gas chromatography. J Chromatogr. 1984;302:303–18.

31. Coskun O. Separation techniques: Chromatography. North Clin Istanb. 2016;3(2):156–60.

32. Mitra S, Kebbekus BB. Environmental chemical analysis. Boca Raton, FL, USA: CRC Press; 2018.

33. Niwa T. Basic theory of mass spectrometry. Clin Chim Acta. 1995;241–242:15–71.

34. Stein S. Mass spectral reference libraries: An ever-expanding resource for chemical identification. Anal Chem. 2012;84(17):7274–82.

35. Abou-Shakra FR. Chapter 12 - Biomedical applications of inductively coupled plasma mass spectrometry (ICP-MS) as an element specific detector for chromatographic separations. In: Wilson I.D., editor. Handbook of analytical separations. 4. Amsterdam: Elsevier Science B.V.; 2003. p. 351–71.

36. Portolés T, Pitarch E, López FJ, Hernández F, Niessen WM. Use of soft and hard ionization techniques for elucidation of unknown compounds by gas chromatography/time-of-flight mass spectrometry. Rapid Commun Mass Spectrom. 2011;25(11):1589–99.

37. Smith RW. Mass spectrometry. In: Siegel J.A., Saukko P.J., Houck M.M., editors. Encyclopedia of forensic sciences (second edition). Waltham: Academic Press; 2013. p. 603–8.

38. Donato P, Cacciola F, Beccaria M, Dugo P, Mondello L. Chapter 8 - Lipidomics. In: Picó Y., editor. Comprehensive analytical chemistry. 68. Amsterdam: Elsevier; 2015. p. 395–439.

39. Gushue JN. Chapter 11 - Principles and applications of gas chromatography quadrupole time-of-flight mass spectrometry. In: Ferrer I., Thurman E.M., editors. Comprehensive analytical chemistry. 61. Amsterdam: Elsevier; 2013. p. 255–70.

40. Lovestead TM, Urness KN. Gas chromatography/mass spectrometry. Mater charact. 10. Almere: ASM International; 2019. p. 1–16.

41. Libarondi M, Binkley J. Comparing the capabilities of time-of-flight and quadrupole mass spectrometers [Internet]. Iselin, NJ, USA: LCGC; 2010 [cited 01.06.2021]. Available from: https://www.chromatographyonline.com/view/comparing-capabilities-time-flight-and-quadrupole-mass-spectrometers-0.

42. Thomas SN. Chapter 10 - mass spectrometry. In: Clarke W., Marzinke M.A., editors. Contemporary practice in clinical chemistry (fourth edition). Washington D.C.: American Association for Clinical Chemistry; 2019. p. 171–85.

43. Radionova A, Filippov I, Derrick PJ. In pursuit of resolution in time-of-flight mass spectrometry: A historical perspective. Mass Spectrom Rev. 2016;35(6):738–57.

44. Guilhaus M. Special feature: Tutorial. Principles and instrumentation in time-of-flight mass spectrometry. Physical and instrumental concepts. J Mass Spectrom. 1995;30(11):1519–32.

45. Katzenstein HS, Friedland SS. New time-of-flight mass spectrometer. Rev Sci Instrum. 1955;26(4):324–7.

46. Rockwood AL, Kushnir MM, Clarke NJ. 2 - Mass spectrometry. In: Rifai N., Horvath A.R., Wittwer C.T., editors. Principles and applications of clinical mass spectrometry. Amsterdam: Elsevier; 2018. p. 33–65.

47. Hinshaw JV. The flame ionization detector. LC GC N Am. 2005;23(12):1262–72.

48. Chaulya SK, Prasad GM. Chapter 3 - Gas sensors for underground mines and hazardous areas. In: Chaulya S.K., Prasad G.M., editors. Sensing and monitoring technologies for mines and hazardous areas. Amsterdam: Elsevier; 2016. p. 161–212.

49. Martyr AJ, Plint MA. Chapter 16 - Engine exhaust emissions. In: Martyr A.J., Plint M.A., editors. Engine testing (fourth edition). Oxford: Butterworth-Heinemann; 2012. p. 407–50.

50. Finlayson BJ, Pitts JN. Photochemistry of the polluted troposphere. Science. 1976;192(4235):111–9.

51. Pereira KL, Dunmore R, Whitehead J, Alfarra MR, Allan JD, Alam MS, Harrison RM, McFiggans G, Hamilton JF. The effect of varying engine

conditions on unregulated VOC diesel exhaust emissions. Atmos Chem Phys Discuss. 2017;2017:1–25.

52. Muñoz A, Ródenas M, Borrás E, Vázquez M, Vera T. The gas-phase degradation of chlorpyrifos and chlorpyrifos-oxon towards oh radical under atmospheric conditions. Chemosphere. 2014;111:522–8.

53. Pereira KL, Dunmore R, Whitehead J, Alfarra MR, Allan JD, Alam MS, Harrison RM, McFiggans G, Hamilton JF. Technical note: Use of an atmospheric simulation chamber to investigate the effect of different engine conditions on unregulated VOC-IVOC diesel exhaust emissions. Atmos Chem Phys. 2018;18(15):11073–96.

54. Hofzumahaus A, Kraus A, Kylling A, Zerefos CS. Solar actinic radiation (280–420 nm) in the cloud-free troposphere between ground and 12 km altitude: Measurements and model results. J Geophys Res Atmos. 2002;107(D18):PAU 6-1–PAU 6-11.

55. Shao Y, Wang Y, Du M, Voliotis A, Alfarra MR, O'Meara SP, Turner SF, McFiggans G. Characterisation of the Manchester aerosol chamber facility. Atmos Meas Tech. 2022;15(2):539–59.

56. Hamilton JF, Rami Alfarra M, Wyche KP, Ward MW, Lewis AC, McFiggans GB, Good N, Monks PS, Carr T, White IR, Purvis RM. Investigating the use of secondary organic aerosol as seed particles in simulation chamber experiments. Atmos Chem Phys. 2011;11(12):5917–29.

57. Byrd G. Gas chromatography problem solving and troubleshooting: What is the deal with water-based samples on a capillary GC column? J Chromatogr Sci. 2005;43(8):305–6.

58. Walker G. Stirling cryocoolers. Cryocoolers: Part 1: Fundamentals. Boston, MA: Springer US; 1983. p. 95–183.

59. Wilson RB, Fitz BD, Mannion BC, Lai T, Olund RK, Hoggard JC, Synovec RE. High-speed cryo-focusing injection for gas chromatography: Reduction of injection band broadening with concentration enrichment. Talanta. 2012;97:9–15.

60. van Lieshout M, Janssen H-G, Cramers C. Combined thermal-desorption and pyrolysis gc using a ptv injector. Part I: Theory and practicle aspects [Internet]. 1996. [cited 17.03.2022]. Available from: https://gcms.cz/labrulez-bucket-strapi-h3hsga3/paper/024_TD_PY-Source-rock.pdf.

61. Armbruster DA, Pry T. Limit of blank, limit of detection and limit of quantitation. Clin Biochem Rev. 2008;29(Suppl 1):S49–S52.

62. Sadler WA. Using the variance function to estimate limit of blank, limit of detection and their confidence intervals. Ann Clin Biochem. 2016;53(1):141–9.

63. Johnson DL. Statistical tools for the comprehensive practice of industrial hygiene and environmental health sciences. Hoboken, NJ: Wiley; 2017.

64. Roessner U, Nahid A, Chapman B, Hunter A, Bellgard M. 1.33 - Metabolomics – the combination of analytical biochemistry, biology, and informatics. In: Moo-Young M., editor. Comprehensive biotechnology (second edition). Burlington, MA: Academic Press; 2011. p. 447–59.

65. Hopkins JR, Lewis AC, Read KA. A two-column method for long-term monitoring of non-methane hydrocarbons (NMHCs) and oxygenated

volatile organic compounds (O-VOCs). J Environ Monit. 2003;5(1):8–13.

66. United States Department of Commerce National Institute of Standards and Technology. Nist chemistry webbook [Internet]. 2022 [cited 20.10.2022]. Available from: https://webbook.nist.gov/chemistry/.

3. Aerosol Formation from VOCs

Abstract

A number of experiments were performed at the University of Manchester Aerosol Chamber that investigated decay of, and particle and secondary organic aerosol intermediate formation from, α-Pinene, toluene, and 1,3,5-trimethylbenzene under a variety of NO_x regimes, and abundance of OH and O_3. To assess the above, a novel GC-MS system incorporating a two-trap thermal desorption unit was used to allow for a finer time resolution during experiments. Particle formation was also observed through measuring particle number during a number of experiments. In experiments using α-Pinene, decay was greatest (>~90%), as was particle formation, where NO_2 was in greater proportion than NO. Decay was also highest where OH and O_3 were in higher concentrations. The greatest particle formation was observed in the experiment dated 31.10.2018, where 9858 particles cm^{-3} were formed. Toluene decay was greatest (67%) where OH was present, and NO_x was not. Particle formation was greatest (27,731 particles cm^{-3}) where NO was in greater proportion than NO_2. Near-complete decay was evident in most experiments using 1,3,5-trimethylbenzene (>98%), where it is seemingly most dependent on OH, with the final experiment using an $NO:NO_2$ ratio of 4:1. NO_x is thought to exert significant influence in the oxidative capacity of the atmosphere, both by controlling the abundance of oxidants, and by influencing new particle formation and, therefore, highly oxygenated molecules. Decay and particle formation is also seen to be affected by the ratio of NO to NO_2, with higher NO_2 leading to greater decay and particle numbers. Twelve SOA intermediates were produced, of which five are in agreement with the existing literature, with the mechanism by which they are created identified in the Master Chemical Mechanism, namely: oxalic acid, benzaldehyde, acetaldehyde, acetic acid, and dimethylbenzaldehyde.

3.1. Introduction

Aerosols serve an important purpose in the atmospheric energy budget, and atmospheric and biogeochemical processes more broadly, through interaction with solar and terrestrial radiation, and through absorption, scattering, and emission [1, 2]. Aerosols, but also cloud cover, water vapour, vegetation, and snow and ice cover — upon which aerosols e.g. black carbon can deposit — can further perturb the radiation balance of the Earth (the balance of absorbed and radiated solar energy) and impact planetary albedo [3-5]. Broadly, radiative forcing is used to measure changes in radiation balance caused by anthropogenic or biogenic elements [3]. Radiative forcing measurements can then be compared to ascertain the impact a given aerosol has on the Earth's climate [3]. The impact of anthropogenic aerosols on radiative forcing is uncertain due to difficulties in accurate quantification [2].

The main components of aerosols are organic and inorganic species, black carbon, mineral species, and primary biological aerosol particles [2]. In the atmosphere, organic aerosols can be emitted by both biogenic and anthropogenic sources, and constitute approximately 20–50% of global aerosol loading [6]. Components of these organic aerosols can be further distinguished as either directly emitted, primary organic aerosols (POAs), or as the result of the oxidation of VOCs; secondary organic aerosols (SOAs) [6]. SOAs are a significant element of organic aerosols, for example, fine particle mass makes up approximately half of organic aerosols in urban areas of the Northern Hemisphere; 65–95% of this fine particle mass is made up of SOAs [6]. POAs and SOAs typically reside in the atmosphere for days (more so for the former) to weeks (more so for the latter) [3]. New particles are formed by the nucleation of low-volatility vapours, forming molecular clusters which can condense, producing aerosols [2].

To initiate SOA formation, VOCs react with multiple species in the atmosphere, most notably OH, O_3, or NO_3 radicals, but also halogen species such as chlorine and bromine [7]. As VOCs begin to degrade, RO_2 and HO_2 radicals are formed, which in turn react with NO, thus converting NO to NO_2. Changes in overall NO_x concentrations, and the ratio between NO_2 and NO therein, will affect the rate at which the VOCs present will degrade [8].The process by which SOAs are formed more generally is illustrated below (adapted from by Kruza et al. [9])

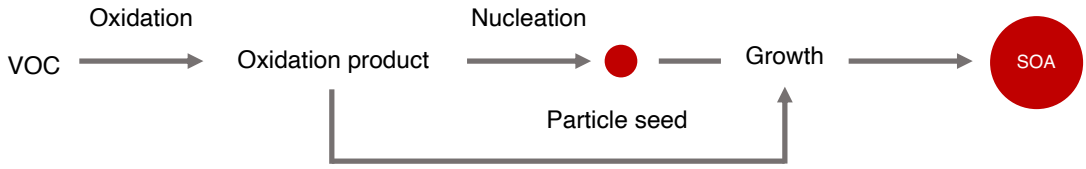

Figure 3.1: SOA formation as adapted from Kruza et al. [9]

Aerosols can also act as cloud condensation nuclei (CCN) and ice nuclei (IN) [2]. CCN are small atmospheric particles (>50–100 nm) that form an aerosol substrate upon which water vapour can condense, and thus develop into cloud droplets [10]. CCNs can be constituted of a number of different atmospheric aerosols, with SOAs formed from VOC oxidation being but one source; the hygroscopicity of different aerosols is the limiting factor of their propensity to form CCNs [11]. As clouds exert significant influence in the Earth's energy budget, an increase in atmospheric SOA concentrations could impact this system notably [10, 12, 13].

SOA precursors can originate from biogenic sources such as forests, peatlands, and other vegetation, and anthropogenic sources such as solvent use, biomass burning, transportation, and industrial processes [6]. Biogenic SOAs are thought to contribute significantly to annual global SOA fluxes, approximately 88 TgC yr^{-1}, as compared to anthropogenic sources at 10 TgC yr^{-1} [6]. Anthropogenic SOA precursors are predominantly alkanes (40%),

aromatics (20%), and alkenes (10%) [6]. These SOAs can then undergo further reaction with oxidants (e.g. OH, O_3, and NO_3) to form less volatile products [6]. In a study of 11 urban areas across three continents, the production rate of anthropogenic SOAs was strongly correlated with species reactivity, with differences between urban areas explained by varying emission rates of aromatics and VOCs [14].

SOA is an important component in $PM_{2.5}$ [15]. Exposure to $PM_{2.5}$ is estimated to cause 3–4 million premature deaths per year [14]. Modelled data linked approximately 340,000 premature deaths related to $PM_{2.5}$ exposure with anthropogenic SOAs per year [14]. Current estimates suggest that ~95% of the world's population live in areas where $PM_{2.5}$ concentrations exceed World Health Organization (WHO) annual average guidelines of 10 μg m^{-3} [14]. This is exacerbated in urban areas where higher population density is linked with both increased emissions of particulate matter and anthropogenic, gas-phase precursors [14].

Evidently SOA formation in urban areas could potentially be a significant issue as emissions of VOCs from commercially available products are now similar to those borne of the transportation sector [16]. Indeed, modelling of future scenarios suggests that globally, SOA burden in the atmosphere exceeds that of sulphate [17]. Moreover, models further predict that there could be a two-fold increase in SOAs over boreal and temperate forests by the year 2100 due to increased forest cover generating more BVOCs, but a reduction over tropical forests due to decreasing forest cover in those areas [17]. Increased average global temperatures could also mean that partition coefficients in the formation of SOAs are reduced, leading to an increase in SOA concentrations by 2100 [17].

As discussed in Chapter 4 and Heeley-Hill et al., VOCs are ubiquitous indoors and are derived from a variety of sources, such as product use, cleaning, cooking, and the infiltration of outdoor air inside [18]. Therefore, the

ubiquity of VOCs implies the production of SOAs. As people spend ~90% of their time indoors, human exposure to SOAs indoors, as opposed to other environments, could be considerable. Peroxy radicals generated following VOC oxidation could influence SOA production via the formation of highly oxygenated organic molecules (HOMs) through autooxidation of these radicals [9, 19]. HOMs are multifunctional, have low volatility and are thought to both increase SOA mass and influence their composition [9]. A study by Pagonis et al. estimates an average 11% yield of HOMs from the ozonolysis of limonene [20].

Terpenoid species are of particular interest as they are readily found in a variety of personal care and cleaning products, and can be off-gassed by existing furnishings [21, 22]. In addition, they are readily sorbed to surfaces due to moderate vapour pressures and via the direct application of cleaning products. Ozone, as an indoor oxidant, is particularly relevant here as primary loss of O_3 is to surface deposition. Singer et al. highlight the vapour pressure (P_0) of limonene as 200 Pa, and an octanal-air coefficient (Log K_{oa}) of 4.21 [23]. The authors calculated the ratio of mass of SOA formed and mass of ozone consumed by ozone-terpenoid surface reactions (ξ_s) as being between 0.70–0.91; this is likely due to changes in relative humidity [23]. To calculate the relative importance of surface chemistry and gas-phase chemistry, particle mass and formation was also calculated. Surface reactions generated between 126–339 no. cm^{-3} μg m^{-3} of formed SOA [23]. Gas-phase reactions generated between 51.1–60.2 no. cm^{-3} μg m^{-3} [23].

To better understand the formation of SOA, this study seeks to identify the formation of SOA intermediates that are created as a result of VOC oxidation, the aerosol chamber at the University of Manchester was used; the methodology is described in detail in Chapter 2. In the literature, SOA intermediates form as a result of successive oxidation processes leading to multigenerational products [24, 25]. Aerosol chambers are widely used in experimental methodologies due to the control that can be exerted during

these studies [26, 27]. They are often constructed of a large inert polymer bag, into which relevant compounds are added [26]. Chamber reactions can either be driven by natural or artificial sunlight, and other parameters such as relative humidity and temperature can be optimised to achieve different experimental conditions [26]. One consideration of chamber use is wall chemistry; this is particularly pertinent in SOA chemistry [28].

Differing chamber designs allow atmospheric chemistry studies to be divided into two main categories: those under artificial light conditions, and those under natural light conditions [26]. Experiments in the former are often performed in sealed polymer bags surrounded by insulation panels, and subject to adjustable light intensities. The latter taking place in 'outdoor' chambers fitted with transparent panelling to allow the infiltration of sunlight into the experimental area [29, 30]. This adaptability of conditions is complemented by the ability to connect a myriad of instruments to the chamber, allowing various facets of the same experiment to be analysed simultaneously [26, 31, 32]. Oxidation experiments are, therefore, well-suited to the chamber environment [26].

Extant studies outline a myriad of different setups, usually using GC-MS instrumentation, but other chromatographic and spectroscopic techniques can be used [31, 32]. Previous studies also highlight the use of chambers in experiments focussed on SOA formation [33, 34]. In these experiments, the aircraft GC-MS (AGC-MS) was used to measure VOC decay and the potential formation of SOA intermediates.

In addition to the chamber experiments, the Master Chemical Mechanism (MCM) was used to further elucidate oxidation processes. The MCM is a near-explicit mechanism that describes gas-phase degradation of 143 VOCs (as of version 3.3.1) in the atmosphere, and the subsequent production of ozone and secondary products, through product and kinetic information as it relates to VOC oxidation [35, 36]. Further, it is assumed that knowledge of

product and kinetic information of a small number of chemicals can be more broadly applied to species for which this information is unknown by virtue of structure-reactivity correlations [35]. The MCM (v.3) details 12,691 reactions of 4,351 organic species and 46 associated inorganic reactions. The mechanism also details the degradation of: 22 alkanes, 20 alkenes (including dienes and monoterpenes), 1 alkyne, 18 aromatics, 6 aldehydes, 10 ketones, 17 alcohols and glycols, 10 ethers and glycoethers, 8 esters, 3 carboxylic acids, 2 other oxygenated VOCs, and 8 chlorinated hydrocarbons [35]. Subsequent updates to MCM the mechanism (to v.3.3.1) have been outlined in the literature [37, 38].

The MCM works to initiate the chemical reaction of a VOC via photolysis, with OH, O_3, or NO_3 [35]. Then, reactions of intermediates following the initial chemistry are considered, with the degradation of first and subsequent generation products allowed for [35]. These degradation steps continue until either CO_2 is generated, or the subsequent chemistry has been previously described elsewhere in the mechanism [35]. See Figure 3.2 which is a flow chart of the process illustrated by Saunders et al. [35]

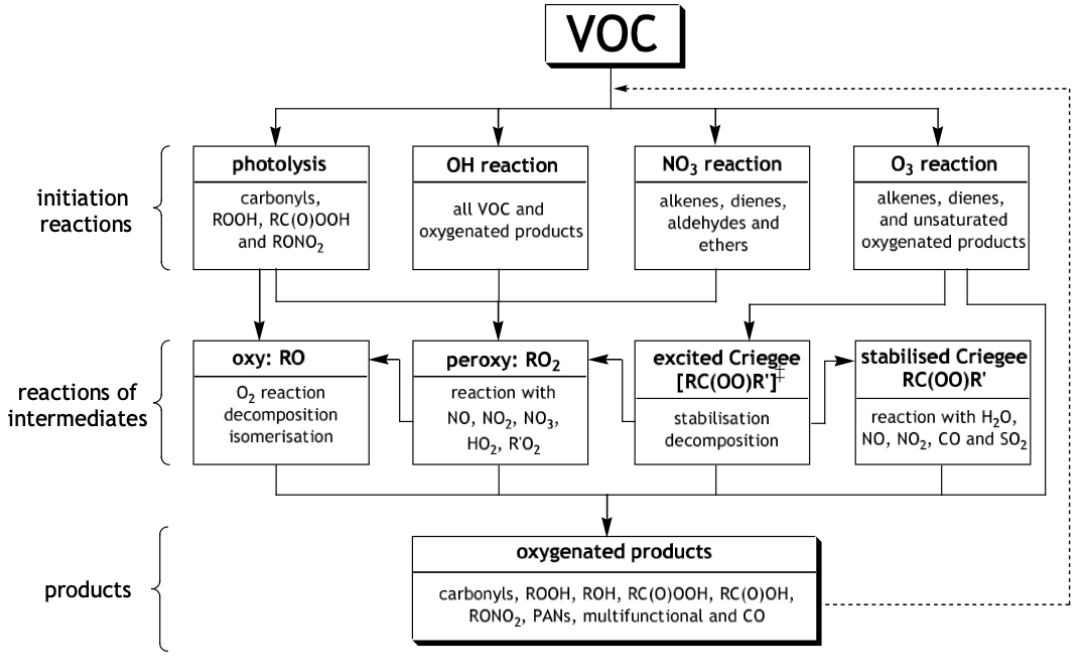

Figure 3.2: Flow chart depicting VOC degradation and product generation chemistry as used in the MCM [35]

The MCM is not fully explicit as the number of reactions from such a mechanism would be not practicable [35]. Therefore, the MCM is necessarily simplified by limiting the proliferation of chemistry via low-probability pathways and by simplifying some degradation schemes [35]. Self and cross-reaction of organic peroxy radicals is also parameterised [35]. The box-model can be downloaded to allow for changes in parameters, and the full mechanism can be browsed online on the MCM website (mcm.york.ac.uk).

3.1.1. Study objectives

A series of experiments was designed to measure the decay of a number of VOCs in different scenarios — namely α-Pinene, toluene, and 1,3,5-trimethylbenzene — along with particle and SOA intermediate production from these experiments (see Table 3.2). Experiments were conducted with differing NO_x and oxidant regimes, in light and dark conditions, and with

differing relative humidities. The AGC-MS was selected to monitor this decay in VOCs and the attendant SOA intermediate production due to the high time resolution in which samples could be taken, and the qualitative information that could be derived from the analysis. Due to significant baseline noise from one trap, results presented herein will be from the functioning trap only, leading to one sample approximately every 16 minutes. These experiments took place in a month-long period between October and November 2018.

3.2. Methodologies

3.2.1. Chamber Description

The University of Manchester Aerosol Chamber is composed of an 18 m^3 fluorinated ethylene propylene Teflon bag suspended within movable aluminium frames, allowing the bag to expand and contract during the experimental process, and is surrounded by reflective plastic sheeting [39, 40]. Lighting is provided by two filtered 6 kW Xenon arc lamps and a series of wall-mounted halogen lamps, replicating the actinic range in the atmosphere, which is between 280–420 nm; the chamber has a wavelength range of 290–800 nm [29, 39, 41]. A heated bulb allows for the injection of VOCs, and NO_x is introduced to the chamber via a cylinder [39].

NOx and oxidant measurements

NO_x (NO and NO_2) was measured using a Thermo Scientific 42i NO_x chemiluminescence analyser [29]. Some disparity between the instrument NO_x readings and NO_x defined as NO + NO_2 is evident from Table 3.1. In all but one instance, where the difference was ~9%, the difference between the two measurements was <5%. Confounding factors in the use of chemiluminescence analysers have been outlined in the literature and include collisional quenching of NO_2, conversion of nitrogen-containing species to NO_x, removal or interconversion of NO/NO_2 within the system,

and through the chemiluminescence of other species; these factors could therefore contribute to the discrepancies observed here [42].

Oxidant mixing ratios were measured throughout each experiment; O_3 was measured using a Thermo Electron Corporation 49C analyser, OH was not measured directly, but calculated by way of an OH 'clock', relative to the decay of the injected VOC and loss of the VOC associated with O_3 [29]. These calculations have been explained in greater detail by Barmet et al. [43] and have been applied to the context of the chamber by Voliotis et al. [44] The calculation follows an integrated first order rate law as detailed in Equation 3.1(a) and (b):

(a)

$$\ln([VOC]) = -k \times [OH] \times t + \ln([VOC]_0)$$

Equation 3.1 (a): Integrated first order rate law to calculate OH mixing ratios, where $\ln([\mathrm{VOC}])$ is the natural logarithm of the concentration of a given VOC, k is the rate constant, t is time (in this instance, seconds), and $\ln([VOC]_0)$ is the natural logarithm of the initial concentration of a given VOC. Therefore, OH concentration is determined by plotting the natural logarithm of the concentration of a given VOC against time, Equation 3.1 (b):

(b)

$$[OH] = \frac{-slope}{k}$$

Equation 3.1 (b): OH concentration determined by slope over rate, k

Wall losses

Chemical adsorption to the chamber (wall loss) is estimated to be significant and can impact reactivity and subsequent chemistry, such as SOA formation [45]. Wall losses have been described by Shao et al. [29] and are presented below in Table 3.1. NO_2 (50 ppb), O_3 (120–350 ppb), and other VOCs (50 ppb) were injected into the chamber and their loss to the walls observed under dark conditions, for four hours. Temperature and relative humidity were maintained at ~25°C and ~50% respectively.

Table 3.1: First-order wall loss rate for NO_2, O_3, α-Pinene, Toluene, and 1,3,5-trimethylbenzene at the University of Manchester Aerosol Chamber

	First-order Wall Loss Rate (s^{-1})
NO_2	$9.40 \pm 7.38 \times 10^{-7}$
O_3	$2.09 \pm 0.97 \times 10^{-6}$
α-Pinene	$2.24 \pm 0.67 \times 10^{-5}$
Toluene	$2.06 \pm 1.25 \times 10^{-5}$
1,3,5-trimethylbenzene	$12.22 \pm 0.90 \times 10^{-5}$

The wall loss of particles is more difficult to define, as it is influenced by a variety of factors such as convection, diffusion, settling, and electrostatics [29]. The use of air conditioning and the attendant agitation of the polymer bag, as well as changes in relative humidity can influence particle wall loss [29].

Particle wall loss was measured via a series of experiments with different humidities and mixing conditions (AC on or off) [29]. An ammonium sulphate (AS) seed was injected into the chamber at a concentration of 50–100 $\mu g\ m^{-3}$, and a modal diameter of ~100 nm, and decayed under dark conditions for approximately four hours [29]. The concentration was observed using a Differential Mobility Particle Sizer (DMPS) at 40–600 nm at a 10 minute scanning time [29]. Thereafter, to derive a decay rate coefficient, an

exponential function was applied to the decay of the particle number in each size bin of the DMPS [29].

Broadly, the particle wall loss rate decreased with increasing particle size, with humidity and mixing conditions having a seemingly moderate impact in reducing wall loss rate [29]. When particle sizes between 100 nm and 500 nm are considered, at 50% RH and with AC on, the mean wall loss rate was estimated to be -1.4– -0.67 x 10^{-4} s^{-1}, with AC off, the mean wall loss rate was reduced to -1.1– -0.4 x 10^{-4} s^{-1}. At 20% humidity with AC on, the mean wall loss rate was estimated to be -1.1– -0.67 x 10^{-4} s^{-1}, with the AC off, the mean wall loss rate was reduced to -0.4– -0.3 x 10^{-4} s^{-1} [29]. particles of <100 nm generally have a slightly higher loss rate than those of 100 nm [29].

3.2.2. Experimental methodology

At the chamber, a variety of VOCs, NO_x and oxidant regimes, and light conditions were used. Experiments varied in duration, with the median duration being 309 minutes. Three different VOCs were used individually in each experiment: α-Pinene, toluene, and 1,3,5-trimethylbenzene, and in varying mixing ratios.

During these experiments only the VOC and NO_x were directly injected into the chamber, wherein OH and O_3 were subsequently generated. O_3 is generated via the photolysis of NO_2 through the following reactions in R 3.1 [46]:

$$NO_2 + h\nu \rightarrow NO + O(^3P)$$
$$O(^3P) + O_2 \rightarrow O_3 \qquad \text{(R 3.1)}$$

O_3 then reacts rapidly with NO to form OH through the following reactions in R 3.2 [47, 48]:

$$\begin{aligned} &O_3 + NO \rightarrow NO_2 \\ &O_3 + h\nu \rightarrow O(^3P) + O_2 \\ &O_3 + h\nu \rightarrow O(^1D) + O_2 \\ &O(^1D) + H_2O \rightarrow 2OH \end{aligned} \qquad \text{(R 3.2)}$$

During the experiments dated 14.11, 15.11, 16.11, 23.11, and 29.11.2018, HONO was used as a source OH radicals. OH is generated through the photolysis of HONO through the following reaction in R 3.3 [49]:

$$HONO + h\nu \rightarrow OH + NO \qquad \text{(R 3.3)}$$

HONO and OH are also generated through the following reaction in R 3.4 [49]:

$$NO_2 + H_2O \rightarrow OH + HONO \qquad \text{(R 3.4)}$$

Table 3.2 details the chamber conditions of each experiment. Each VOC is listed with the assumed injected mixing ratio. RH refers to relative humidity, Lights specifies whether the chamber remained lit (on) or whether the experiment was performed under dark conditions (off). The maxima of NO, NO_2, NO_x, O_3, and OH are provided in mixing ratios, expressed as ppb. Directly measured mixing ratios are reported to three significant figures by default, but values are truncated to fewer significant figures where additional decades may confer artificial precision.

Table 3.2: Overview of experimental conditions of the chamber. NO_x data were not collected for the experiments dated 21.11.2018 and 23.11.2018

Date	VOC	Duration (mins)	RH (%)	Lights	NO (ppb)	NO_2 (ppb)	NO_x (ppb)	O_3 (ppb)	OH (ppb)
23.10.18	α-Pinene (100 ppb)	286	50	On	36	144	180	34.7	6.18×10^{-5}
24.10.18	α-Pinene (100 ppb)	367	53	On	140	67.5	189	1.92	1.05×10^{-4}
26.10.18	α-Pinene (100 ppb)	227	50	Off	91.2	90.5	181	-	-
31.10.18	α-Pinene (100 ppb)	314	50	On	8.5	6	14.5	25.3	8.75×10^{-5}
01.11.18	α-Pinene (100 ppb)	349	55	On	70.5	130	195	40	9.06×10^{-5}
02.11.18	α-Pinene (100 ppb)	365	10	On	70.5	133	195	60.9	3.81×10^{-4}
13.11.18	Toluene (200 ppb)	309	55	On	96	294	380	-	6.07×10^{-4}
14.11.18	Toluene (200 ppb)	297	50	On	384	306	690	-	0.00411
15.11.18	Toluene (200 ppb)	367	50	On	17.6	39.3	55.5	-	0.00242
16.11.18	Toluene (200 ppb)	255	20	On	19.2	45.1	63.9	-	8.92×10^{-4}
21.11.18	1,3,5-tmb (200 ppb)	317	20	On	-	-	-	-	4.11×10^{-4}

23.11.18	1,3,5-tmb (200 ppb)	275	20	On	-	-	-	-	0.002
29.11.18	1,3,5-tmb (200 ppb)	122	20	On	206	908	1113	-	0.00473

Analysis of samples was performed using the AGC-MS composite instrument, consisting of a Markes TT24-7 thermal desorption unit (Markes International, Llantrisant, UK), an Agilent 6850 gas chromatograph, and an Agilent 5875C mass spectrometer (both Agilent Technologies, Santa Clara, CA, USA). The GC was equipped with a generic diphenyl dimethyl polysiloxane column, which allows for the analysis of hydrocarbons and semi-volatile compounds. The AGC-MS was calibrated using a high pressure gravimetrically prepared custom standard gas prepared at the Wolfson Atmospheric Chemistry Laboratories, University of York.

A list of nine chemical species was prepared that encompassed commonly found BTEX species, monoterpenes, isoprene, and 1,3,5-trimethylbenzene. These species were identified by the University of Manchester chamber group as potential species of interest in their experiments. Liquid standards were procured, and calculations performed to identify the volume of standard required to correspond to parts per billion volume of each species when diluted. Subsequently, liquid standard was injected, at one end of the cylinder, directly into a modified evacuated Restek 1 L cylinder via a one directional tap and a GC septum secured to the cylinder with a 1” Swagelok nut. This allowed the liquid standard to be transferred from the syringe to the cylinder with minimal loss of vacuum in the cylinder. The opposing end of the cylinder was again modified with a one directional tap and a length of ¼” stainless steel tubing. Depending on configuration, this setup ensures flow through the cylinder in only one direction.

As stated, prior to injection, the 1 L cylinder was evacuated to sub-atmospheric pressure, refilled with ambient air, and evacuated. This cycle was repeated three times. The 1 L cylinder was then attached to an evacuated 10 L cylinder, that had been evacuated to sub-atmospheric pressure (~300 Pa), to allow for dilution. To transfer the standard mixture to the larger cylinder, the 1 L cylinder was connected to a high-pressure CP-grade nitrogen cylinder at one end, and the larger cylinder at the other.

Initially, the 1 L cylinder was washed through with a low flow of nitrogen for several minutes. The 1 L cylinder was then disconnected, and the 10 L was attached directly to the nitrogen cylinder, where it was filled to 5 MPa. It was then vented to atmospheric pressure and refilled to 5 MPa, resulting in a two-stage dilution to a mixing ratio per compound of approximately 5 ppb. Figure 3.3 displays a typical chromatogram of the described gas standard provided by the AGC-MS.

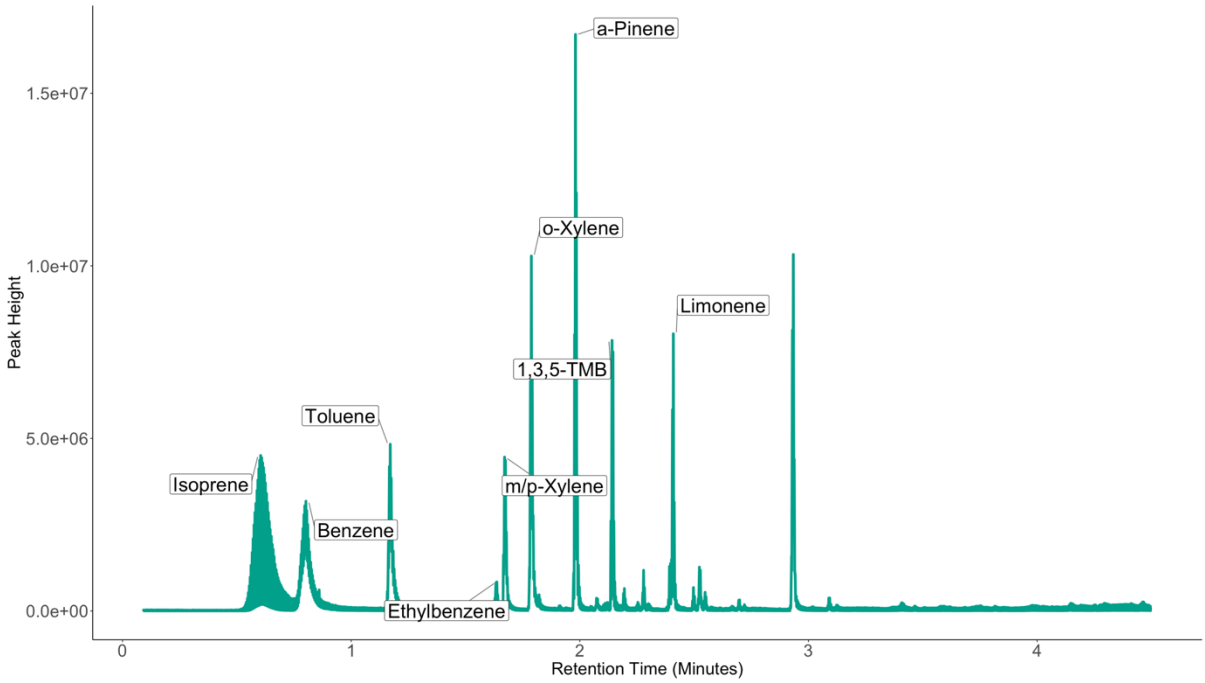

Figure 3.3: AGC-MS signal for the custom blended gas calibration mix for the oven programme outlined in Table 2.6

The AGC-MS was situated adjacent to the chamber. The chamber sample outlet was connected to the sample inlet of the AGC-MS. Carrier gas was provided by a CP-grade helium cylinder; this also powered the pneumatic valves in the TDU. Whilst the chamber was prepared for experimentation, the GC-MS was set to run a series (~6) of instrument blank samples, where no sample or calibration gas was flowing through the system, but the thermal

desorption traps were set to fire as per the experiment sampling times. A calibration run of four to six samples, followed by a number of instrument blanks, until the experiment start time, was then set. To maintain a fast time resolution, the GC-MS was set to run throughout the entire experimentation period of a given day and operated in TIC mode. During the sampling phase, a flow rate of 100 mL was maintained for six minutes, resulting in a sample of 600 mL.

In addition to the AGC-MS, a DMPS (TSI Instruments, Shoreview, MN, USA) was attached to the chamber to measure particle formation during VOC oxidation. The DMPS is managed by the Centre for Atmospheric Science at the University of Manchester. Particle number results from the DMPS are presented alongside the VOC decay plots later in this chapter.

3.2.3. Statistical methodology

As described in Chapter 2, VOCs and potential SOA intermediates were identified and quantified using Agilent MassHunter qualitative and quantitative software. To account for instrument background readings, the mean of AGC-MS blank peak areas summed with peak areas from the chamber background data were subtracted from the compound peak areas to create blank corrected data.

Decay percentage is defined as the decrease between the maximum mixing ratio in ppb and the mixing ratio recorded at the end of the experiment period in ppb, expressed as a percentage. The decay rate is defined as the difference in mixing ratio between the maximum and end mixing ratios divided by the duration of the experiment in minutes. The decay rate value is given in ppb decrease per minute (ppb min^{-1}); see Table 3.3

Data manipulation and visualisation was conducted using R v.4.02 “Taking off Again” and the RStudio environment v.1.3.1073 “Golden Rod”, using the

dplyr (v.1.0.2) package and plotted using *ggplot2* (v.3.3.2) of the *tidyverse* (v.1.3.0) package. Mixing ratio data in the VOC decay plots were displayed using geom_line(). Particle formation and decay plots were displayed using twin axis line plots in Microsoft Excel software.

Table 3.3: Overview of maximum and end VOC mixing ratios (MR) and decay statistics.

Experiment Date	Duration (mins)	Maximum VOC MR (ppb)	End VOC MR (ppb)	Decay (%)	Decay Rate (ppb min^{-1})
23.10.18	286	11.5	1.4	88.2	0.04
24.10.18	367	22.8	15.5	32.2	0.02
26.10.18	227	35.1	30	14.7	0.02
31.10.18	314	29.2	12.6	56.9	0.05
01.11.18	349	22.8	2.3	89.9	0.06
02.11.18	365	38.5	0.5	98.7	0.10
13.11.18	309	76.3	57	25.3	0.06
14.11.18	297	20.9	9.1	56.6	0.04
15.11.18	367	25.1	8.4	66.6	0.05
16.11.18	255	55.5	30.1	45.8	0.10
21.11.18	317	61.3	42	31.4	0.06
23.11.18	275	201	4	98	0.72
29.11.18	122	8726	50.2	99.4	71.1

3.3. Results and Discussion

3.3.1. Decay and particle formation

A grid of all decay experiments per compound is presented displaying mixing ratio data of the parent VOC, of the pertinent oxidants, and of NO_x (see Figure 3.3). Individual decay experiments are displayed with the same mixing ratio data for the parent compound, alongside particle number data. This is to illustrate the point at which particles are formed, and the extent to which they are formed, in relation to decay of the parent VOC.

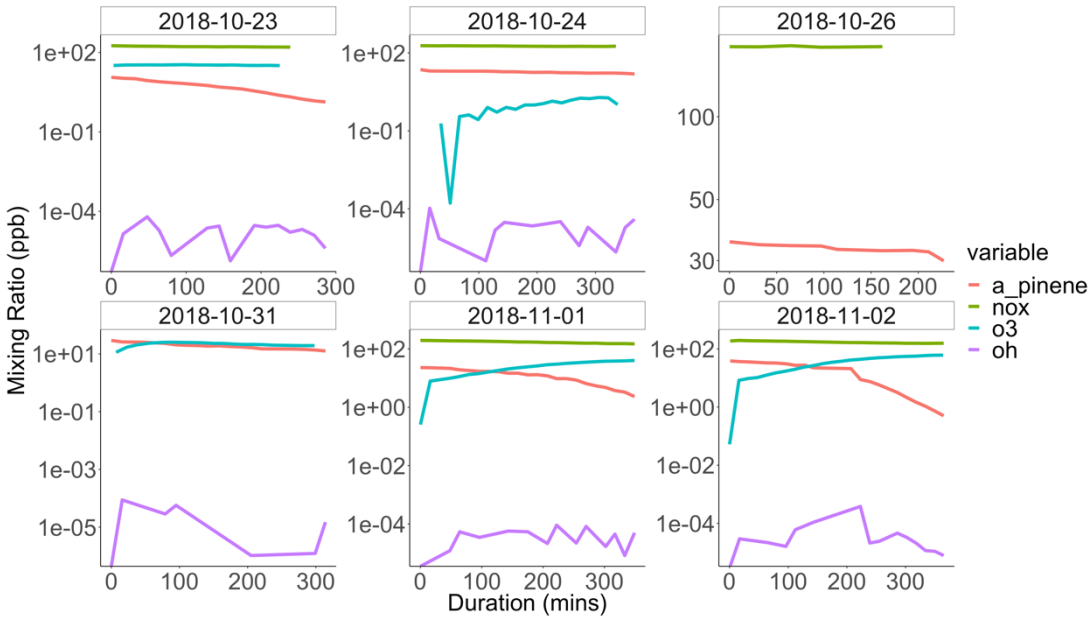

Figure 3.3: α-Pinene decay during multiple experiments between 23.10.2018 and 02.11.2018. The red line represents α-Pinene decay, the green line represents NO_x, the blue line represents O_3, and the purple line represents OH. All mixing ratios are expressed in ppb and on a $\log_{10}$ scale. Experiment duration is expressed in minutes.

Regarding α-Pinene (see Figure 3.3), the greatest decay was observed during the experiment dated 02.11.2018 (~99%), with experiments dated 01.11.2018 and 23.10.2018 also displaying decay above 88%. As outlined in

Table 3.2, these experiments had a 3:1 $NO:NO_2$ ratio. The experiment dated 02.11.2018 also had significantly higher mixing ratios of other oxidants, explaining, at least in part, the greater decay in the experiment period. By contrast, in the experiment dated 24.10.2018, decay was measured at 32%. Here, the $NO:NO_2$ ratio was reversed so that the mixing ratio of NO was significantly higher than that of NO_2. O_3 was also measured at less than 2 ppb, whilst the mixing ratio of OH remained consistent with the latter experiments. The least decay was observed during the experiment dated 26.10.2018 (~15%), where the $NO:NO_2$ ratio was 1:1, O_3 and OH was not present, and the chamber lights were turned off, therefore limiting any photolysis.

As can be seen in the majority of the experiments using α-Pinene, OH often peaked multiple times in the experiment, and as OH is an effective oxidant, these peaks often triggered greater levels of decay. This was particularly apparent in the experiments dated 23.10.2018, 24.10.2018, and 02.11.2018. Mixing ratios of NO_x remained relatively consistent, but as described in Tables 3.2 and 3.3, the ratio of NO to NO_2 remained important in overall VOC decay. This is explained in more detail later in this section, but briefly, decay was greatest in experiments where NO was in greater proportion to NO_2. The experiment dated 31.10.2018 measured dark decay, so decay via photolysis was extremely limited.

NO_x mixing ratios were also very low. NO_x mixing ratios lower than parts per billion are very difficult to achieve at the aerosol chamber due to the ambient levels observed in urban central Manchester, UK, where the chamber is located [44]. As such, oxidants were relatively unhindered in abundance; decay was greatest when OH and O_3 mixing ratios are highest. Where O_3 was present in the experiment, total decay was notably higher, implying that O_3 contributed significantly to the overall oxidation of α-Pinene. Ozonolysis of α-Pinene is identified in the literature as a major contributor to new particle

and SOA formation, and as explained later in Section 3.3.2, triggers autoxidation in α-Pinene [50, 51].

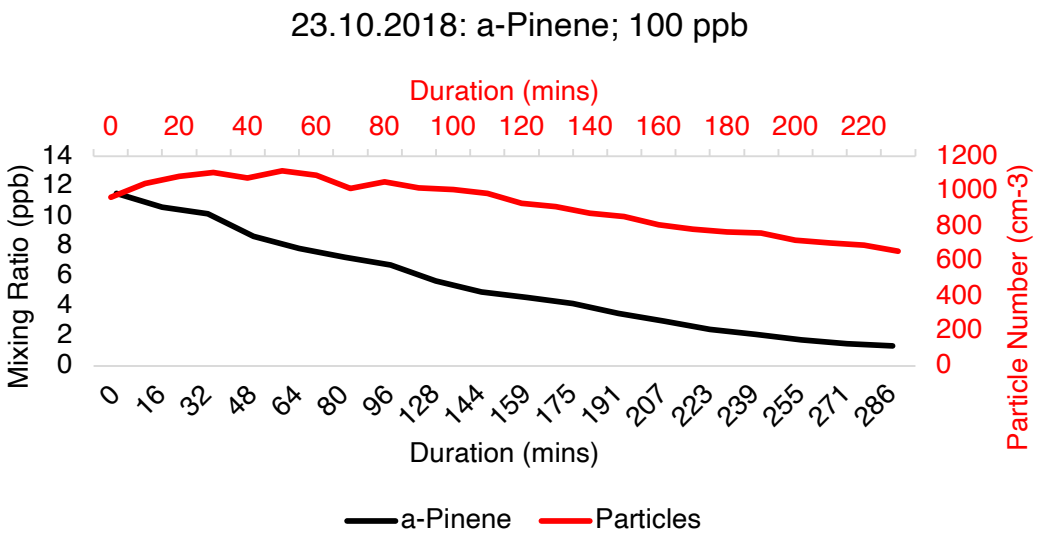

Figure 3.4: α-Pinene decay and particle number. The black line represents α-Pinene decay and is expressed in ppb, and the red line represents particle number in no. cm^{-3}. Duration is expressed in minutes

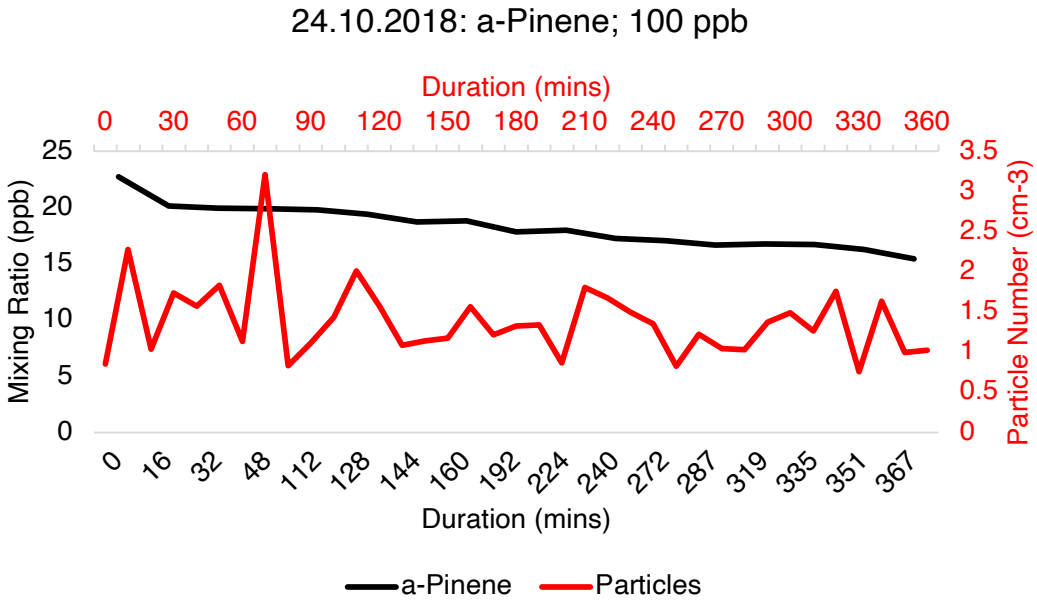

Figure 3.5: α-Pinene decay and particle number. The black line represents α-Pinene decay and is expressed in ppb, and the red line represents particle number in no. cm^{-3}. Duration is expressed in minutes

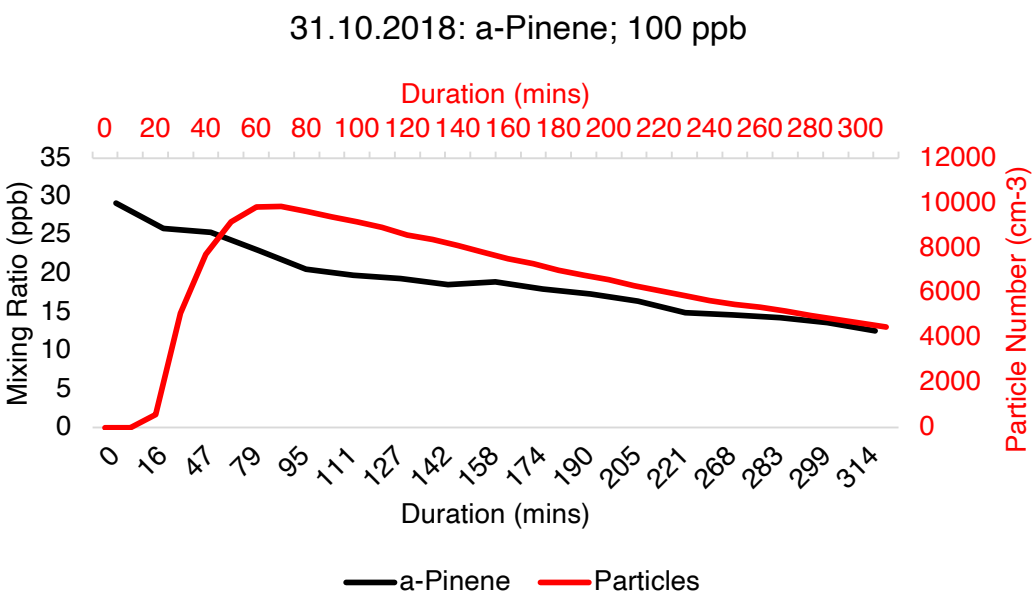

Figure 3.5: α-Pinene decay and particle number. The black line represents α-Pinene decay and is expressed in ppb, and the red line represents particle number in no. cm^{-3}. Duration is expressed in minutes

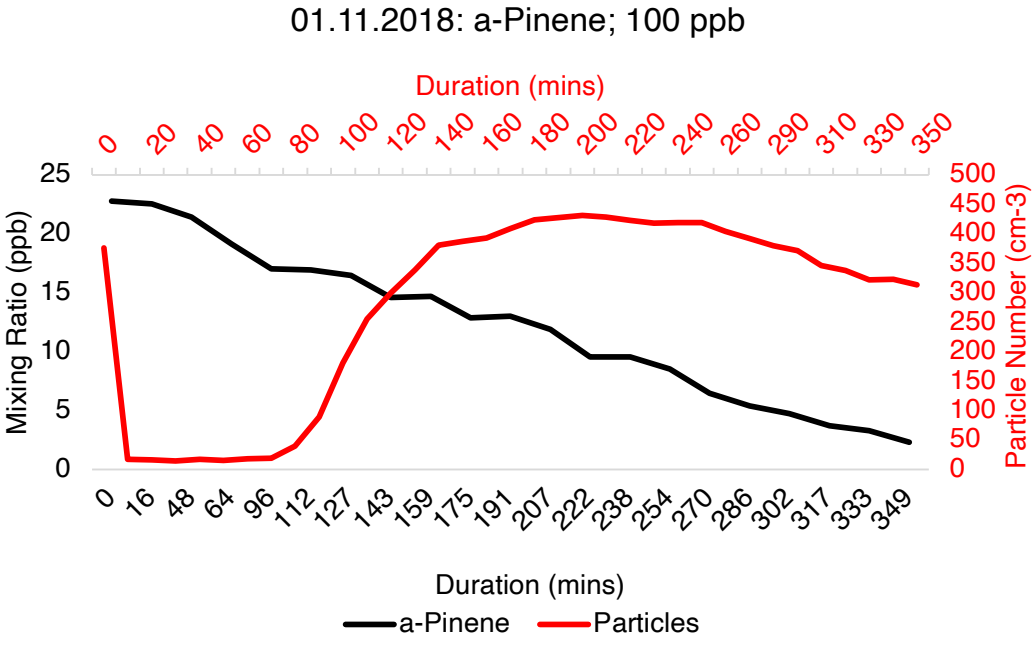

Figure 3.6: α-Pinene decay and particle number. The black line represents α-Pinene decay and is expressed in ppb, and the red line represents particle number in no. cm^{-3}. Duration is expressed in minutes

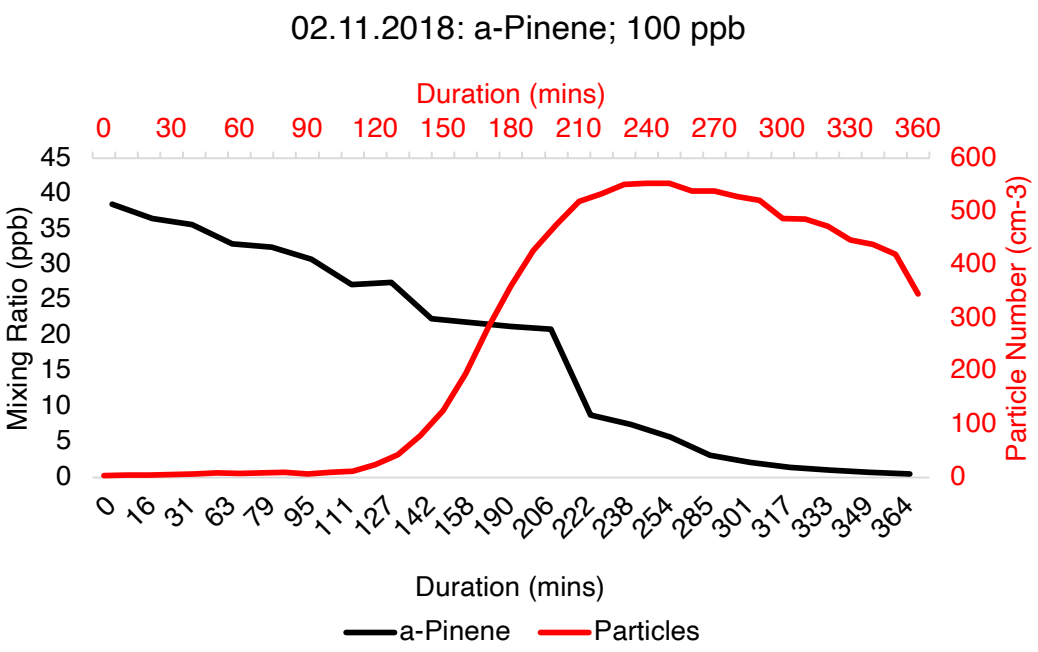

Figure 3.7: α-Pinene decay and particle number. The black line represents α-Pinene decay and is expressed in ppb, and the red line represents particle number in no. cm^{-3}. Duration is expressed in minutes

Similarly to trends found when considering the decay data solely, particle formation was greatest in experiments where the NO_x ratio used contained a larger proportion of NO_2 than NO. Conversely, particle formation was depressed when the NO proportion was larger than NO_2. The greatest number of particles were produced during the experiment dated 31.10.2018 with a maximum of 9858 particles cm^{-3} formed. The experiment dated 24.10.2018 produced the lowest number of particles, with a maximum of 3.2 particles cm^{-3} produced.

Regarding particle formation, the least particle formation was observed in the experiment dated 24.10.2018 (maximum = 3.21 particles cm^{-3}). This experiment used an NO:NO_2 ratio of 1:2. A relatively low mixing ratio of O_3 was present (1.9 ppb) as was a relatively high OH mixing ratio. The highest mixing ratio, as mentioned earlier, was observed during the experiment dated 31.10.2018 (9,858 particles cm^{-3}). In this experiment, NO was in

greater abundance than NO_2, but abundance of both was very low (8.5 and 6 ppb respectively). This suggests that the presence of NO_x, above a certain mixing ratio, could inhibit particle production from α-Pinene decay. Perhaps notably, in experiments dated 01.11.2018 and 02.11.2018, particle formation was evidently delayed following injection of α-Pinene. In other experiments detailed, particle formation was almost concurrent with α-Pinene decay. As discussed earlier, in the experiments dated 01.11.2018 and 02.11.2018, the $NO:NO_2$ ratio was 2:1, and O_3 mixing ratios were higher. It is also noteworthy that near-complete decay was observed by the conclusion of the experiment in both instances. No particle data were collected during the experiment dated 26.10.2018.

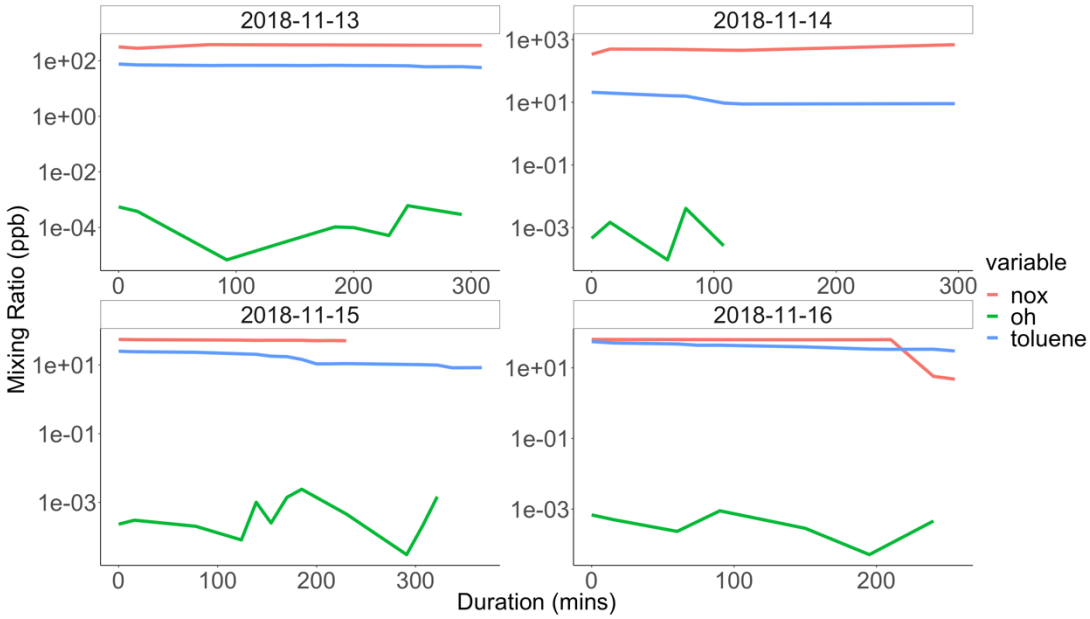

Figure 3.8: Toluene decay during multiple experiments between 13.11.2018 and 16.11.2018. The blue line represents toluene decay, the red line represents NO_x, and the green line represents OH. All mixing ratios are expressed in ppb and on a log_{10} scale. Experiment duration is expressed in minutes.

Regarding toluene (see Figure 3.8), the greatest decay (67%) was observed during the experiment dated 15.11.2018, where the $NO:NO_2$ ratio was

approximately 2:1, albeit in low mixing ratios, but the OH mixing ratio was relatively high. Similar NO_x conditions, i.e. 2:1 $NO:NO_2$ ratio, were observed in the experiment dated 16.11.2018. These conditions resulted in a decay of ~46%, likely because OH mixing ratios were relatively low. Similar results were observed during the experiment dated 14.11.2018, where decay was 56% with a higher OH mixing ratio, but with a 4:3 $NO:NO_2$ ratio; no O_3 was present. Unfortunately, only limited NO_x data were available for this experiment. The least decay (25%) was observed in the experiment dated 13.11.2018, where OH was in low concentration and the $NO:NO_2$ ratio was 3:1.

Similarly to those experiments using α-Pinene, OH peaked several times during the experiment, often at the start, in the middle, and towards the end of the experiment. Where OH peaks, decay rates often increased, perhaps most notably in the experiments dated the 14 and 15.11.2018. In the experiments dated 13 and 14.11.2018, NO_x increased as toluene began to decay, and during the experiment dated 14.11.2018, NO_x continued to increase towards the end of the experiment concurrent with the decay of toluene.

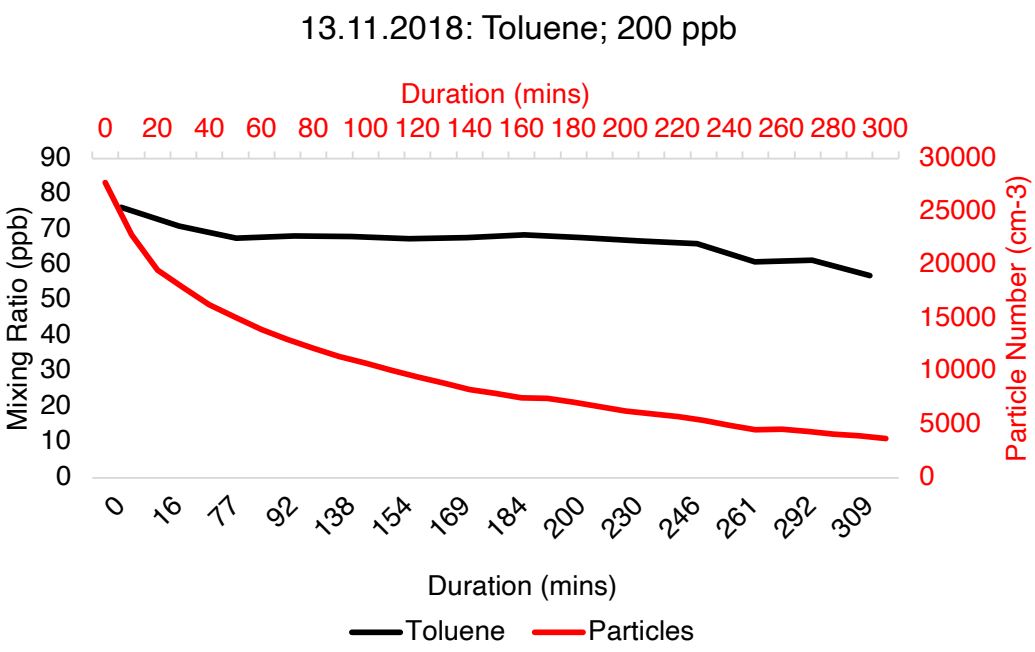

Figure 3.9: Toluene decay and particle number. The black line represents toluene decay and is expressed in ppb, and the red line represents particle number in no. cm^{-3}. Duration is expressed in minutes

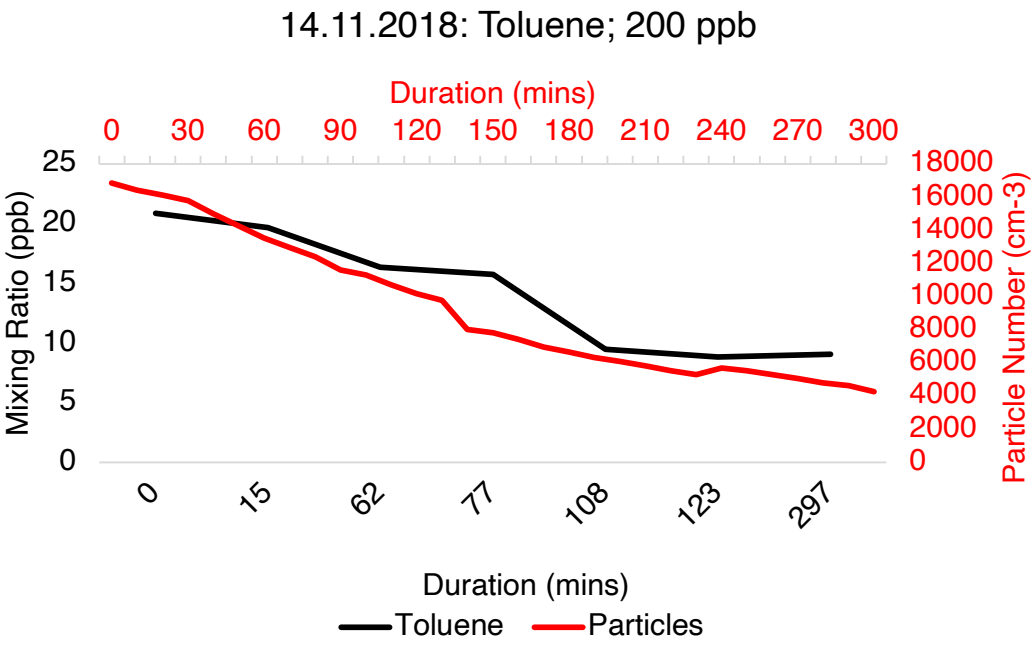

Figure 3.10: Toluene decay and particle number. The black line represents toluene decay and is expressed in ppb, and the red line represents particle number in no. cm^{-3}. Duration is expressed in minutes

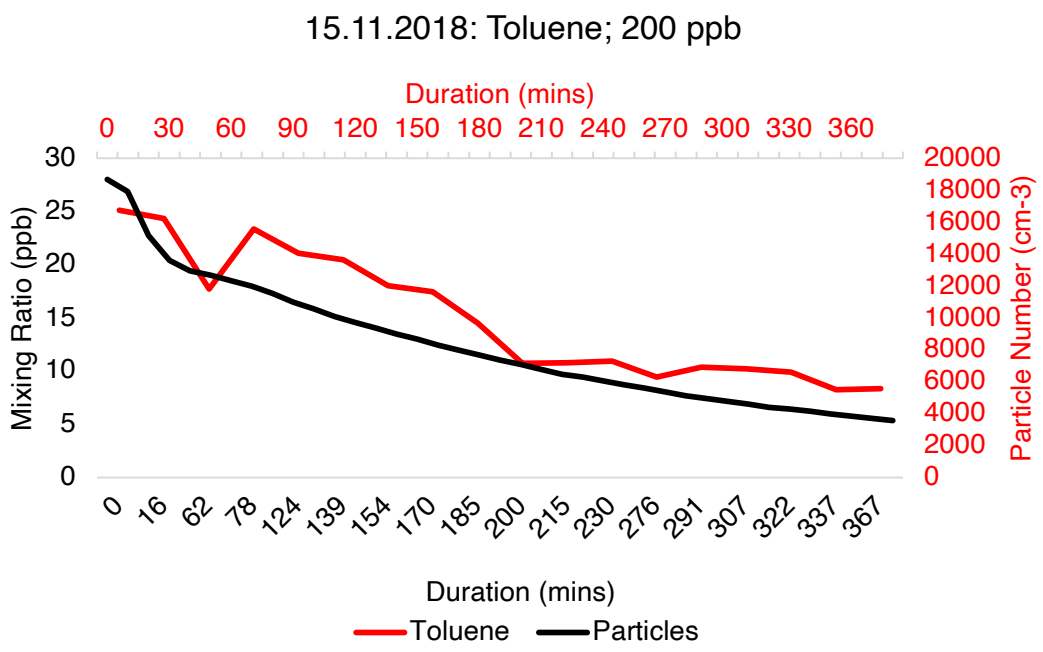

Figure 3.11: Toluene decay and particle number. The black line represents toluene decay and is expressed in ppb, and the red line represents particle number in no. cm^{-3}. Duration is expressed in minutes

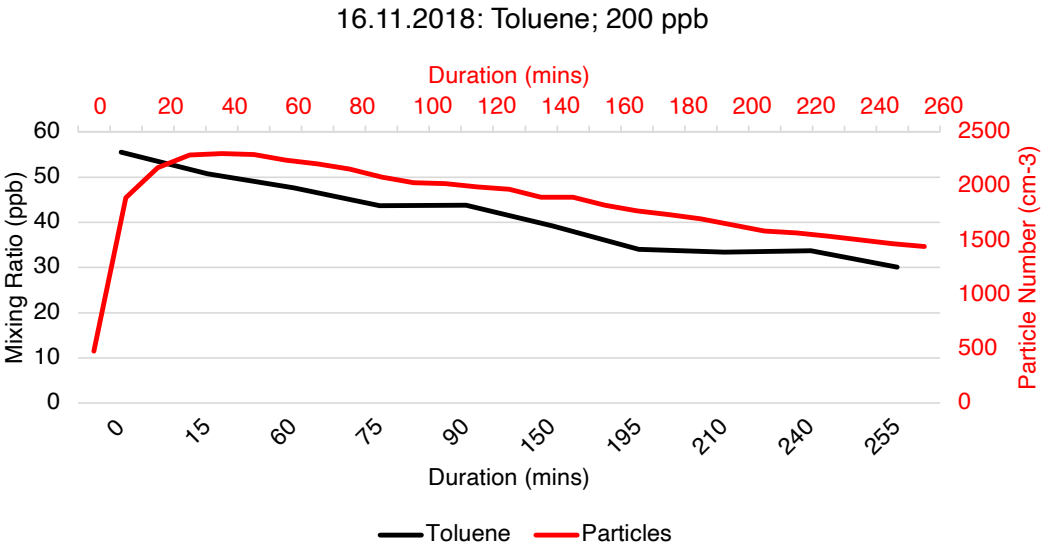

Figure 3.12: Toluene decay and particle number. The black line represents toluene decay and is expressed in ppb, and the red line represents particle number in no. cm^{-3}. Duration is expressed in minutes

Regarding particle formation from toluene decay, the maximum number of particles (27,731 particles cm^{-3}) was observed during the experiment dated 13.11.2018. The lowest maximum particle number was observed in the experiment dated 16.11.2018, with 2,299 particles cm^{-3}. In contrast to results observed in α-Pinene decay particle formation, the highest particle numbers were evident when NO was in higher abundance than NO_2 (3:1). Significant particle formation was also observed in the experiment dated 14.11.2018 — where the NO:NO_2 ratio was 1:1 and the OH mixing ratio was the highest of all the toluene experiments (0.004 ppb) — and during the experiment dated 15.11.2018 where no NO_x was used, but OH was relatively high (0.002 ppb). The experiment with the least particles formed did not use NO_x, and OH mixing ratios were low (8.92×10^{-4} ppb). O_3 was not used in any of the toluene experiments.

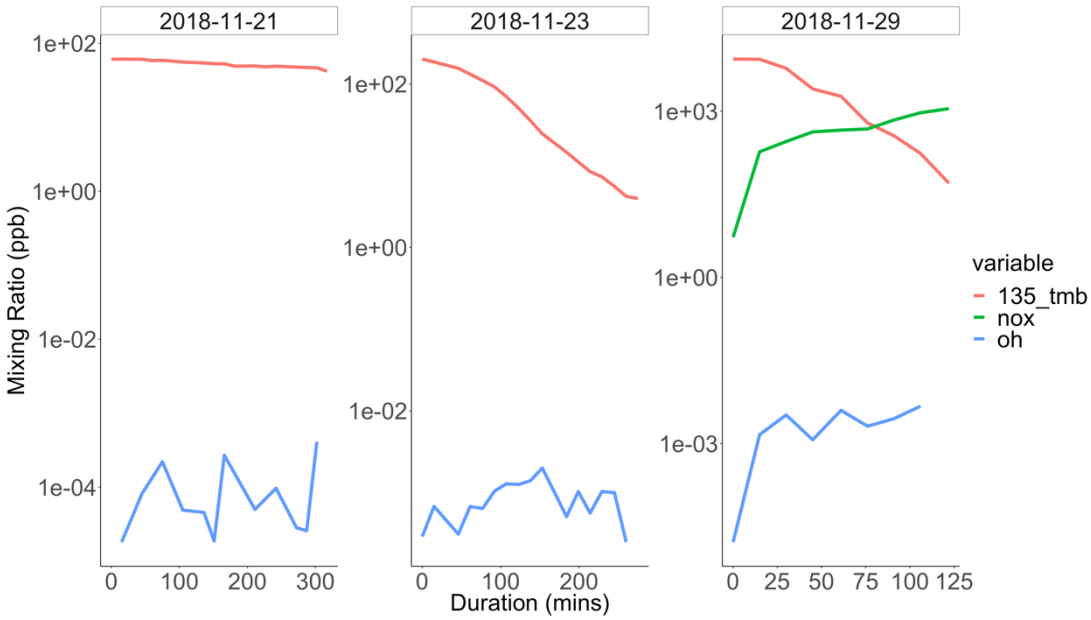

Figure 3.13: 1,3,5-trimethylbenzene decay during multiple experiments between 21.11.2018 and 29.11.2018. The red line represents 1,3,5-trimethylbenzene decay, the green line represents NO_x, and the blue line represents OH. All mixing ratios are expressed in ppb and on a log_{10} scale. Experiment duration is expressed in minutes.

Regarding experiments where 1,3,5-trimethylbenzene was used (see Figure 3.13), the greatest decay (>98%) was observed in the experiments dated 23.11.2018 and 29.11.2018. Both experiments used OH in relatively higher concentrations as compared to the experiment dated 21.11.2018; in the experiment dated 29.11.2018, NO_x mixing ratios were approximately 4:1. The least decay (31%) was observed in the experiment dated 21.11.2018, where OH mixing ratios were relatively low and neither O_3 nor NO_x were present.

As in the experiments using α-Pinene and toluene, OH often peaked at the beginning, in the middle, and at the end of the experiment, perhaps most noticeably in the experiments dated 21 and 23.11.2018. Interestingly, in the experiment dated 29.11.2018, in the presence of NO_x, OH continued to rise relatively consistently throughout the experiment. In OH mixing ratios above 10^{-3}, the decay of 1,3,5-trimethylbenzene was much more apparent. In the experiment dated 29.11.2018, NO_x increased as 1,3,5-trimethylbenzene continued to decay.

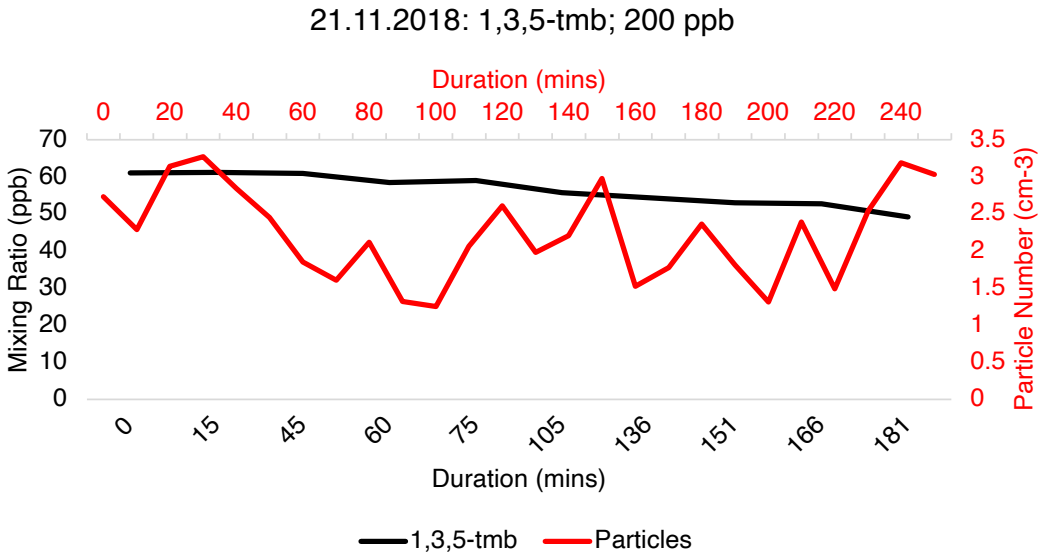

Figure 3.14: 1,3,5-trimethylbenzene decay and particle number. The black line represents 1,3,5-trimethylbenzene decay and is expressed in ppb, and the red line represents particle number in no. cm^{-3}. Duration is expressed in minutes

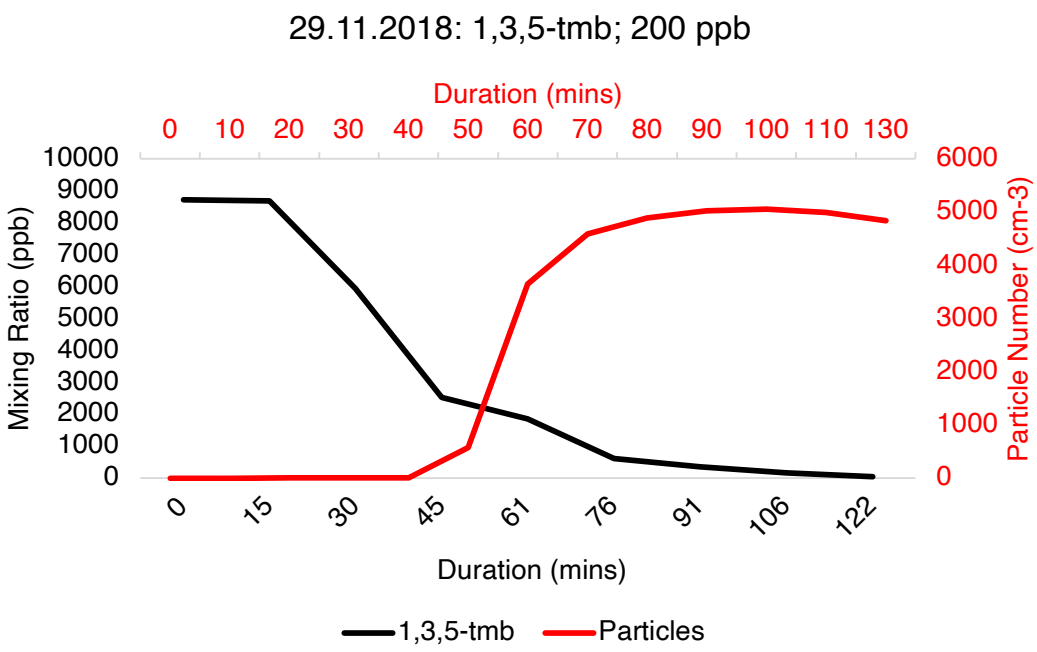

Figure 3.15: 1,3,5-trimethylbenzene decay and particle number. The black line represents 1,3,5-trimethylbenzene decay and is expressed in ppb, and the red line represents particle number in no. cm^{-3}. Duration is expressed in minutes

Regarding particle formation, the greatest number of particles (5,056 particles cm^{-3}) was observed in the experiment dated 29.11.2018. This experiment had a NO:NO_2 ratio of approximately 4:1 and an OH mixing ratio of 0.004 ppb. Minimal particle formation (3.27 particles cm^{-3}) was observed in the experiment dated 21.11.2018. This experiment had a relatively low OH mixing ratio of 4.11 x 10^{-4} ppb and no NO_x was present. Again, no O_3 was present during these experiments. No particle data were collected in the experiment dated 23.11.2018.

As outlined in Chapter 1, NO_x plays a significant role in the oxidative capacity of the atmosphere through its control of atmospheric radicals via reactions with peroxy radicals [52]. To form peroxy radicals (RO_2), a given VOC reacts with a radical to form an alkyl radical, which subsequently reacts with oxygen to form RO_2 [52]. Further reactions between RO_2 and NO lead to the net

production of O_3. This usually dominates in continental areas where sources of anthropogenic NO_x abound [52]. These reactions also form alkoxy radicals and NO_2, and propagate HO_x and NO_x radical chains [52]. Reactions of alkoxy species ultimately complete the HO_x cycle — through the formation of HO_2 and OH — and the simultaneous interconversion of NO and NO_2 completes the NO_x cycle [52]. High NO_x areas can potentially lead to the competition between NO and RO_2 reactions and the autoxidation of RO_2, impacting highly oxygenated organic molecules (HOMs). Both by controlling oxidant amount and the chemistry of peroxy radicals, NO_x impacts atmospheric chemistry significantly [53].

As mentioned in the Introduction, HOMs derived from the autooxidation of radical species could have a significant impact on indoor air chemistry through its potential influence on SOA mass and composition [20]. Further work performed by Yan et al. suggests that HOMs could significantly drive new particle formation (NPF), wherein NO_x plays a substantial role [54]. Generally, NO_x supresses particle growth in a non-uniform way, but in a way that is dependent on the size of the new particle [54]. Further, because NO_x also changes the volatility of HOMs, particle growth is also impacted [54].

As outlined in Figure 3.1 in Section 3.1, the mechanism by which SOA is formed proceeds through the nucleation of an oxidation product and its growth to an SOA [9]. This part of the mechanism is defined by Yan et al. as NPF [54]. Many particles are formed during particle nucleation, but are quenched by pre-existing particles if growth is too slow [54]. Sulphuric acid is often key in particle nucleation under most atmospheric conditions, but clusters can be stabilised by organic vapours which are themselves dominant in particle growth, making it crucial in the survival of newly formed particles [54]. In chamber experiments performed by Yan et al., where a 2:1 mix of α-Pinene and Δ-3-carene was injected into a chamber with different ppb mixing ratios of NO_x, the presence of NO_x was associated with changes in HOM composition, leading to suppression in NPF and particle growth [54].

This suppression in growth was most pronounced in smaller diameter particles (~2 nm), with negligible suppression in larger diameter particles (>30 nm) [54]. The authors also observed the more significant role that NO plays over NO_2 in this suppression [54].

NPF from monoterpene oxidation is thought to be particularly susceptible to NO_x, and NO especially, owing to permutation reactions of higher-generation peroxy radical-like intermediates limiting the rate at which new particles form [55]. This could explain, at least in part, why the numbers of particles formed was low in experiments in which α-Pinene was used, contrasted with those using toluene. For example, greatest particle numbers were observed in the experiment with the lowest NO_x mixing ratios (~15 ppb), and where NO_2 was in greater abundance than NO. Tsiligiannis et al. suggest that 1,3,5-trimethylbenzene produces HOMs in a NO_x-free environment under elevated OH [53]. This could help to explain raised particle numbers in experiments using NO_x but with comparatively high OH mixing ratios relative to other experiments using 1,3,5-trimethylbenzene carried out here.

HOM production is also expected to be impacted by temperature. Simon et al. state that HOM yield from the ozonolysis of α-Pinene is approximately 6.2% at 25°C, decreasing to 0.7% at -50°C [51]. At 5°C, yield is expected to be 3.2%, and at 20°C, 7% [19, 56]. Lower temperatures are also expected to lower the oxidation state of the products, increase the rate of new particle formation, and decrease the saturated vapour pressure of each oxidation state [51]. With reduced volatility at lower temperature, nucleation rates are expected be up to three orders of magnitude higher at -50°C than they are at 25°C [51].

3.3.2. SOA intermediate formation

For the purposes of this study, a potential SOA intermediate is identified as a peak that develops and persists in the chromatograms from the experimental

periods, with particular focus on peaks developing around the elution time of the main VOC peak. Potential SOA intermediates were identified using the National Institute of Standards and Technology (NIST) library installed in the MassHunter Qualitative Analysis software.

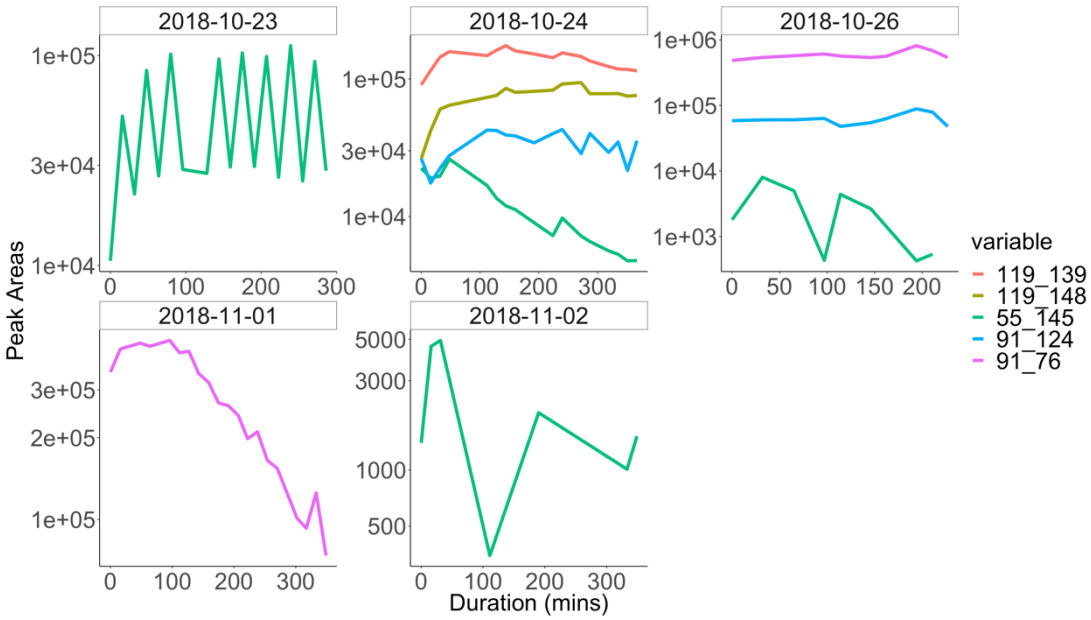

Figure 3.16: α-Pinene SOA intermediate formation during multiple experiments between 23.10 and 02.11.2018. SOA intermediate values are expressed as peak areas and on a $\log_{10}$ scale. Duration is expressed in minutes. The first number of the variable category refers to the m/z of the identified ion, the second number refers to the elapsed sample time, in seconds, at which the ion appears

Ion 55, occurring at 145 seconds, was identified as a potential SOA intermediate in the experiment dated 23.10.2018. Ion 55 had a maximum abundance of 1.11 x 10^5 peak areas, and an abundance of 2.83 x 10^4 peak areas by the conclusion of the experiment. As can be seen in Figure 3.14, there is significant spiking displayed, suggesting an instrument issue. Despite this, there is evidently an upward trend in the abundance of ion 55.

Four potential SOA intermediates were identified in the experiment dated 24.10.2018: two 119 ions, and ions 55 and 91. The 119 ion forming at 139 seconds had a maximum peak area of 1.74 x 10^5, the second 119 ion occurring at 148 seconds had a maximum peak area of 9.41 x 10^4 peak areas. Both ions increased in abundance following VOC injection before a gradual decline (end peak area of 119 at 140 seconds = 1.14 x 10^5; end peak area of 119 at 149 seconds = 7.59 x 10^4 peak areas). A further ion, ion 91, was detected at 125 seconds. This ion had a maximum peak area of 3.56 x 10^4 peak areas, before increasing to 4.29 x 10^4 by the conclusion of the experiment. Ion 55 occurred at 145 seconds and had a maximum abundance of 2.61 x 10^4 peak areas, and an abundance of 4.78 x 10^3 peak areas by the conclusion of the experiment. All ions in this experiment began to increase in abundance shortly after the experiment began. Unlike the other ions highlighted in this experiment, ion 55 declined sharply shortly after peaking, whilst the other ions begin to plateau.

Three potential SOA intermediates were identified in the experiment dated 26.10.2018, ion 91 occurring at 76 and 124 seconds, and ion 55 occurring at 145 seconds. 91 occurring at 76 seconds peaked at 8.12 x 10^5 peak areas and declined to 5.37 x 10^5 peak areas at the conclusion of the experiment. The 91 ion occurring at 124 seconds peaked at 8.85 x 10^4 peak areas and declined to 4.76 x 10^4 peak areas at the conclusion of the experiment. Ion 55 had a maximum abundance of 7.99 x 10^3, and an abundance of 5.36 x 10^3 peak area by the conclusion of the experiment. Both 91 ions remained at a relatively constant abundance throughout the experiment, peaking towards the end. Ion 55 formed quickly shortly after the beginning of the experiment, before again declining rapidly as the experiment progressed.

Ion 91 was detected as a potential SOA intermediate during the experiment dated 01.11.2018. Ion 91, occurring at 76 seconds, peaked at 4.56 x 10^5 peak areas and declined to 7.37 x 10^4 peak areas by the conclusion of the

experiment. Ion 91 formed very quickly at the beginning of the experiment, before declining as the experiment progressed.

Ion 55 was detected during the experiment dated 02.11.2018. Ion 55, occurring at 145 seconds, had a maximum peak area of 4.93 x 10^3 peak areas and concluded at 1.51 x 10^3 peak areas. Despite the presence of some additional ions in the experiment dated 31.10.2018, these have not been included for discussion here as abundance remained relatively constant throughout the experiment and could not be considered SOA intermediates.

Ion 55 was identified as oxalic acid, cyclobutyl hexyl ester (NIST search match factor = 711, probability = 37.1%). Oxalic acid is formed from the oxidation of α-Pinene and has been shown to derive from isoprene, for example from biogenic sources such as forests [57]. Ion 91 occurring at 76 seconds was identified as benzaldehyde, 4-benzyloxy-3-methoxy-2-nitro- (NIST search match factor = 801, probability = 15.1%). Ion 91 occurring at 124 seconds was identified as 1,2-propanediol, 3-benzyloxy-1,2-diacetyl (NIST search match factor = 592, probability = 75.1%). Ion 119 occurring at 139 seconds was identified as 1,3,8-p-methatriene (NIST search match factor = 831, probability = 24.6%). Ion 119 occurring at 148 seconds was identified as benzene, 1-methyl-3-(1-methylethyl)- (NIST search match factor = 802, probability = 10.5%).

In the literature, α-Pinene is cited as being a significant contributor to SOAs in the atmosphere, and is readily oxidised by the OH radical and O_3, forming semi-volatile organic compounds [51]. During ozonolysis of α-Pinene, it can undergo rapid autoxidation by virtue of its carbon-carbon double bond [51]. Autoxidation is the process wherein repeated hydrogen shifts occur within peroxy radicals [51]. The subsequent addition of O_2 to each H-shift forms highly oxygenated, multifunctional peroxy radicals, which, under low NO_x conditions terminate at highly oxygenated peroxy radicals [51]. First, a primary

ozonide is formed, subsequently leading to the formation of Criegee Intermediates, approximately 60–90% of which undergoes H-shift forming vinyl hydroperoxides following O_2 addition [50]. This releases OH radicals, forming peroxy radicals in the presence of O_2 [50], Eddingsaas, Loza et al. [58] performed α-Pinene oxidation experiments under low and high NO_x conditions to measure OH oxidation in a chamber. Under low NO_x conditions, hydroxy hydroperoxides and pinonaldehyde were the most abundant oxidation products, with pinonaldehyde also present in high NO_x experiments. Pinonaldehyde, as well as formaldehyde and acetone were also identified in chamber experiments by Rolletter, Kaminski et al. [59]

As discussed later, benzaldehyde is an oxidation product of other VOCs used in the chamber campaign, namely toluene and 1,3,5-trimethylbenzene. Due to the lack of a benzene ring in the structure of α-Pinene, benzaldehyde is evidently not an oxidation product of α-Pinene; rather its presence in experiments using α-Pinene could be due to direct contamination with benzaldehyde, or the oxidation of other artefacts leading to benzaldehyde formation, in the chamber or in the experiment apparatus. Ion 91 could also be misidentified as benzaldehyde. These scenarios could also be the case regarding the presence of ion 91 occurring at 124 seconds being identified as 1,2-propandiol. p-Menthatriene (ion 119; 139 seconds) and m-Cymene (ion 119; 148 seconds) are both monoterpenes, so are likely a misidentification of an α-Pinene oxidation product.

The experiments dated 23.10.2018, 01.11.2018, and 02.11.2018 yielded the greatest decay, but the least number of intermediate species. These experiments also had a 3:1 $NO:NO_2$ ratio. By contrast, the most number of intermediate species were observed in the experiments dated 24.10.2018 and 26.10.2018. Interestingly, the greatest decay of SOA intermediate was observed during the experiment dated 01.11.2018, which had a 3:1 $NO:NO_2$ ratio. The lowest abundance of SOA intermediate and the lowest number of intermediate species was observed in the experiment dated 02.10.2018,

despite having high mixing ratios of OH and O_3 relative to other experiments that used α-Pinene, but a 3:1 NO:NO_2 ratio was used. This demonstrates the potential importance of NO_x, and the ratio of NO to NO_2, in SOA intermediate formation, and the relative unimportance of the mixing ratios of OH and O_3.

When the MCM was used for the ozonolysis of α-Pinene, two products are identified (see R 3.5 and 3.6). Ozonolysis proceeds with a rate coefficient of 8.05×10^{-16} exp(-640/t) and the branching ratio of each reaction is given in parentheses proceeding the product:

α-Pinene + O_3 → APINOOA (0.6) (R 3.5)

α-Pinene + O_3 → APINOOB (0.4) (R 3.6)

When the MCM was used for the oxidation of α-Pinene via OH, three products are identified (see R 3.7–3.9). Oxidation with OH proceeds with a rate coefficient of 1.2×10^{-11} exp(440/t) and the branching ratio of each reaction is given in parentheses proceeding the product:

α-Pinene + OH → APINAO2 (0.572) (R 3.7)

α-Pinene + OH → APINBO2 (0.353) (R 3.8)

α-Pinene + OH → APINCO2 (0.075) (R 3.9)

When α-Pinene undergoes oxidation with OH, the OH adds to the carbon-carbon double bond, forming the three peroxy radicals shown above: APINAO2, APINBO2, and APINCO2 [59]. Subsequently, reactions with NO proceed to form the alkoxy radicals: APINAO and APINBO [59]. These alkoxy radicals undergo ring opening, and, when reacted with O_2, form pinonaldehyde and HO_2 [59]. Reactions with NO also produce APINCO, which subsequently forms acetone and HCHO, which are also formed following the oxidation of pinonaldehyde [59]. Ozonolysis of α-Pinene, two Criegee

intermediates are formed: APINOOA and APINOOB [60]. APINOOA decays to two peroxy radical species: C107O2 and C109O2 [60]. APINOOB again decays to a peroxy radical (C96O2) and to pinonaldehyde [60, 61].

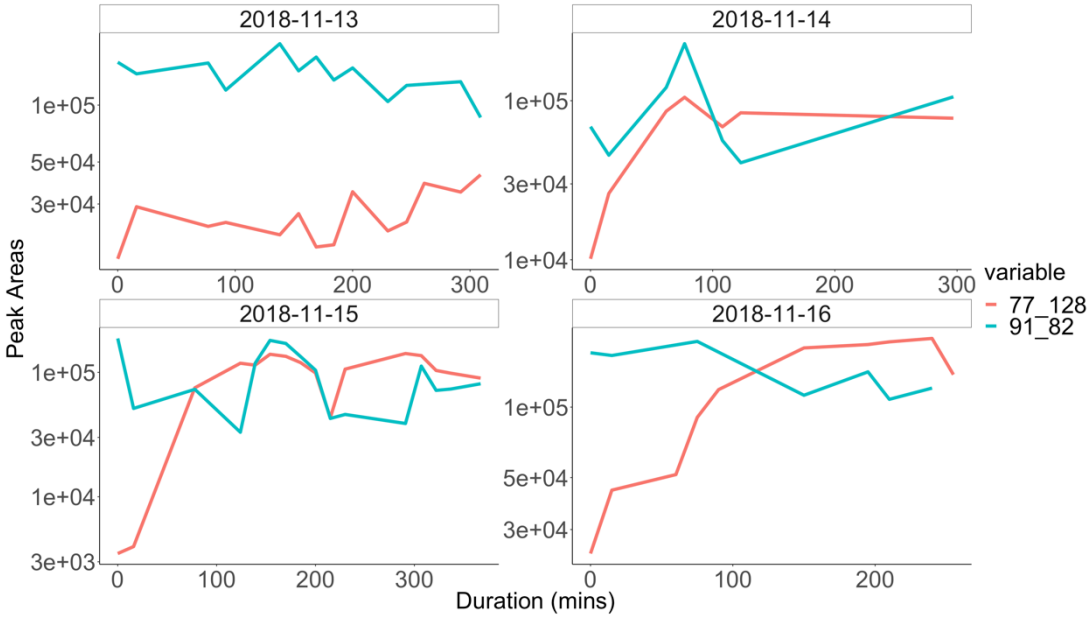

Figure 3.17: Toluene SOA intermediate formation during multiple experiments between 13.11 and 16.11.2018. SOA intermediate values are expressed as peak areas and on a $\log_{10}$ scale. Duration is expressed in minutes. The first number of the variable category refers to the m/z of the identified ion, the second number refers to the elapsed sample time, in seconds, at which the ion appears

Two potential SOA intermediate was identified in all experiments using toluene: ions 77 and 91. During the experiment dated 13.11.2018, ion 77, occurring at 128 seconds, had a maximum peak area of 4.28 x 10^4 peak areas. The same value was observed by the conclusion of the experiment, indicating that the ion peaked in abundance at the end of the experiment; the median abundance was 2.40 x 10^4 peak areas. Ion 91, occurring at 82 seconds, had a maximum abundance of 2.11 x 10^5 peak areas, and an abundance of 8.60 x 10^4 peak areas by the conclusion of the experiment. Ion 91 abundance remained relatively constant, though there was a small peak

approximately halfway through the experiment. Ion 77 formed rapidly following the start of the experiment and gradually increased towards the experiment's conclusion.

During the experiment dated 14.11.2018, ion 77 peaked at 1.06 x 10^5 peak areas, and had an abundance of 7.76 x 10^4 peak areas by the conclusion of the experiment. Ion 91 had a peak abundance of 2.28 x 10^5 peak areas, and an abundance of 1.06 x 10^5 peak areas by the conclusion of the experiment. Both ion 77 and 91 peaked at approximately the same time (~80 minutes). From this point, abundance of ion 77 decreased slightly before recovering and plateauing to the conclusion of the experiment. Ion 91 decreased more significantly before increasing again to the end of the experiment.

During the experiment dated 15.11.2018, ion 77 had a maximum abundance of 1.42 x 10^5 peak areas and had an abundance of 8.99 x 10^4 peak areas by the conclusion of the experiment. Ion 77 increased in abundance significantly shortly after the start of the experiment before broadly plateauing for the remainder of the experiment. Ion 91 presented an interesting pattern, peaking at the beginning, in the middle, and towards the end of the experiment.

During the experiment dated 16.11.2018, ion 77 had a maximum abundance of 1.96 x 10^5 peak areas, and an abundance of 1.38 x 10^5 peak areas by the conclusion of the experiment. Ion 91 had a peak abundance of 1.91 x 10^5 peak areas, and an abundance of 1.21 x 10^5 peak areas by the conclusion of the experiment. Ion 77 increased in abundance sharply over approximately the first ~100 minutes of the experiment, before increasing much more gradually until the conclusion of the experiment, though there was a sharp decline at the very end of the experiment. Unfortunately, since the experiment ended at this point, it is not possible to determine if this is a definite trend. Ion 91 increased gradually in abundance shortly after the start

of the experiment, before declining more substantially and recovering slightly towards the end of the experiment.

Ion 77 was identified as benzaldehyde (NIST search match factor = 938, probability = 73.9%). Benzaldehyde is a recognised oxidation product of toluene [62]. Ion 91 was identified as benzaldehyde, 4-benzyloxy-3-methoxy-2-nitro- (NIST search match factor = 796, probability = 15.4%). The NIST library also identified ion 91 more probably as hydrazinecarbothioamide and ethanamine. However, due to the presence of a benzene ring in toluene, benzaldehyde, 4-benzyloxy-3-methoxy-2-nitro- was chosen as a more suitable match.

In existing studies, toluene has been identified as a compound for the formation of SOAs. Hamilton, Webb et al. [63] performed an experiment on the photooxidation of toluene in the atmosphere at the European Photo-Reactor (EUPHORE) chamber in Valencia, Spain. The experiment involved injecting 2119 ppb toluene and 214 ppb dimethyl-sulphide, with NO_x maintained at 15–20 ppb throughout the experiment, which is representative of suburban areas. In total, 74 compounds were identified, including acetic acid, benzaldehyde, benzyl alcohol, across a variety of functional groups including furans, aromatics and acids. A number of low concentration fragments were also identified and determined to be fragments of larger compounds which were formed during the analytical process. This is a significant challenge posed by such analyses when trying to determine secondary products. Benzyl alcohol was determined as a significant SOA intermediate from the oxidation of toluene, and is widely used in a variety of consumer products [64].

SOA intermediate abundance remained relatively consistent across all four experiments that used toluene. In all experiments, with the exception of the experiment dated 13.11.2018, the two intermediates increased to similar abundances and began to plateau towards the end of the experiments. In the

experiment dated 13.11.2018, the two intermediates increased in abundance at much slower rates. This could potentially be explained by the 3:1 NO:NO_2 ratio used.

When the MCM was used for the oxidation of toluene by OH, four products are identified (see R 3.10–13). Oxidation with OH proceeds with a rate coefficient of 1.8 x 10^{-12} exp(340/t) and the branching ratio of each reaction is given in parentheses proceeding the product:

Toluene + OH → C6H5CH2O2 (0.07) (R 3.10)

Toluene + OH → CRESOL (0.18) (R 3.11)

Toluene + OH → TLBIPERO2 (0.65) (R 3.12)

Toluene + OH → TLEPOXMUC (0.10) (R 3.13)

Toluene is oxidised by OH in two ways: first is via the abstraction of the hydrogen atom from the methyl group (approximately 10% of OH oxidation via this route), the second is via addition to the aromatic ring (approximately 90% of OH oxidation via this route) [65, 66]. The H-atom abstraction route proceeds to the formation of benzaldehyde products through the reaction of a peroxy intermediate with either HO_2 or NO [65]. The addition route is categorised in three ways dependent on the compounds produced: (1) phenol, (2) epoxide, and (3) those products formed as a result of peroxy-bicyclic ring-opening [65]. In the literature, this OH addition, proceeds to the formation of dienals and dicarbonyls such as glyoxal and methylglyoxal [67]. OH oxidation can also form benzaldehyde and cresol, where the ring is retained [68].

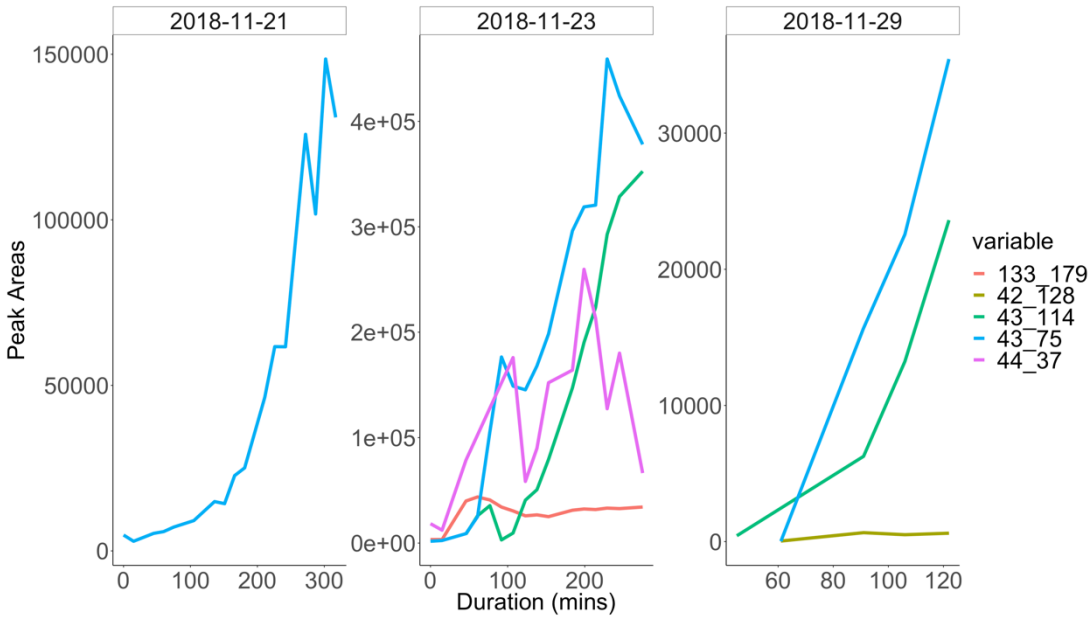

Figure 3.18: 1,3,5-tmb SOA intermediate formation during multiple experiments between 21.11 and 29.11.2018. SOA intermediate values are expressed as peak areas and on a $\log_{10}$ scale. Duration is expressed in minutes. The first number of the variable category refers to the m/z of the identified ion, the second number refers to the elapsed sample time, in seconds, at which the ion appears

During the experiment dated 21.11.2018, ion 43 was identified as a potential SOA intermediate, occurring at 75 seconds. Ion 43 had a maximum abundance of 1.49 x 10^5 peak areas, and an abundance of 1.31 x 10^5 peak areas by the conclusion of the experiment. Ion 43 increased rapidly from the beginning of the experiment until the end of the experiment.

Four ions were identified as potential SOA intermediates during the experiment dated 23.11.2018. Two 43 ions were identified at 75 and 114 seconds. The former had a maximum abundance of 4.59 x 10^5 peak areas and an abundance of 3.78 x 10^5 by the conclusion of the experiment. The latter had a maximum abundance of 3.53 x 10^5 peak areas. The same abundance was observed at the conclusion of the experiment, indicating that the ion peaked in abundance at the end of the experiment; the median

abundance was 6.50 x 10^4 peak areas. Ion 44 occurred at 37 seconds and had a maximum abundance of 2.60 x 10^5, and an abundance of 6.64 x 10^4 by the conclusion of the experiment. Ion 133 occurred at 179 seconds and had a maximum abundance of 4.37 x 10^4 peak areas, with an abundance of 3.42 x 10^4 peak areas by the conclusion of the experiment. Both 43 ions increased rapidly from the beginning of the experiment until the end of the experiment. Ion 44 increases from the start of the experiment and peaks around the middle of the experiment, before declining by its conclusion.

Three ions were identified during the experiment dated 29.11.2018. Ion 42 occurred at 128 seconds and had a maximum abundance of 6.58 x 10^2 peak areas, and an abundance of 6.19 x 10^2 peak areas by the conclusion of the experiment. Two 43 ions occurred at 74 and 114 seconds. The former had a maximum abundance of 3.54 x 10^4 peak areas. The same abundance was observed at the conclusion of the experiment, indicating that the ion peaked in abundance at the end of the experiment; the median abundance was 1.91 x 10^4 peak areas. The latter had a maximum abundance of 2.36 x 10^4 peak areas. The same abundance was observed at the conclusion of the experiment, indicating that the ion peaked in abundance at the end of the experiment; the median abundance was 9.74 x 10^3 peak areas. Both 43 ions increase rapidly from the beginning of the experiment to the end. The abundance of ion 42 remained relatively consistent throughout the experiment, though abundance slightly peaked in the middle of the experiment.

Ion 43 occurring at 75 seconds was identified as acetic acid (NIST search match factor = 765, probability = 54.7%). Ion 43 occurring at 77 seconds was identified as 2-phenoxyethyl isobutyrate (NIST search match factor = 353, probability = 20.5%). Ion 43 occurring at 114 seconds was identified as acetic anhydride (NIST search match factor = 867, probability = 57.6%). Ion 44 was identified as acetaldehyde (NIST search match factor = 717, probability 38%). Ion 133 was identified as benzaldehyde,

2,5-dimethyl- (NIST search match factor = 869, probability = 41%).

Acetic acid (ion 43; 75 seconds) was identified as a product in in the oxidation of 1,3,5-trimethylbenzene by Wyche et al. [69] Acetic anhydride (ion 43; 114 seconds) is not recorded in the literature as an oxidation product of 1,3,5-trimethylbenzene, but when hydrated, proceeds to form acetic acid. Acetaldehyde (ion 44) was tentatively identified by Wyche et al. in the photooxidation of 1,3,5-trimethylbenzene, though it is not widely reported as an oxidation product elsewhere in the literature [69]. 2-phenoxyethyl isobutyrate is not identified as an oxidation product, so it was likely to be either a misidentified ion, or a contaminant in the chamber or experimental apparatus. Dimethylbenzaldehyde (ion 133) is widely identified in the literature as an oxidation product [70, 71].

Metzger et al. investigated NO_x oxidation of 1,3,5-trimethylbenzene using a chamber [72]. Methylglyoxal was the significant oxidation product of 1,3,5-trimethylbenzene, along with furanones and 2-methyl-4-oxopent-2-enal. An additional chamber study by Huang et al. investigating OH oxidation of 1,3,5-trimethylbenzene also concluded that 2-methyl-4-oxopent-2-enal was a significant oxidation product in the experiments, along with 3,5-dimethyl benzaldehyde, 2,4,6-trimethylphenol and 3,5-dimethyl-2-furanone [73].

In the experiment dated 23.11.2018, the greatest SOA intermediate abundance and number of intermediate species was observed. This experiment contained no NO_x and a relatively high mixing ratio of OH. The experiment dated 29.11.2018 also contained a high mixing ratio of OH, but also NO_x. Increasing NO_x during the experiment could help to explain the lower abundance and the fewer number of intermediate species observed as compared to the experiment dated 23.11.2018. Conversely, the second highest abundance of SOA intermediates was observed in the experiment dated 21.11.2018, where NO_x wasn't present and OH was in relatively low abundance.

When the MCM is used for the oxidation of 1,3,5-trimethylbenzene by OH, four products are identified (see R 3.14–17). Oxidation with OH proceeds with a rate coefficient of 5.67×10^{-11} and the branching ratio of each reaction is given in parentheses proceeding the product:

1,3,5-trimethylbenzene + OH → TM135BPRO2 (0.79) (R 3.14)

1,3,5-trimethylbenzene + OH → TM135BZOL (0.04) (R 3.15)

1,3,5-trimethylbenzene + OH → TM135OXMUC (0.14) (R 3.16)

1,3,5-trimethylbenzene + OH → TMBO2 (0.03) (R 3.17)

Oxidation of 1,3,5-trimethylbenzene via OH can proceed in two ways: first via H-atom abstraction, either from the methyl group or the aromatic carbon; the former cited as more favourable, or second, by OH addition to the aromatic ring and thus forming TMB-OH adducts [74]. Radicals initially formed in this chemistry subsequently react with O_2 to form peroxy radical intermediates [74]. Further reactions with HO_2 and NO subsequently form trimethylphenol, bicyclic peroxides, bicyclic carbonyl and methylglyoxal [74].

In the literature, it is noted higher NO_x environments can lead to a greater proportion of organonitrates being present, the formation of which can compete with and supress the autoxidation process that leads to HOM formation, more specifically, HOM accretion products (see R 3.18 and 3.19) [53, 75]. HOM accretion products themselves are known to have a high molecular mass and are potentially important for SOA formation in low-NO_x environments.

$RO_2 + NO \rightarrow RONO_2$, (R 3.18)

$\rightarrow RO + NO_2$. (R 3.19)

3.3.3. Summary of tentative SOA intermediate compounds

Table 3.4: Summary table of potential SOA intermediates from the experiments listed in Table 3.2

VOC	m/z	Retention Time (seconds)	Compound	Match	Probability (%)
α-Pinene	91	76	Benzaldehyde, 4-benzyloxy-3-methoxy-2-nitro-	801	15.1
	91	124	1,2-Propanediol, 3-benzyloxy-1,2-diacetyl	592	75.1
	119	139	1,3,8-p-Menthatriene	831	24.6
	55	145	Oxalic acid, cyclobutyl hexyl ester	711	37.1
	119	148	m-Cymene	802	10.5
Toluene	91	82	Benzaldehyde, 4-benzyloxy-3-methoxy-2-nitro-	796	15.4
	77	128	Benzaldehyde	938	73.9
1,3,5-tmb	44	37	Acetaldehyde	717	38
	43	75	Acetic acid, anhydride with formic acid	765	54.7
	43	77	2-Phenoxyethyl isobutyrate	353	20.5
	43	114	Acetic anhydride	867	57.6
	133	179	Benzaldehyde, 2,5-dimethyl-	869	41

3.4. Study Limitations

Identifying potential SOA intermediates in experiments of this nature is confounded by several factors. SOA intermediate formation potentially results in very small quantities of the ion of interest being produced which could be difficult to quantify separately from background concentrations. Similarly, it is difficult to distinguish those compounds that could be SOA intermediates from compounds that appear in background experiments, or as a result of contamination. This is especially so given the numerous elements

that constitute the experimental apparatus; contamination could occur with the injection of the VOC into the chamber, in the chamber itself, in the connection between the chamber and the AGC-MS, and in the various instruments of the AGC-MS.

As briefly described earlier, one trap in the thermal desorption unit of the AGC-MS experienced significant malfunctioning at the beginning of the autumn 2018 campaign. This resulted in unreliable results from these samples. With one functioning trap remaining, this significantly decreased the time resolution of data derived from the experiments. Due to the nature of chamber campaigns, e,g, significant cost and time constraints, it wasn't possible to perform anything other than the most basic maintenance on the instrument; as such, data from the malfunctioning trap remained unused for the entire campaign. A second campaign took place during Spring 2019. During this campaign, another fault developed in the thermal desorption unit, where concentration data proved unreliable across both traps, meaning data from the campaign was unusable. A third campaign was planned for the beginning of 2020, but due to the COVID-19 pandemic and subsequent cessation of laboratory activities at both the University of York and the University of Manchester, the winter 2020 chamber campaign was cancelled.

Due to these complications, and additional data cleaning, data collection from the chamber was severely limited. Unfortunately, instrument errors pertaining to the AGC-MS likely occurred during transit between York and Manchester. Ideally, any future campaigns involving the AGC-MS, and its movement from one laboratory to another, should allow sufficient time for installation and troubleshooting prior to the commencement of the campaign. Despite these challenges, a valuable experimental dataset was collected, observing SOA decay, oxidant behaviour, and the formation of particles and SOA intermediates.

Clearly, using GC-MS has significant potential in chamber experiments as it offers qualitative and quantitative data to observe both VOC decay and the formation of SOA intermediates under a variety of conditions. The use of a two-trap thermal desorption unit in the AGC-MS also allows for a faster time resolution than provided by traditional GC-MS, allowing it to capture greater levels of experimental detail. However, a number of challenges present themselves in this context, such as difficulties in accurately measuring such small quantities of SOA intermediates and accurately identifying the compounds themselves using existing libraries.

3.5. Conclusions

In this study, the decay of α-Pinene, toluene, and 1,3,5-trimethylbenzene, and the abundance of OH and O_3 was measured in relation to the mixing ratio of NO_x, particle data was collected to quantify the number of particles formed during each experiment, and the formation of SOA intermediates from each VOC was also observed. Finally, the Master Chemical Mechanism was browsed to elucidate the process by which expected SOA intermediates in these experiments.

From the reviewed literature and as evidenced in these experiments, NO_x has a significant role in the oxidative capacity of the atmosphere by not only controlling the abundance of oxidants, but by also potentially impacting NPF and therefore HOMs. Generally, these experiments show that decay is governed by OH; where mixing ratios of OH are highest, decay tends to increase. Where O_3 was present, total decay was greater than in experiments where OH was the sole oxidant, suggesting that O_3 does contribute a large part to oxidation. Where NO_x was present, decay and particle formation tended to be greatest when NO_2 constituted a larger portion of the NO:NO_2 ratio.

Across all the chamber experiments, a total of 12 SOA intermediates were identified: five from experiments using α-Pinene, two from experiments using toluene, and five from experiments using 1,3,5-trimethylbenzene. Of these, five are recognised in the literature as observed oxidation products. The remaining seven are thought to be either misidentified ions, potential contaminants in the experimental apparatus, or artefacts from previous experiments. Browsing the Master Chemical Mechanism has also elucidated some of the mechanisms that are the result of OH and O_3 oxidation of α-Pinene, toluene, and 1,3,5-trimethylbenzene.

These experiments were, unfortunately, subject to a number of issues mainly regarding instrumentation, contributing to a significantly smaller dataset than was anticipated. As such, only one campaign at the chamber was possible, and of this, only part of the available dataset was viable for discussion. These issues highlight the potentially complex nature of chamber experiments, but the data collected suggests the use of GC-MS is a feasible and appropriate methodology for future experiments.

References

1. Charlson RJ, Lovelock JE, Andreae MO, Warren SG. Oceanic phytoplankton, atmospheric sulphur, cloud albedo and climate. Nature. 1987;326(6114):655–61.

2. Boucher O, Randall D, Artaxo P, Bretherton C, Feingold G, Forster P, Kerminen V-M, Kondo Y, Liao H, Lohmann U, Rasch P, Satheesh SK, Sherwood S, Stevens B, Zhang XY. Clouds and aerosols. In: Stocker T.F., Qin D., Plattner G.-K., Tignor M., Allen S.K., Boschung J., Nauels A., Xia Y., Bex V., Midgley P.M., editors. Climate change 2013: The physical science basis contribution of Working Group I to the fifth assessment report of the Intergovernmental Panel on Climate Change. Cambridge, United Kingdom and New York, NY, USA: Cambridge University Press; 2013. p. 571–658.

3. Myhre G, Lund Myhre C, Samset BH, Storelvmo T. Aerosols and their relation to global climate and climate sensitivity. Nature Education Knowledge. 2013;4:7.

4. Arvesen A, Cherubini F, del Alamo Serrano G, Astrup R, Becidan M, Belbo H, Goile F, Grytli T, Guest G, Lausselet C, Rørstad PK, Rydså L, Seljeskog M, Skreiberg Ø, Vezhapparambu S, Strømman AH. Cooling aerosols and changes in albedo counteract warming from CO_2 and black carbon from forest bioenergy in Norway. Sci Rep. 2018;8(1):1–13.

5. Wild M, Liepert B. The earth radiation balance as driver of the global hydrological cycle. Environ Res Lett. 2010;5(2):1–8.

6. Srivastava D, Vu TV, Tong S, Shi Z, Harrison RM. Formation of secondary organic aerosols from anthropogenic precursors in laboratory studies. NPJ Clim Atmos Sci. 2022;5(1):1–30.

7. Finlayson-Pitts BJ. Halogens in the troposphere. Anal Chem. 2010;82(3):770–6.

8. Atkinson R. Atmospheric chemistry of VOCs and NO_x. Atmos Environ. 2000;34(12):2063–101.

9. Kruza M, McFiggans G, Waring MS, Wells JR, Carslaw N. Indoor secondary organic aerosols: Towards an improved representation of their formation and composition in models. Atmos Environ. 2020;240:1–10.

10. Svensmark H, Enghoff MB, Shaviv NJ, Svensmark J. Increased ionization supports growth of aerosols into cloud condensation nuclei. Nat Commun. 2017;8(1):1–9.

11. Bouzidi H, Fayad L, Coeur C, Houzel N, Petitprez D, Faccinetto A, Wu J, Tomas A, Ondráček J, Schwarz J, Ždímal V, Zuend A. Hygroscopic growth and ccn activity of secondary organic aerosol produced from dark ozonolysis of γ-terpinene. Sci Total Environ. 2022;817:1–16.

12. Liu C, Wang T, Rosenfeld D, Zhu Y, Yue Z, Yu X, Xie X, Li S, Zhuang B, Cheng T, Niu S. Anthropogenic effects on cloud condensation nuclei distribution and rain initiation in east Asia. Geophys Res Lett. 2020;47(2):1–10.

13. Tao J, Kuang Y, Ma N, Hong J, Sun Y, Xu W, Zhang Y, He Y, Luo Q, Xie L, Su H, Cheng Y. Secondary aerosol formation alters CCN activity in the North China Plain. Atmos Chem Phys. 2021;21(9):7409–27.

14. Nault BA, Jo DS, McDonald BC, Campuzano-Jost P, Day DA, Hu W, Schroder JC, Allan J, Blake DR, Canagaratna MR, Coe H, Coggon MM, DeCarlo PF, Diskin GS, Dunmore R, Flocke F, Fried A, Gilman JB, Gkatzelis G, Hamilton JF, Hanisco TF, Hayes PL, Henze DK, Hodzic A, Hopkins J, Hu M, Huey LG, Jobson BT, Kuster WC, Lewis A, Li M, Liao J, Nawaz MO, Pollack IB, Peischl J, Rappenglück B, Reeves CE, Richter D, Roberts JM, Ryerson TB, Shao M, Sommers JM, Walega J, Warneke C, Weibring P, Wolfe GM, Young DE, Yuan B, Zhang Q, de Gouw JA, Jimenez JL. Secondary organic aerosols from anthropogenic volatile organic compounds contribute substantially to air pollution mortality. Atmos Chem Phys. 2021;21(14):11201–24.

15. Zhang S, Tang H, Li Q, Li L, Ge C, Li L, Feng J. Secondary organic aerosols in $PM_{2.5}$ in Bengbu, a typical city in central China: Concentration, seasonal variation and sources. Atmosphere. 2021;12(7):1–16.

16. McDonald BC, de Gouw JA, Gilman JB, Jathar SH, Akherati A, Cappa CD, Jimenez JL, Lee-Taylor J, Hayes PL, McKeen SA, Cui YY, Kim S-W, Gentner DR, Isaacman-VanWertz G, Goldstein AH, Harley RA, Frost GJ, Roberts JM, Ryerson TB, Trainer M. Volatile chemical products emerging as largest petrochemical source of urban organic emissions. Science. 2018;359(6377):760–4.

17. Tsigaridis K, Kanakidou M. Secondary organic aerosol importance in the future atmosphere. Atmos Environ. 2007;41(22):4682–92.

18. Heeley-Hill AC, Grange SK, Ward MW, Lewis AC, Owen N, Jordan C, Hodgson G, Adamson G. Frequency of use of household products containing VOCs and indoor atmospheric concentrations in homes. Environ Sci Process Impacts. 2021;23(5):699–713.

19. Ehn M, Thornton JA, Kleist E, Sipilä M, Junninen H, Pullinen I, Springer M, Rubach F, Tillmann R, Lee B, Lopez-Hilfiker F, Andres S, Acir I-H, Rissanen M, Jokinen T, Schobesberger S, Kangasluoma J, Kontkanen J, Nieminen T, Kurtén T, Nielsen LB, Jørgensen S, Kjaergaard HG, Canagaratna M, Maso MD, Berndt T, Petäjä T, Wahner A, Kerminen V-M, Kulmala M, Worsnop DR, Wildt J, Mentel TF. A large source of low-volatility secondary organic aerosol. Nature. 2014;506(7489):476–9.

20. Pagonis D, Algrim LB, Price DJ, Day DA, Handschy AV, Stark H, Miller SL, de Gouw JA, Jimenez JL, Ziemann PJ. Autoxidation of limonene emitted in a university art museum. Environ Sci Technol Lett. 2019;6(9):520–4.

21. Skulberg K, Nyrud A, Goffeng L, Wisthaler A. Health and exposure to vocs from pinewood in indoor environments. Front Built Environ. 2019;5:1–11.

22. Waring MS, Siegel JA. Indoor secondary organic aerosol formation initiated from reactions between ozone and surface-sorbed d-limonene. Environ Sci Technol. 2013;47(12):6341–8.

23. Singer BC, Revzan KL, Hotchi T, Hodgson AT, Brown NJ. Sorption of organic gases in a furnished room. Atmos Environ. 2004;38(16):2483–94.

24. Aumont B, Valorso R, Mouchel-Vallon C, Camredon M, Lee-Taylor J, Madronich S. Modeling soa formation from the oxidation of intermediate volatility *n*-alkanes. Atmos Chem Phys. 2012;12(16):7577–89.

25. Surratt JD, Chan AWH, Eddingsaas NC, Chan M, Loza CL, Kwan AJ, Hersey SP, Flagan RC, Wennberg PO, Seinfeld JH. Reactive

intermediates revealed in secondary organic aerosol formation from isoprene. Proc Natl Acad Sci U S A. 2010;107(15):6640–5.

26. Cocker DR, Flagan RC, Seinfeld JH. State-of-the-art chamber facility for studying atmospheric aerosol chemistry. Environ Sci Technol. 2001;35(12):2594–601.

27. Finlayson BJ, Pitts JN. Photochemistry of the polluted troposphere. Science. 1976;192(4235):111–9.

28. Trump ER, Epstein SA, Riipinen I, Donahue NM. Wall effects in smog chamber experiments: A model study. Aerosol Sci Technol. 2016;50(11):1180–200.

29. Shao Y, Wang Y, Du M, Voliotis A, Alfarra MR, O'Meara SP, Turner SF, McFiggans G. Characterisation of the Manchester aerosol chamber facility. Atmos Meas Tech. 2022;15(2):539–59.

30. Jeffries H, Fox D, Kamens R. Outdoor smog chamber studies: Light effects relative to indoor chambers. Environ Sci Technol. 1976;10(10):1006–11.

31. Paulson SE, Pandis SN, Baltensperger U, Seinfeld JH, Flagan RC, Palen EJ, Allen DT, Schaffner C, Giger W, Portmann A. Characterization of photochemical aerosols from biogenic hydrocarbons. J Aerosol Sci. 1990;21:S245–S8.

32. Hurley MD, Sokolov O, Wallington TJ, Takekawa H, Karasawa M, Klotz B, Barnes I, Becker KH. Organic aerosol formation during the atmospheric degradation of toluene. Environ Sci Technol. 2001;35(7):1358–66.

33. Kalberer M, Paulsen D, Sax M, Steinbacher M, Dommen J, Prevot ASH, Fisseha R, Weingartner E, Frankevich V, Zenobi R, Baltensperger U. Identification of polymers as major components of atmospheric organic aerosols. Science. 2004;303(5664):1659–62.

34. Lambe AT, Chhabra PS, Onasch TB, Brune WH, Hunter JF, Kroll JH, Cummings MJ, Brogan JF, Parmar Y, Worsnop DR, Kolb CE, Davidovits P. Effect of oxidant concentration, exposure time, and seed particles on secondary organic aerosol chemical composition and yield. Atmos Chem Phys. 2015;15(6):3063–75.

35. Saunders SM, Jenkin ME, Derwent RG, Pilling MJ. Protocol for the development of the Master Chemical Mechanism, MCM v3 (part a): Tropospheric degradation of non-aromatic volatile organic compounds. Atmos Chem Phys. 2003;3(1):161–80.

36. Sommariva R, Cox S, Martin C, Borońska K, Young J, Jimack PK, Pilling MJ, Matthaios VN, Nelson BS, Newland MJ, Panagi M, Bloss WJ, Monks PS, Rickard AR. Atchem (version 1), an open-source box model for the Master Chemical Mechanism. Geosci Model Dev. 2020;13(1):169–83.

37. Jenkin ME, Young JC, Rickard AR. The MCM v3.3.1 degradation scheme for isoprene. Atmos Chem Phys. 2015;15(20):11433–59.

38. Bloss C, Wagner V, Jenkin ME, Volkamer R, Bloss WJ, Lee JD, Heard DE, Wirtz K, Martin-Reviejo M, Rea G, Wenger JC, Pilling MJ. Development of a detailed chemical mechanism (MCMv3.1) for the atmospheric oxidation of aromatic hydrocarbons. Atmos Chem Phys. 2005;5(3):641–64.

39. Hamilton JF, Rami Alfarra M, Wyche KP, Ward MW, Lewis AC, McFiggans GB, Good N, Monks PS, Carr T, White IR, Purvis RM.

Investigating the use of secondary organic aerosol as seed particles in simulation chamber experiments. Atmos Chem Phys. 2011;11(12):5917–29.

40. Pereira KL, Dunmore R, Whitehead J, Alfarra MR, Allan JD, Alam MS, Harrison RM, McFiggans G, Hamilton JF. Technical note: Use of an atmospheric simulation chamber to investigate the effect of different engine conditions on unregulated VOC-IVOC diesel exhaust emissions. Atmos Chem Phys. 2018;18(15):11073–96.

41. Hofzumahaus A, Kraus A, Kylling A, Zerefos CS. Solar actinic radiation (280–420 nm) in the cloud-free troposphere between ground and 12 km altitude: Measurements and model results. J Geophys Res Atmos. 2002;107(D18):PAU 6-1–PAU 6-11.

42. Alam MS, Crilley LR, Lee JD, Kramer LJ, Pfrang C, Vázquez-Moreno M, Ródenas M, Muñoz A, Bloss WJ. Interference from alkenes in chemiluminescent NO_x measurements. Atmos Meas Tech. 2020;13(11):5977–91.

43. Barmet P, Dommen J, DeCarlo PF, Tritscher T, Praplan AP, Platt SM, Prévôt ASH, Donahue NM, Baltensperger U. OH clock determination by proton transfer reaction mass spectrometry at an environmental chamber. Atmos Meas Tech. 2012;5(3):647–56.

44. Voliotis A, Du M, Wang Y, Shao Y, Alfarra MR, Bannan TJ, Hu D, Pereira KL, Hamilton JF, Hallquist M, Mentel TF, McFiggans G. Chamber investigation of the formation and transformation of secondary organic aerosol in mixtures of biogenic and anthropogenic volatile organic compounds. Atmos Chem Phys Discuss. 2022;2022:1–49.

45. Krechmer JE, Day DA, Jimenez JL. Always lost but never forgotten: Gas-phase wall losses are important in all Teflon environmental chambers. Environ Sci Technol. 2020;54(20):12890–7.

46. Tadic I, Nussbaumer CM, Bohn B, Harder H, Marno D, Martinez M, Obersteiner F, Parchatka U, Pozzer A, Rohloff R, Zöger M, Lelieveld J, Fischer H. Central role of nitric oxide in ozone production in the upper tropical troposphere over the Atlantic Ocean and western Africa. Atmos Chem Phys. 2021;21(10):8195–211.

47. Hagenbjörk A, Malmqvist E, Mattisson K, Sommar NJ, Modig L. The spatial variation of O_3, NO, NO_2 and NO_x and the relation between them in two Swedish cities. Environ Monit Assess. 2017;189(4):1–12.

48. Crutzen PJ. The role of NO and NO_2 in the chemistry of the troposphere and stratosphere. Annu Rev Earth Planet Sci. 1979;7(1):443–72.

49. Czader BH, Rappenglück B, Percell P, Byun DW, Ngan F, Kim S. Modeling nitrous acid and its impact on ozone and hydroxyl radical during the Texas Air Quality Study 2006. Atmos Chem Phys. 2012;12(15):6939–51.

50. Zhao Z, Zhang W, Alexander T, Zhang X, Martin DBC, Zhang H. Isolating α-pinene ozonolysis pathways reveals new insights into peroxy radical chemistry and secondary organic aerosol formation. Environ Sci Technol. 2021;55(10):6700–9.

51. Simon M, Dada L, Heinritzi M, Scholz W, Stolzenburg D, Fischer L, Wagner AC, Kürten A, Rörup B, He XC, Almeida J, Baalbaki R, Baccarini A, Bauer PS, Beck L, Bergen A, Bianchi F, Bräkling S, Brilke S, Caudillo L, Chen D, Chu B, Dias A, Draper DC, Duplissy J, El-Haddad I, Finkenzeller H, Frege C, Gonzalez-Carracedo L, Gordon H,

Granzin M, Hakala J, Hofbauer V, Hoyle CR, Kim C, Kong W, Lamkaddam H, Lee CP, Lehtipalo K, Leiminger M, Mai H, Manninen HE, Marie G, Marten R, Mentler B, Molteni U, Nichman L, Nie W, Ojdanic A, Onnela A, Partoll E, Petäjä T, Pfeifer J, Philippov M, Quéléver LLJ, Ranjithkumar A, Rissanen MP, Schallhart S, Schobesberger S, Schuchmann S, Shen J, Sipilä M, Steiner G, Stozhkov Y, Tauber C, Tham YJ, Tomé AR, Vazquez-Pufleau M, Vogel AL, Wagner R, Wang M, Wang DS, Wang Y, Weber SK, Wu Y, Xiao M, Yan C, Ye P, Ye Q, Zauner-Wieczorek M, Zhou X, Baltensperger U, Dommen J, Flagan RC, Hansel A, Kulmala M, Volkamer R, Winkler PM, Worsnop DR, Donahue NM, Kirkby J, Curtius J. Molecular understanding of new-particle formation from α-pinene between –50 and +25°C. Atmos Chem Phys. 2020;20(15):9183–207.

52. Orlando JJ, Tyndall GS. Laboratory studies of organic peroxy radical chemistry: An overview with emphasis on recent issues of atmospheric significance. Chem Soc Rev. 2012;41(19):6294–317.

53. Tsiligiannis E, Hammes J, Salvador CM, Mentel TF, Hallquist M. Effect of NO_x on 1,3,5-trimethylbenzene (tmb) oxidation product distribution and particle formation. Atmos Chem Phys. 2019;19(23):15073–86.

54. Yan C, Nie W, Vogel AL, Dada L, Lehtipalo K, Stolzenburg D, Wagner R, Rissanen MP, Xiao M, Ahonen L, Fischer L, Rose C, Bianchi F, Gordon H, Simon M, Heinritzi M, Garmash O, Roldin P, Dias A, Ye P, Hofbauer V, Amorim A, Bauer PS, Bergen A, Bernhammer A-K, Breitenlechner M, Brilke S, Buchholz A, Mazon SB, Canagaratna MR, Chen X, Ding A, Dommen J, Draper DC, Duplissy J, Frege C, Heyn C, Guida R, Hakala J, Heikkinen L, Hoyle CR, Jokinen T, Kangasluoma J, Kirkby J, Kontkanen J, Kürten A, Lawler MJ, Mai H, Mathot S, Mauldin RL, Molteni U, Nichman L, Nieminen T, Nowak J, Ojdanic A,

Onnela A, Pajunoja A, Petäjä T, Piel F, Quéléver LLJ, Sarnela N, Schallhart S, Sengupta K, Sipilä M, Tomé A, Tröstl J, Väisänen O, Wagner AC, Ylisirniö A, Zha Q, Baltensperger U, Carslaw KS, Curtius J, Flagan RC, Hansel A, Riipinen I, Smith JN, Virtanen A, Winkler PM, Donahue NM, Kerminen V-M, Kulmala M, Ehn M, Worsnop DR. Size-dependent influence of no_x on the growth rates of organic aerosol particles. Sci Adv. 2020;6(22):1–9.

55. Wildt J, Mentel TF, Kiendler-Scharr A, Hoffmann T, Andres S, Ehn M, Kleist E, Müsgen P, Rohrer F, Rudich Y, Springer M, Tillmann R, Wahner A. Suppression of new particle formation from monoterpene oxidation by NO_x. Atmos Chem Phys. 2014;14(6):2789–804.

56. Kirkby J, Duplissy J, Sengupta K, Frege C, Gordon H, Williamson C, Heinritzi M, Simon M, Yan C, Almeida J, Tröstl J, Nieminen T, Ortega IK, Wagner R, Adamov A, Amorim A, Bernhammer A-K, Bianchi F, Breitenlechner M, Brilke S, Chen X, Craven J, Dias A, Ehrhart S, Flagan RC, Franchin A, Fuchs C, Guida R, Hakala J, Hoyle CR, Jokinen T, Junninen H, Kangasluoma J, Kim J, Krapf M, Kürten A, Laaksonen A, Lehtipalo K, Makhmutov V, Mathot S, Molteni U, Onnela A, Peräkylä O, Piel F, Petäjä T, Praplan AP, Pringle K, Rap A, Richards NAD, Riipinen I, Rissanen MP, Rondo L, Sarnela N, Schobesberger S, Scott CE, Seinfeld JH, Sipilä M, Steiner G, Stozhkov Y, Stratmann F, Tomé A, Virtanen A, Vogel AL, Wagner AC, Wagner PE, Weingartner E, Wimmer D, Winkler PM, Ye P, Zhang X, Hansel A, Dommen J, Donahue NM, Worsnop DR, Baltensperger U, Kulmala M, Carslaw KS, Curtius J. Ion-induced nucleation of pure biogenic particles. Nature. 2016;533(7604):521–6.

57. Mochizuki T, Kawamura K, Miyazaki Y, Wada R, Takahashi Y, Saigusa N, Tani A. Secondary formation of oxalic acid and related organic species from biogenic sources in a larch forest at the northern slope of Mt. Fuji. Atmos Environ. 2017;166:255–62.

58. Eddingsaas NC, Loza CL, Yee LD, Seinfeld JH, Wennberg PO. a-pinene photooxidation under controlled chemical conditions – Part 1: Gas-phase composition in low- and high-NO_x environments. Atmos Chem Phys. 2012;12(14):6489–504.

59. Rolletter M, Kaminski M, Acir IH, Bohn B, Dorn HP, Li X, Lutz A, Nehr S, Rohrer F, Tillmann R, Wegener R, Hofzumahaus A, Kiendler-Scharr A, Wahner A, Fuchs H. Investigation of the α-pinene photooxidation by OH in the atmospheric simulation chamber saphir. Atmos Chem Phys. 2019;19(18):11635–49.

60. Molteni U, Simon M, Heinritzi M, Hoyle CR, Bernhammer A-K, Bianchi F, Breitenlechner M, Brilke S, Dias A, Duplissy J, Frege C, Gordon H, Heyn C, Jokinen T, Kürten A, Lehtipalo K, Makhmutov V, Petäjä T, Pieber SM, Praplan AP, Schobesberger S, Steiner G, Stozhkov Y, Tomé A, Tröstl J, Wagner AC, Wagner R, Williamson C, Yan C, Baltensperger U, Curtius J, Donahue NM, Hansel A, Kirkby J, Kulmala M, Worsnop DR, Dommen J. Formation of highly oxygenated organic molecules from α-pinene ozonolysis: Chemical characteristics, mechanism, and kinetic model development. ACS Earth Space Chem. 2019;3(5):873–83.

61. Rickly P, Stevens PS. Measurements of a potential interference with laser-induced fluorescence measurements of ambient OH from the ozonolysis of biogenic alkenes. Atmos Meas Tech. 2018;11(1):1–16.

62. Wagner V, Jenkin ME, Saunders SM, Stanton J, Wirtz K, Pilling MJ. Modelling of the photooxidation of toluene: Conceptual ideas for validating detailed mechanisms. Atmos Chem Phys. 2003;3(1):89–106.

63. Hamilton JF, Webb PJ, Lewis AC, Reviejo MM. Quantifying small molecules in secondary organic aerosol formed during the photo-

oxidation of toluene with hydroxyl radicals. Atmos Environ. 2005;39(38):7263–75.

64. Charan SM, Buenconsejo RS, Seinfeld JH. Secondary organic aerosol yields from the oxidation of benzyl alcohol. Atmos Chem Phys. 2020;20(21):13167–90.

65. Baltaretu CO, Lichtman EI, Hadler AB, Elrod MJ. Primary atmospheric oxidation mechanism for toluene. J Phys Chem A. 2009;113(1):221–30.

66. Ji Y, Zhao J, Terazono H, Misawa K, Levitt NP, Li Y, Lin Y, Peng J, Wang Y, Duan L, Pan B, Zhang F, Feng X, An T, Marrero-Ortiz W, Secrest J, Zhang AL, Shibuya K, Molina MJ, Zhang R. Reassessing the atmospheric oxidation mechanism of toluene. Proc Natl Acad Sci U S A. 2017;114(31):8169–74.

67. Newland MJ, Jenkin ME, Rickard AR. Elucidating the fate of the OH-adduct in toluene oxidation under tropospheric boundary layer conditions. Proc Natl Acad Sci U S A. 2017;114(38):E7856–E7.

68. Birdsall AW, Andreoni JF, Elrod MJ. Investigation of the role of bicyclic peroxy radicals in the oxidation mechanism of toluene. J Phys Chem A. 2010;114(39):10655–63.

69. Wyche KP, Monks PS, Ellis AM, Cordell RL, Parker AE, Whyte C, Metzger A, Dommen J, Duplissy J, Prevot ASH, Baltensperger U, Rickard AR, Wulfert F. Gas phase precursors to anthropogenic secondary organic aerosol: Detailed observations of 1,3,5-trimethylbenzene photooxidation. Atmos Chem Phys. 2009;9(2):635–65.

70. Paulsen D, Dommen J, Kalberer M, Prévôt ASH, Richter R, Sax M, Steinbacher M, Weingartner E, Baltensperger U. Secondary organic aerosol formation by irradiation of 1,3,5-trimethylbenzene–NO_x–H_2O in a new reaction chamber for atmospheric chemistry and physics. Environ Sci Technol. 2005;39(8):2668–78.

71. Lin X, Tang X, Wen Z, Long B, Fittschen C, Gu X, Zhang Y, Zhang W. Data of chemical composition of the particles from OH-initiated oxidation of 1,3,5-trimethylbenzene. Data Brief. 2022;42:1–8.

72. Metzger A, Dommen J, Gaeggeler K, Duplissy J, Prevot ASH, Kleffmann J, Elshorbany Y, Wisthaler A, Baltensperger U. Evaluation of 1,3,5 trimethylbenzene degradation in the detailed tropospheric chemistry mechanism, MCMv3.1, using environmental chamber data. Atmos Chem Phys. 2008;8(21):6453–68.

73. Huang M, Hu C, Guo X, Gu X, Zhao W, Wang Z, Fang L, Zhang W. Chemical composition of gas and particle–phase products of OH–initiated oxidation of 1,3,5–trimethylbenzene. Atmos Pollut Res. 2014;5(1):73–8.

74. Ponnusamy S, Sandhiya L, Senthilkumar K. The atmospheric oxidation mechanism and kinetics of 1,3,5-trimethylbenzene initiated by OH radicals – a theoretical study. New J Chem. 2017;41(18):10259–71.

75. Pullinen I, Schmitt S, Kang S, Sarrafzadeh M, Schlag P, Andres S, Kleist E, Mentel TF, Rohrer F, Springer M, Tillmann R, Wildt J, Wu C, Zhao D, Wahner A, Kiendler-Scharr A. Impact of NO_x on secondary organic aerosol (SOA) formation from α-pinene and β-pinene photooxidation: The role of highly oxygenated organic nitrates. Atmos Chem Phys. 2020;20(17):10125–47.

4. Population Study

This work was originally published, in part, in Environmental Science: Processes & Impacts, 12th April 2021[1]

Abstract

Volatile organic compounds (VOCs) are a key class of atmospheric emission released from highly complex petrochemical, transport and solvent sources both outdoors and indoors. This study established the concentrations and speciation of VOCs in 60 homes (204 individuals, 360 x 72 h samples, 40 species) in summer and winter, along with outdoor controls. Self-reported daily statistics were collected in each home on the use of cleaning, household and personal care products, all of which are known to release VOCs. Frequency of product use varied widely: deodorants: 2.9 uses $home^{-1}$ d^{-1}; sealant-mastics 0.02 uses $home^{-1}$ d^{-1}. The total concentration of VOCs indoors (range C_2–C_{10}) was highly variable between homes e.g. range 16–8,146 $\mu g\ m^{-3}$ in winter. Indoor concentrations of VOCs exceeded outdoor for 84% of households studied in summer and 100% of homes in winter. the most abundant VOCs found indoors in this study were *n*-butane (wintertime range: 1.4–4,630 $\mu g\ m^{-3}$), likely released as aerosol propellant, ethanol, acetone and propane. The cumulative use VOC-containing products over multiday timescales by occupants provided little predictive power to infer 72 hour averaged indoor concentrations. However, there was weak covariance between the cumulative usage of certain products and individual VOCs. From a domestic emissions perspective, reducing the use of hydrocarbon-based aerosol propellants indoors would likely have the largest impact.

[1] DOI: https://doi.org/10.1039/D0EM00504E. N.B: since publication, and during thesis write-up, a duplicate canister ID was discovered in the original dataset. As this was only one household, this issue will likely cause minimal, if any, changes to figures 4.6, 4.7, 4.8, and 4.11. Affected figures remain as published in Heeley-Hill et al. (2021).

4.1. Introduction

Contemporary observations have indicated that, on average, people in high income countries spend up to 90% of their time in enclosed indoor spaces [1]. This motivates the need to understand the chemistry of indoor environments, and to quantify any public health risk that may exist in the built environment where it may be a significant vector for exposure to air pollution [2-4].

Indoor environments are influenced by a multitude of factors, with outdoor air being a major contributor to indoor pollution [5]. Sources of pollution outdoors are various, with vehicular emissions being a primary driver, though industrial sources can also exert significant influence [6]. Ventilation, both mechanical (e.g. HVAC) and non-mechanical (e.g. open windows and doors), is thought to impact concentrations of pollutants indoors, though further research is needed to determine the exact influence of either. A study by Montgomery et al. [7] found higher TVOC concentrations in a non-mechanically ventilated office space than in a mechanically ventilated one, <100 μg m^{-3} and <50 μg m^{-3} toluene equivalent respectively (using a conversion factor as described by Mizukoshi et al. [8]) In the context of office spaces during dust storm events, concentrations of $PM_{2.5}$ and PM_{10} were approximately three times higher indoors. (e.g. $PM_{2.5}$ indoor non-storm = 15.9 μg m^{-3}, indoor storm = 46.5 μg m^{-3}) [9]. This was attributed to the use of a HEPA-filtered ventilation system [9].

Even in air-borne microbial communities, similarity between outdoor and indoor spaces due to ventilation systems was observed (approximately 88% of indoor species were also observed outdoors) [10]. In models, effectiveness in different filtration types was also observed by Azimi et al. [11] Higher efficiency filters, such as high-efficiency particulate air (HEPA) filters were proven to reduce the concentrations of $PM_{2.5}$ and ultra-fine particulates over lower efficiency, minimum efficiency reporting value (MERV) filters, with a reported average effectiveness of HEPA filters of >20% to 50% for both

$PM_{2.5}$ and ultra-fine particulates, as compared to <5% for the lowest efficiency filters, across multiple housing types and climates in the United States [11]. Beyond the ingress of outdoor air inside, indoor air quality is also affected by a range of biological agents, such as pet dander, dust, mould, and mildew [12]. Presence of radon gas is important as a source of exposure to ionising radiation in homes, depending on the local geology [13, 14]. These factors are further influenced by multiple parameters, such as humidity and temperature [12].

Indoor chemistry and exposure science literature shows how multiple factors can influence indoor emissions and air quality [6]. For volatile organic compounds (VOCs) specifically, air exchange rate is critical, as is the ingress of outdoor air, the internal combustion of fuels, cooking activities, off-gassing from building materials and furnishings, and the use of VOC-containing products. All potentially impact on indoor concentrations [15]. Occupants themselves are also a living source of VOCs, from breath, skin, sweat and so on [16-19]. The overall balance of human exposure to VOCs is therefore a blend of air inhaled indoors and when outside. Outdoor VOCs have been monitored routinely in many countries for decades and much is known about representative concentrations, variability and exposure. Indoor atmospheres are more difficult to representatively characterise for VOCs than outdoors as each built environment is unique. Detailed chemical inventories of indoor VOC concentrations are a developing aspect of research in the context of larger population studies [20-25]. Existing studies suggest that concentrations, and therefore exposure to VOCs are very frequently greater indoors than outdoors [22-24].

Indoor VOC measurements have historically used passive diffusion sampling tubes containing a chemical sorbent material. This can limit the range of VOCs detected and the sensitivity of that detection [26] but has the practical advantage of being cheap, flexible and scaleable to large numbers of homes. Contemporaneous studies have utilised alternative analytical methods, such

as proton-transfer-reaction mass spectrometry (PTR-MS) and chemical ionisation mass spectrometry (CIMS). These online methods provide chemical analysis in real-time, but this is often impractical to set-up in domestic environments [27-29]. This highlights a key dilemma in studying VOCs indoors. Simple, scalable methods for population studies must rely on slow time integrated collection of samples over hours to many days, whilst advanced mass spectrometric methods can provide immense detail on second-by-second processes, but only for one or two test homes at a time. Neither method is 'better', insight emerges from the blending of information from both.

Often missing from on-line MS and adsorbent tubes used in indoor studies are measurements of the most volatile VOCs. Though more materials-intensive, an alternative is to deploy within homes internally silica-treated stainless-steel canisters, with flow restrictors as samplers; outlined in the United States Environmental Protection Agency Toxic Organic 15 Compendium Method [30]. Offline laboratory analysis of canister-collected samples using, for example, combinations of both gas chromatography-mass spectrometry (GC-MS) and gas chromatography-flame ionisation detection (GC-FID) analysis thus broadens the range of gas-phase VOCs that can be screened [31, 32].

In recent years, there has been particular interest in the role of terpenoid VOCs within indoor settings. These are commonly released from consumer fragrances and are contained in personal care and cleaning products; these are mostly derived from plant oils [33-35]. Terpenoids are also emitted indoors from natural sources: plants, flowers, fruit, herbs, and spices. Toxicological assessments show that monoterpene VOCs are not themselves harmful at typical part per billion concentrations that might be encountered indoors. For instance, d-limonene has been demonstrated to have a low order of toxicity potential at low inhalation exposure levels (ECHA REACH Registration [36]), or when compared to REACH-compliant Derived No Effect Levels [37]. Similar

conclusions have been reached in other studies examining VOC emissions and indoor air exposures that were below critical exposure limits [38].
An area of uncertainty has been the potential for these classes of relatively reactive VOCs to degrade to form secondary pollutants through indoor oxidation with ozone. Ozone can be drawn indoors from outside, and other possible oxidation routes include reactions with OH, Cl, and NO_3 radicals that can be generated indoors [39]. Gas phase by-products from the oxidation of VOCs indoors include formaldehyde, acetaldehyde - both species being formed as part of the atmospheric degradation of many different VOCs - and secondary organic aerosols (SOA) [40, 41].

Undertaking broad, and ideally non-targeted, screening of the full range of VOCs present indoors is central to the attribution of observed abundances to their different contributing sources and to assess the relative balance of VOC exposure between indoors and outside. Whilst few VOCs are emitted by only one activity indoors, some do have distinctive contributing sources where it may be hypothesised that indoor speciation could be influenced by the consumption or usage patterns of the originating products albeit it with other factors such as air exchange rate possibly controlling absolute concentrations. For example, acetone, ethanol, dichloromethane, limonene and *n*-pentane are used as solvents within both professional and domestic cleaning products [42-45]. Acetone and ethanol emissions can also be observed in human breath as a result of biological processes [46]. Moreover, ethanol is emitted from food, such as bread [47]. *iso*-butane and *n*-butane are the major VOCs used as propellants within compressed gas products, often combined with propane and with ethanol as a cosolvent, dependent on manufacturer and product [45, 48]. Toluene, ethylbenzene and *m, p* and *o* xylene species are commonly associated with paints, glues and varnishes [49] and ethane and propane are minor components of fossil methane gas [50], found indoors via small gas leaks. VOCs can be released indoors from leakage of the fuels used for heating and cooking, the speciation of these depending on the fuels used. In this UK study the dominant fuel used in all

homes was natural gas, comprising methane with ~8% ethane and trace propane and butane. Other locations and countries can have different fuel blends often comprising propane and butane,

Another consideration, though not within the scope of this study, is further chemical interactions, such as the formation of secondary organic aerosols (SOAs) and the influence of surface reservoirs. Heterogeneous surface chemistry is an emerging topic in indoor chemistry and is covered in the recent literature [51-53]. SOA production is driven predominantly by the oxidants OH and O_3 [54]. Though indoor data on these species were not collected in this study, it is likely that species with a short indoor residence time will be affected by different oxidant concentrations between seasons [55, 56].

Domestic usage of VOC-containing products can be simplistically placed into one of two classifications. '*Large dose - low frequency*' emissions are those arising from infrequent activities such as painting and decorating, or the installation of new furniture. These have relatively well-described effects in the research literature [3, 57]. The contribution of these sources is reflected in efforts to reduce VOC content in building products and paints, for example in the EU via the Construction Products Directive 89/106/EEC and Paints Directive 2004/42/EC.

By contrast, the effects of '*small dose - high frequency*' emissions are much more uncertain contributors to both indoor air quality and as a source of outdoor VOC pollution as well. Whilst many different products contain trace amounts of VOCs, the connections between the use of small dose - high frequency products, and overall domestic VOC emissions and concentrations is uncertain in real-world settings. These products are diverse in their applications and are used, potentially, multiple times per day and by multiple occupants. This source classification can include personal care and household products [57-60].

In the public reporting and general discussion of the relationships between VOCs and indoor air quality there is often anecdotal linkage made between particular types of consumer products and adverse indoor air quality outcomes. Fragranced candles, for example, are frequently cited in the context of personal indoor VOC exposure [37]. There is however little direct evidence showing a quantitative and causal relationship between frequency of use of a specific product and the observed concentrations of a particular VOC indoors, rather it is inferred from product formulation. We note however the work of Adgate, Church et al. [22] which did suggest a correlation between indoor VOC concentrations and the use of cleaning products.

4.1.1. Study objectives

In this study we set out to evaluate the potential association between real-world indoor VOC concentrations, the speciation of the VOCs found indoors, and the consumption patterns of consumer products. An association between the cumulative frequency of use of an individual product (over a period of three days), or use of many products, and changes in indoor VOC speciation and concentrations would potentially provide an attractive predictive method to estimate VOCs more widely, should consumption statistics be known. We focus on the metric of culminative 'frequency of recorded uses' of products, since it is simple and reliable data to collect in a population study. We readily acknowledge that other, more difficult to quantify factors such as the size of dose in each use, and the differences in product-to-product formulation from different manufacturers will also be very important controlling variables that influence VOC emissions. By collecting both indoor and outdoor samples simultaneously, we have been able to then assess the relative significance of indoors versus outdoors as locations for exposure to VOCs for this study cohort. Since we use only simple methods we do not have data on real-time activities such as ventilation rates, or wider environmental conditions such as in-room photolysis. We do however collect

some proxy data such as building, age, type, occupancy and so on that allows some of these aspects to be explored further.

4.2. Methods

4.2.1. Experimental methodology

A cohort of 204 volunteer participants was drawn from an existing and well-characterised panel of naïve consumer product testers, based in Ashford, United Kingdom. All the homes are located within the Ashford town region, meaning the homes here should be typically characterised as experiencing suburban UK background conditions for outdoor pollutants The study used 60 individual homes (all primary residences) with a median occupancy of 4 people per home. The demographics of the participants and information of the property types are shown in Tables 4.1 and 4.2.

Table 4.1: Demographic information of participants by season

	Winter	Summer
Male	95	104
Under 18	32	35
18–30	16	20
31–45	25	25
46–60	17	17
61–75	5	7
Female	109	100
Under 18	34	33
18–30	18	14
31–45	30	26
46–60	18	17
61–75	9	10
Gender not disclosed	1	0
18–30	1	0

Table 4.2: Property information by season

	Winter	Summer
Property Era		
Victorian, or earlier	21	23
1920–1930	6	5
1940–1950	8	13
1960–1970	36	38
1980–2000	45	44
2000+	64	57
Property Type		
Detached	91	85
Semi-Detached	55	66
Studio Apartment	6	6
Terraced	28	23
Number of Residents		
1	9	9
2	42	46
3	27	26
4	69	68
5+	33	31
Number of Bedrooms		
2	29	29
3	87	82
4	38	45
5+	26	24

Of the participants in the first winter sampling experiments, 91.7% also participated in the summer experiment. Five new replacement homes were added in the summer experiment to maintain a constant sample size, since a small number of participants were unavailable for both seasons. The broader purpose and hypothesis of the study was not divulged to the participants, who were asked only to place the canister samplers in their homes and record statistical information daily on a tablet-based information system. Study participant identities and home locations were known to Givaudan UK, but these were not divulged to the University of York. Households were given a unique household ID, to which canister IDs were assigned during the experimental periods. These actions were performed to preserve participant and home anonymity.

A total of 360 indoor air samples and 55 outdoor background control samples were collected over two, nine-week sampling periods between February and April 2019 (defined as winter), and July and September 2019 (summer). Feb–April 2019 - period average minimum outdoor temperature 4.7 ºC; max 11.4 ºC. July–Sept 2019 - period average minimum outdoor temperature 14.9 ºC; max 20.5 ºC. Three indoor samples were taken in each house per sampling campaign, giving a total of six samples per house for the study. Three households were randomly selected each week to collect a control outdoor sample, placing a sampler in a back garden away from the home.

Samples were collected indoors over three days into 6 L internally silica-treated stainless-steel canisters. These canisters were evacuated initially to 300 Pa. They used 72-hour equivalent flow controllers to create a linearly averaged 48-hour sampling time (Entech, CA, USA and Restek, PA, USA), and then a reduced flow rate for the final 24 hours. A sampling period of 72 hours allowed the capture of VOC concentration spikes accompanying product use, in addition to the longer decay attendant to product evaporation, such as from skin or hair. Canisters were evacuated, in the laboratory, on a high-vacuum rig before use. Field and laboratory blank canisters were interspersed randomly amongst the samples during the automated laboratory analysis. Samplers were only placed in a living room or kitchen-living room if the property was open plan. Guidance was given to avoid placing samplers directly near sources of VOCs such as flowers, diffusers, plug-ins and so on. The most common location for samplers was on the floor which, when the inlet restrictor is included, meant a sampling height of ~50 cm above the floor level. The sampling gas flow profile of a typical sampler is shown in Figure 4.1.

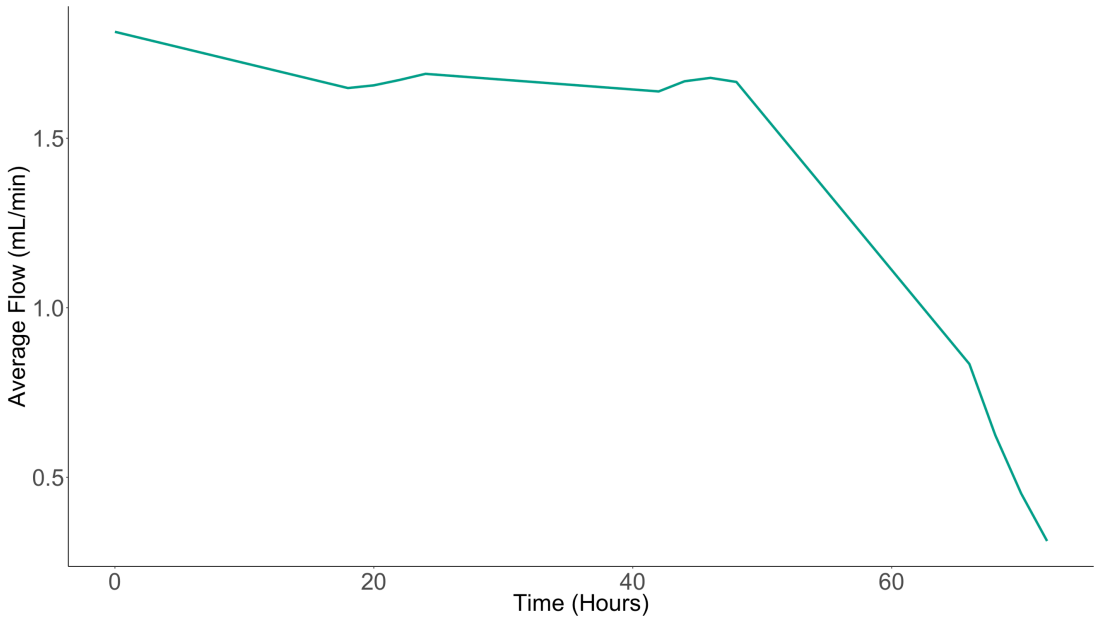

Figure 4.1: Sampling flow profile of a typical sampler used in the study

Following sample collection in homes participants returned their canisters to a central collection point in Ashford and these were couriered to the University of York. Samples were analysed within seven days of collection, with canisters then evacuated for re-use and returned to Ashford. Each canister sample was pressurised to 179 kPa using highly purified air, whereupon they were connected to autosamplers. Field blanks and calibration standards were included in the sample sequence. Two separate instruments were used in this study and samples run on both instruments: 1) a thermal desorption GC-FID-FID system, an Agilent 7890B (Agilent Technologies, Santa Clara, CA, USA), used to quantify C_2–C_8 non-methane hydrocarbons and short chain oxygenates, based on the method of Hopkins, Lewis et al. [61] This used two PLOT columns connected to a Markes CIA Advantage xr autosampler, a Markes Kori xr water condenser, and a Markes Unity xr thermal desorption system. (Markes International, Llantrisant, UK). 2) Thermal desorption GC-ToF-MS based on the methods in Shaw, Lidster et al. [62] using a Markes Unity 2 thermal desorption system, an Agilent 7890A with volatility-based GC separation on methyl siloxane GC column and an Almsco ToF detector (Almsco International, Llantrisant, UK). This

provided quantification of C_4–C_{12} VOCs. Per 6 L sample, a total of 1 l was taken (500 mL for each analytical system). The species quantified in this study are listed in Table 4.5; in some cases, the same VOC was measured on both analytical systems, providing a further crosscheck of analytical performance.

Calibration was based on gravimetrically prepared high pressure (10 MPa) standards, a combination of a 4 ppb, 30 component NMHC ozone precursor non-methane hydrocarbon standard (National Physical Laboratory, Teddington UK) and custom-blended multicomponent standard including terpenes and oxygenated VOCs based on in-house dilution of part per million gravimetric standards into secondary high pressure passivated cylinders with individual VOCs in the part per billion range. In all cases the calibration standard balance gas was high purity nitrogen (chromatograms shown in Figures 4.2 and 4.3). The limit of detection for individual VOCs on both systems was typically in the 5–50 parts per trillion range. On appropriate molecular weight conversion at 25 °C to VOC-specific mass concentrations, this equated to detection limits (defined as 3 times S/N) for individual VOCs typically in the range 0.015–0.2 μg m^{-3}. The range of different detection limits reflects differing carbon responses by FID and differing fragmentation patterns and ionisation efficiency in the MS.

Measurement uncertainty was dominated by uncertainties carried forward in calibration from the gravimetric primary gas standards. These were quoted by manufacturers as 5% uncertainty. Further uncertainty arises from run to run analytical reproducibility, itself a function of VOC concentration. For measurements of VOCs more than 10 times the detection limit, reproducibility of analysis was typically better than 1% for GC-FID. When other components of the sampling system are considered, such as variability in inlet flow rate and blank canister artefacts, an expanded uncertainty of ~7% results. For measurements of VOCs closer to the detection limit uncertainties are considerably greater, rising to 50% for chromatographic

peaks that are 3 times signal to noise. Our measurements cover a very wide range concentrations, often high values relative to detection limits. We report concentrations by default to three significant figures, unless the concentration was sufficiently low that the third figure decade was equivalent to or greater than the estimated uncertainty, in which case values were truncated to fewer significant figures to avoid artificial precision being inferred.

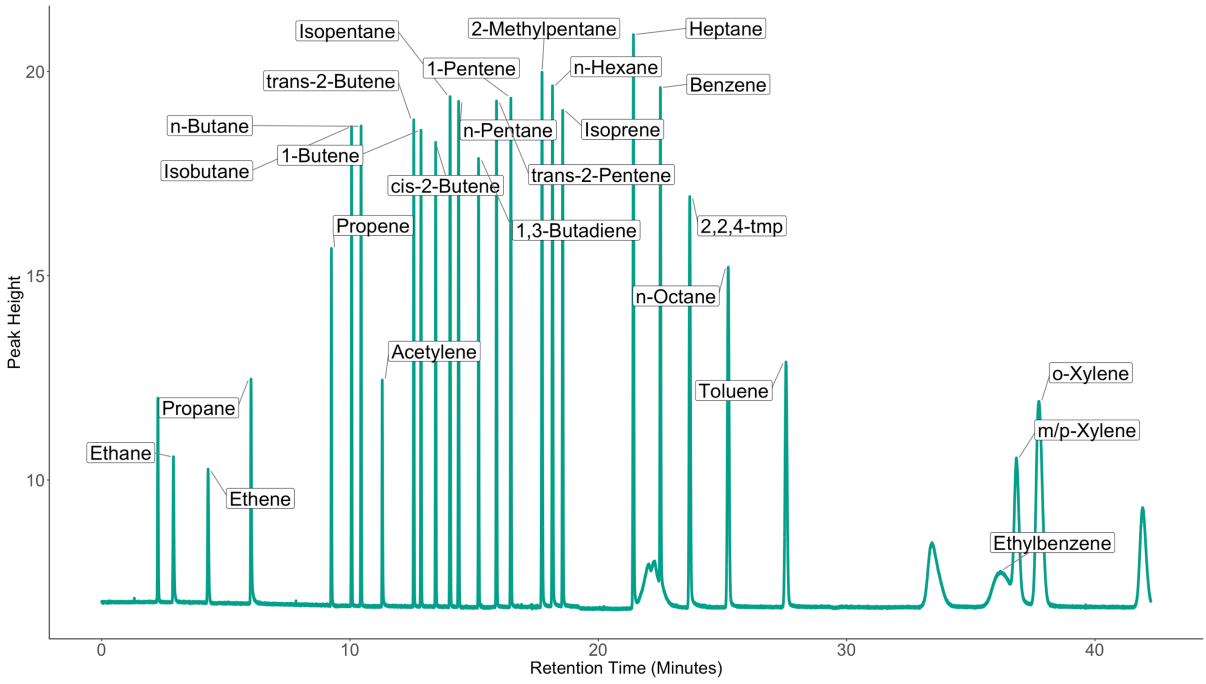

Figure 4.2: GC-FID chromatogram for NPL 30 NMHC calibration gas at 4 ppb per VOC

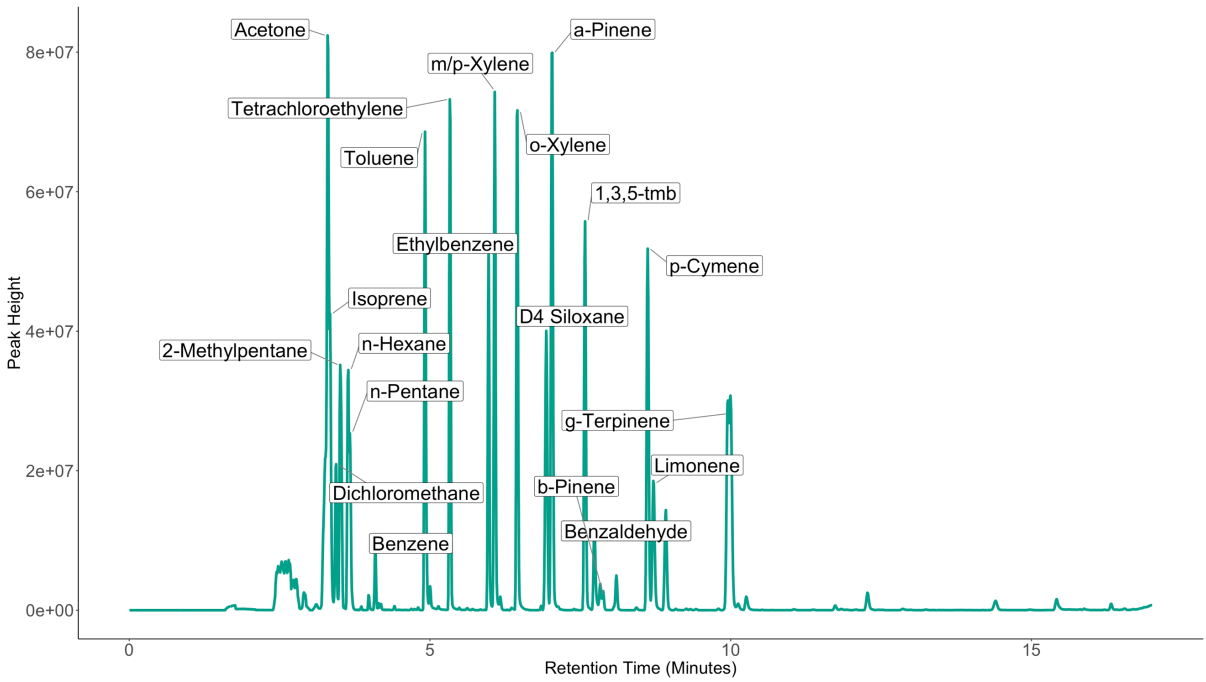

Figure 4.3: GC-MS chromatogram for custom-blended calibration gas including monoterpenes and oxygenates

4.2.2. Survey methodology

A participant and activity survey was developed to place the chemical data in the context of property information, residence occupancy, and resident demographics. A daily log was then completed to obtain information about the use of VOC-containing products by residents in each home. The survey was based on pre-existing panel study methodologies used by Givaudan UK, and was digitised for user inputs on a supplied tablet computer. Products included in the survey were selected to cover a wide range of different VOC-emitters commonly found in the home. The survey considered only VOCs likely to be conventionally used within the main domestic living space of the home (see Tables 4.3 and 4.4). In combination, complete data log records and matching chemical analysis were generated for 92% of the deployed samplers. Around 8% of sampling opportunities were lost due to participant sampling errors, failure to complete diary logs, or the sample analysis not meeting the required laboratory QA/QC standards.

Table 4.3: Additional questions posed in the participant household survey

Additional Household Questions	
Built-in Garage	Yes
	No
Glazing	Single
	Double or triple
Heating Method	Solid fuel; wood stove
	Solid fuel; coal
	Solid fuel; log burner
	Solid fuel; other - please specify
	Solid fuel; gas central heating
	Solid fuel; electric central heating
	Solid fuel; oil central heating
	Solid fuel; LPG central heating
Cooking Method	Gas
	Electric
	Solid fuel
	Other; please specify
Presence of Smokers	Yes
	No
Presence of Cut Flowers	Yes
	No

Table 4.4: Product-use log provided to study households. Participants were asked to complete the log each day of the study period and an average was taken to identity mean product usage for each household, per study period.

	Product Type	Uses
Day 1	Aftershave/Perfume	n
	Air freshener	n
	Antiperspirant Deodorant	n
	Candles	n
	Cleaning Sprays	n
	Furniture Polish	n
	Hairspray	n
	Insecticide-Fly Sprays	n
	Paint	n
	Plug-ins	n
	Sealant-Mastics	n
Day 2	Aftershave/Perfume	n
	...	n
Day 3	Aftershave/Perfume	n
	...	n

The study was limited to recording occupants' frequency of use of products as a numerical value of number of times per day. Frequency of use is clearly only part of the overall behaviour that defines VOC emissions from a particular product when in use. The size of dose used will also be a factor in determining emissions, but this is complex to estimate in a self-led diary study. A further important influence is individual product composition, though participants were not asked to record manufacturer or brand. We discuss this further in the conclusions section.

4.2.3. Statistical methodology

Data analysis was performed using R v.4.02 "Taking off Again" and the RStudio environment v.1.3.1073 "Golden Rod", data manipulation was

performed using the *dplyr* (v.1.0.2) package. The majority of the methods used in this manuscript utilise descriptive statistics, with attendant visualisation therein. 25th and 75th and 5th and 95th percentiles were used to ascertain high and low concentrations where appropriate. Median values were favoured over mean values so as not to confound outlier influence and concentration values when considering averages. Correlation analysis was performed using the *cor* function of the *stats* (v. 4.0.2) package in R. Visualisation of the correlation matrix was achieved using the *corrplot* function of the *corrplot* package (v. 0.84). Correlation is displayed as follows: a narrow, forward-slanting straight line represents a strong correlation, a full circle represents no correlation and a backward-slanting straight line represents an anti-correlation. Darker blues indicate greater correlation, darker reds represent lesser correlation. Numbers are on a scale of -1 to 1, with -1 being anticorrelated and 1 being fully correlated. Covariance analysis was performed after rescaling the raw concentration data on a scale of 0–1, and rescaling the covariance values from 0-100 using the normalize function of the *BBmisc* package in R (v.1.11). Data normality was tested using the Anderson-Darling Test. The Wilcoxon Rank Sum Test was performed to test statistical difference between the mean of two groups of data. The test is non-parametric so assumes non-normal data distribution. Regression analysis was performed using the *lm* function in the *stats* R package.

Total indoor VOC concentrations, henceforth referred to as TVOC, is a widely used metric in the literature to measure total VOC mass indoors. TVOC is typically measured by dedicated sensors which make an operationally defined determination of concentrations. There is no absolute traceable methodology for TVOC; Total carbon by FID is the closest approximation, often yielding similar values to the summation of the individual parts as quantified by GC-MS or GC-FID. Here we use the sum concentration of all VOCs analysed by GC-FID and GC-MS a methodology common to other studies [63-66].

4.3. Results

4.3.1. Product use statistics

An initial analysis was performed on the frequency of use of individual classes of VOC-containing products, and a summary of total recorded uses in each home is shown in Figure 4.4.

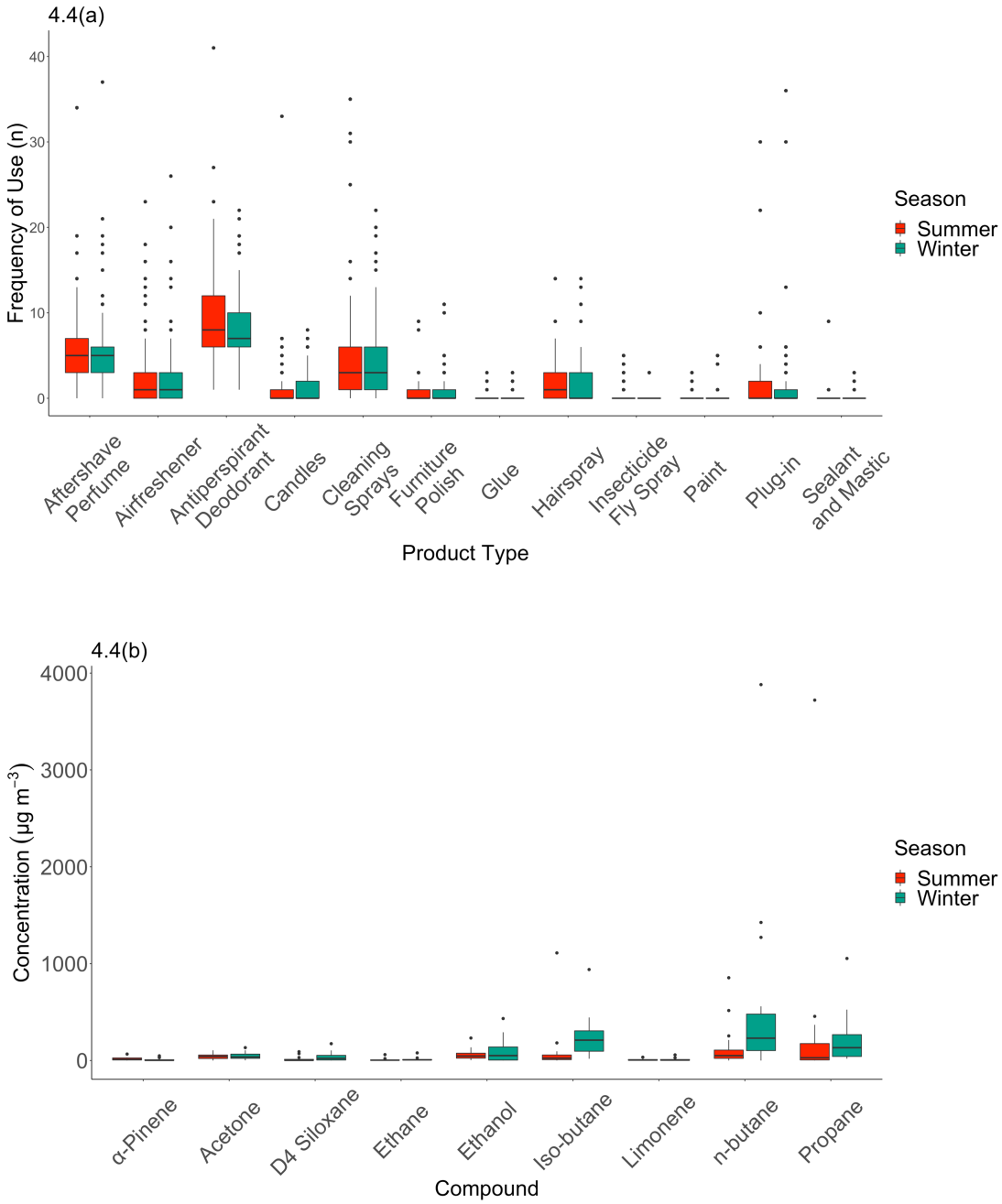

Figure 4.4: (a) Frequency of use of product types per sampling period across all households by season and (b) concentration ranges of selected VOCs from 60 homes by season (red is summer, green winter). Box size is defined by the 25th and 75th percentiles, with the middle line of the boxes the median value. No greater than 1.5 times the interquartile range from both percentiles defines the whiskers. Outliers are plotted as individual data points beyond the whiskers. To aid visualisation in (b), outliers beyond the 10th and 90th percentiles on *n*-butane are not included in the plot, but are included in calculations used to define box plot parameters

Many of these products are typically listed in review literature as being contributors to indoor VOCs. We note that there are, in practice, a very wide range of frequencies of actual use in real-world settings, something that is rarely quantified or discussed in reviews. VOC sources such as paints are only used infrequently in homes, as would be expected from a likely large dose - low frequency product; 72% of homes never used any paints during this study. We do recognise however that decorating products, such as paints, will continue to emit VOCs at some level for an extended period after initial application and may contribute to what is measured [67].

The most commonly-used consumer product source of VOCs indoors were aerosol antiperspirant deodorants. These were used in all 60 homes that were studied and with an average frequency across the cohort of 2.9 uses per home per day. Some VOC-containing products such as plug-in air fresheners were used in relatively few of the UK homes studied, but frequency of their use varied widely from only occasional use to up to > 35 uses per sampling 72 hour period. This very wide variability in types of products used, and the frequency of use of any given product, highlights the inappropriateness of generalising about the contributions of particular product types as contributors to indoor VOC concentrations. Little commonality existed in VOC product usage, or frequency of use between

homes, beyond the almost universal use of deodorants, cleaning sprays and perfumes.

There were some modest differences in the seasonal use of different product types (Figure 4.4(a) and Table 4.6). For instance, personal care products (i.e. antiperspirant/deodorants) were reported as being in greater use during the summer than in the winter (frequency of use median = 8 per sampling period in summer, 7 in winter). Usage of other product types remained largely constant between seasons.

Table 4.5: Indoor VOC concentration statistics (median, 5th percentile, 95th percentile and standard deviation values) for 60 homes combining winter and summer samples, n = 360. All values are given as concentrations in μg m^{-3}. Measurement uncertainty was typically ±7%. Compounds analysed via GC-FID have limit of detection values as outlined by Hopkins et al. [61]

	Median Concentration	5th%ile	95th%ile	SD	DL
n-butane	107	2.3	1180	547	0.005
Propane	44.2	1.2	609	456	0.004
Acetone	43.8	4.2	156	53.8	0.1
iso-butane	40.4	1.5	597	227	0.005
Ethanol	40.1	dl	283	184	<0.001
α-Pinene	8.0	dl	56.7	24.4	1.6
D4 Siloxane	6.6	dl	96.1	33.7	2.7
Ethane	4.3	0.9	45.9	41.6	0.01
Limonene	3.8	0.3	24.0	10.0	10.8
iso-pentane	3.7	0.6	40.8	38.1	0.006
Toluene	1.5	0.2	28.1	72.6	0.008
m/p-xylene	1.5	0.2	10.4	54.0	3.9
iso-butene	1.2	0.1	10.8	23.4	0.005
o-xylene	1.2	dl	15.2	54.6	2.6
n-pentane	1.1	0.4	10.3	102	2.1
Isoprene	1.0	0.1	3.1	17.7	0.4
Ethene	0.8	0.2	2.8	2.6	0.008
Ethylbenzene	0.8	0.07	6.7	6.3	2.4
cis-2-butene	0.8	0.06	6.7	15.5	0.005

p-cymene	0.7	0.05	4.1	2.6	3.2
Benzene	0.5	0.2	1.8	28.8	2.2
2-methylpentane	0.4	0.06	3.0	881	0.176
1-pentene	0.7	0.03	5.1	2.3	0.006
n-hexane	0.4	0.06	1.6	21.6	0.74
Propene	0.4	0.10	1.1	1.9	0.003
n-heptane	0.3	0.06	2.4	9.9	0.008
Acetylene	0.3	0.05	1.1	0.4	0.002
Methanol	0.3	dl	18.8	32.6	0.1
1-butene	0.3	0.04	1.2	0.7	0.005
n-octane	0.2	0.03	3.7	5.8	0.009
trans-2-pentene	0.2	0.01	10.7	5.8	0.006
Dichloromethane	0.2	dl	1.9	5.5	1.2
1,3,5-trimethylbenzene	0.2	dl	4.4	1.8	1.3
1,3-butadiene	0.2	0.03	2.9	6.7	0.004
β-pinene	0.1	dl	12.4	7.4	12
2,2,4-trimethylpentane	0.1	0.01	3.2	30.5	0.009
trans-2-butene	0.07	dl	0.4	0.2	0.005
Tetrachloroethylene	0.03	dl	0.4	2.1	3.2
γ-Terpinene	dl	dl	0.7	3.0	1.7

Table 4.6: Descriptive statistics for product type and frequency of use over a standard 72-hour participant recording period. Data drawn from 60 homes, including both summer and winter campaigns

	Winter Number of uses in 72 hrs				Summer Number of uses in 72 hrs			
	Range	Median	IQR	SD	Range	Median	IQR	SD
Aftershave Perfume	0–37	5	3	4.33	0–34	5	4	3.71
Air freshener	0–26	1	3	3.72	0–23	1	3	3.57
Antiperspirant Deodorant	1–22	7	4	4.1	1–41	8	6	4.75
Candles	0–8	0	2	1.66	0–33	0	1	2.8
Cleaning Sprays	0–22	3	5	4.07	0–35	3	5	5.6
Furniture Polish	0–11	0	1	1.55	0–9	0	1	1.29
Glue	0–3	0	0	0.485	0–3	0	0	0.42
Hairspray	0–14	0	3	2.33	0–14	1	3	2

Insecticide-Fly Spray	0–3	0	0	0.223	0–5	0	0	1.05
Paint	0–5	0	0	0.674	0–3	0	0	0.5
Plug-in	0–36	0	1	4.67	0–30	0	2	3.95
Sealant Mastic	0–3	0	0	0.319	0–9	0	0	0.695

4.3.2. VOC concentrations across the study cohort and comparison with outdoors

A summary of the VOCs found indoors is shown in Table 4.5. As has been reported in many previous studies, the variability between homes was very large. A small number of VOCs do, however, stand out as being dominant in terms of contribution to the overall VOC concentration indoors. *n*-butane had the highest median concentration in the homes measured, with multiple homes having 72-hour averages exceeding 1,000 μg m^{-3}. Two other commonly used solvents (and with other indoor sources), ethanol and acetone, were also observed in significant concentrations. The distribution statistics for the most abundant VOCs by season are shown in Figure 4.4(b).

TVOC was calculated by season for each home shown in Figure 4.5. Median TVOC in summer was 370 μg m^{-3}, and 426 μg m^{-3} in winter; this was a statistically insignificant difference (Wilcoxon Rank Sum Test, $W = 14356$, $p = 0.126$).

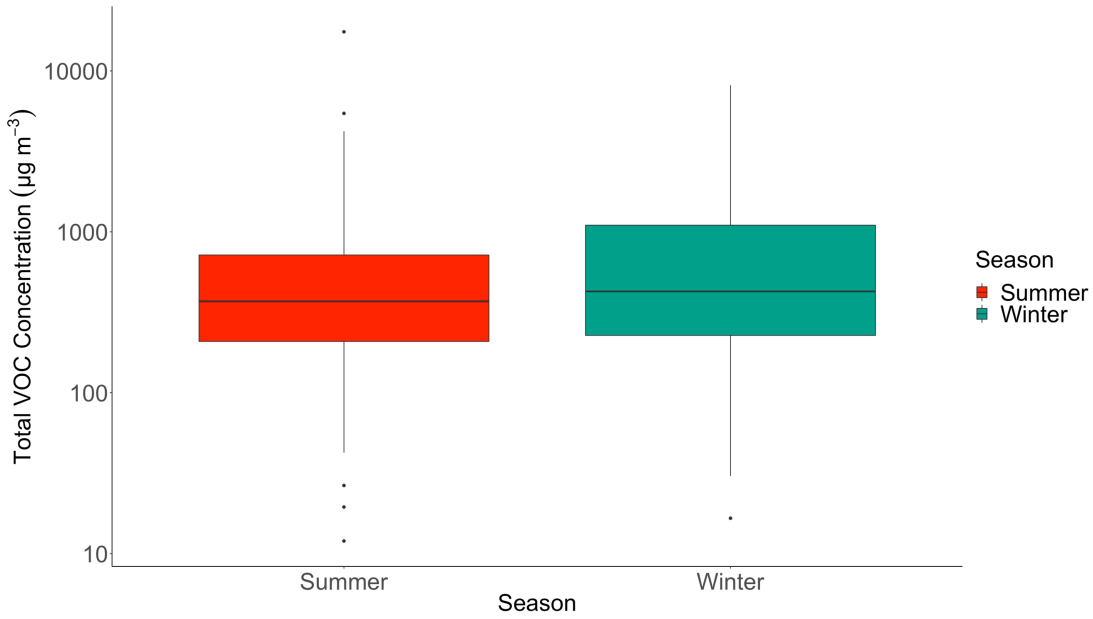

Figure 4.5: Total VOC concentration ranges by season. Box size is defined by the 25th and 75th percentiles of the data. The middle line of the boxes defines the median value. No greater than 1.5 times the interquartile range from both percentiles defines the whiskers. Outliers are plotted beyond the whiskers. Outliers outside the 10th and 90th percentiles are not included in the plot, but are included in calculations used to define box plot parameters

Notable in Figure 4.4(b) was the difference in median *n*-butane concentrations between winter and summer (summer = 69.4 μg m^{-3}, winter = 185 μg m^{-3}). Although frequency of use in this product category was lower in winter, the higher concentrations observed in winter may reflect lower ventilation rates, and its accumulation indoors given it is a relatively unreactive VOC. This was also in evidence for *iso*-butane, a linked emission from aerosols propellants.

Statistically significant seasonal differences in indoor concentrations were observed for certain species. For α-pinene, the summer median concentration was considerably higher than winter (summer = 11.9 μg m^{-3}, winter = 2.9 μg m^{-3}), the median concentration of α-pinene indoors was 8 μg m^{-3} and outdoors was only 0.8 μg m^{-3}, suggestive of more significant possible

sources of emissions from outgassing of wood products from within the fabric of the house[29]. In contrast, limonene had lower median concentrations indoors in summer: 3.6 μg m^{-3}, winter: 4.7 μg m^{-3}, potentially reflective of its accumulation in winter from use of cleaning and fragranced products, and other food sources. The median concentration indoors was 3.8 μg m^{-3} and outdoors was only 0.2 μg m^{-3}, again indicative of a potent inside source, rather than significant ingress from outdoors.

There are relatively few comprehensively speciated indoor studies in the literature to compare these new observations against. A study of a broadly similar nature was the European EXPOLIS study of VOC emissions in Helsinki by Edwards, Jurvelin et al. [68] This reported concentrations of aromatic, halocarbon, and monoterpenes that were, in general, higher than seen in this study. More recent changes in legislation and product composition could have led to lower emissions, ergo lower concentrations in 2019, given the significant near 20 years gap between studies. Seasonal differences in concentrations were reported as negligible, though the EXPOLIS study incorporated spring and autumn measurements when temperatures were broadly similar. A study of the indoor quality of apartments by Schlink, Thiem et al. [69] reported higher concentrations of aromatics and monoterpene species than were found in this study. Jia, Batterman et al. [70] also reported higher concentrations of several VOCs than in this study, with the exception of α-pinene, with samples collected from a number of individual residences over winter and summer. In accordance with this study, seasonality had little influence on indoor concentrations, and correlations between individual species were limited.

4.3.3. VOC concentrations in relation to building characteristics and demographics

Air exchange rates (AER) are a critical factor in controlling indoor VOC concentrations, whether through allowing the ingress of outdoor VOCs, or

through increased concentrations accumulating from sources indoors due to lower dilution [71]. AER is not straightforwardly measured in large numbers of homes simultaneously and could not be directly measured in these homes due to the practicalities involved. Instead, property age and type, and glazing were considered as possible proxies for ventilation – it might be assumed that older buildings (*e.g.* older than 1900) would have the poorest insulation and highest rates of ventilation than modern buildings (*e.g.* post 2000) built to higher energy efficiency standards. Each house in the study was placed into one of six age categories and four building types. In Figure 4.6 we show the concentration statistics (median, interquartile, 95th percentile values) for total VOC (TVOC) as a function of building age and as a function of building type in Figure 4.7.

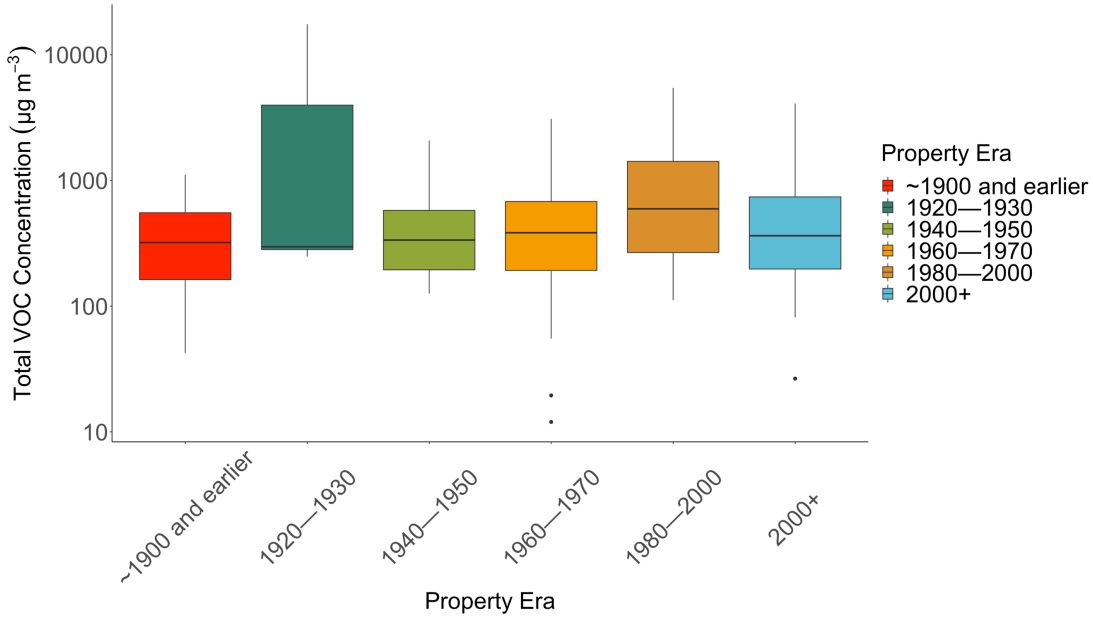

Figure 4.6: Indoor TVOC statistics as a function of building age. Solid black line shows median value, boxes interquartile range and vertical lines 95th percentile values

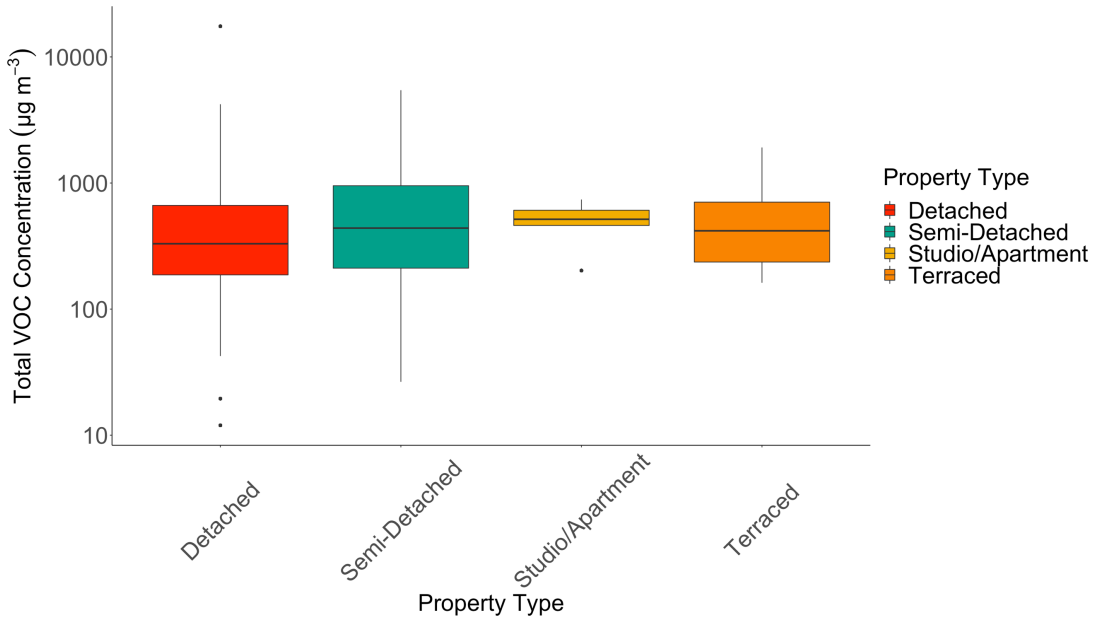

Figure 4.7: Indoor TVOC statistics as a function of property type. Solid black line shows median value, boxes interquartile range and vertical lines 95th percentile values

In our dataset there were no statistically significant differences between TVOC and building age (Kruskal-Wallis Rank Sum Test, $\chi^2(5) = 7.47$, $p = 0.188$). We would note that for all building ages a wide range of concentrations were observed in each class. The highest median TVOC was found in buildings in the era 1960–1979. Similarly, no substantial differences were seen in the median TVOC of homes of different type (Kruskal-Wallis Rank Sum Test, $\chi^2(3) = 2.77$, $p = 0.428$). Slightly higher values were seen in studio and apartments, although again the differences were not statistically significant. Whilst building type and ventilation are without doubt critical factors that influence indoor TVOC concentrations, no systematic differences emerged in this dataset suggesting that factors such as ventilation do not provide an overwhelming degree of control on concentrations.

Number of bedrooms, window glazing type and the presence of an integrated garage were also considered. Calculating median TVOC concentrations

across number of bedrooms per residence resulted in the following observations: 2 bedrooms: 374 μg m^{-3}, 3 bedrooms: 439 μg m^{-3}, 4 bedrooms: 264 μg m^{-3}, 5 plus: 561 μg m^{-3}, see Figure 4.8. No statistical significance was observed between TVOC concentration per household, and number of bedrooms (Kruskal-Wallis Rank Sum Test, $\chi^2(3) = 5.99$, $p = 0.112$). There is a scarcity of literature concerning number of bedrooms and indoor VOC concentrations. A lack of statistical significance could be explained thusly: Larger properties could induce more significant dilution of VOCs, but a greater number of bedrooms does not ipso facto imply a larger property; nor does it imply a greater number of residents and therefore potentially greater concentrations of VOCs.

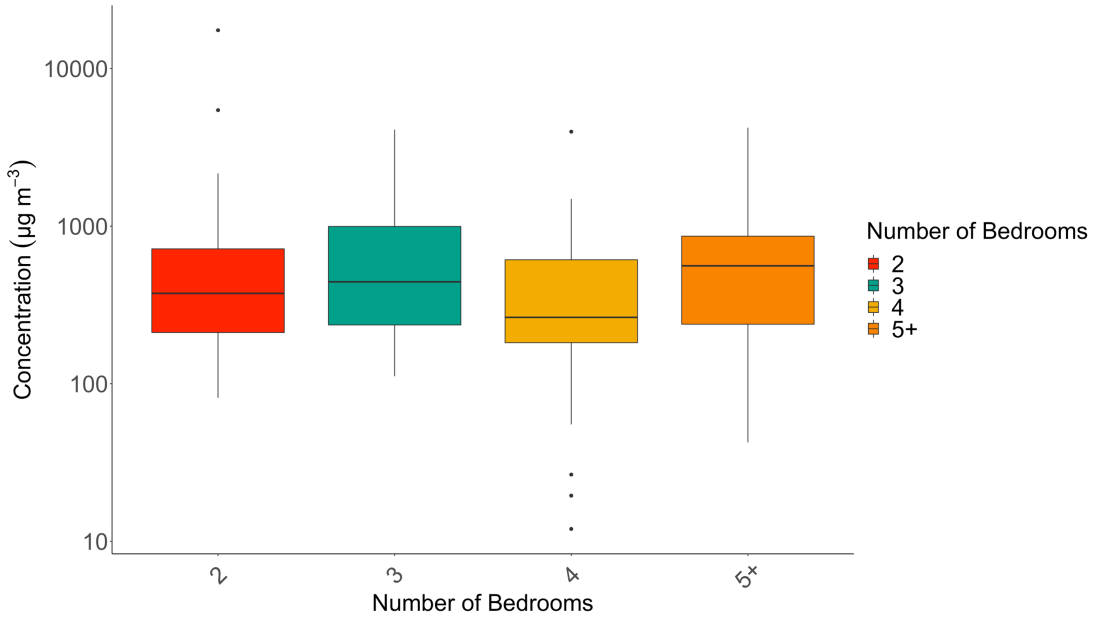

Figure 4.8: Indoor TVOC statistics as a function of the number of bedrooms. Solid black line shows median value, boxes interquartile range and vertical lines 95th percentile values *n*-butane

Calculating median TVOC concentrations across window glazing type resulted in the following observations: double and triple glazed properties: 374 μg m^{-3}, and single glazed properties: 524 μg m^{-3}, see Figure 4.9; no statistical significance was observed (Wilcoxon Rank Sum Test, $W = 503$, $p = 0.94$). Please note that no distinction was made between double and triple

glazed properties. Research is currently lacking as to the potential impacts of window glazing type on indoor VOC concentrations. Existing research places greater emphasis on the role of window opening and air quality. One potentially important factor in determining the impact of glazing type and VOC concentrations is the air exchange rate. Ridley, Fox et al. [72] estimated that the mean background air exchange rate in a house with an absence of double-glazing was 0.9 changes h^{-1}, this reduced to 0.64 changes h^{-1} with the presence of double-glazing. Wang, Barratt et al. [39] observed that there was no statistically significant relationship between eight different VOC concentrations and glazing type.

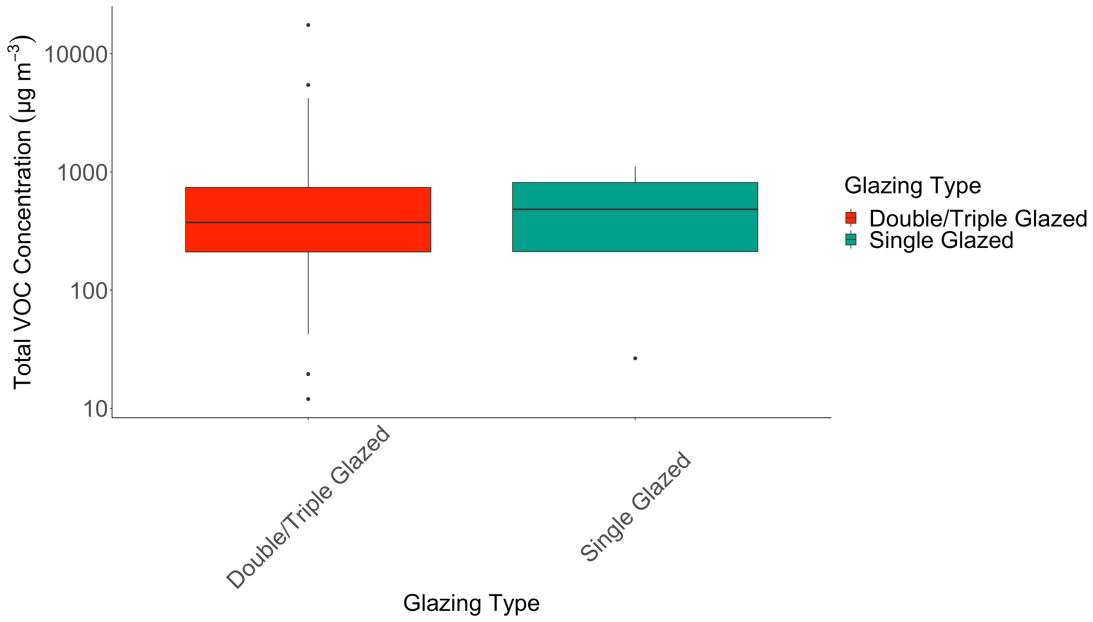

Figure 4.9: Indoor TVOC statistics as a function of glazing type. Solid black line shows media value, boxes interquartile range and vertical lines 95th percentile values

Raw, Coward et al. [73] reported that mean TVOC (defined in the study as the sum of all C_6 – C_{16} hydrocarbon peaks) was higher in English houses with integrated garages (244 μg m^{-3}) than with no garage (218 μg m^{-3}), or a detached garage (179 μg m^{-3}). The authors recognise that TVOC could be higher in houses with no garage present than with a detached garage due to

VOC-emitting materials being stored indoors in the absence of a suitable outdoor space. Dodson, Levy et al. [74] reported that in Boston, MA homes, in-garage concentrations of mobile source pollutants e.g. BTEX were 5 to 10 times higher than in ambient indoor atmospheres. They added further that 20–40% of indoor concentrations of gasoline related VOCs e.g. BTEX could be attributed to integrated garages.

In this study, properties with an integrated garage had a median TVOC concentration of 351 μg $m^{-3,}$ those without, a median of 425 μg m^{-3}, see Figure 4.10; no statistical significance was observed (Wilcoxon Rank Sum Test, $W = 3626$, $p = 0.227$). No statistically significant relationships were observed between BTEX species and the presence of an integrated garage, though m/p-Xylene did approach significance (Wilcoxon Rank Sum Test, $W = 2706$, $p = 0.08$), see Figure 4.11. It should be noted that the presence of an integrated garage was the only criterion specified; no distinction was made between the absence of an integrated garage and the presence of a detached garage. Further, Batterman, Hatzivasilis et al. [75] considered characteristics about the physical characteristics of the garages. Garage size did not appear to be a significant influence on VOC concentrations.

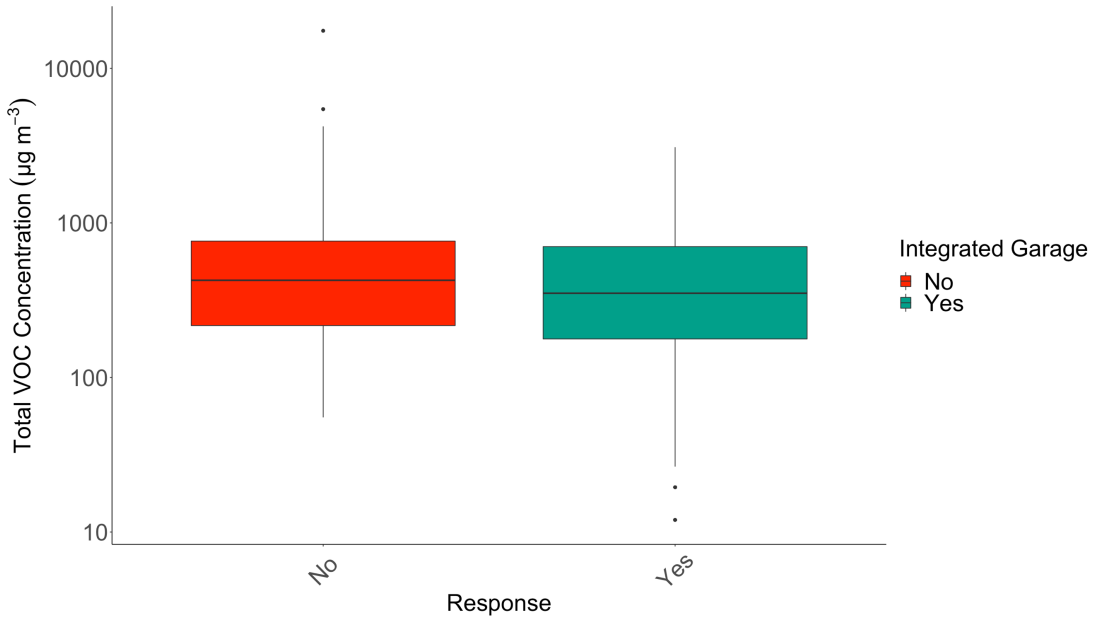

Figure 4.10: Indoor TVOC statistics as a function of integrated garage presence. Solid black line shows media value, boxes interquartile range and vertical lines 95th percentile values

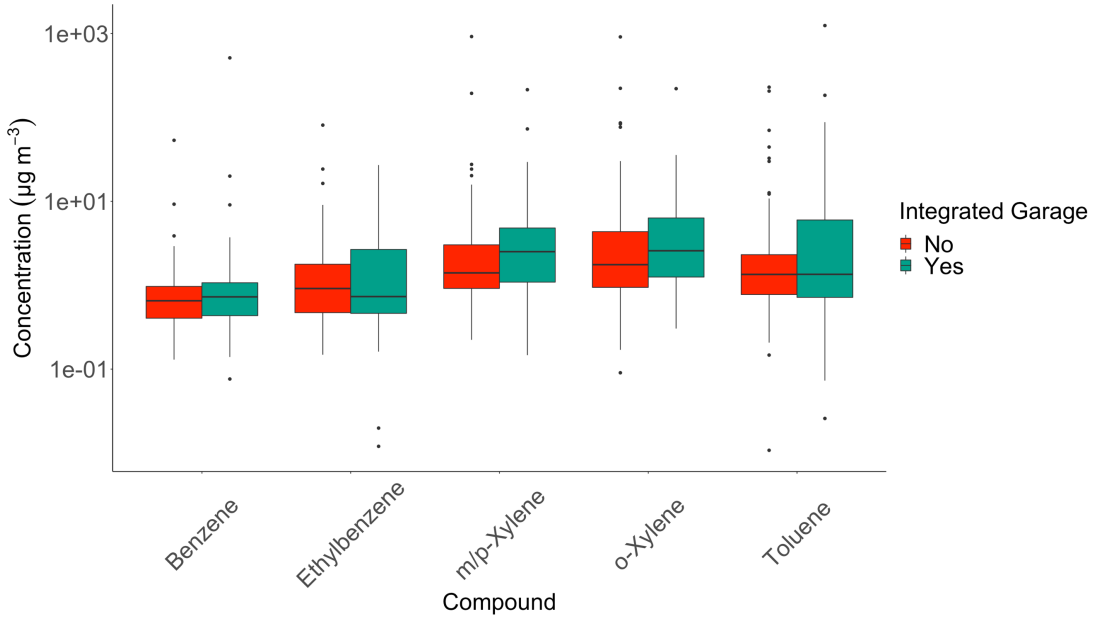

Figure 4.11: Influence of the presence of integrated garages on indoor BTEX concentrations. Results displayed on a $\log_{10}$ scale

Tobacco smoke has been well-cited in the existing literature as a significant influence on indoor air quality [3, 15]. BTEX species are commonly associated with smoking [76, 77]. No statistically significant difference was observed between presence of smoking/vaping per household and TVOC concentrations (Wilcoxon Rank Sum Test, $W = 2466$, $p = 0.737$); properties with instances of smoking/vaping had a median TVOC concentration of 374 $\mu g\ m^{-3}$ and properties without had a median concentration of 333 $\mu g\ m^{-3}$, see Figure 4.12. No statistically significant relationships were observed between concentrations of BTEX species and presence of smoking and vaping, with the exception of ethylbenzene (Wilcoxon Rank Sum Test, $W = 3100$, $p = 0.005$), see Figure 4.13. This is a surprising conclusion as higher ethylbenzene concentrations in homes with smokers is typically recorded in the literature [78, 79]. A potential reason for this observation could include higher ventilation rates e.g. open windows during a smoking event or increased ventilation more generally, but as air exchange rates weren't recorded during this study, it is difficult to substantiate this argument without further investigation in future studies. Some studies have documented decreased concentrations of tobacco smoke more generally in well-ventilated spaces however [80, 81] (e.g. average indoor winter $PM_{2.5} = 10.3\ \mu g\ m^{-3}$, summer = 8 $\mu g\ m^{-3}$ and average indoor winter nicotine = 620 ng m^{-3-}, summer = 85 ng m^{-3} [80]). Further elucidation of frequency of smoking in the study homes would also ascertain whether the frequency of smoking would necessarily confer higher concentrations of ethylbenzene.

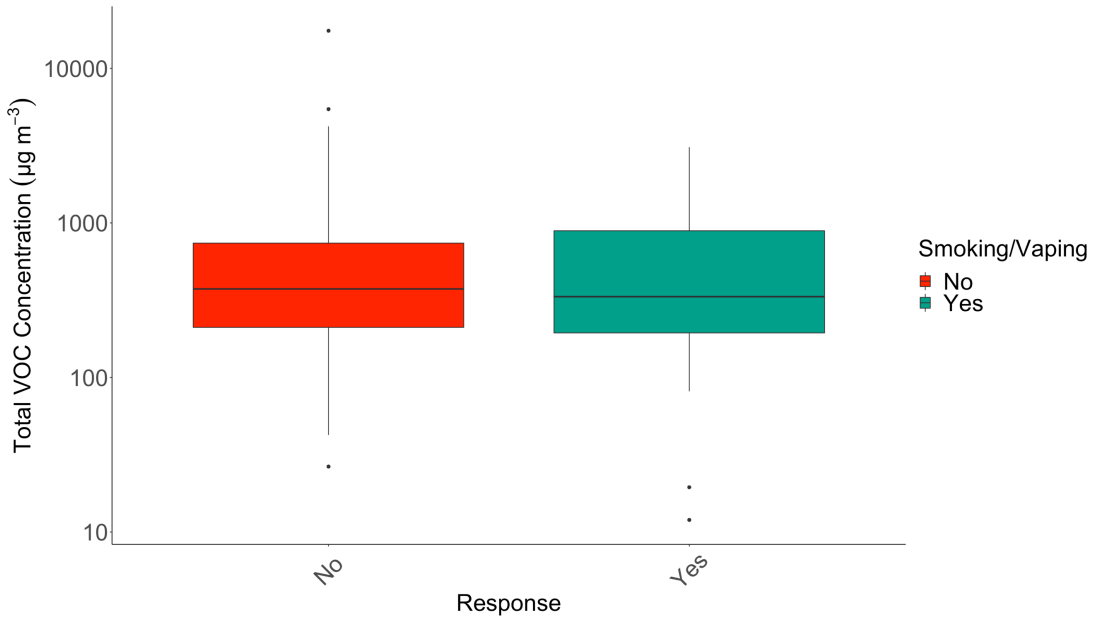

Figure 4.12: Indoor TVOC statistics as a function of smoking/vaping presence. Solid black line shows median value, boxes interquartile range and vertical lines 95th percentile values

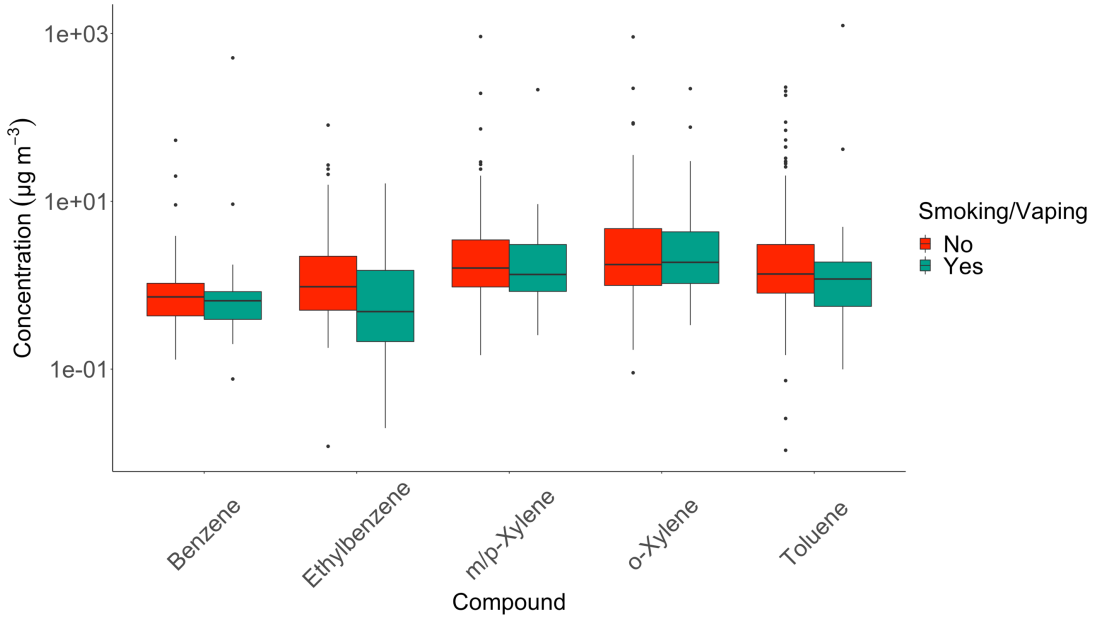

Figure 4.13: Influence of smoking and vaping on indoor BTEX concentrations. Results displayed on a $\log_{10}$ scale

No statistical significance was observed between the number of residents per household and TVOC concentrations (Kruskal-Wallis Rank Sum Test, $\chi^2(4) = 6.64$, $p = 0.156$). Median TVOC concentrations was as follows: 1 person = 608 μg m^{-3}, 2 people = 328 μg m^{-3}, 3 people = 580 μg m^{-3}, 4 people = 318 μg m^{-3}, and 5 people and more = 565 μg m^{-3}, see Figure 4.14. Similarly to the number of bedrooms per residence, there is a lack of research in the existing literature exploring the relationship between indoor VOC concentrations and number of residents per property. It would be reasonable to assume that a greater number of residents would increase indoor TVOC concentrations, given the contemporary research linking product use and VOC concentrations, but this conclusion is not borne out by the data in this study; other variables may be more influential.

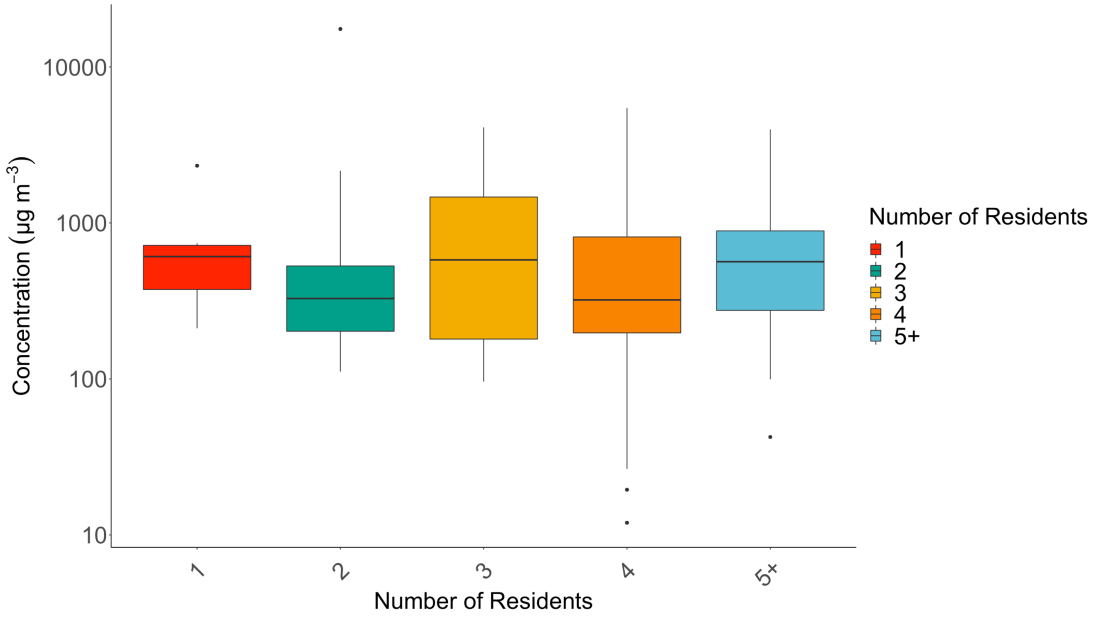

Figure 4.14: Indoor TVOC statistics as a function of number of residents. Solid black line shows median value, boxes interquartile range and vertical lines 95th percentile values

4.3.4. Balance of VOCs between indoor and outdoor air

Indoor/outdoor ratios for the ten most abundant species by season can be seen in Figure 4.15. This data can largely be rationalised by consideration of the indoor sources. *n*-butane for example had a high indoor to outdoor ratio (indoor median = 107 μg m^{-3}, outdoor median = 5.2 μg m^{-3}) reflecting the frequently use of aerosols in the study, whereas a long-lived VOC such as ethane from widespread natural gas leakage had broadly similar concentrations both indoors and out. Of these ten species, only pentane had higher abundance outdoors, which likely reflects its dominant emission from gasoline evaporation and relatively limited use in household products.

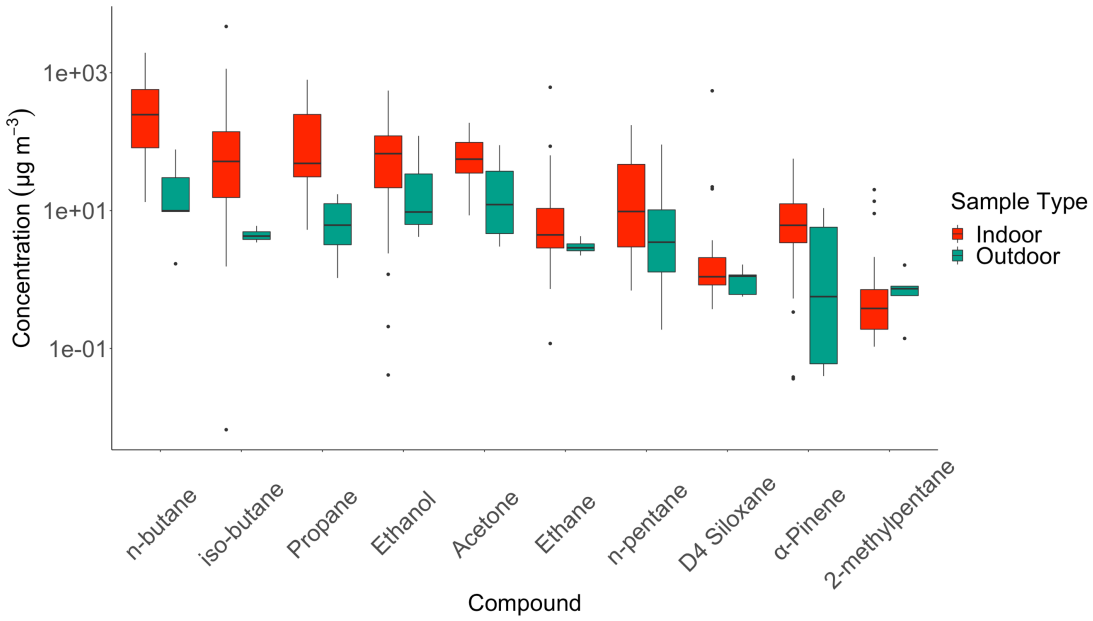

Figure 4.15: Rank order plot of the indoor/outdoor ratios for ten most abundant species across both campaigns and all households. The y-axis has been transformed to a $\log_{10}$ scale to aid visualisation

The TVOC concentrations measured in each household are shown as a rank order plot in Figure 4.16, along with the winter and summer outdoor concentrations. The mean value for each home is shown with a black bar. The mean winter outdoor TVOC concentration was recorded at 102 μg m^{-3},

the lowest recorded group mean TVOC value in the data set shown in Figure 4.16. The mean summer outdoor value was 261 μg m^{-3}.

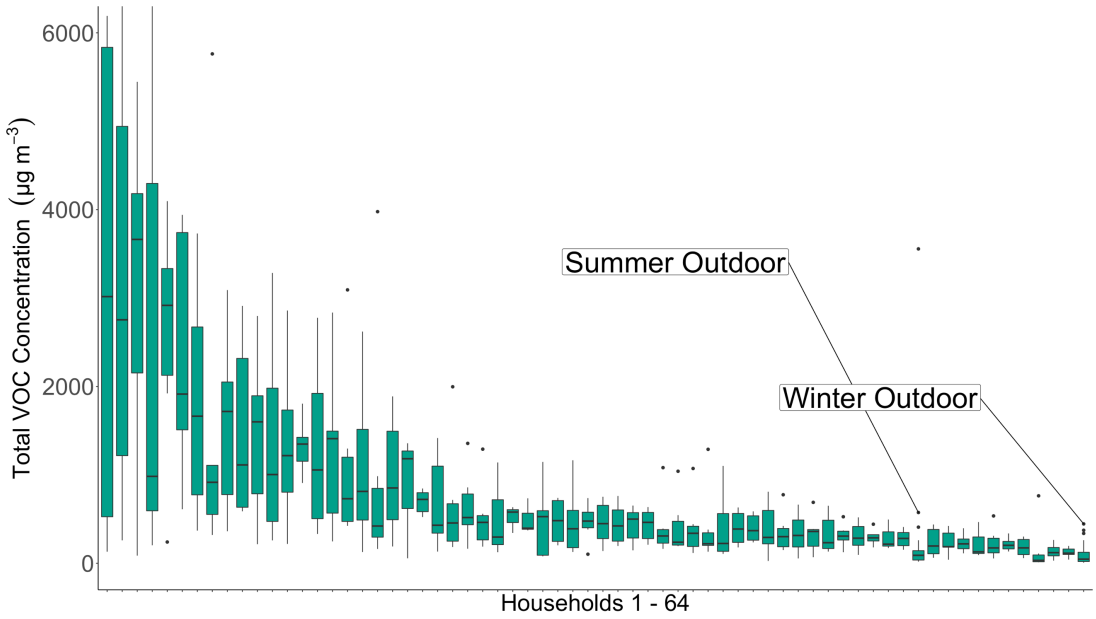

Figure 4.16: TVOC concentrations in all samples by household in rank order from highest mean to lowest household. Included are the outdoor TVOC for all outdoor samples, grouped by season. To aid visualisation, the y axis has an upper limit of 10,000 μg m^{-3}. Outliers higher than this value are not shown (relevant only to Household ranked No.1), but are included in the calculation of the mean values. A small number of individual samples (n = 39) have absent GC-FID or GC-MS data. Therefore, mean TVOC will be skewed lower than if full samples were taken.

TVOC concentrations indoors exceeded outdoors in 84% of households when compared to the mean summertime outdoor concentration and in 100% of households when compared to the wintertime mean outdoor concentration. A small number (seven) of high indoor concentration households were detected in the study, but with a long tail of homes where indoor air concentrations were within a factor of two of outdoors. Across the cohort as a whole the median indoor TVOC concentration was 413 μg m^{-3}, approximately 1.5 and 4 times higher than outdoors in summer and winter

respectively. Whilst the number of outdoor samples collected in this study was smaller than those collected indoors, and not every home had a matching control outdoor sample, it is clear that the more significant route for VOC exposure in this study group would be from inhalation of indoor air, rather than outdoors when considered solely on a like-for-like concentration basis. If a weighting for the greater time typically spent indoors compared to outdoors was applied then the differential between the two possible routes for exposure for an individual grows further, although in this study we did not collect data on individual time in each environment. Time spent indoors, daily is typically cited as 90%, so we can confidently assume that people will experience the majority of their VOC exposure indoors. Of the many species found indoors, recent studies have identified toluene, hexane and formaldehyde as priority chemicals for further study as they promote respiratory irritation and an inflammatory response [82].

4.3.5. Relationships between individual VOCs indoors

Since VOCs come from many sources, the relationships between them are complex, but speciation may carry with it information that provides insight into the contributing sources. The relationships between VOCs, correlated / uncorrelated etc, is a variable that is somewhat independent of AER, if one assumes that dilution is generally with outdoor air that is much lower in VOCs than the indoor air. Some VOCs are closely linked to one another in terms of their abundance and variability, whilst others have behaviours that is completely decoupled. Significant correlations between VOCs were evident between indoor concentrations of some alkanes, likely due to their common use as solvents in different types of household and personal care products. Correlations were also seen between benzene, toluene, ethylbenzene, and the xylene isomers (BTEX) again consistent with them having common sources. These VOCs are often combined together in refined solvent materials such as paints and glues. Weaker correlations were observed

between different monoterpenes, or between different functional group classes.

A matrix correlation plot is shown in Figure 4.17 and provides a visual indicator that indoor VOCs do not behave as a single pollutant. There are many complex relationships between the different VOCs within this matrix, from the very highly correlated *e.g*. benzene and *n*-heptane (r = 0.98), *iso*-butane and *n*-butane (r = 0.91), to fully uncorrelated. The significance of the relationships between individual VOCs was found to be broadly similar between seasons, although some relationships became stronger in the summer months, such as those between the individual BTEX species.

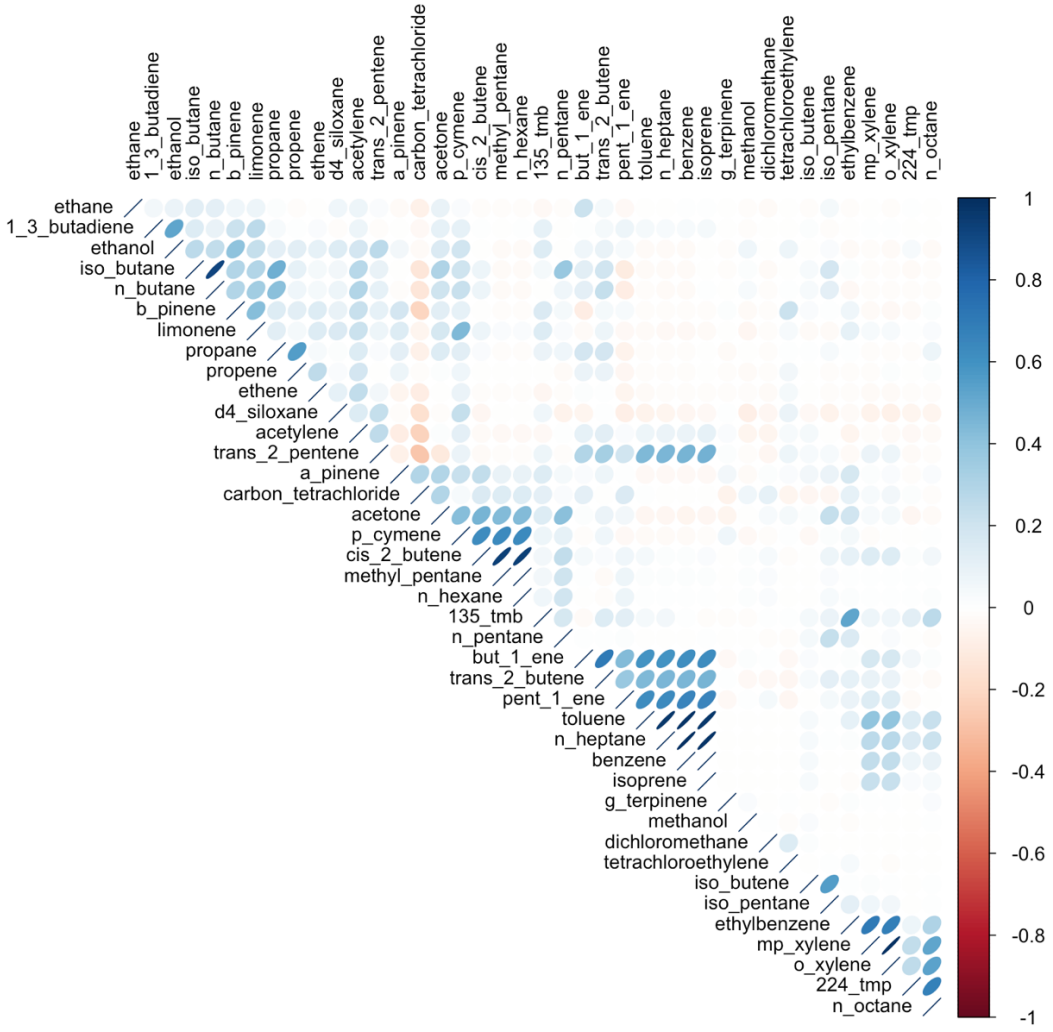

Figure 4.17: Correlation matrix for VOCs observed indoors in 60 homes during both winter and summer. Correlation results are displayed visually; a narrow, forward-slanting straight line represents a strong correlation, a full circle represents no correlation and a backward-slanting straight line represents an anti-correlation. Darker blues indicate greater correlation, darker reds represent lesser correlation. Numbers are on a scale of -1 to 1, with -1 being anticorrelated and 1 being fully correlated

Literature surrounding the correlations between VOC concentrations indoors is sparse, though Esplugues, Ballester et al. [83] identified strong correlations between BTEX species indoors. Current literature has apportioned emissions to large-scale sources because of the similar VOCs released, e.g. use of paints, renovation work, traffic etc. [23], but there is a dearth of literature

attributing particular VOC emissions to the use of specific household product types.

4.3.6. Indoor VOC concentrations and frequency of product use

Section 3.3 showed there were no clear links between TVOC and building age or type, and this lack of systematic connection also extended to other factors such as occupant number, age, or bedroom count. Given these factors did not provide significant predictive power for indoor VOCs a hypothesis in this study was that the combined frequency of use of all VOC-containing products in the home could be reflected in the indoor speciation and possibly concentrations of VOCs observed. Homes that had similar building characteristics (and therefore AER), and that frequently used VOC-containing products, might show on average higher indoor VOC concentrations than the homes of infrequent users. A secondary hypothesis was that frequent users of specific VOC-containing products may also, on average, have distinctive distributions of VOCs (a speciation) that could be linked to particular products. An initial analysis of the relationships between TVOC concentrations and the total number of household recorded uses of all products for the duration of each sample is shown in Figure 4.18. No statistically significant relationship between these two variables was found, likely confirming that other factors such as AER variability overwhelm any signal remaining from household product use.

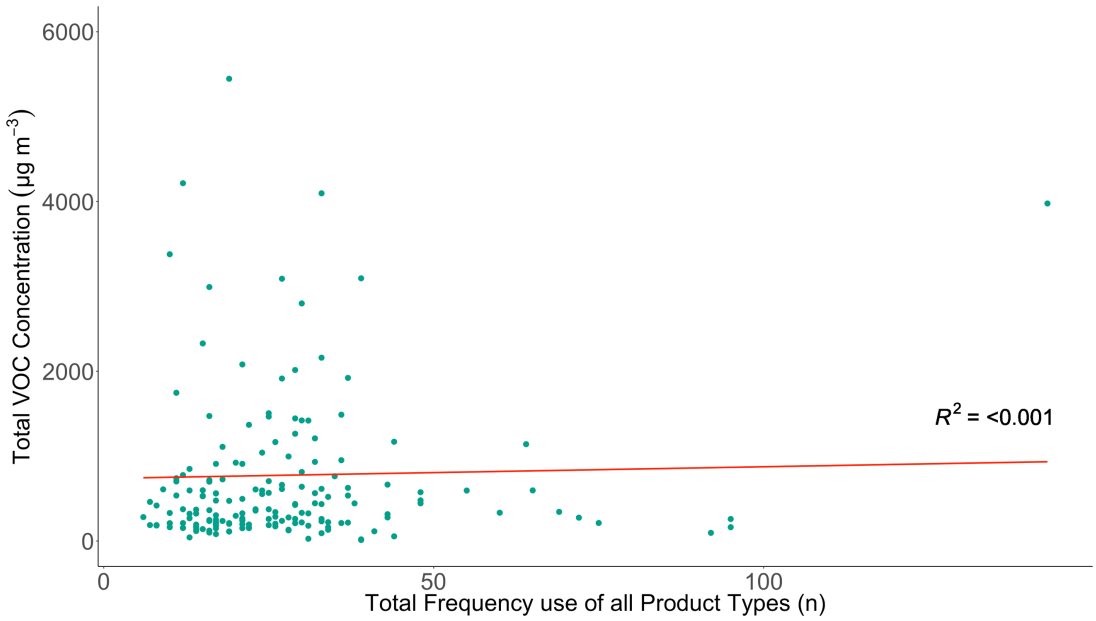

Figure 4.18: Relationship between the total VOC concentration indoors (sum of all VOCs measured) and the total number of household recorded uses of all VOC-containing products for the duration of that sample. The red line represents a regression line generated by a linear model.

Given that there was no canonical distribution in the speciation of indoor VOCs, TVOC would be expected to be a poor metric to use when attempting to link indoor concentrations with product use. For example, TVOC may be overly sensitive to contributions from a dominant indoor VOC source that may not have any association or emissions from household products. Figure 4.19 explores how the concentrations of individual VOCs vary as a function of total frequency of all products used for the duration of each sample. As with TVOC, there is no statistically significant relationship between the concentrations of individual VOCs and the total frequency of recorded uses of all products in each home. Using a metric of combined frequency of use of VOC-containing products in a home is therefore not a predictor of indoor VOC concentrations in that home, either expressed as a TVOC value, or for the concentration of any individual VOC.

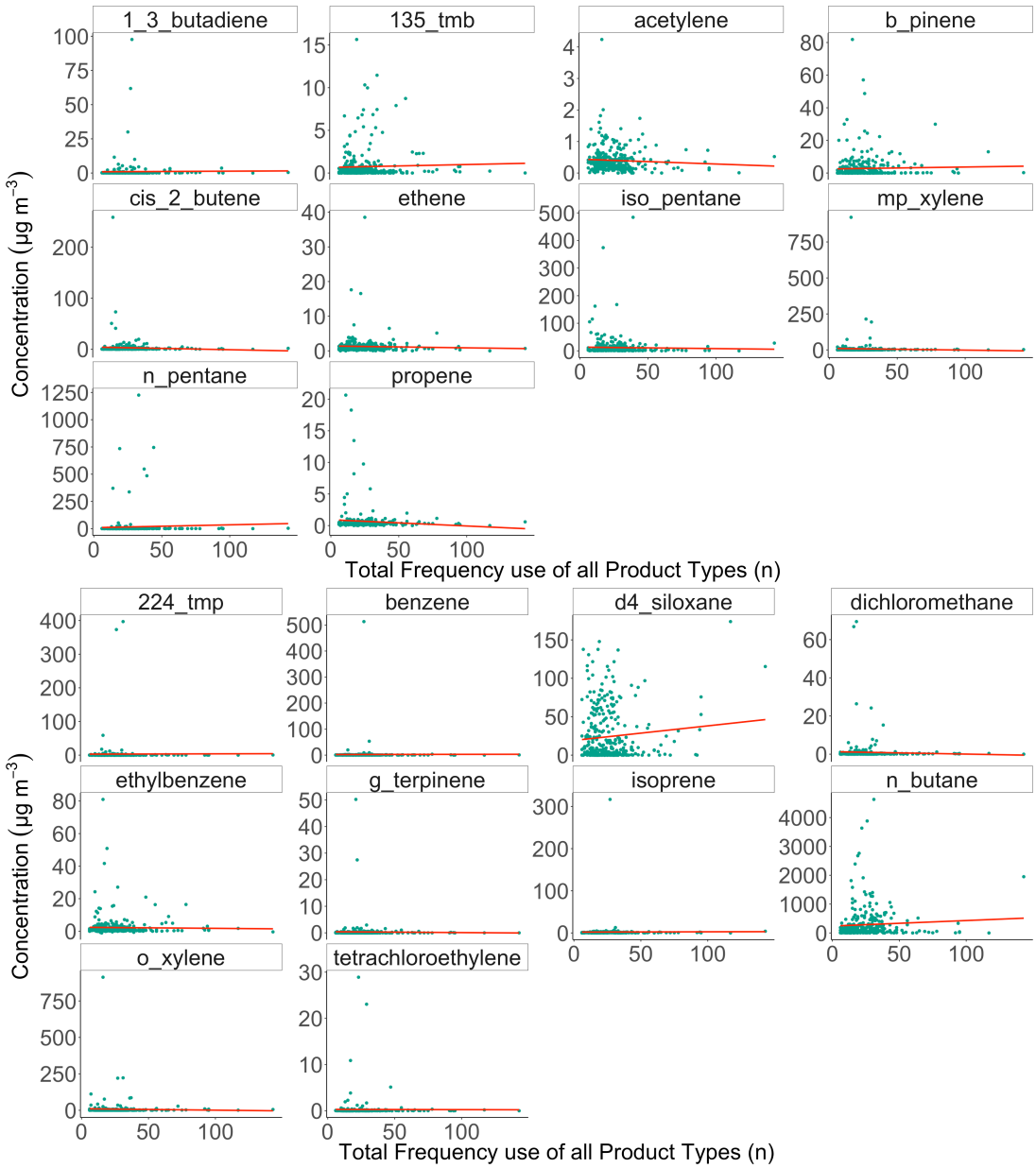
1_3_butadiene
135_tmb
acetylene
b_pinene
cis_2_butene
ethene
iso_pentane
mp_xylene
n_pentane
propene
Concentration (µg m^{-3})
Total Frequency use of all Product Types (n)
224_tmp
benzene
d4_siloxane
dichloromethane
ethylbenzene
g_terpinene
isoprene
n_butane
o_xylene
tetrachloroethylene
Concentration (µg m^{-3})
Total Frequency use of all Product Types (n)

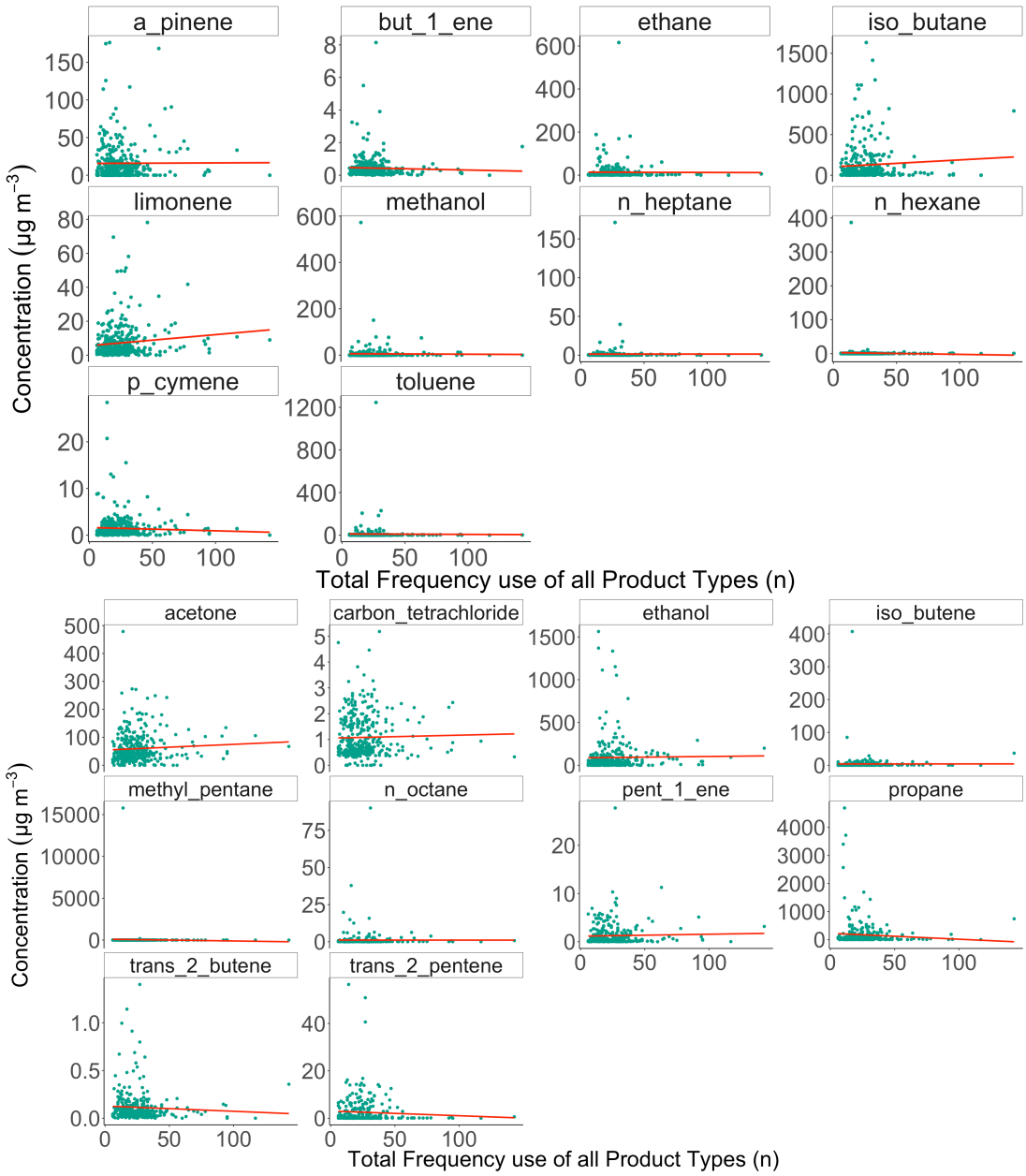

Figure 4.19: Relationships between individual VOC concentrations and the total number of recorded uses of all VOC-containing products in each sampling period. The red lines represent regression lines generated by a linear model

The differences in the nature and variance of the two datasets (e.g. unit integer vs continuous) may mean that *x y* correlation and linear interpolation of product use frequency against VOC concentration may lead to a poor fit. Covariance, however, provides an alternative measure of the degree of

relationship between the two data sets, scaled to be independent of unit of measurement. Covariance is determined as the product of deviations of data points from their respective mean values.

Each dataset was rescaled from 0 to 100, and the covariance between a selected range of parameter pairs then shown as a matrix plot in Figure 4.20. To simplify the figure, we select six of the most frequently used product types and six of the more abundant VOCs. Using this methodology, some weak relationships between variables begin to emerge. There is covariance in the frequency of use of different product types (e.g. the frequency of use of household cleaning sprays co-varies with insecticides). Some of these inter-product covariance relationships can be rationalised as being a consequence of occupant preferences and behaviours. Some weak but statistically significant covariance also emerged between frequencies of individual product usage and indoor concentrations of specific individual VOCs. For example, there was weak covariance between indoor limonene concentrations and the frequency of use of insecticides and plug-in air fresheners. The relationships are plausible based on the known composition of the products themselves.

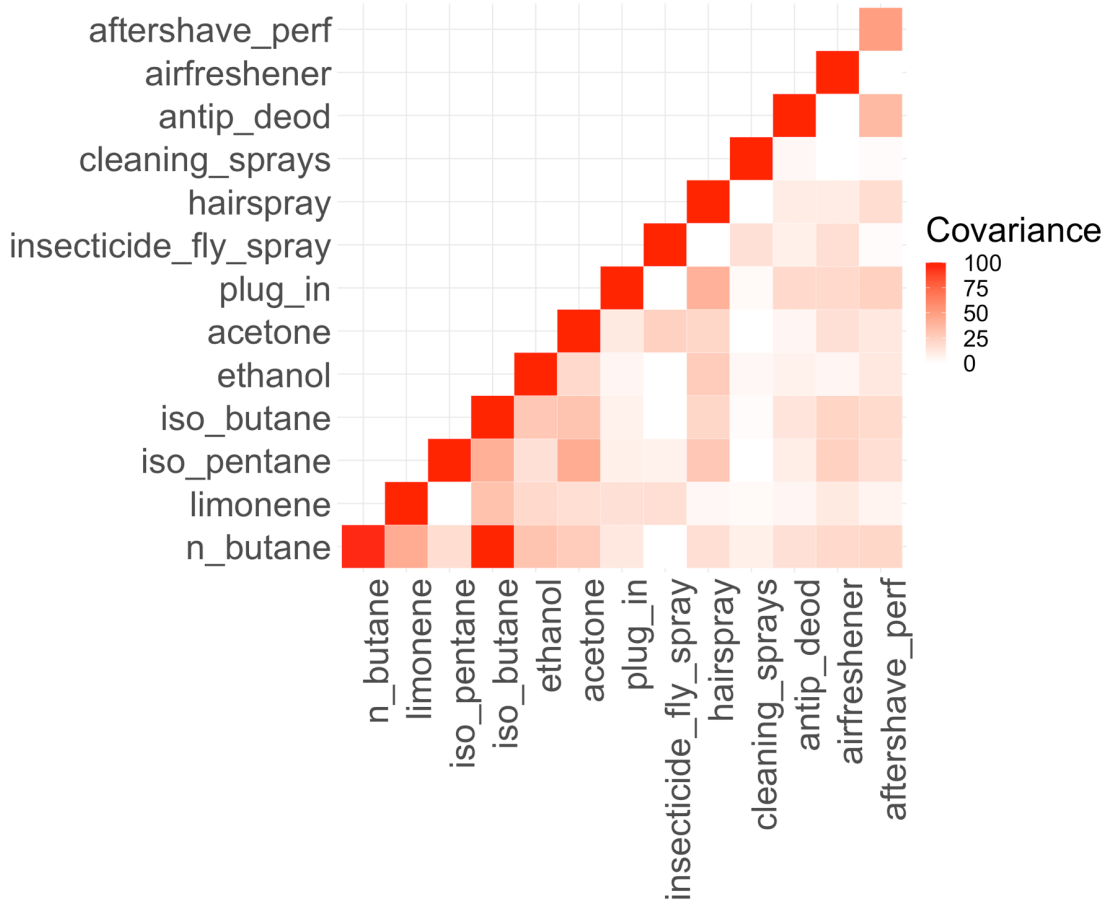

Figure 4.20: Covariance values for selected VOC and product use frequency pairs. Covariance values are derived from concentration and product usage data, all data rescaled from 0 to 100

The conclusions drawn here linking concentrations with usage of products have no direct comparators in the literature. However, the general outcomes can be compared to Rösch, Kohajda et al. [23] who assessed associations between VOC emissions and pattern scenarios (common activities that release VOCs). The authors noted that for patterns where VOC emission profiles are similar, it was impossible to apportion a particular profile to a particular source. As mentioned earlier, Adgate, Church et al. [22] reported that use of cleaning products was associated with higher concentrations of d-limonene and lower concentrations of β-pinene. They also indicate that room deodoriser use was associated with higher α-Pinene concentrations.

4.3.7. Comparison with literature

There are relatively few contemporary comparator studies in existing literature, however, some larger population studies do exist and will be discussed here. Adgate, Church et al. [22] examined three exposure scenarios for 153 school-aged children in Minneapolis, MN, USA, namely outdoors, indoors at school, indoors at home and personal exposure. Organic vapour monitors were used to measure 15 common VOCs in these different scenarios in winter and spring 2000. Sexton, Adgate et al. [24] measured outdoor, indoor and personal exposure concentrations of 15 VOCs for 71 adults in three urban areas of the Minneapolis-Saint Paul metropolitan area, MN, USA, again using passive air samplers. Finally, Rösch, Kohajda et al. [23] measured 60 VOCs in 622 apartments in Leipzig, Germany. Median concentrations for VOCs that are common to this and at least one other study are shown in Table 4.7.

Table 4.7. Comparison of median indoor VOC concentrations of this study with other recent reports in literature, all units in μg m^{-3}.

	This Study	Adgate, Church et al. [22]	Sexton, Adgate et al. [24]	Rösch, Kohajda et al. [23]
1,3,5-tmb	0.2	-	-	0.21
α-Pinene	8.03	2.4		15.53
β-Pinene	0.14	2.5	1.2	1.84
Benzene	0.52	2.2	1.9	1.09
Dichloromethane	0.2	0.4	1.1	-
Ethylbenzene	0.81	1	1.40	0.9
Limonene	3.83	28.6	9	13.03
m/p-xylene	1.5	3.7	1.6	1.84
n-heptane	0.32	-	-	1.2
n-hexane	0.4	-	-	1.12
n-octane	0.21	-	-	0.56
o-xylene	1.2	1.2	1.6	0.61
Tetrachloroethylene	0.03	0.5	0.6	-

Toluene	1.52	8.2	12.3	8.06

The concentrations of monoterpenes were consistently lower in this work than those recorded in the other studies. With regards to BTEX species, benzene and toluene were in lower concentrations here, whilst the xylenes and ethylbenzene were broadly similar. Alkanes were considerably lower here and 1,3,5-trimethylbenzene concentrations broadly similar. Results in other studies, such as the National Human Exposure Assessment Survey (NHEXAS) and the Toxics Exposure Assessment Columbia-Harvard (TEACH) studies also report similar values to existing literature [20, 84].

We note however the rather limited range of species where a direct comparison between studies can be made. Table 4.6 is in a sense misleading, since it does not include the four most abundant VOCs that we observe, since they were not measured in these other studies, likely because of incompatibility with the sampling and/or analytical methods used. There is potential therefore for a literature bias towards discussing those particular VOCs which are commonly measured in indoor population studies e.g. mid-volatility, Tenax-compatible compounds that can be quantitatively collected using either pumped or diffusive sampling tubes. When more universal 'whole air' sampling methods are used a different set of VOCs come to the fore as most abundant, such as butane, ethanol, acetone, cyclic siloxanes etc.

4.4. Discussion

This study has surveyed the indoor concentrations of a wide range of VOCs (~C_2–C_{10}) in 60 UK homes alongside collecting contextual information and a diary of frequency of household use of VOC-containing consumer products. Using whole air sampling as the collection methodology has allowed for a comprehensive screening of VOCs without any biases associated with the upper-limit of compound volatility, and has included infrequently measured

very volatile species such as ethane, ethene, acetylene, methanol, ethanol, propane and butane. Whilst physical factors such as air exchange rate might be anticipated to exert a significant control over indoor VOCs, our study showed no systematic differences between TVOC and different eras and construction type, despite covering a range from pre-1900 to post 2000. Each property type group included homes that spanned a very wide range of indoor VOC concentrations, from below 100 ppb TVOC to in excess of 1000 ppb. The presence of other factors, such as smoking and integrated garages, did not exert significant influence over TVOC, though significance was observed between ethylbenzene and houses where smoking/vaping was recorded. Additionally, the number of residents and the number of bedrooms did not influence TVOC.

Whilst VOC-containing domestic products are undoubtedly a source of emissions of VOCs in the home, the cumulative frequency of their use is not, in isolation, a predictor of overall abundance of VOCs indoors when averaged over a three-day period. The total recorded uses of VOC-containing products varied widely across 60 homes, but this was not reflected systematically in the resulting time-averaged indoor concentrations of either the total amount of VOC present, or the concentrations of individual VOCs. Whilst many different consumer products contain VOCs, the frequency with which those products are used in real-life varied widely. This behavioural component of indoor air quality emissions is not well-understood or widely reported in the research literature. Whilst this study is likely only directly reflective of UK habits, products, and behaviour, it shows that some VOC-containing products are used only very infrequently, whilst others such as deodorant aerosols are used in virtually all homes and at high frequencies. Even for commonly-used products such as deodorants which have simple and distinctive chemical formulations, no strong relationships were found between their frequency of use and the indoor concentrations of the key ingredients, *n*-butane or *iso*-butane.

The release of VOCs from consumer products is often cited as having links to adverse indoor air quality, however in this study we find few statistically robust connections between concentrations and the frequency of use of those products which contain VOCs. This is not to suggest that these products are not contributors to emissions and indoor concentrations — they clearly are — however, other factors such as the size of dose of product used, product-to-product variability between manufacturers, persistent indoor VOC emissions from other sources (like off-gassing from wood, furniture etc.), episodic emissions from food and cooking and physical factors such as ventilation, exert greater influence over indoor concentrations over longer averaging periods. The limitations of time-averaged measurements are acknowledged, and no doubt if followed at higher time resolution (e.g. by PTR-MS) linkage between transient concentrations of VOCs and product use would be clearer, as has been seen in many highly instrumented test homes.

Whilst the vast majority of VOCs are emitted directly from sources within the homes, such as consumer products, from cooking, furnishings and so on, some VOCs may be generated as secondary by-products following gas phase oxidation. Most VOCs reported in this study are primary hydrocarbons, halocarbons or siloxanes, and so by their nature are not secondary. It is possible however that some fraction of alcohols and ketones measured could derive from oxidation of those primary hydrocarbon-like VOCs, although the strength of that source is very uncertain.

VOCs such as *n*-butane are linked to a relatively limited number of possible indoor sources. The very high concentrations seen in some homes will almost certainly have arisen from the use of compressed aerosols, where product composition between manufacturers and brands is reasonably consistent and therefore largely discountable as a confounding variable. Recording only frequency of use, and not dose size, is possibly a confounding influence. We note the very limited information available on consumer use of aerosols, beyond overall national consumption statistics (in

the UK ~10 aerosol cans per person per year [85]. Reducing frequency of use of aerosols containing *n*-butane would appear to be the most effective intervention to reduce the overall total indoor concentrations of VOCs and overall emissions of VOCs arising from domestic product use.

TVOC may be an inadequate metric to use when attempting to link indoor concentrations with VOC product use, but it does provide an interesting insight into potential exposure routes for VOCs overall. Concentrations of VOCs in this study were higher indoors than outdoors for all homes in winter and for 84% of homes during the summer. A small number of homes had high concentrations, but the majority were within around a factor of two of outdoor concentrations. Exposure to ambient concentrations up to 25,000 μg m^{-3} have previously been reported to be unlikely to cause any ill-effects beyond sensory irritation [63].

No households in this study reached this threshold on a mean concentration basis, but this TVOC value was exceeded in one three-day sample in one household. Those very high concentrations were driven by hydrocarbons from aerosol sources. From a study of this limited sample size robust statistics are therefore not available on the likely population prevalence of homes routinely exceeding the 25,000 μg m^{-3} value, but it is clearly possible, and may occur perhaps at the frequency >1 in 100 homes.

VOCs released indoors are not limited in their effects to the indoor environment. Since indoor oxidation rates are relatively slow compared to outside, the fate for a fraction of indoor-released VOCs is for them to be ventilated outdoors where they contribute, as other VOC sources do, to tropospheric ozone and SOA formation [86]. Domestic and industrial solvents are now thought to comprise the largest component of the urban VOC emissions budget in high-income countries [87], overtaking VOC emissions from road transport. This emissions sector may be subject to further controls to support attainment of obligations in international treaties such as the

UNECE Convention on Long-range Transboundary Air Pollution and EC National Emissions Ceiling Directive [88, 89].

Indoor observations shed some light on the scale of VOC emissions from domestic consumer products, an area with widely acknowledged uncertainties in international reporting and national emission inventories. The high concentrations of VOCs that derive from aerosol propellants seen in virtually all the homes studied here, and that are used with high frequencies, highlights that there may be particular policy value in considering reformulation or removal of this specific source of emissions. Measured purely as mass of VOC emissions, *iso* and *n*-butane from aerosols appear to form the largest contribution from indoor emissions as assessed from real-life behaviours. This is also borne out by estimates of VOCs in emissions inventories that are resolved in sufficient sectoral and speciated detail. From the UK National Atmospheric Emissions Inventory in 2017, ~ 34 ktonnes of VOCs were estimated to be emitted from aerosols in the source categories of 'cosmetics and toiletries' and 'household products', representing around 4% of total UK VOC emissions. Placed in context, VOC emissions originating from domestic use of aerosols within the home are broadly similar in magnitude to the total estimated VOC emissions from all road transport sources in the UK (2017 data: ~ 49 ktonnes).

The air quality impacts of VOCs released indoors are not equal between different species, and we note that many of the most abundant VOCs seen here are relatively unreactive in the context of indoor oxidation chemistry. Translation of mass concentrations into metrics that reflect the formation of atmospheric by-products, such as secondary product creation potential is one means to evaluate this effect [54]. Although it is beyond this study, it is likely that the air quality role and influence of alkenes, monoterpenes and aromatic compounds would be elevated, relative to their contributions when expressed only in mass terms.

References

1. Carslaw N. A new detailed chemical model for indoor air pollution. Atmos Environ. 2007;41(6):1164–79.

2. Redlich CA, Sparer J, Cullen MR. Sick-building syndrome. Lancet. 1997;349(9057):1013–6.

3. Spengler JD, Sexton K. Indoor air pollution: A public health perspective. Science. 1983;221(4605):9–17.

4. Stolwijk JAJ. Risk assessment of acute health and comfort effects of indoor air pollution. Ann N Y Acad Sci. 1992;641(1):56–62.

5. Shrestha PM, Humphrey JL, Carlton EJ, Adgate JL, Barton KE, Root ED, Miller SL. Impact of outdoor air pollution on indoor air quality in low-income homes during wildfire seasons. Int J Environ Res Public Health. 2019;16(19):1–21.

6. Leung DYC. Outdoor-indoor air pollution in urban environment: Challenges and opportunity. Front Environ Sci. 2015;2(69):1–7.

7. Montgomery JF, Storey S, Bartlett K. Comparison of the indoor air quality in an office operating with natural or mechanical ventilation using short-term intensive pollutant monitoring. Indoor Built Environ. 2015;24(6):777–87.

8. Mizukoshi A, Kumagai K, Yamamoto N, Noguchi M, Yoshiuchi K, Kumano H, Yanagisawa Y. A novel methodology to evaluate health impacts caused by voc exposures using real-time VOC and Holter monitors. Int J Environ Res Public Health. 2010;7(12):4127–38.

9. Kuo H-W, Shen H-Y. Indoor and outdoor $PM_{2.5}$ and PM_{10} concentrations in the air during a dust storm. Build Environ. 2010;45(3):610–4.

10. Meadow JF, Altrichter AE, Kembel SW, Kline J, Mhuireach G, Moriyama M, Northcutt D, O'Connor TK, Womack AM, Brown GZ, Green JL, Bohannan BJM. Indoor airborne bacterial communities are influenced by ventilation, occupancy, and outdoor air source. Indoor Air. 2014;24(1):41–8.

11. Azimi P, Zhao D, Stephens B. Modeling the impact of residential HVAC filtration on indoor particles of outdoor origin (RP-1691). Sci Technol Built Environ. 2016;22(4):431–62.

12. Saini J, Dutta M, Marques G. A comprehensive review on indoor air quality monitoring systems for enhanced public health. Sustainable Environment Research. 2020;30(1):1–12.

13. Tsapalov A, Kovler K. Studying temporal variations of indoor radon as a vital step towards rational and harmonized international regulation. Environmental Challenges. 2021;4:1–13.

14. Petermann E, Bossew P. Mapping indoor radon hazard in Germany: The geogenic component. Sci Total Environ. 2021;780:1–14.

15. Jones AP. Indoor air quality and health. Atmos Environ. 1999;33(28):4535–64.

16. Veres PR, Faber P, Drewnick F, Lelieveld J, Williams J. Anthropogenic sources of voc in a football stadium: Assessing human emissions in the atmosphere. Atmos Environ. 2013;77:1052–9.

17. Wisthaler A, Weschler CJ. Reactions of ozone with human skin lipids: Sources of carbonyls, dicarbonyls, and hydroxycarbonyls in indoor air. Proc Natl Acad Sci U S A. 2010;107(15):6568–75.

18. Zou Z, He J, Yang X. An experimental method for measuring VOC emissions from individual human whole-body skin under controlled conditions. Build Environ. 2020;181:1–9.

19. Gallagher M, Wysocki CJ, Leyden JJ, Spielman AI, Sun X, Preti G. Analyses of volatile organic compounds from human skin. Br J Dermatol. 2008;159(4):780–91.

20. Gordon SM, Callahan PJ, Nishioka MG, Brinkman MC, O'Rourke MK, Lebowitz MD, Moschandreas DJ. Residential environmental measurements in the National Human Exposure Assessment Survey (NHEXAS) Pilot Study in Arizona: Preliminary results for pesticides and VOCs. J Expo Anal Environ Epidemiol. 1999;9(5):456–70.

21. Lin YS, Egeghy PP, Rappaport SM. Relationships between levels of volatile organic compounds in air and blood from the general population. J Expo Sci Environ Epidemiol. 2008;18(4):421–9.

22. Adgate JL, Church TR, Ryan AD, Ramachandran G, Fredrickson AL, Stock TH, Morandi MT, Sexton K. Outdoor, indoor, and personal exposure to VOCs in children. Environ Health Perspect. 2004;112(14):1386–92.

23. Rösch C, Kohajda T, Röder S, Bergen Mv, Schlink U. Relationship between sources and patterns of VOCs in indoor air. Atmos Pollut Res. 2014;5(1):129–37.

24. Sexton K, Adgate JL, Ramachandran G, Pratt GC, Mongin SJ, Stock TH, Morandi MT. Comparison of personal, indoor, and outdoor

exposures to hazardous air pollutants in three urban communities. Environ Sci Technol. 2004;38(2):423–30.

25. Rappaport SM, Kupper LL. Variability of environmental exposures to volatile organic compounds. J Expo Anal Environ Epidemiol. 2004;14:92–107.

26. Woolfenden E. Monitoring vocs in air using sorbent tubes followed by thermal desorption-capillary GC analysis: Summary of data and practical guidelines. J Air Waste Manage Assoc. 1997;47(1):20–36.

27. Price DJ, Day DA, Pagonis D, Stark H, Algrim LB, Handschy AV, Liu S, Krechmer JE, Miller SL, Hunter JF, de Gouw JA, Ziemann PJ, Jimenez JL. Budgets of organic carbon composition and oxidation in indoor air. Environ Sci Technol. 2019;53(22):13053–63.

28. Schripp T, Etienne S, Fauck C, Fuhrmann F, Märk L, Salthammer T. Application of proton-transfer-reaction-mass-spectrometry for indoor air quality research. Indoor Air. 2014;24(2):178–89.

29. Liu Y, Misztal PK, Xiong J, Tian Y, Arata C, Weber RJ, Nazaroff WW, Goldstein AH. Characterizing sources and emissions of volatile organic compounds in a Northern California residence using space- and time-resolved measurements. Indoor Air. 2019;29(4):630–44.

30. McClenny WA, and Holdren, M. W. Compendium of methods for the determination of toxic organic compounds in ambient air -second edition - compendium method TO-15: Determination of volatile organic compounds (VOCs) in air collected in specially-prepared canisters and analyzed by gas chromatography/ mass spectrometry (GC/MS) [Internet]. Cincinnati, OH, USA: United States Environmental Protection Agency; 1999. [cited 27.11.2017]. Available from: https://www3.epa.gov/ttnamti1/files/ambient/airtox/to-15r.pdf.

31. Herrington JS. Rapid determination of TO-15 volatile organic compounds (VOCs) in air [Internet]. Bellefonte, PA: Restek; 2016. [cited 08.05.2018]. Available from: http://www.restek.com/pdfs/EVAN1725B-UNV.pdf.

32. de Blas M, Navazo M, Alonso L, Durana N, Iza J. Automatic on-line monitoring of atmospheric volatile organic compounds: Gas chromatography–mass spectrometry and gas chromatography–flame ionization detection as complementary systems. Sci Total Environ. 2011;409(24):5459–69.

33. Matura M, Sköld M, Börje A, Andersen KE, Bruze M, Frosch P, Goossens A, Johansen JD, Svedman C, White IR, Karlberg A-T. Selected oxidized fragrance terpenes are common contact allergens. Contact Dermatitis. 2005;52(6):320–8.

34. Singer BC, Destaillats H, Hodgson AT, Nazaroff WW. Cleaning products and air fresheners: Emissions and resulting concentrations of glycol ethers and terpenoids. Indoor Air. 2006;16(3):179–91.

35. Stepanyuk A, Kirschning A. Synthetic terpenoids in the world of fragrances: Iso E Super® is the showcase. Beilstein J Org Chem. 2019;15:2590–602.

36. Kirkpatrick DT. A two-week inhalation toxicity study of aerosolized d-limonene in the Sprague Dawley rat. 2013.

37. Petry T, Vitale D, Joachim FJ, Smith B, Cruse L, Mascarenhas R, Schneider S, Singal M. Human health risk evaluation of selected VOC, SVOC and particulate emissions from scented candles. Regul Toxicol Pharmacol. 2014;69(1):55–70.

38. Trantallidi M, Dimitroulopoulou C, Wolkoff P, Kephalopoulos S, Carrer P. Ephect iii: Health risk assessment of exposure to household consumer products. Sci Total Environ. 2015;536(Supplement C):903–13.

39. Wang CM, Barratt B, Carslaw N, Doutsi A, Dunmore RE, Ward MW, Lewis AC. Unexpectedly high concentrations of monoterpenes in a study of UK homes. Environ Sci Process Impacts. 2017;19(4):528–37.

40. Jenkin ME, Watson LA, Utembe SR, Shallcross DE. A common representative intermediates (CRI) mechanism for VOC degradation. Part 1: Gas phase mechanism development. Atmos Environ. 2008;42(31):7185–95.

41. Waring MS. Secondary organic aerosol in residences: Predicting its fraction of fine particle mass and determinants of formation strength. Indoor Air. 2014;24(4):376–89.

42. Nazaroff WW, Weschler CJ. Cleaning products and air fresheners: Exposure to primary and secondary air pollutants. Atmos Environ. 2004;38(18):2841–65.

43. Vincent G, Marquaire PM, Zahraa O. Abatement of volatile organic compounds using an annular photocatalytic reactor: Study of gaseous acetone. J Photochem Photobiol A: Chem. 2008;197(2):177–89.

44. Byrne FP, Jin S, Paggiola G, Petchey THM, Clark JH, Farmer TJ, Hunt AJ, Robert McElroy C, Sherwood J. Tools and techniques for solvent selection: Green solvent selection guides. Sustainable Chemical Processes. 2016;4(1):1–24.

45. Salthammer T. Very volatile organic compounds: An understudied class of indoor air pollutants. Indoor Air. 2016;26(1):25–38.

46. Galassetti PR, Novak B, Nemet D, Rose-Gottron C, Cooper DM, Meinardi S, Newcomb R, Zaldivar F, Blake DR. Breath ethanol and acetone as indicators of serum glucose levels: An initial report. Diabetes Technol Ther. 2005;7(1):115–23.

47. Gorgus E, Hittinger M, Schrenk D. Estimates of ethanol exposure in children from food not labeled as alcohol-containing. J Anal Toxicol. 2016;40(7):537–42.

48. Journal of the American College of Toxicology. Final report of the safety assessment of isobutane, isopentane, n-butane, and propane. J Am Coll Toxicol. 1982;1(1):127–42.

49. Słomińska M, Konieczka P, Namieśnik J. The fate of BTEX compounds in ambient air. Crit Rev Environ Sci Technol. 2014;44(5):455–72.

50. Chang Y-M, Hu W-H, Fang W-B, Chen S-S, Chang C-T, Ching H-W. A study on dynamic volatile organic compound emission characterization of water-based paints. J Air Waste Manage Assoc. 2011;61(1):35–45.

51. Weschler CJ, Nazaroff WW. Semivolatile organic compounds in indoor environments. Atmos Environ. 2008;42(40):9018–40.

52. Wang C, Collins DB, Arata C, Goldstein AH, Mattila JM, Farmer DK, Ampollini L, DeCarlo PF, Novoselac A, Vance ME, Nazaroff WW, Abbatt JPD. Surface reservoirs dominate dynamic gas-surface partitioning of many indoor air constituents. Sci Adv. 2020;6(8):1–11.

53. Lunderberg DM, Kristensen K, Tian Y, Arata C, Misztal PK, Liu Y, Kreisberg N, Katz EF, DeCarlo PF, Patel S, Vance ME, Nazaroff WW, Goldstein AH. Surface emissions modulate indoor SVOC

concentrations through volatility-dependent partitioning. Environ Sci Technol. 2020;54(11):6751–60.

54. Carslaw N, Shaw D. Secondary product creation potential (SPCP): A metric for assessing the potential impact of indoor air pollution on human health. Environ Sci Process Impacts. 2019;21(8):1313–22.

55. Weschler CJ. Ozone in indoor environments: Concentration and chemistry. Indoor Air. 2000;10(4):269–88.

56. Pytel K, Marcinkowska R, Zabiegała B. Investigation of the dynamism of nanosized SOA particle formation in indoor air by a scanning mobility particle sizer and proton-transfer-reaction mass spectrometry. Molecules. 2020;25(9):1–23.

57. Wormuth M, Scheringer M, Hungerbühler K. Linking the use of scented consumer products to consumer exposure to polycyclic musk fragrances. J Ind Ecol. 2005;9(1-2):237–58.

58. Wu XM, Bennett DH, Ritz B, Cassady DL, Lee K, Hertz-Picciotto I. Usage pattern of personal care products in California households. Food Chem Toxicol. 2010;48(11):3109–19.

59. Carslaw N, Fletcher L, Heard D, Ingham T, Walker H. Significant OH production under surface cleaning and air cleaning conditions: Impact on indoor air quality. Indoor Air. 2017;27(6):1091–100.

60. Garcia-Hidalgo E, von Goetz N, Siegrist M, Hungerbühler K. Use-patterns of personal care and household cleaning products in Switzerland. Food Chem Toxicol. 2017;99:24–39.

61. Hopkins JR, Lewis AC, Read KA. A two-column method for long-term monitoring of non-methane hydrocarbons (NMHCs) and oxygenated

volatile organic compounds (O-VOCs). J Environ Monit. 2003;5(1):8–13.

62. Shaw JT, Lidster RT, Cryer DR, Ramirez N, Whiting FC, Boustead GA, Whalley LK, Ingham T, Rickard AR, Dunmore RE, Heard DE, Lewis AC, Carpenter LJ, Hamilton JF, Dillon TJ. A self-consistent, multivariate method for the determination of gas-phase rate coefficients, applied to reactions of atmospheric VOCs and the hydroxyl radical. Atmos Chem Phys. 2018;18(6):4039–54.

63. European Commission. EUR 17675 EN European collaborative action indoor air quality and its impact on man – environment and quality of life – Report No 19: Total volatile organic compounds (TVOC) in indoor air quality investigations [Internet]. Luxembourg, Luxembourg: European Commission; 1997. [cited 08.12.2020]. Available from: https://op.europa.eu/en/publication-detail/-/publication/34beabd5-f38b-4336-ac69-3eec614bbad4.

64. De Bortoli M, Knöppel H, Pecchio E, Peil A, Rogora L, Schauenburg H, Schlitt H, Vissers H. Concentrations of selected organic pollutants in indoor and outdoor air in northern italy. Environ Int. 1986;12(1):343–50.

65. Mølhave L. Volatile organic compounds, indoor air quality and health. Indoor Air. 1991;1(4):357–76.

66. Noguchi M, Mizukoshi A, Yanagisawa Y, Yamasaki A. Measurements of volatile organic compounds in a newly built daycare center. Int J Environ Res Public Health. 2016;13(5):1–14.

67. Sparks LE, Guo Z, Chang JC, Tichenor BA. Volatile organic compound emissions from latex paint – Part 1. Chamber experiments and source model development. Indoor Air. 1999;9(1):10–7.

68. Edwards RD, Jurvelin J, Saarela K, Jantunen M. VOC concentrations measured in personal samples and residential indoor, outdoor and workplace microenvironments in EXPOLIS-Helsinki, finland. Atmos Environ. 2001;35(27):4531–43.

69. Schlink U, Thiem A, Kohajda T, Richter M, Strebel K. Quantile regression of indoor air concentrations of volatile organic compounds (VOC). Sci Total Environ. 2010;408(18):3840–51.

70. Jia C, Batterman S, Godwin C. VOCs in industrial, urban and suburban neighborhoods, Part 1: Indoor and outdoor concentrations, variation, and risk drivers. Atmos Environ. 2008;42(9):2083–100.

71. Hernandez G, Wallis SL, Graves I, Narain S, Birchmore R, Berry T-A. The effect of ventilation on volatile organic compounds produced by new furnishings in residential buildings. Atmos Environ X. 2020;6:1–11.

72. Ridley I, Fox J, Oreszczyn T, Hong SH. The impact of replacement windows on air infiltration and indoor air quality in dwellings. International Journal of Ventilation. 2003;1(3):209–18.

73. Raw GJ, Coward SKD, Brown VM, Crump DR. Exposure to air pollutants in English homes. J Expo Anal Environ Epidemiol. 2004;14:S85–S94.

74. Dodson RE, Levy JI, Spengler JD, Shine JP, Bennett DH. Influence of basements, garages, and common hallways on indoor residential volatile organic compound concentrations. Atmos Environ. 2008;42(7):1569–81.

75. Batterman S, Hatzivasilis G, Jia C. Concentrations and emissions of gasoline and other vapors from residential vehicle garages. Atmos Environ. 2006;40(10):1828–44.

76. Wallace L, Pellizzari E, Hartwell TD, Perritt R, Ziegenfus R. Exposures to benzene and other volatile compounds from active and passive smoking. Arch Environ Health. 1987;42(5):272–9.

77. Wickliffe JK, Stock TH, Howard JL, Frahm E, Simon-Friedt BR, Montgomery K, Wilson MJ, Lichtveld MY, Harville E. Increased long-term health risks attributable to select volatile organic compounds in residential indoor air in Southeast Louisiana. Sci Rep. 2020;10(1):1–12.

78. Nazaroff WW, Singer BC. Inhalation of hazardous air pollutants from environmental tobacco smoke in US residences. J Expo Anal Environ Epidemiol. 2004;14 Suppl 1:S71–S7.

79. Wallace LA, Pellizzari ED. Personal air exposures and breath concentrations of benzene and other volatile hydrocarbons for smokers and nonsmokers. Toxicol Lett. 1987;35(1):113–6.

80. Arku RE, Adamkiewicz G, Vallarino J, Spengler JD, Levy DE. Seasonal variability in environmental tobacco smoke exposure in public housing developments. Indoor Air. 2015;25(1):13–20.

81. Antonucci A, Vitali M, Martellucci S, Mattei V, Protano C. A cross-sectional study on benzene exposure in pediatric age and parental smoking habits at home. Int J Environ Res Public Health. 2020;17(15):1–17.

82. Dezest M, Le Bechec M, Chavatte L, Desauziers V, Chaput B, Grolleau J-L, Descargues P, Nizard C, Schnebert S, Lacombe S,

Bulteau A-L. Oxidative damage and impairment of protein quality control systems in keratinocytes exposed to a volatile organic compounds cocktail. Sci Rep. 2017;7(1):1–14.

83. Esplugues A, Ballester F, Estarlich M, Llop S, Fuentes-Leonarte V, Mantilla E, Iñiguez C. Indoor and outdoor air concentrations of BTEX and determinants in a cohort of one-year old children in Valencia, Spain. Sci Total Environ. 2010;409(1):63–9.

84. Sax SN, Bennett DH, Chillrud SN, Kinney PL, Spengler JD. Differences in source emission rates of volatile organic compounds in inner-city residences of New York City and Los Angeles. J Expo Sci Environ Epidemiol. 2004;14(1):S95–S109.

85. National Atmospheric Emissions Inventory. National Atmospheric Emissions Inventory [Internet]. London, UK: Department for Environment Food and Rural Affairs; 2017. [cited 05.03.2021]. Available from: https://naei.beis.gov.uk.

86. Abbatt JPD, Wang C. The atmospheric chemistry of indoor environments. Environ Sci Process Impacts. 2020;22(1):25–48.

87. McDonald BC, de Gouw JA, Gilman JB, Jathar SH, Akherati A, Cappa CD, Jimenez JL, Lee-Taylor J, Hayes PL, McKeen SA, Cui YY, Kim S-W, Gentner DR, Isaacman-VanWertz G, Goldstein AH, Harley RA, Frost GJ, Roberts JM, Ryerson TB, Trainer M. Volatile chemical products emerging as largest petrochemical source of urban organic emissions. Science. 2018;359(6377):760–4.

88. European Parliament. Directive (EU) 2016/2284 of the European Parliament and of the Council of 14 December 2016 on the Reduction of national emissions of certain atmospheric pollutants, amending Directive 2003.35/EC and repealing Directive 2001/81/EC [Internet].

Brussels, Belgium: European Parliament; 2016. [cited 05.03.2021]. Available from: https://eur-lex.europa.eu/legal-content/EN/TXT/?uri=uriserv%3AOJ.L_.2016.344.01.0001.01.ENG.

89. United Nations. 1979 Geneva Convention on Long-Range Transboundary Air Pollution [Internet]. Geneva, Switzerland: United Nations; 1979. [cited 05.03.2021]. Available from: https://eur-lex.europa.eu/legal-content/EN/TXT/?uri=LEGISSUM:l28162.

5. Reactivity of VOCs Indoors

Abstract

Volatile organic compounds (VOCs), thought to be in significant concentrations indoors, are emitted from a myriad of sources and can contribute significantly to secondary organic aerosol (SOA) formation, conferring a deleterious effect on indoor air quality and human health. The reactive potential (defined as the product of the rate constant of a given VOC with a given oxidant the concentration of the VOC) and pseudo-first order reaction rates were calculated between the following 39 commonly found indoor VOCs: 1,3-butadiene, 1,3,5-trimethylbenzene, 2,2,4-trimethylpentane, α-Pinene, acetone, acetylene, β-Pinene, benzene, 1-butene, cis-2-butene, D4 siloxane, dichloromethane, ethane, ethanol, ethene, ethylbenzene, γ-Terpinene, *iso*-butane, *iso*-butene, *iso*-pentane, isoprene, limonene, ethanol, 2-methylpentane, m/p, Xylene, *n*-butane, *n*-heptane, *n*-hexane, *n*-octane, *n*-pentane, o-Xylene, p-cymene, 1-pentene, propane, propene, tetrachloroethylene, toluene, trans-2-butene, trans-2-pentene, and three major oxidants, OH, O_3 and NO_3. Regarding reactive potential, OH had the greatest reactive potential with *n*-butane (median reactive potential = 2.83 s^{-1}), O_3 had the greatest reactive potential with limonene (median reactive potential = 1.10 x 10^{-5} s^{-1}), and NO_3 had the greatest reactive potential with α-Pinene (median reactive potential = 2.06 x 10^{-1} s^{-1}). α-Pinene had the greatest reaction rate when median pseudo-first order reaction rates for all oxidants were summed (5.39 x 10^6 molecules cm^{-3} s^{-1}). Limonene also had a high reaction rate in this scenario (4.46 x 10^6 molecules cm^{-3} s^{-1}); NO_3 was the dominant oxidant in these reactions (median NO_3 pseudo-first order reaction rate; α-Pinene = 5.07 x 10^6 molecules cm^{-3} s^{-1}, limonene = 3.92 x 10^6 molecules cm^{-3} s^{-1}). Generally, monoterpenes had the greatest pseudo-first order reaction rate, followed by alkanes and alkenes. An indoor environment model provided data regarding $PM_{2.5}$, NO_x, O_3, and the Secondary Product Creation Potential (SPCP) metric, amongst others. The

median mixing ratio of NO_x was lower in summer and in the lockdown period, whilst O_3 was higher. SPCP was highest during lockdown, and lowest during winter. This presents an interesting scenario where a low-NO_x environment is created through future legislation, but the potential for possibly hazardous secondary products to be created is increased.

5.1. Introduction

In recent years, assessing the quality of indoor air has become increasingly important. More time spent indoors in developed countries and, more generally, the ubiquitous use of multiple aerosol products, such as cleaning sprays and personal care products, has only heightened the need for additional research [1-3]. With greater product use comes an increased likelihood of the formation of secondary organic aerosols (SOA), especially from terpenoid and alkene-containing products [4]. Though further research is needed, it is thought that SOAs have a deleterious impact on indoor air quality and human health [5]. Studies in the 1990s confirmed that indoor VOC and formaldehyde concentrations were not sufficiently high to be warranted as the cause of 'sick-building syndrome', and so reactive chemistry became the locus of research [6].

The House Observations of Microbial and Environmental Chemistry (HOMEChem) study of 2018 is widely-reported in the literature due to the extensive nature of the experiments and observations made. Broadly, over a month-long period in summer 2018, HOMEChem sought to investigate the influence of everyday activities on chemistry indoors, such as cooking and cleaning activities, as well as differing occupancy levels and ventilation [7]. These experiments were located at a test home positioned on the campus of the University of Texas at Austin [7]. In one HOMEChem study, SOA formation as the result of bleach cleaning was observed [8]. The use of bleach (sodium hypochlorite; NaOCl) in cleaning activities can invoke radical chemistry by producing OH and Cl radicals through photolysis [8].

Oxygenated VOCs (OVOCs) can be subsequently produced via the oxidation of VOCs by OH and Cl, which can condense onto existing particulate matter to form SOAs [8]. In outdoor environments, OVOCs can often form SOAs due to having a lower vapour pressure than the volatile precursors from which they are derived [8]. In the study, SOA formation was monitored following cooking and cleaning activities. Organic aerosol fragments were observed following the cleaning episode that were likely derived from OVOCs produced during cleaning that condensed to particulate matter generated from earlier cooking activities [8]. There was a 25% increase in the summed analytical signal of fragments from a pre-cleaning baseline; however this did not translate to a significant increase (<3%) in sub-micrometer organic aerosol mass [8]. This was attributed to an air exchange rate that may have been too rapid for meaningful SOA production (~0.5 h^{-1}) [8]. Another potential complication was the large surface sinks available for OVOCs in the test home [8]. Similarly, Wang et al. observed SOA production from the reaction of limonene and HOCl and Cl_2 in an atmospheric chamber [9]. Following dark mixing and UV irradiation, there was an average 40% mass yield of mass loading secondary particles relative to limonene consumed [9].

Outdoors, many thousands of different chemicals reside in the atmosphere, and the complexity of the mixture invariably means many thousands of structurally different compounds are contained therein [5]. Indoor atmospheres are arguably more complex due to indoor-outdoor air exchange, and the release of a number of different compounds from multiple sources, including product use and from cooking and heating systems [10, 11]. These complex environments provide an opportunity for SOAs to form. SOAs are formed from gas-to-particle phase transfer of partially oxidised material.

Organic matter constitutes a significant proportion of atmospheric particulate matter (20–90%) in the lower troposphere [12]. Organic aerosols are derived from direct emissions of anthropogenic and biogenic sources, with

subsequent reactions forming SOAs. SOAs can have significant impacts on air quality, human health and climate change, but due to the complexity of these reactions, full understanding of their formation is elusive; indeed, using the Master Chemical Mechanism (MCM), the degradation of methane to carbon dioxide and water is represented in 23 reactions and 17 species, with more complex compounds represented in a greater number of reactions and species [13, 14]. The MCM is a near-explicit mechanism detailing VOC degradation in the troposphere and is often used in the literature to further elucidate chemical reactions in the atmosphere [15].

In 2019, a population-scale study was performed to measure the concentrations of commonly-found VOCs indoors, with full details provided in Chapter 4 and Heeley-Hill et al. [16] Existing studies have focussed on acquiring the concentration data of a variety of compounds thought to be typical in indoor environments, usually including alkane and monoterpene groups, due to their assumed prevalence in indoors. Analysis in the 2019 study was extended to include lighter-weight alkenes, so that a range of VOCs could be monitored in the range C_2–C_{10}. Numerous chemical classes were analysed to comprise a large number of VOCs commonly found indoors. Acetone, dichloromethane, ethanol, limonene, and *n*-pentane are used as solvents. Butane species are used as propellants and often in conjunction with ethanol and propane as a cosolvent [17-19]. Toluene, ethylbenzene, and the xylene isomers are often components in decorative products, such as paints and varnishes [20, 21]. Ethanol and propane are minor components in fossil methane gas; terpenoid species are often released from consumer fragrance products [22]. To further analysis from the above work, this study will explore the indoor reactions of these commonly found VOCs with OH, O_3, and NO_3. Analysis will also include a secondary product metric derived from the Indoor Detailed Chemical Model, named the Secondary Product Creation Potential.

Also considered is the impact of a set of behavioural and mobility restrictions, known as 'lockdowns', implemented during the COVID-19 pandemic of 2020 to the present day, on indoor air quality. These periods can be considered reflective of potential future low NO_x scenarios. Lockdowns are a non-pharmaceutical intervention, implemented across many countries globally, and were used to contain SARS-CoV-2 outbreaks and to limit subsequent COVID-19 infections [23]. Lockdowns typically included restrictions on social gatherings and introduced social distancing guidelines to limit close contact between individuals [24]. The first cases of COVID-19 were identified in Wuhan, China in late-2019, the first case in Europe was detected in France on 24th January, with the UK declaring its first case on 31st January [25, 26]. The World Health Organisation declared COVID-19 a pandemic on 11th March and the first lockdown period in the UK was implemented shortly thereafter on 23rd March [26, 27].

Due to the closure of many workplaces and restrictions on travel during lockdown periods, traffic congestion significantly reduced in many areas, thus having an impact on typical air pollution as compared to 'normal' periods [28]. Lockdown periods could also be thought to reflect future air quality conditions as legislation against the sale of new diesel and petrol cars will be implemented in the United Kingdom from 2030, and proposed legislation in the European Union will effectively ban diesel and petrol-fuelled cars from 2035 to meet a proposal that cuts CO_2 emissions in the EU by 100% [29, 30]. The United Kingdom has been subject to a number of lockdown periods throughout 2020 and 2021, this study considers the first between March and May 2020.

5.1.1. Reactive chemistry

One important dynamic is the presence of oxidants indoors, in this study, OH, O_3, and NO_3 are considered. OH is a highly reactive compound meaning

its residence time outdoors is often less than a second [31]. Outdoors, as detailed in Chapter 1, multiple pathways exist for the formation of OH: i) photolysis of ozone (O_3), nitrous acid (HONO), hydrogen peroxide (H_2O_2), or methyl hydroperoxide (CH_3OOH) [2, 32, 33] ii) the reaction of nitrous oxide (NO) with the hydroperoxyl radical (HO_2) [34] iii) the reaction of alkene species with O_3 [2]. It is likely that the third pathway is the principal method by which OH is formed indoors; the first pathway relies on the presence of sunlight which, whilst present indoors, will not be in significant quantities to be a major contributor, unless reactive chemistry adjacent to windows is being considered [35]. The reaction mechanism between OH and alkanes can be seen below in Figure 5.1, as illustrated by Ziemann [36]

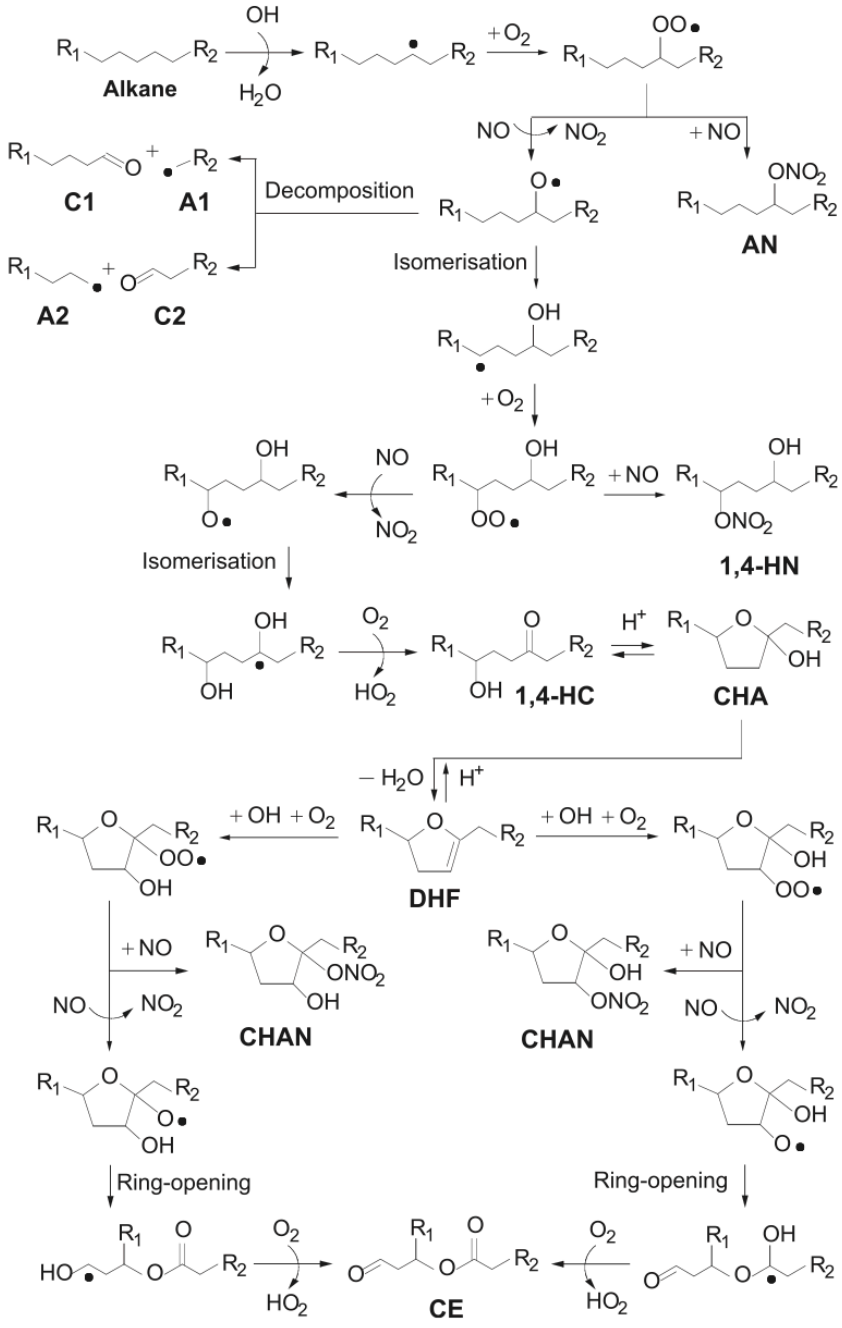

Figure 5.1: Reaction mechanism of OH and alkanes

In the reaction of OH and alkanes, oxidation is initiated by H-atom abstraction, forming H_2O and an alkyl radical [36]. These alkyl radicals go onto react with O_2, forming an alkyl peroxy radical [36]. Further reactions are dependent on whether the system is low- or high-NO_x [36]. In low NO_x

environments, the radicals either react with each other or with HO_2 [36]. In high-NO_x environments, the radicals react with NO or NO_2 [37]. If continued reactions continue with NO, alkyl nitrates or alkoxy radicals are formed, which decompose to carbonyls and alkyl radicals or they isomerise [37]. Through NO_2, alkyl peroxy nitrates are formed, but they decompose rapidly and form alkoxy peroxy radicals and NO_2 [36].

The reaction mechanism between OH and alkenes can be seen below in Figure 5.2, as illustrated by Teng et al. [38]

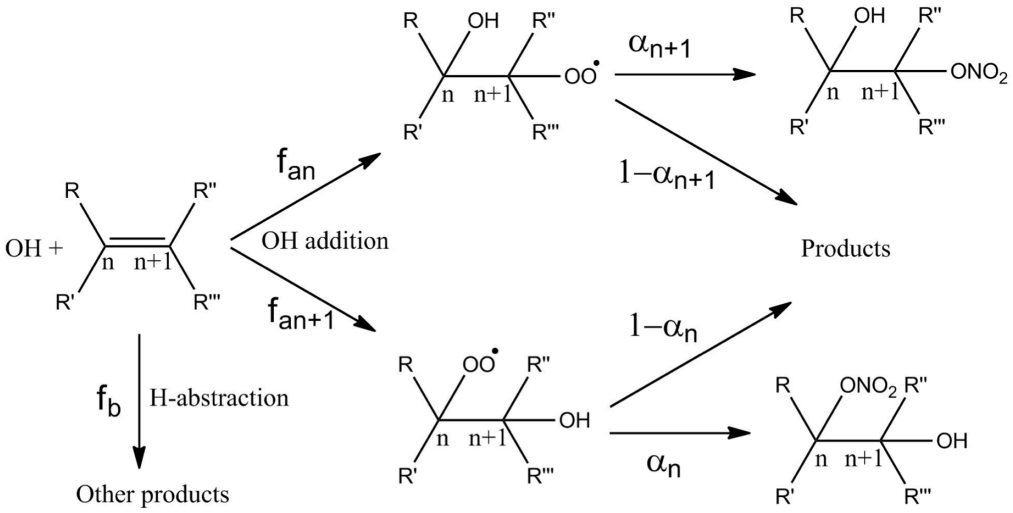

Figure 5.2: Reaction mechanism of OH and alkenes

The reaction of OH and alkenes can be initiated either through H-atom abstraction, resulting in H_2O and alkyl radicals [36]. These reactions proceed similarly to OH and alkane reactions, but with an additional hydroxy group [36]. OH and alkene reactions can also be initiated by OH addition to carbon-carbon double bonds [36]. Subsequent O_2 addition in these reactions forms β-hydroperoxy radicals, and further reaction with NO forms β-hydroxy nitrates [38].

O_3 is primarily found indoors due to indoor-outdoor air exchange, and concentrations are driven predominantly by this, a building's air exchange rate, and O_3 interaction with surfaces [39]. Emissions from electrical appliances are also a contributing factor [40]. Indoor O_3 concentrations are in the range of 30–70% of outdoor levels [41]. O_3 reacts quickly with alkenes to form a significant contribution to indoor OH concentrations. Subsequent OH reactions with VOCs contribute to the formation of radicals and, in turn, transform to oxidised compounds [41]. The reaction between O_3 and alkanes is not thought to be significant, so only the reaction mechanism of the ozonolysis of alkenes is considered here [42, 43]. The reaction mechanism between O_3 and alkenes can be seen below in Figure 5.3, as illustrated by Newland et al. [44]

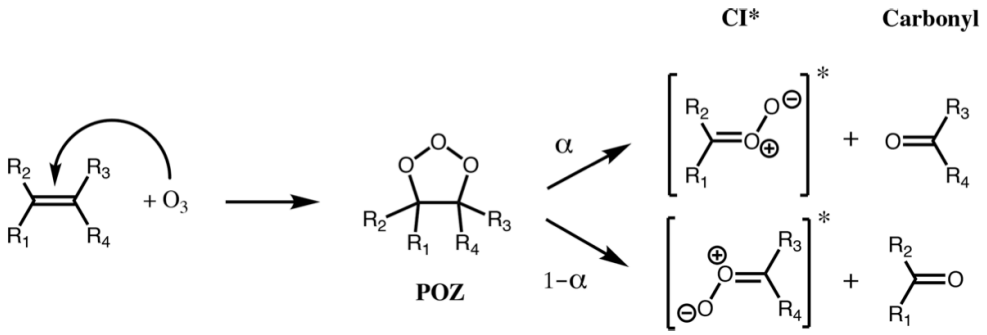

Figure 5.3: Reaction mechanism of O_3 and alkenes

Ozonolysis of alkenes is initated by O-addition to the carbon-carbon double bonds [44]. This reaction forms a short-lived primary ozonide (POZ) that then fragments to a pair of carbonyls and a pair of Criegee Intermediates [44]. The Criegee Intermediate is either then quenched to form a Stabililised Criegee Intermediate that can react with either water or an oxygenated organic, or it can form a hydroperoxide, decomposing to an alkyl radical and OH [39].

NO_3 is proposed as a significant oxidant indoors by Weschler and Carslaw [35] as NO_3 is rapidly photolysed outdoors. NO_3 is the result of reactions between O_3 and NO_2 to form NO_3 and O_2. The likely concurrence of O_3 and

NO_2 indoors increases the importance of NO_3 as an oxidant. Further interaction between NO_2 and NO_3 is in equilibrium with N_2O_5, potentially forming HNO_3. NO_3 reactions with VOCs again yield the formation of radicals and oxidised compounds. [11, 45, 46]. The reaction mechanism between NO_3 and alkanes can be seen below in Figure 5.4, as illustrated by Fry and Sakinger. [47]

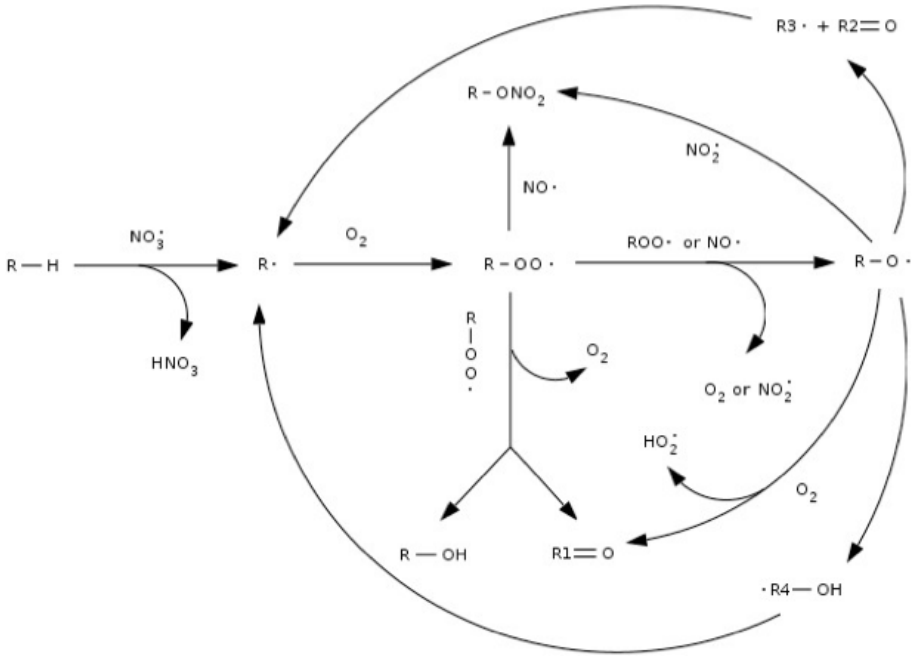

Figure 5.4: Reaction mechanism of NO_3 and alkanes

The reaction mechanism between NO_3 and alkenes can be seen below in Figure 5.5, as illustrated by Fry and Sakinger [47].

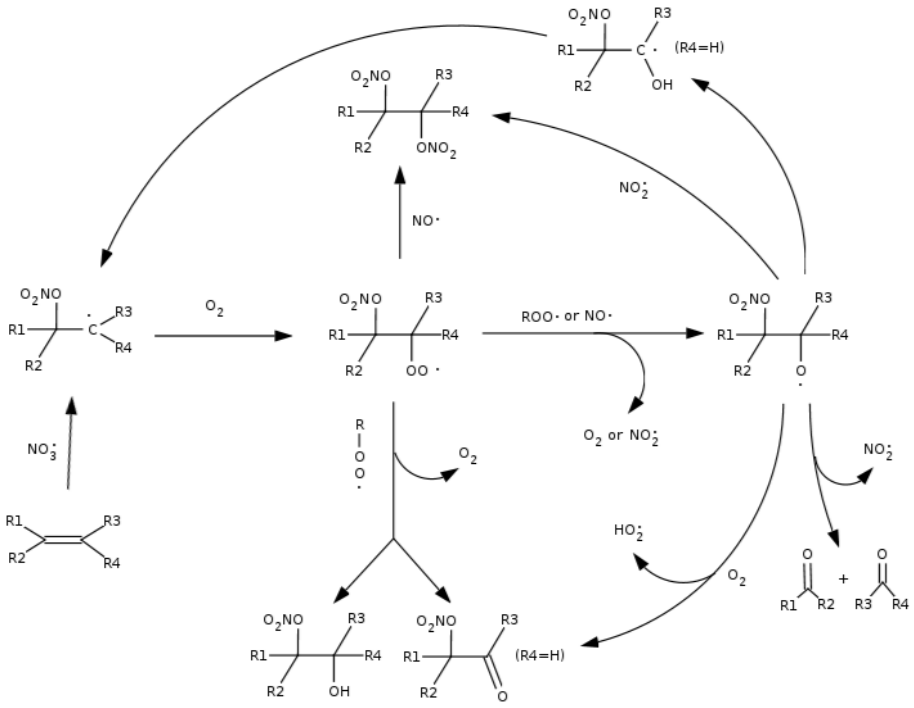

Figure 5.5: Reaction mechanism of NO_3 and alkenes

NO_3 oxidation of alkanes, see Figure 5.4, proceeds via H-atom abstraction, forming peroxy radicals [48]. In the oxidation of alkenes, see Figure 5.5, NO_3 addition forms oxidised intermediate organic products e.g aldehydes and nitrooxy-substituted compounds [49].

In general, alkenes are more reactive than alkanes due to the presence of carbon-carbon double bonds [50]. In the ozonolysis of alkenes, carbon-carbon double bonds undergo addition of O_3, where the double bonds are replaced with oxygen [44, 51]. This forms a molozonide intermediate [52]. The reaction continues until the intermediates break apart and form carbonyls and carbonyl oxides (Criegee intermediates), and ultimately, a stable ozonide [51]. Reactions between NO_3 and alkenes similarly attack these carbon-carbon double bonds via NO_3 addition [47]. NO_3-initiated oxidation leads to the

formation of aldehydes and nitrooxy-substituted compounds [49]. OH reacts with alkenes through OH addition, further reaction with O_2 forms hydroxy peroxy radicals [38] . Conversely, alkanes are constructed of single carbon bonds and are oxidised almost exclusively by OH, and to a lesser extent by NO_3 and O_3, through H-atom abstraction [42, 53-55]. Oxidation of alkanes by NO_3 is not thought to be significant, except in areas with high alkane concentrations e.g. oil and gas basins [43]. Initial degradation of alkanes forms alkyl radicals which are thus converted to alkyl peroxy radicals via reactions with O_2 [55].

Typical indoor concentrations of OH, O_3, and NO_3 were obtained from the literature and are detailed below in Table 5.1.

Table 5.1: Typical concentrations of oxidants in indoor environment from existing literature [56-58].

	Concentration (molecule^{-1} cm^{-3})
OH	1.7 x 10^5 [56]
O_3	1.06 x 10^{10} [57]
NO_3	2.46 x 10^7 [58]

In Table 5.2, the rate constant of each VOC with OH, O_3, and NO_3 is listed, and the atmospheric lifetime has been calculated using the following equation:

$$\tau_{VOC} = \frac{1}{k[O_x]}$$

Equation 5.1: Calculating the atmospheric lifetime of VOCs based on reaction with OH, O_3, or NO_3, where k is the rate constant of a VOC with the oxidant, O_x.

VOCs indoors aren't oxidised by one oxidant in isolation, so to predict VOC lifetime based on reaction with the three considered in this study, τ_{total} was calculated, which sums VOC lifetime based on oxidation with OH, O_3, and NO_3 (see equation 5.2).

$$\tau_{total} = \frac{1}{\left(\frac{1}{\tau_{OH}} + \frac{1}{\tau_{O3}} + \frac{1}{\tau_{NO3}}\right)}$$

Equation 5.2: Calculating the atmospheric lifetime of VOCs based on the combined reaction with OH, O_3, or NO_3, where $\tau_{OH/O3/NO3}$ is as defined in Equation 5.1

Table 5.2: Rate constants for observed VOCs with OH, O_3, and NO_3 in molecules cm^{-1} s^{-1}. Indoor atmospheric lifetimes have been calculated and defined in seconds

	k_{OH} (molecules cm^{-1} s^{-1})	k_{O3} (molecules cm^{-1} s^{-1})	k_{NO3} (molecules cm^{-1} s^{-1})	τ_{OH} (s^{-1})	τ_{O3} (s^{-1})	τ_{NO3} (s^{-1})	τ_{total} (s^{-1})
1,3-butadiene	6.66×10^{-11}	6.24×10^{-18}	1.00×10^{-13}	8.83×10^{4}	1.51×10^{7}	4.07×10^{5}	7.22×10^{4}
1,3,5-trimethylbenzene	5.73×10^{-11}	2.20×10^{-21}	2.40×10^{-16}	1.03×10^{5}	4.29×10^{10}	1.69×10^{8}	1.03×10^{5}
2,2,4-trimethylpentane	3.68×10^{-12}	1.00×10^{-23}	9.00×10^{-17}	1.60×10^{6}	9.43×10^{12}	4.52×10^{8}	1.59×10^{6}
α-Pinene	5.37×10^{-11}	4.30×10^{-18}	5.80×10^{-12}	1.10×10^{5}	2.19×10^{7}	7.01×10^{3}	6.59×10^{3}
Acetone	2.19×10^{-13}	N/A	8.50×10^{-18}	2.69×10^{7}	N/A	4.78×10^{9}	2.67×10^{7}
Acetylene	8.15×10^{-13}	3.00×10^{-20}	2.30×10^{-17}	7.22×10^{6}	3.14×10^{9}	1.77×10^{9}	7.17×10^{6}
β-Pinene	1.47×10^{-11}	1.20×10^{-17}	2.51×10^{-12}	4.00×10^{5}	7.86×10^{6}	1.62×10^{4}	1.55×10^{4}
Benzene	1.23×10^{-12}	1.00×10^{-23}	3.00×10^{-17}	4.78×10^{6}	9.43×10^{12}	1.36×10^{9}	4.77×10^{6}
1-butene	3.14×10^{-11}	1.20×10^{-17}	5.40×10^{-15}	1.87×10^{5}	7.86×10^{6}	7.53×10^{6}	1.79×10^{5}
cis-2-butene	6.02×10^{-11}	1.30×10^{-16}	1.89×10^{-13}	9.77×10^{4}	7.26×10^{5}	2.15×10^{5}	6.15×10^{4}
D4 Siloxane	1.01×10^{-12}	3.00×10^{-20}	2.00×10^{-16}	5.82×10^{6}	3.14×10^{9}	2.03×10^{8}	5.65×10^{6}
Dichloromethane	1.42×10^{-13}	N/A	4.80×10^{-18}	4.14×10^{7}	N/A	8.47×10^{9}	4.12×10^{7}
Ethane	2.68×10^{-13}	1.00×10^{-23}	7.90×10^{-18}	2.19×10^{7}	9.43×10^{12}	5.15×10^{9}	2.19×10^{7}
Ethanol	3.27×10^{-12}	N/A	1.37×10^{-15}	1.80×10^{6}	N/A	2.97×10^{7}	1.70×10^{6}
Ethene	8.52×10^{-12}	1.80×10^{-18}	2.14×10^{-16}	6.90×10^{5}	5.24×10^{7}	1.90×10^{8}	6.79×10^{5}
Ethylbenzene	7.10×10^{-12}	1.00×10^{-20}	5.71×10^{-16}	8.29×10^{5}	9.43×10^{9}	7.12×10^{7}	8.19×10^{5}
γ-Terpinene	1.77×10^{-10}	1.40×10^{-16}	2.90×10^{-11}	3.32×10^{4}	6.74×10^{5}	1.40×10^{3}	1.34×10^{3}
iso-butane	2.34×10^{-12}	1.00×10^{-23}	8.20×10^{-17}	2.51×10^{6}	9.43×10^{12}	4.96×10^{8}	2.50×10^{6}

iso-butene	5.14×10^{-11}	1.20×10^{-17}	1.35×10^{-14}	1.14×10^{5}	7.86×10^{6}	3.01×10^{6}	1.09×10^{5}
iso-pentane	3.90×10^{-12}	1.00×10^{-23}	1.56×10^{-16}	1.51×10^{6}	9.43×10^{12}	2.61×10^{8}	1.50×10^{6}
Isoprene	1.01×10^{-10}	1.40×10^{-17}	6.78×10^{-13}	5.82×10^{4}	6.74×10^{6}	6.00×10^{4}	2.94×10^{4}
Limonene	1.49×10^{-10}	6.50×10^{-16}	9.40×10^{-12}	3.95×10^{4}	1.45×10^{5}	4.32×10^{3}	3.80×10^{3}
Methanol	9.44×10^{-13}	N/A	2.10×10^{-16}	6.23×10^{6}	N/A	1.94×10^{8}	6.04×10^{6}
2-methylpentane	5.60×10^{-12}	1.00×10^{-23}	2.04×10^{-12}	1.05×10^{6}	9.43×10^{12}	1.99×10^{4}	1.96×10^{4}
m/p-Xylene	1.90×10^{-11}	1.10×10^{-21}	3.42×10^{-16}	3.10×10^{5}	8.58×10^{10}	1.19×10^{8}	3.09×10^{5}
n-butane	2.54×10^{-12}	1.00×10^{-23}	4.59×10^{-17}	2.32×10^{6}	9.43×10^{12}	8.86×10^{8}	2.31×10^{6}
n-heptane	7.15×10^{-12}	1.00×10^{-23}	1.36×10^{-16}	8.23×10^{5}	9.43×10^{12}	2.99×10^{8}	8.20×10^{5}
n-hexane	5.61×10^{-12}	1.00×10^{-23}	1.10×10^{-16}	1.05×10^{6}	9.43×10^{12}	3.70×10^{8}	1.05×10^{6}
n-octane	8.68×10^{-12}	1.00×10^{-23}	1.90×10^{-16}	6.78×10^{5}	9.43×10^{12}	2.14×10^{8}	6.76×10^{5}
n-pentane	3.94×10^{-12}	1.00×10^{-23}	8.70×10^{-17}	1.49×10^{6}	9.43×10^{12}	4.67×10^{8}	1.49×10^{6}
o-Xylene	1.22×10^{-11}	1.72×10^{-21}	3.77×10^{-16}	4.82×10^{5}	5.48×10^{10}	1.08×10^{8}	4.80×10^{5}
p-cymene	1.51×10^{-11}	5.00×10^{-20}	1.51×10^{-11}	3.90×10^{5}	1.89×10^{9}	2.69×10^{3}	2.67×10^{3}
1-pentene	3.19×10^{-11}	1.00×10^{-17}	3.14×10^{-11}	1.84×10^{5}	9.43×10^{6}	1.29×10^{3}	1.29×10^{3}
Propane	1.15×10^{-12}	1.00×10^{-23}	9.20×10^{-18}	5.12×10^{6}	9.43×10^{12}	4.42×10^{9}	5.11×10^{6}
Propene	2.63×10^{-11}	1.20×10^{-17}	6.40×10^{-15}	2.24×10^{5}	7.86×10^{6}	6.35×10^{6}	2.10×10^{5}
Tetrachloroethylene	1.67×10^{-13}	N/A	N/A	3.52×10^{7}	N/A	N/A	3.52×10^{7}
Toluene	5.96×10^{-12}	4.10×10^{-22}	6.80×10^{-17}	9.87×10^{5}	2.30×10^{11}	5.98×10^{8}	9.85×10^{5}
trans-2-butene	6.02×10^{-11}	2.65×10^{-16}	1.89×10^{-17}	9.77×10^{4}	3.56×10^{5}	2.15×10^{9}	7.67×10^{4}
trans-2-pentene	6.69×10^{-11}	3.15×10^{-16}	3.80×10^{-13}	8.79×10^{4}	2.99×10^{5}	1.07×10^{5}	4.16×10^{4}

OH, O_3, and NO_3 rate constants outlined in Table 5.2 were derived from the United States National Institutes of Health PubChem database (National Insititutes of Health [59] and references therein) and the available literature [43, 60-68].

As can be seen by the indoor lifetime calculations of the VOCs with the relevant oxidants, reaction with the OH radical is significant in the majority of reactions with few exceptions e.g. monoterpene species react much more readily with the NO_3 radical. Thus, OH is largely responsible for the total indoor atmospheric lifetime of VOCs when indoor lifetimes with OH, O_3, and NO_3 are combined. There is clearly a significant difference in the lifetimes of compounds outside and indoors, for example, Atkinson and Arey estimate the outdoor lifetime of limonene when in reaction with OH as 49 minutes, with an outdoor OH concentration estimated to be 2.0×10^6 molecules cm^{-3} [69]; here the calculation for the same reaction indoors, but with less OH, estimates this to be nearly 11 hours.

5.2. Methodologies

Two methods are considered with which to estimate the oxidation potential of these VOCs. The first method calculates OH, O_3 and NO_3 reactions based on the product of the individual VOC concentration and its oxidant rate constant. The second uses a box model developed by Carslaw [2] and is detailed below.

5.2.1. Experimental methodology

In the aforementioned population-scale study, 351 indoor and 53 outdoor air samples were obtained across 60 households in winter and summer 2019. Silica treated stainless-steel canisters and attached flow restrictors were used to collect three-day time-weighted average samples. This method broadly aligns with the sampling protocol outlined in the United States Environmental Protection Agency Toxic Organics Compendium Method TO-15 [70]. A cohort of 204 participants was drawn from an existing and well-characterised panel of consumer product testers who were not privy to the hypothesis of the study. Participants were asked to complete two surveys, one regarding property information, residence occupancy, and resident demographics and the second a product usage log recording each individual

usage of a given product type. Samples were collected each week and shipped to the University of York for analysis via GC-ToF-MS and GC-FID.

5.2.2. Reactive potential and pseudo-first order reaction rate calculations

Reactive potential and pseudo-first reaction rates are of interest in this study as the more reactive a species is, its propensity to form harmful secondary compounds increases, depending on the atmospheric lifetime and abundance of the compounds [13]. First, the reactive potential is determined, where the product of the bimolecular rate constant with the concentration of VOC present is assessed, and second, the pseudo-first order reaction rate is determined, this measures the rate of loss of VOC using indoor concentrations of the pertinent oxidants.

The first calculation, shown in Equation 5.3, gives a metric that measures the likely generation of secondary products based on the concentration of the VOC in the atmosphere and its rate constant with the given oxidant, independent of how abundant the oxidant is.

$$Reactive\ potential = \ kOx[VOC]$$

Equation 5.3: Equation for determining reactive potential, where kOx is the rate constant of a given VOC with a given oxidant, and $[VOC]$ is the concentration of the given VOC

The second calculation, shown in Equation 5.4, gives a metric that extends the first by considering the concentration of the oxidant in the environment. This reaction is considered a pseudo-first order, or bimolecular, reaction, as the concentration of the oxidant is considered constant in the environment.

Pseudo-first order reaction rates were calculated using two equations in Equations 5.4 (a) and (b) below:

(a)

$$k' = kOx[Ox]$$

Equation 5.4 (a): Equation for determining k', where kOx is the bimolecular rate constant, and Ox is the concentration of the oxidant as stated in Table 5.1

(b)

$$Rate\ of\ loss\ of\ VOC = k'[VOC]$$

Equation 5.4 (b): Equation for determining pseudo-first order reaction rates, where k' is defined as in Equation 5.4 (a)

5.2.3. Modelling

5.2.3.1. INdoor Detailed Chemical Mechanism (INDCM)[2]

Mechanism

The Indoor Detailed Chemical Model (INDCM) is a box model, assuming a single, well-mixed environment, based on the Master Chemical Mechanism (MCM, v.3.2), that takes chemical mechanisms and places them in a context relevant to chemistry undertaken indoors. INDCM considers the reactions of ~140 VOCs with OH, O_3, and NO_3. Several physical processes are also accounted for, including air exchange rates, chemical deposition, photolysis,

[2] Summarised from Carslaw [2]

internal emissions and gas-to-particle partitioning. Outdoor mixing ratios of O_3, NO_2 and NO can also be set [2]. The model degrades each VOC with OH, O_3, and NO_3, and photolysis, if appropriate. Radicals subsequently generated include peroxy, oxy, and excited and stable Criegee species. Further reaction results ultimately in CO_2 and H_2O. In total, this model contains approximately 20,000 reactions and 5,000 species [13]. Critically, INDCM deviates from the MCM by incorporating additional species found more readily indoors — such as limonene and terpinene — which are modelled after their structure compared to α-Pinene or β-Pinene, both of which are included in the MCM [2].

The concentration of each species in INDCM can be calculated using the following equation:

$$\frac{\mathrm{d}C_\mathrm{i}}{\mathrm{d}t} = V_\mathrm{d}\left(\frac{A_\mathrm{i}}{V_\mathrm{i}}\right)C_\mathrm{i} + \lambda_\mathrm{r} f C_\mathrm{o} - \lambda_\mathrm{r} C_\mathrm{i} + \frac{Q_\mathrm{i}}{V_\mathrm{i}} + \sum_{j=1}^{n} Rij,$$

Equation 5.5: Calculation to determine concentration of a given species in INDCM, where: C_i = indoor concentration of a species, C_o = outdoor concentration of a species, V_d = deposition velocity of a species, A_i = surface area of a room, V_i = volume of a room, λ_r = indoor/outdoor air exchange rate, f = building filtration factor, Q_i = indoor emission rate, Rij = reaction rate between species i and *j*.

Deposition velocities

In this model, deposition was assumed to be irreversible and calculated according to the term V_d in Equation 5.5. Table 5.3 lists the deposition velocities of a number of species indoors

Table 5.3: The deposition velocities for a number of species indoors

	Deposition velocity (cm s^{-1})
Organic peroxides	0.07
NO_2	0.06
O_3/SO_2	0.036
$HONO/HNO_3/HO_2NO_2/H_2O_2/NO_3/N_2O_5/HO_2/OH$	0.007
$HCHO/CH_3CHO$	0.005
Aldehydes (excluding HCHO and CH_3CHO)	0.005
PAN and organic nitrates	0.002
CO/NO	0

Surface production reactions

HONO production is the only surface production reaction considered by INDCM, though the author recognises other potentially important surface reactions that take place indoors (e.g. O_3 and carpet).

The photolysis of HONO is believed to contribute to the production of OH, and in the presence of a vented combustion source, mixing ratios can be considerable at 5–15 ppb. Without a combustion source, indoor concentrations of HONO can still exceed outdoor concentrations. This is thought to be because of NO_2 infiltrations indoors. HONO produced from the reaction of OH and NO is slow, so surface formation with H_2O and NO_2 is the largest contributor to indoor HONO concentrations. A heterogeneous production rate of $2.9 \pm 1.8 \times 10^{-3}$ m min^{-1} was used in INDCM.

Photolysis

Light indoors was treated as two compartments in INDCM; one in the ultraviolet range (300–400 nm) and the visible range (400–760 nm). Flat spectral distribution was assumed in each compartment.

The photolysis coefficient (j) of a given VOC (i) is calculated via Equation 5.6(a):

$$j_i = h_{\mathrm{uv}} I_{\mathrm{uv}} + h_{\mathrm{vis}} I_{\mathrm{vis}},$$

Equation 5.6 (a): Indoor photolysis coefficient calculation, where: I_{uv} = spherically integrated photon flux in the ultraviolet range (set as 2.3 x 10^{13} photons cm^{-2} s^{-1}), I_{vis} = spherically integrated photon flux in the visible range (set as 2.3 x 10^{13} photons cm^{-2} s^{-1}). These values are assumed typical of indoor artificial light fluxes

h_{uv} is calculated via:

$$h_{\mathrm{uv}} = (100\ \mathrm{nm})^{-1} \int_{300\ \mathrm{nm}}^{400\ \mathrm{nm}} \sigma \phi \mathrm{d}\lambda,$$

Equation 5.6 (b): Definition of h_{uv}, where: σ = the molecule's absorption cross-section, ϕ = quantum yield, $\mathrm{d}\lambda$ = relevant wavelength interval

h_{vis} is calculated via:

$$h_{\mathrm{vis}} = (360\ \mathrm{nm})^{-1} \int_{400\ \mathrm{nm}}^{760\ \mathrm{nm}} \sigma \phi \mathrm{d}\lambda,$$

Equation 5.6 (c): Definition of h_{vis}, where: σ = the molecule's absorption cross-section, ϕ = quantum yield, $\mathrm{d}\lambda$ = relevant wavelength interval

Photolysis outdoors was derived from a two-stream scattering model and attenuated to values more relevant to indoor environments; as such, set ratio values are an attenuation of 0.1 for visible light to 0.03 for ultraviolet light. Carslaw and Shaw (and references therein) suggest that approximately three times more light is transmitted indoors as visible over ultraviolet light [13]. The

total photolysis rate for a given species is then defined as the sum of indoor and outdoor contributions.

Outdoor exchange and air exchange rate

Indoor concentrations of some species are significantly impacted by exchange with outdoor air. H_2O_2 and HNO_3 remained approximately consistent over a diurnal cycle, and was set at 2 ppb. OH, HO_2, and CH_3O_2 are photolysed rapidly, with the noon maxima concentrations set at 5 x 10^6, 1 x 10^8, and 2.5 x 10^7 molecules cm^{-3}. Finally, HONO, is also photolysed rapidly, with mixing ratios peaking overnight; set at 300 ppt at night, and 20 ppt at noon.

Exchange with indoor air is derived from the right-side of Equation 5.5., with the building filtration factor (f) assumed to be 1. Air exchange rate is assumed to be 0.76 h^{-1} (an average representative of British housing stock from research of ~2900 homes) studies have shown that AER can vary between 0.2 h^{-1} and 2 h^{-1} depending on building tightness.

5.2.3.2. Secondary Product Creation Potential (SPCP)[3]

An addition to the INDCM model was the creation of the Secondary Product Creation Potential (SPCP) metric. SPCP was borne of a need for a standardised metric that measured the oxidation potential of a variety of VOCs found indoors and, therefore, their propensity to form potentially hazardous products. Models do exist that measure potential reactivity through the amount of ozone produced by VOCs, for example the Photochemical Ozone Creation Potential (POCP) and the Maximum Incremental Reactivity (MIR) metrics. In the existing literature, ozone is proven to be harmful to human health, and the health of plant crops, and so

[3] Summarised from Carslaw and Shaw [13]

measuring the ozone production potential from VOC oxidation is of clear importance [71]. Bowman and Seinfeld outline the various mechanisms through which ozone is generated by VOC chemistry in the atmosphere, as is discussed in more detail in Chapter 1 [72]. In simple terms, VOCs have different ozone-forming potentials owing to their structure and their reaction with OH, as in a VOC/NO_x system, ozone production is primarily initiated by OH [72]. Ozone production is also dependent on atmospheric NO_x concentration, and other VOCs present [72]. POCP was developed as a way of estimating ozone formation from VOC degradation using a photochemical trajectory model [73]. POCP estimates changes in ozone following incremental mass emissions of a compound [71]. The ratio of these increases in ozone are compared relative to the same incremental emission of ethene, and a POCP value is obtained [71, 73]. Akin to POCP, MIR measures ozone formation resulting from the addition of a given VOC, divided by the amount of VOC added [74]. However, neither of these models can explore indoor chemistry in a nuanced way, as photolysis—which is the primary driver of chemistry outdoors—is less applicable indoors, and ozone is rapidly removed indoors [13]. SPCP accounts for various constituents in indoor air that influence secondary product formation, such as PANs and organic nitrates. This methodology subsequently provides a more relevant framework for indoor air specifically over existing oxidation prediction metrics e.g. POCP and MIR. SPCP values were calculated using Equation 5.7.

$$SPCP = \sum (organic\ nitrates + PANs + HCHO + O_3 + glyoxal + acetaldehyde)$$

Equation 5.7: Equation for determining SPCP values

Where total organic nitrate, peroxyacetyl nitrate, formaldehyde, ozone, glyoxal and acetaldehyde mixing ratios generated is summed. In Carslaw and Shaw, SPCP is divided by the mixing ratio of a given VOC in ppb (β) to calculate the SPCP of each VOC (in ppb secondary products produced per

ppb of added VOC); however, this is not the case in this study. Here, SPCP is the total value of secondary products generated in a mixture; the result is expressed in ppb of secondary products produced. Formaldehyde, glyoxal, and acetaldehyde mixing ratios are considered by the model due to their potential or confirmed toxicity in the human body.

As explained by Carslaw and Shaw, SPCP is based on 63 VOCs thought to be commonly found indoors, see Table 5.4 [13]. 53 species were identified from four studies, highlighting compounds found in cleaning products and air fresheners. Another two studies identified six additional compounds, another three compounds were identified as degradation products already found in the Master Chemical Mechanism, and 2-methyl-2-buten-2-ol was included due it being derived from biogenic sources; this resulted in a total of 63 compounds being considered.

Table 5.4: Compounds included in SPCP calculations outlined by Carslaw and Shaw [13]; where MBO = 2-methly-2-buten-2-ol, MEK = Methyl ethyl ketone, MIBK = Methyl-isobutylketone, MIBKAOH = 4-hydroxy-4-methylpentan-2-one, and MRPK = 2-Pentanone

1-butene	Decanal	Methylpropene
1,2-Dichloropropane	Decane	MIBK
1,2,3-Trimethylbenzene	Dodecane	MIBKAOH
1,2,4-Trimethylbenzene	Ethane	MPRK
1,3-butadiene	Ethanol	*n*-butane
1,3,5-Trimethylbenzene	Ethene	*n*-butanol
2-butoxyethanol	Ethylbenzene	*n*-heptane
3-pentanol	Ethylene glycol	*n*-hexane
α-Pinene	Formic acid	*n*-pentane
Acetaldehyde	Formaldehyde	*n*-propanol
Acetic acid	Heptanal	Nonanal
Acetone	Hexanal	o-Xylene
β-Pinene	i-propanol	Octanal
Benzaldehyde	i-propylbenzene	Propene
Benzene	Isoprene	Styrene
Dichloromethane	Limonene	Tetrachlorethene

Methyl chloroform	m-Xylene	Toluene
Chloroform	MBO	*trans*-2-butene
cis-2-butene	MEK	*trans*-butanol
Cyclohexane	Methacrolein	Trichloroethene
Cyclohexanone	Methanol	Undecane

In the SPCP model used by Carslaw and Shaw [13], the mixing ratio of each VOC was set to 10 ppb, and changes in the concentration of OH, HO_2, RO_2, the sum of organic nitrates, the sum of PANs, HCHO, O_3, glyoxal, and acetaldehyde were observed. The summed species are included as they are well-documented in the literature as potentially mutagenic, carcinogenic, allergenic, or otherwise have impacts on cardiovascular or pulmonary health [13]. A baseline model was run where no VOC was added to the system, and subsequent runs were made for relevant changes in parameters, with changes in the concentration of the above species observed. Once SPCP values had been derived, the units were given as ppb secondary products produced per ppb of added VOC to the system. In this study, rather than VOC mixing ratios being set to 10 ppb, they were set to observations as described in Heeley-Hill et al. [16], with zero, 25th percentile, median, 75th percentile, and maximum observed values. As mentioned earlier, SPCP calculations in this study refer to total secondary products generated by a mixture, and not per ppb of VOC added. Critically, this allowed the SPCP model to be used with observed mixing ratios.

In the original study, sensitivity runs were performed to assess the impact of changing parameters on indoor chemistry. Briefly, lowering the AER (0.2 h^{-1}) reduces O_3 mixing ratios (7.9 to 2.7 ppb) and in turn supresses VOC-O_3 chemistry, which reduces OH [13]. Raising AER (2 h^{-1}) increases O_3 mixing ratios (7.9 to 15 ppb), stimulating VOC-O_3 chemistry [13]. Adjusting light attenuation also has an impact, with greater light attenuation resulting in increased SPCP; the converse is also true [13]. In the latter scenario, NO_2 was photolysed more rapidly, stimulating O_3 production [13].

The SPCP model is somewhat restricted as it does not consider e.g. particle formation. The authors state that while the INDCM does include particle formation for some species e.g. terpenes, it does not include particle formation for others, so particle formation has been disregarded entirely in SPCP calculations. In addition, the calculation used in the original study gives the health effects of each VOC equal weighting so that, in effect, each compound is considered just as potentially toxic as another.

Experimental

The method used here is as described in Carslaw and Shaw [13]. The INDCM was initialised to replicate a typical residence in a polluted European city as described in Kruza et al. [75], namely: an apartment consisting of three bedrooms (7.5 m^2), an open-plan kitchen/living room (12.5 m^2 and 20.9 m^2 respectively), a WC (2.8 m^2), a bathroom (7.8 m^2), a corridor (3.9 m^2), and a ceiling height of 2.4 m; these dimensions equate to a surface area of 70 m^2 and a volume of 168 m^2. Temperature was set to 300 K and relative humidity at 45%. The air exchange rate was set to 0.76 h^{-1}. Outdoor light attenuated indoors was set at 3% ultraviolet and 10% visible light. Outdoor O_3 and NO_x concentrations followed a diurnal profile derived from data observed at the London Air Quality Network Greenwich site (see Table 5.5) as a proxy for conditions in Ashford, Kent; this site is referenced as a suburban background site by the Department for Environment, Food, and Rural Affairs (DEFRA). These values inferred two-day averaged indoor mixing ratios in the model as outlined in Tables 5.6–5.8 The model was run for two days, with the model run commencing at 07:00 and finishing at 00:00 the following day. The first 17 hours (07:00—00:00) allowed the model to stabilise, with results presented from the final 24 hours (00:00 to 00:00).

To reflect potential seasonality in the data, model runs were performed for each campaign separately – winter/spring (WS) and summer/autumn (SA) – considering the observed minimum, 25th percentile, median, 75th percentile

and maximum concentrations for each VOC individually, and an additional run where VOC concentrations were set to zero. Outdoor VOC concentrations were set to median observed values in each season, whilst NO_x and O_3 concentrations had the same respective concentrations across both seasons. An additional campaign was modelled – 'lockdown' – to inform the potential impacts on indoor air chemistry of travel and activity restrictions imposed by the UK government during the COVID-19 pandemic. This period was dated from 23.03.2020 to 31.04.2020. In this campaign, VOC load scenarios were the same as in the SA campaign, but outdoor O_3 and NO_x concentrations were adjusted to the dates of the lockdown period.

Table 5.5: Outdoor minimum and maximum mixing ratios for O_3, NO, and NO_2 for all campaigns

	WS		SA		Lockdown	
	Min	Max	Min	Max	Min	Max
O_3	17	33	15	36	20	43
NO	3	15	2	6	1	5
NO_2	7	15	5	9	5	10

Table 5.6. Modelled indoor mixing ratios for O_3, NO, and NO_2 for the winter campaign

	Zero	Min	25th	Median	75th	Max
O_3	7.21	7.21	7.45	7.83	8.20	5.90
NO	0.61	0.61	0.53	0.39	0.22	0.04
NO_2	6.39	6.39	6.34	6.27	6.16	5.48

Table 5.7. Modelled indoor mixing ratios for O_3, NO, and NO_2 for the summer campaign

	Zero	Min	25th	Median	75th	Max
O_3	8.5	8.5	8.6	8.7	8.8	4.7
NO	0.2	0.2	0.2	0.1	0.1	0.0
NO_2	3.3	3.3	3.2	3.2	3.1	2.9

Table 5.8. Modelled indoor mixing ratios for O_3, NO, and NO_2 for the lockdown campaign

	Zero	Min	25th	Median	75th	Max
O_3	7.21	7.21	7.45	7.83	8.20	5.90
NO	0.610	0.610	0.527	0.386	0.218	0.041
NO_2	6.389	6.389	6.341	6.275	6.164	5.479

5.2.4. Statistical methodology

Data manipulation and visualisation was conducted using R v.4.02 “Taking off Again” and the RStudio environment v.1.3.1073 “Golden Rod”, using the *dplyr* (v.1.0.2) package and plotted using *ggplot2* (v.3.3.2) of the *tidyverse* (v.1.3.0) package. Median values were used, where stated explicitly, to temper outlier bias in relevant results and visualisations. Summed values were used, where stated explicitly, to define total reactive potential across all indoor samples. Trends in the data from INDCM were highlighted using geom_smooth(), using the default method. The default method uses generalised additive modelling when n>1000.

5.3. Results and Discussion

5.3.1. Reactive potential and pseudo-first order reaction rate results

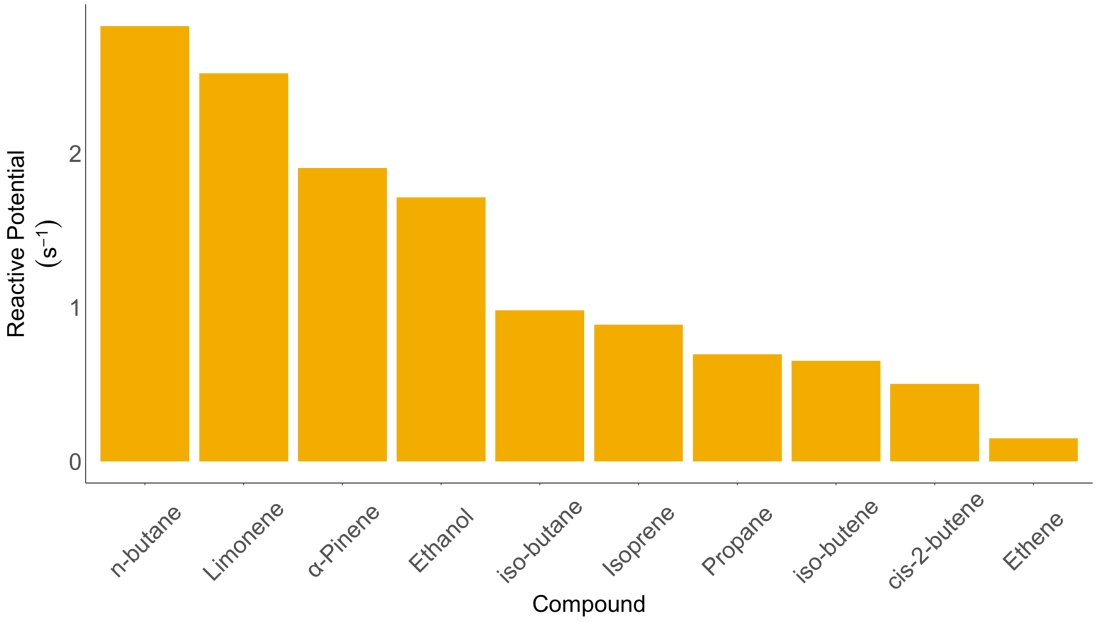

Figure 5.6: Ten VOCs with the greatest median reactive potential with OH across all households

n-butane was the largest sink of OH, with a reactive potential of 2.83 s^{-1}, followed by the monoterpenes limonene and α-Pinene at 2.52 and 1.91 s^{-1} respectively. The reactive potential of alkenes generally decreased, with ethene having the lowest reactive potential in this subset of the ten species with the greatest reactive potential at 1.5 x 10^{-1} s^{-1}; see Figure 5.6. The dominance of OH in *n*-butane reactive potential is in accordance with existing literature [76]. OH is seen as a universal oxidiser in the atmosphere, particularly of alkanes, but as seen in Figure 5.6, alkenes are also readily oxidised by OH, mainly through H-atom abstraction [42, 55, 77].

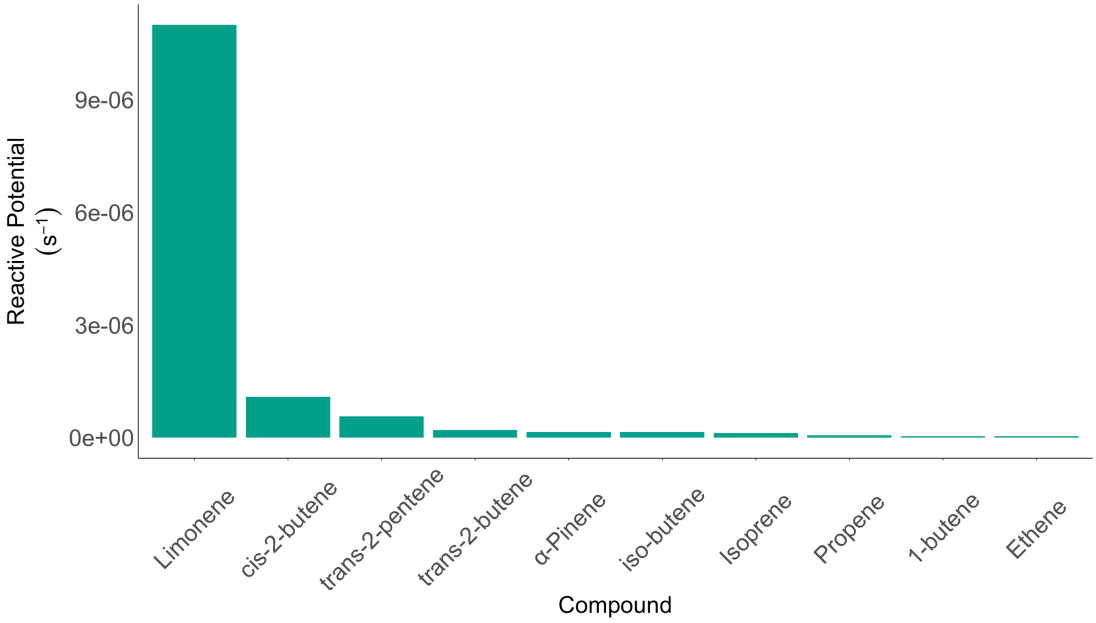

Figure 5.7: Ten VOCs with the greatest median reactive potential with O_3 across all households

Limonene was the largest sink of O_3 at 1.10 x 10^{-5} s^{-1}. A notable conclusion is the greater reactive potential of alkene species more generally e.g. cis-2-butene (1.09 x 10^{-6} s^{-1}) with ethene having the lowest reactive potential in this subset of ten species with the greatest reactive potential (3.17 x 10^{-8} s^{-1}), see Figure 5.7. Alkenes dominate the ten species with the greatest reactive potential; as mentioned earlier, alkenes are most readily oxidised by O_3, as opposed to e.g. alkanes, owing to O-atom addition to the carbon-carbon double bonds inherent in alkene species.

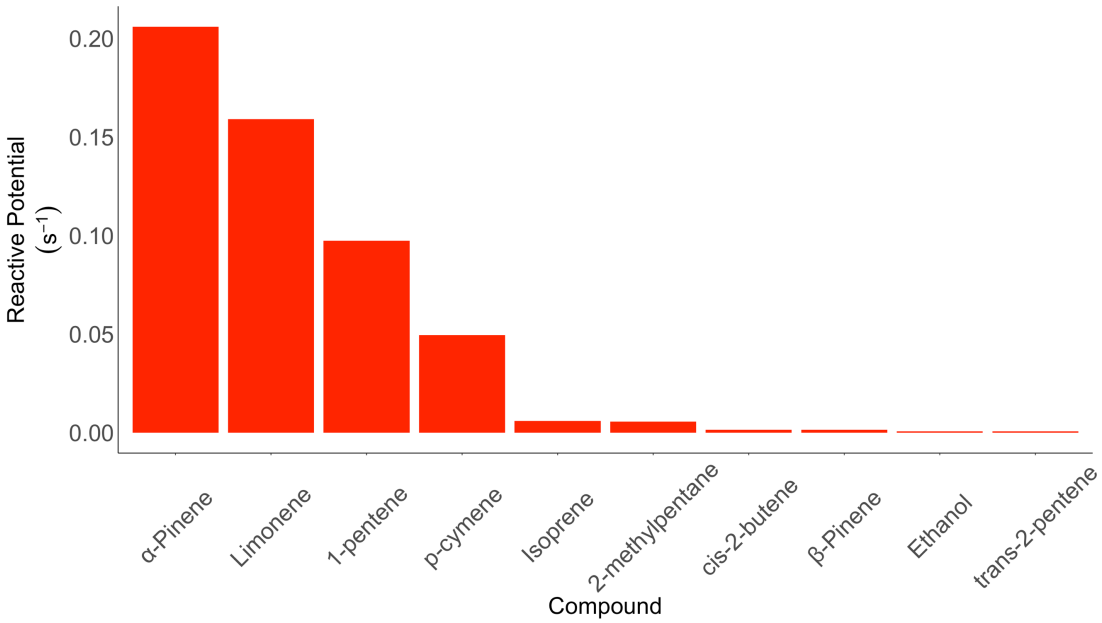

Figure 5.8: Ten VOCs with the greatest median reactive potential with NO_3 across all households

α-Pinene and limonene were the largest sinks of NO_3 at 2.06 x 10^{-1} and 1.59 x 10^{-1} s^{-1} respectively. Reactive potential decreased significantly, with alkenes forming the majority of the species with the greatest reactive potential, with trans-2-pentene having the lowest reactive potential in this subset of the ten species with the greatest reactive potential at 6.81 x 10^{-4} s^{-1}, see Figure 5.8. Similarly to the O_3 reactive potential as described above, NO_3 adds oxygen to carbon-carbon double bonds, hence why alkenes again dominate the species with the greatest reactive potential. Notably, monoterpenes have the greatest reactive potential. Monoterpenes are often cited for their highly-reactive nature; this is due to [78-80]. NO_3 oxidation of monoterpenes is cited in the literature as a source of SOA production [79, 81]. This could be particularly relevant indoors, where NO_3 exerts greater influence in reactive potential than outdoors [82].

Measuring reactive potential has revealed that OH clearly dominates VOC chemistry indoors, particularly that of alkanes, whilst O_3 and NO_3 dominate alkene chemistry. The reaction between OH and *n*-butane is evidently the

process that leads to the greatest number of reactions and thus potentially the greatest number of secondary products. From this metric, it is evident that OH is most reactive with VOCs indoors than both O_3 and NO_3, however, because O_3 occurs at higher concentrations than OH, oxidation with O_3 is still significant.

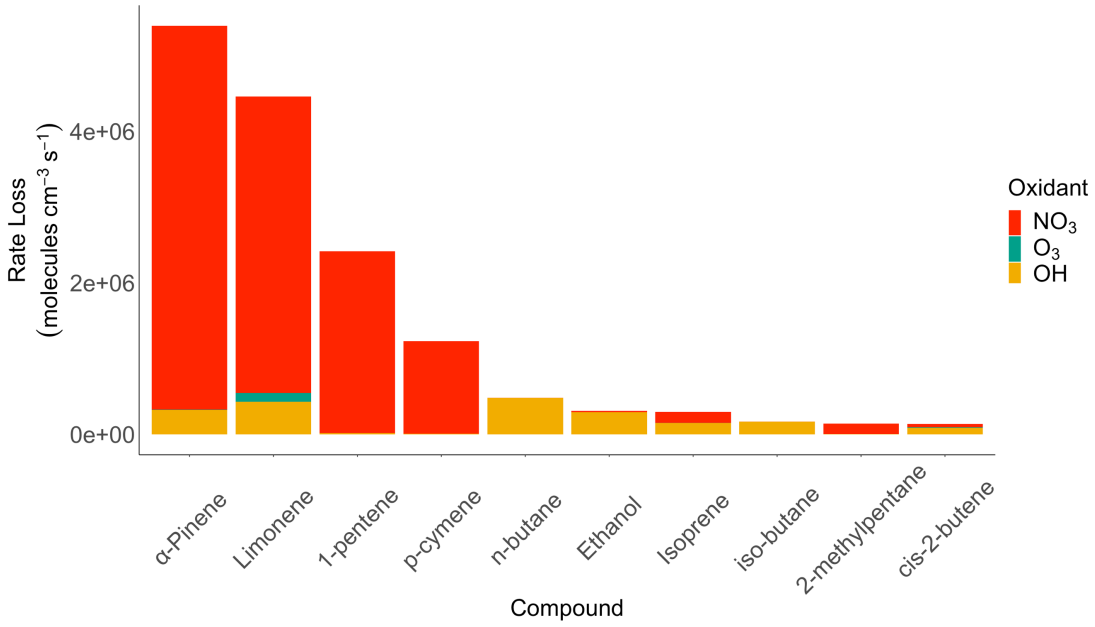

Figure 5.9: Combined median pseudo-first order reaction rate for the ten species with the greatest oxidation rate. Oxidant concentrations assumed to be: OH: 1.7 x 10^5 molecule^{-1} cm^{-3} [56], O_3: 1.06 x 10^{10} molecule^{-1} cm^{-3} [57], NO_3: 2.46 x 10^7 molecule^{-1} cm^{-3} [58]

When the median pseudo-first order reaction rate for each oxidant is summed, see Figure 5.9, the total median pseudo-first order reaction rate of VOCs by the most prevalent indoor oxidants is considered. The monoterpenes α-Pinene and limonene had the greatest first-order pseudo reaction rate at 5.39 and 4.46 x 10^6 molecules cm^{-3} s^{-1}. This plot is also useful for visualising the dominant oxidant per variable. One notable conclusion is that α-Pinene, limonene, 1-pentene and p-cymene oxidation was dominated by reactions with NO_3; Arata, Zarzana et al. [82] predicted that NO_3 was the primary oxidant of monoterpenes. *n*-butane and *iso*-butane

have pseudo-first order reaction rate of 4.82 and 1.68 x 10^5 molecules cm^{-3} s^{-1}, reactions that were dominated by OH. Remaining VOCs in this subset were a mix of alkanes and alkenes, with cis-2-butene having the lowest pseudo-first order reaction rate overall at 1.36 x 10^5 molecules cm^{-3} s^{-1}.

Initial oxidation of VOCs leads to the formation of polar oxygenated functional groups, resulting in less volatile and more water-soluble intermediates, continuing further cycles of oxidation. Properties such as reactivity, photolysis, volatility, and solubility will all impact SOA formation and are different for each chemical present in the mixture [5]. Outdoors, monoterpenes have a calculated lifetime of between minutes and hours [66]. Oxidation products resulting from NO_x-α-Pinene reactions are formaldehyde, acetone and pinonaldehyde. NO_x -β-Pinene reactions lead to formaldehyde, acetone and nopinone. NO_x-limonene reactions result in the formation of formaldehyde and 4-acetyl-1-methylcyclohexene. These first-generation products, in most of their experimental cases, were as reactive as the parent compound with O_3 and OH, with the exception of nopinone [83]. An oft-cited example of SOA production indoors is the formation of formaldehyde from limonene-containing cleaning products, a known respiratory irritant and carcinogen in humans. [84-87].

5.3.2. Indoor Detailed Chemical Model results

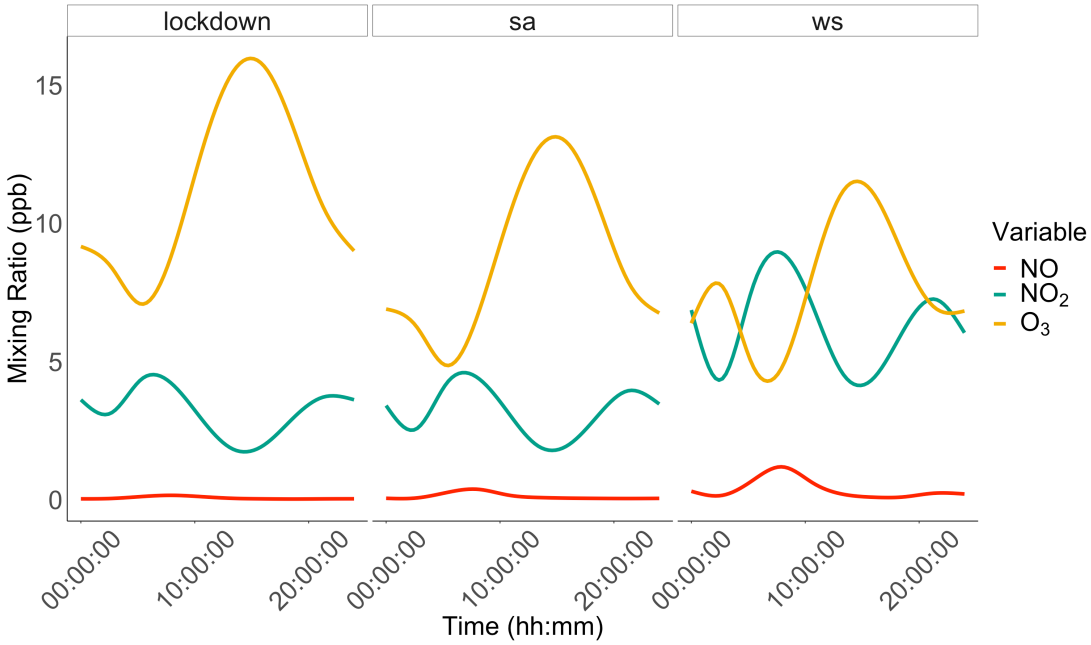

Figure 5.10: O_3 and NO_x mixing ratios across all three campaign periods using the median VOC load. Mixing ratio values are in ppb

In Figure 5.10, the mixing ratios of O_3, NO, and NO_2 are displayed for all three campaigns, using the median VOC load. The mixing ratio of O_3 across all VOC loads was highest during the lockdown period (median lockdown = 9.72 ppb). During the lockdown and summer periods, NO_2 mixing ratios were similar, but in winter, there was a notable increase; NO remained low throughout the summer and lockdown periods (NO_2 median: summer = 3.24 ppb, lockdown = 3.19 ppb, winter = 6.23 ppb; NO median: summer = 0.08 ppb, lockdown = 0.05 ppb, winter = 0.24 ppb).

In accordance with the literature, NO_x followed a diurnal pattern, where it peaks twice per day, usually around rush-hour periods where traffic congestion is highest [88]. An inverse relationship between O_3 and NO_x is evident and is shown in the reactions below in R 5.1 [89]:

$$\begin{aligned} &NO_2 + h\nu \rightarrow NO + O \\ &O + O_2 + M \rightarrow O_3 + M \\ &O_3 + NO \rightarrow NO_2 + O_2 \end{aligned} \qquad \text{(R 5.1)}$$

O_3 is shown to peak in the afternoon as a result of photochemistry with O_3 precursors e.g. VOCs; a process which is maximised around mid-day [90, 91]. Grange, Lee et al. [28] estimated that NO_2 concentrations were up to 34% lower during lockdown than in 'normal' scenarios, but O_3 increased by up to 30% in the same period, based on modelled data. A decrease in NO_x but an increase in O_3 mixing ratios was attributed to less O_3 being lost via the NO titration mechanism; this is borne out by existing studies [92, 93]. O_3 has two precursors in the atmosphere: NO_x and VOCs. Studies suggest that O_3 concentrations can either be NO_x-sensitive or VOC-sensitive; these regimes can preclude effective management of these pollutants [28, 89, 93].

NO_x concentrations tend to be higher in the summer than winter due to the oxidation mechanisms of NO_x and is typically lost through oxidation with OH, and the formation of HNO_3 at night through N_2O_5 hydrolysis. In the winter, the concentrations of these oxidants are lower, leading to longer residence times in the atmosphere [94]. O_3 concentrations are typically higher in summer due to higher temperatures, relative humidity, and increased irradiance [95].

A tangential consequence of lockdown periods globally has been an observed reduction in NO_x; satellite observations between January and April 2020 place a reduction of 20–38% in the NO_2 column over the United States and western Europe. Reductions increased to ~40% over China [96]. These results are broadly reflected in the UK by Lee et al. who reported an estimated 48% reduction in surface-level NO_x concentrations, using data

from the Automatic Urban and Rural Network (AURN) network [97]. Venter et al. reported a population-weighted concentration reduction of 60% in 34 countries, the majority of which was associated with changes in transportation behaviour [98]. Lee et al. report that during lockdown in the UK, road traffic was reduced by 73%, according to Google mobility data, and that consequently, there was a reduction of NO_2 of 40% in urban background sites [97].

According to the National Atmospheric Emissions Inventory (NAEI), approximately 53% of NO_x in urban areas is emitted from traffic sources; there is obviously some nuance within those statistics with some vehicle types emitting more NO_x than other vehicles, and also how lockdowns impacted their usage e.g. heavy goods vehicles — a heavy emitter — impacted comparatively mildly compared to passenger vehicles — a low emitter — which were used significantly less [97]. More widely, it is thought that the decrease in NO_x concentrations during lockdown was coincident with a 50% increase in atmospheric methane. This is thought to be a result of a decrease in OH from lower NO_x concentrations, thus increasing the residence time of methane in the atmosphere [99]. More widely, it is thought that the decrease in NO_x concentrations during lockdown was coincident with a 50% increase in atmospheric methane. This is thought to be a result of a decrease in OH from lower NO_x concentrations, thus increasing the residence time of methane in the atmosphere [99].

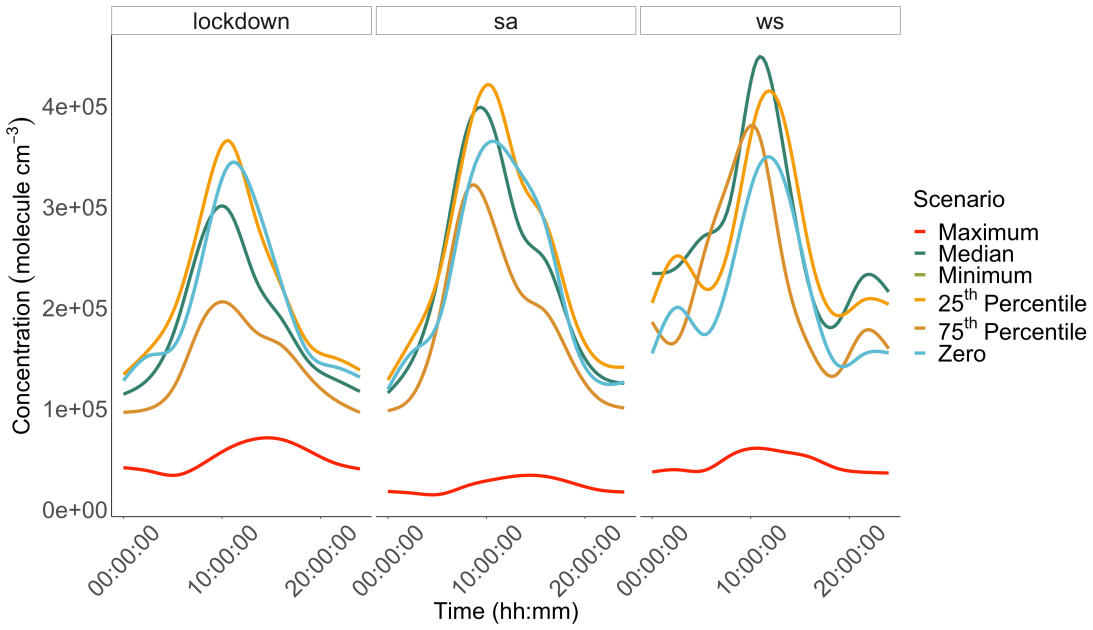

Figure 5.11: OH concentrations across all VOC load scenarios for all three campaign periods. Concentration values are in molecule cm^{-3}

Regarding OH, during the lockdown and summer campaigns, the 25th percentile of concentrations produces the highest OH concentrations. In winter, median VOC concentrations produce the most OH. Concentrations of OH were significantly depressed in the maximum VOC load when compared with other scenarios (OH 'maximum' scenario median: summer = 2.29 x 10^4 molecule cm^{-3}, winter = 4.22 x 10^4 molecule cm^{-3}, lockdown = 4.94 x 10^4 molecule cm^{-3}). The lockdown period yielded the lowest OH concentrations, and winter the highest (OH median: lockdown = 1.59 x 10^5 molecule cm^{-3}, summer = 1.73 x 10^5 molecule cm^{-3}, winter = 2.03 x 10^5 molecule cm^{-3}), see Figure 5.11. As discussed earlier, OH radicals are produced by the oxidation of VOCs, particularly in the ozonolysis of alkenes, so it is not surprising that increasing VOC concentrations, to an extent, imply higher OH concentrations. However, when VOC concentrations reach significant levels, diminishing O_3 concentrations become the limiting factor in OH formation, with neither being replenished. This system is also impacted when increasing peroxy radical concentration, from increased VOC loading, consumes NO, reducing OH replenishment still further. Literature regarding seasonality in

OH concentrations is sparse but OH concentrations were observed to be lower in winter than in summer, though the difference was moderate [100-102].

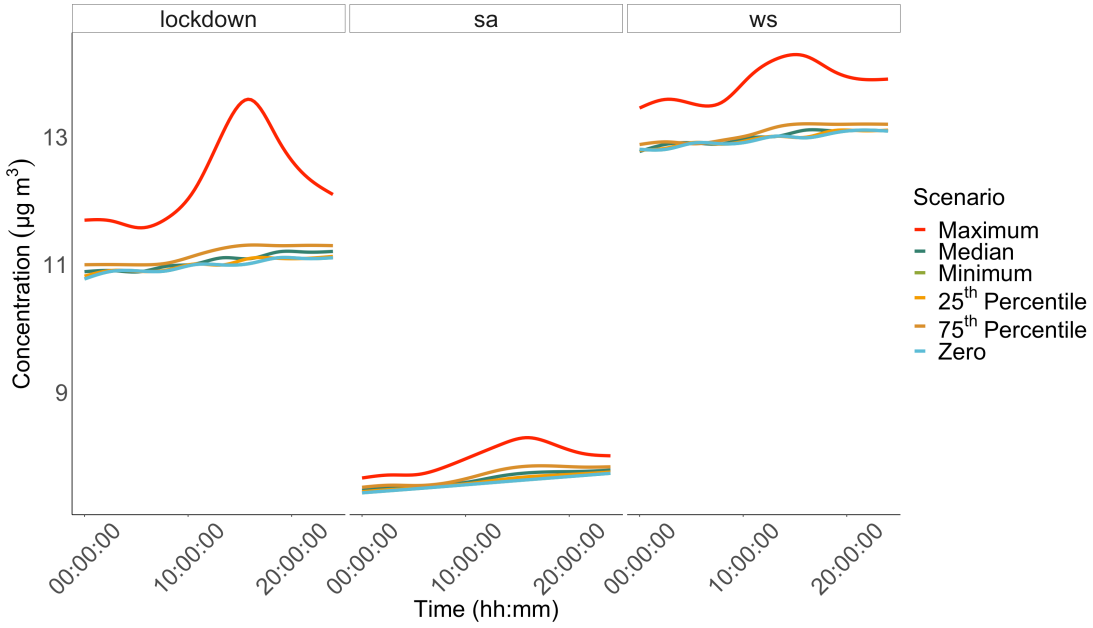

Figure 5.12: $PM_{2.5}$ concentrations across all VOC load scenarios for all three campaign periods. Concentration values are in $\mu g\ m^3$

$PM_{2.5}$ concentrations were significantly enhanced in the maximum VOC load scenario, particularly in the winter and lockdown periods ($PM_{2.5}$ 'maximum' scenario median: winter = 13.9 $\mu g\ m^3$, lockdown = 12.2 $\mu g\ m^3$). Notably, $PM_{2.5}$ concentrations were significantly lower in summer than in winter ($PM_{2,5}$ 'median' scenario median summer = 7.65 $\mu g\ m^3$, winter = 13 $\mu g\ m^3$), see Figure 5.11. This has been linked to decreased ventilation rates during winter, thus leading to a greater accumulation of fine particles indoors [103]. This trend is also reflected outdoors by Rogula-Kozłowska, Klejnowski et al. [104] who attribute this seasonality to energy usage and prevailing meteorological conditions. Meteorology is also considered a significant factor in PM concentrations by Ali, Shahzadi et al. [105]

In terms of $PM_{2.5}$ pollution, lockdown measures again saw a decrease in concentrations. Chauhan and Singh reported decreases in $PM_{2.5}$

concentrations during lockdown, as compared to the previous year, in the United States, Europe, and Asia. In New York City, concentrations decreased by 32%; by 58% in Zaragoza, and by 35% in Delhi [106]. These decreases are thought to be derived primarily from less traffic [106]. From a UK perspective, this is in contrast to what was reported by Dobson and Semple, who observed that outdoor concentrations of $PM_{2.5}$ in Scotland in 2020 were not significantly different to those of previous years e.g. 2017 = 6.7 μg m^{-3}, 2020 = 6.6 μg m^{-3} [107]. Indoor daily mean $PM_{2.5}$ concentrations were reported by Domínguez-Amarillo et al. to have increased during the lockdown in Madrid by 12–20% [108]. This is attributed to a lack of appropriate ventilation and more intensive use of cleaning products due to the pandemic [108].

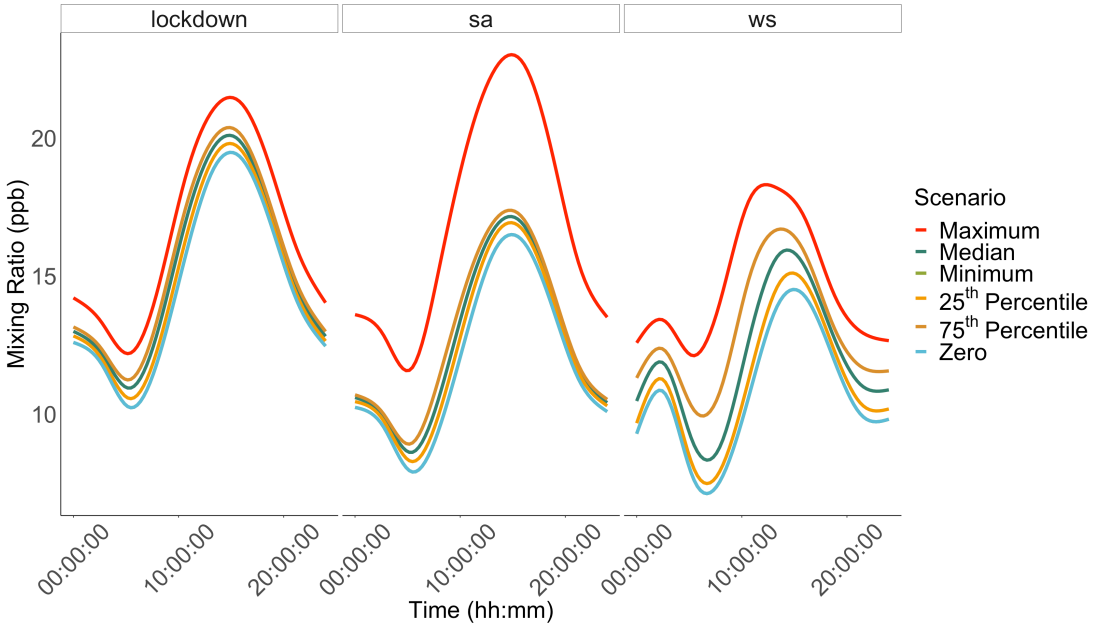

Figure 5.13: SPCP mixing ratios across all VOC load scenarios for all three campaign periods. Mixing ratio values are in ppb

SPCP mixing ratios were enhanced in the 'maximum' VOC load scenario, particularly in regard to the summer period, though mixing ratios in the 'maximum' scenario were similar between summer and the lockdown period (SPCP 'maximum' scenario median: winter = 13.7 ppb, lockdown = 16.2 ppb,

summer = 16.4 ppb). SPCP mixing ratios were higher during the lockdown period than in summer and winter across all VOC load scenarios (SPCP median: winter = 11.9 ppb, summer = 12.6 ppb, lockdown = 14.7 ppb), see Figure 5.12. As discussed elsewhere in this chapter, product use, particularly the use of cleaning and personal care products — which contain very reactive compounds such as monoterpenes — increased during lockdown, possibly influencing the production of potentially harmful compounds. Due to the unique nature of the lockdown scenario, and its impact on product use, it is unlikely that the increase in SPCP mixing ratios will be represented in future scenarios discussed elsewhere in this chapter

Regarding individual VOCs, Carslaw and Shaw [13] reported that in terms of SPCP values, alkenes and monoterpenes had greater potential of forming SOAs than other chemicals. Further analysis combined this data with typical mixing ratios, found in existing literature, to create a metric that ranks SOA potential in relation to mixing ratios. This placed monoterpenes, more specifically limonene and α-Pinene, significantly higher in terms of potential than other compounds.

As SPCP is still, to date, a novel metric, direct comparisons cannot be made with the literature. Instead, comparisons will be made where VOCs in general, or total VOC concentrations, are considered. Uchiyama, Tomizawa et al. [109] observed that higher concentrations of VOCs generally were found in summer than in winter indoors. This was attributed to outdoor-indoor exchange and indoor sources. Other studies observe the inverse; that VOCs are lower in summer than in winter [110]

The impacts of lockdown on human behaviour, and thus product use, is a complex area of discussion. The nature of the March–June 2020 lockdown period in the UK, and similar restrictions in other nations, meant that people were only permitted to leave their residences for certain activities – if they were key workers or were mandated to continue working, if they were

exercising outdoors, or if they were leaving their home to purchase essential items or to attend medical appointments. Due to these restrictions, people left their homes less frequently and as such it is likely that, generally, people used fewer personal care products e.g. antiperspirant deodorants, perfumes etc., though there is some evidence to suggest that product categories vary in importance for consumers e.g. skincare products being more important than make-up [111]. Gerstell et al. reported a decrease in sales of make-up and fragrances of up to 75%, but up to an eight-fold increase in the sale of other cosmetics skincare products [112].

Conversely, as people spent more time at home, it is possible people used cleaning products more frequently, as a precautionary measure to prevent infection with COVID-19 and to improve general cleanliness whilst occupying the same space for extended periods, and potentially engaged in home renovation and hobby activities, and thereby increasing concentrations of VOCs still further [113, 114]. In Italy, an interesting aspect to this hypothesis was manifest in an increase in exposure to disinfectants and surface cleansers that warranted contacting poison centres during lockdown (A 7.7 % and 6.8% increase respectively) [115]. During lockdown in Turkey, an increase of 69% in frequency of cleaning in homes was observed, along with an increase of 75% in time spent cleaning, and an increase of 74% in the number of products used [116]. Cooking is also likely to have contributed to increased pollutant concentrations over lockdown, as restaurants and cafés were forced to close. Laltrello et al. reported that $PM_{2.5}$ concentrations increased by ~190%, though cooking was listed only as a contributing factor, not as the sole reason [117]. Similarly, in Malaysia, an increase in average concentrations of $PM_{2.5}$ was recorded between a median average outdoor concentration of 12 μg m^{-3} to an average maximum of 52 μg m^{-3} indoors [118].

As mentioned earlier, air exchange rates are an important consideration in SOA production as significant reactions can take place indoors before air exchange rates can exert influence on the compounds in question [6]. Several

models in the literature detail the impact of AER on SOA production through the running of low and high AER scenarios. In Carslaw and Shaw [13], and their development of the SPCP metric, AER was investigated as a confounding variable on results returned by the model. Low AER was associated with lower O_3 concentrations, affecting O_3-reactive VOCs, which subsequently resulted in lower OH and secondary pollutants involved in calculating SPCP. High AER was associated with higher O_3 concentrations and therefore higher SPCP. Similar results in different AERs and attendant O_3 concentrations were observed in Weschler, Shields et al. [119] Surface interactions are a significant contributor to chemistry indoors [120]. Kruza, Lewis et al. [75] estimate that approximately 80% of ozone indoors is lost to surface deposition, with soft furnishings and painted walls acting as the most reactive surfaces. NO_2 and indoor surface reactions can result in the production of HONO [119]. Other factors e.g. solubility and reactivity also exert influence in SOA formation [5].

Here, two principal methods were presented by which indoor oxidation of VOCs can be measured. The first, calculating reactive potential and pseudo-first order reaction rates, suggested that indoor oxidation mechanisms are driven primarily by OH in a majority of commonly found VOCs, but NO_3 and O_3 also exert significant influence indoors. Monoterpenes were lost most quickly when combined median pseudo-first order reaction rates and had the greatest reactive potential when NO_3 and O_3 were considered. *n*-butane was the largest sink of OH, and the reaction between the two has the potential to produce the greatest number of secondary products of any VOCs in this study. The second, calculating SPCP values using an indoor chemistry model, predicted that total VOC oxidation potential will be higher in summer than in winter, and that it is significantly enhanced during lockdown conditions, where O_3 mixing ratios are higher and NO_x mixing ratios are lower. The indoor environment model also provided some additional data regarding $PM_{2.5}$ and OH indoors. $PM_{2.5}$ was significantly higher in winter than summer, with concentrations under lockdown conditions more closely

reflecting those in winter. OH mixing ratios were generally higher in winter than in summer and under lockdown conditions, but differences between winter and summer were more modest. Future legislation under which NO_x would be reduced due to the prohibition of the sale of diesel and petrol cars in the UK could be reflected in the lockdown period presented in this study.

References

1. Jones AP. Indoor air quality and health. Atmos Environ. 1999;33(28):4535–64.

2. Carslaw N. A new detailed chemical model for indoor air pollution. Atmos Environ. 2007;41(6):1164–79.

3. Yeoman AM, Lewis AC. Global emissions of VOCs from compressed aerosol products. Elementa (Wash D C). 2021;9(1):1–15.

4. McDonald BC, de Gouw JA, Gilman JB, Jathar SH, Akherati A, Cappa CD, Jimenez JL, Lee-Taylor J, Hayes PL, McKeen SA, Cui YY, Kim S-W, Gentner DR, Isaacman-VanWertz G, Goldstein AH, Harley RA, Frost GJ, Roberts JM, Ryerson TB, Trainer M. Volatile chemical products emerging as largest petrochemical source of urban organic emissions. Science. 2018;359(6377):760–4.

5. Hallquist M, Wenger JC, Baltensperger U, Rudich Y, Simpson D, Claeys M, Dommen J, Donahue NM, George C, Goldstein AH, Hamilton JF, Herrmann H, Hoffmann T, Iinuma Y, Jang M, Jenkin ME, Jimenez JL, Kiendler-Scharr A, Maenhaut W, McFiggans G, Mentel TF, Monod A, Prévôt ASH, Seinfeld JH, Surratt JD, Szmigielski R, Wildt J. The formation, properties and impact of secondary organic aerosol: Current and emerging issues. Atmos Chem Phys. 2009;9(14):5155–236.

6. Wolkoff P. Indoor air chemistry: Terpene reaction products and airway effects. Int J Hyg Environ Health. 2020;225:1–8.

7. Farmer DK, Vance ME, Abbatt JPD, Abeleira A, Alves MR, Arata C, Boedicker E, Bourne S, Cardoso-Saldaña F, Corsi R, DeCarlo PF, Goldstein AH, Grassian VH, Hildebrandt Ruiz L, Jimenez JL, Kahan

TF, Katz EF, Mattila JM, Nazaroff WW, Novoselac A, O'Brien RE, Or VW, Patel S, Sankhyan S, Stevens PS, Tian Y, Wade M, Wang C, Zhou S, Zhou Y. Overview of HOMEchem: House observations of microbial and environmental chemistry. Environ Sci Process Impacts. 2019;21(8):1280–300.

8. Mattila JM, Arata C, Wang C, Katz EF, Abeleira A, Zhou Y, Zhou S, Goldstein AH, Abbatt JPD, DeCarlo PF, Farmer DK. Dark chemistry during bleach cleaning enhances oxidation of organics and secondary organic aerosol production indoors. Environ Sci Technol Lett. 2020;7(11):795–801.

9. Wang C, Collins DB, Abbatt JPD. Indoor illumination of terpenes and bleach emissions leads to particle formation and growth. Environ Sci Technol. 2019;53(20):11792–800.

10. Spengler JD, Sexton K. Indoor air pollution: A public health perspective. Science. 1983;221(4605):9–17.

11. Nazaroff WW, Goldstein AH. Indoor chemistry: Research opportunities and challenges. Indoor Air. 2015;25(4):357–61.

12. Kroll JH, Seinfeld JH. Chemistry of secondary organic aerosol: Formation and evolution of low-volatility organics in the atmosphere. Atmos Environ. 2008;42(16):3593–624.

13. Carslaw N, Shaw D. Secondary product creation potential (SPCP): A metric for assessing the potential impact of indoor air pollution on human health. Environ Sci Process Impacts. 2019;21(8):1313–22.

14. Zhu J, Penner JE, Lin G, Zhou C, Xu L, Zhuang B. Mechanism of SOA formation determines magnitude of radiative effects. Proc Natl Acad Sci U S A. 2017;114(48):12685–90.

15. Saunders SM, Jenkin ME, Derwent RG, Pilling MJ. Protocol for the development of the Master Chemical Mechanism, MCM v3 (Part A): Tropospheric degradation of non-aromatic volatile organic compounds. Atmos Chem Phys. 2003;3(1):161–80.

16. Heeley-Hill AC, Grange SK, Ward MW, Lewis AC, Owen N, Jordan C, Hodgson G, Adamson G. Frequency of use of household products containing VOCs and indoor atmospheric concentrations in homes. Environ Sci Process Impacts. 2021;23(5):699–713.

17. Byrne FP, Jin S, Paggiola G, Petchey THM, Clark JH, Farmer TJ, Hunt AJ, Robert McElroy C, Sherwood J. Tools and techniques for solvent selection: Green solvent selection guides. Sustainable Chemical Processes. 2016;4(1):1–24.

18. Journal of the American College of Toxicology. Final report of the safety assessment of isobutane, isopentane, n-butane, and propane. J Am Coll Toxicol. 1982;1(1):127–42.

19. Salthammer T. Very volatile organic compounds: An understudied class of indoor air pollutants. Indoor Air. 2016;26(1):25–38.

20. Chang Y-M, Hu W-H, Fang W-B, Chen S-S, Chang C-T, Ching H-W. A study on dynamic volatile organic compound emission characterization of water-based paints. J Air Waste Manage Assoc. 2011;61(1):35–45.

21. Słomińska M, Konieczka P, Namieśnik J. The fate of BTEX compounds in ambient air. Crit Rev Environ Sci Technol. 2014;44(5):455–72.

22. Singer BC, Destaillats H, Hodgson AT, Nazaroff WW. Cleaning products and air fresheners: Emissions and resulting concentrations of glycol ethers and terpenoids. Indoor Air. 2006;16(3):179–91.

23. Meyerowitz-Katz G, Bhatt S, Ratmann O, Brauner JM, Flaxman S, Mishra S, Sharma M, Mindermann S, Bradley V, Vollmer M, Merone L, Yamey G. Is the cure really worse than the disease? The health impacts of lockdowns during COVID-19. BMJ Global Health. 2021;6(8):1–6.

24. Coroiu A, Moran C, Campbell T, Geller AC. Barriers and facilitators of adherence to social distancing recommendations during COVID-19 among a large international sample of adults. PLoS One. 2020;15(10):1–20.

25. Lescure F-X, Bouadma L, Nguyen D, Parisey M, Wicky P-H, Behillil S, Gaymard A, Bouscambert-Duchamp M, Donati F, Le Hingrat Q, Enouf V, Houhou-Fidouh N, Valette M, Mailles A, Lucet J-C, Mentre F, Duval X, Descamps D, Malvy D, Timsit J-F, Lina B, van-der-Werf S, Yazdanpanah Y. Clinical and virological data of the first cases of COVID-19 in europe: A case series. Lancet Infect Dis. 2020;20(6):697–706.

26. Hadjidemetriou GM, Sasidharan M, Kouyialis G, Parlikad AK. The impact of government measures and human mobility trend on COVID-19 related deaths in the UK. Transp Res Interdiscip Perspect. 2020;6:1–6.

27. Mallah SI, Ghorab OK, Al-Salmi S, Abdellatif OS, Tharmaratnam T, Iskandar MA, Sefen JAN, Sidhu P, Atallah B, El-Lababidi R, Al-Qahtani M. COVID-19: Breaking down a global health crisis. Ann Clin Microbiol Antimicrob. 2021;20(1):1–36.

28. Grange SK, Lee JD, Drysdale WS, Lewis AC, Hueglin C, Emmenegger L, Carslaw DC. COVID–19 lockdowns highlight a risk of increasing ozone pollution in European urban areas. Atmos Chem Phys. 2021;21(5):4169–85.

29. Carey N, Steitz C. EU proposes effective ban for new fossil-fuel cars from 2035 [Internet]. London, UK: Reuters; 2021 [cited 10.08.2021]. Available from: https://www.reuters.com/business/retail-consumer/eu-proposes-effective-ban-new-fossil-fuel-car-sales-2035-2021-07-14/.

30. Raugei M, Kamran M, Hutchinson A. Environmental implications of the ongoing electrification of the UK light duty vehicle fleet. Resour Conserv Recycl. 2021;174:1–14.

31. Isaksen ISA, Dalsøren SB. Getting a better estimate of an atmospheric radical. Science. 2011;331(6013):38–9.

32. Gómez Alvarez E, Amedro D, Afif C, Gligorovski S, Schoemaecker C, Fittschen C, Doussin J-F, Wortham H. Unexpectedly high indoor hydroxyl radical concentrations associated with nitrous acid. Proc Natl Acad Sci U S A. 2013;110(33):13294–9.

33. Anglada JM, Crehuet R, Martins-Costa M, Francisco JS, Ruiz-López M. The atmospheric oxidation of CH3OOH by the OH radical: The effect of water vapor. Phys Chem Chem Phys. 2017;19(19):12331–42.

34. Smith SC, Lee JD, Bloss WJ, Johnson GP, Ingham T, Heard DE. Concentrations of OH and HO_2 radicals during NAMBLEX: Measurements and steady state analysis. Atmos Chem Phys. 2006;6(5):1435–53.

35. Weschler CJ, Carslaw N. Indoor chemistry. Environ Sci Technol. 2018;52(5):2419–28.

36. Ziemann PJ. Effects of molecular structure on the chemistry of aerosol formation from the OH-radical-initiated oxidation of alkanes and alkenes. Int Rev Phys Chem. 2011;30(2):161–95.

37. Finewax Z, Pagonis D, Claflin MS, Handschy AV, Brown WL, Jenks O, Nault BA, Day DA, Lerner BM, Jimenez JL, Ziemann PJ, de Gouw JA. Quantification and source characterization of volatile organic compounds from exercising and application of chlorine-based cleaning products in a university athletic center. Indoor Air. 2021;31(5):1323–39.

38. Teng AP, Crounse JD, Lee L, St. Clair JM, Cohen RC, Wennberg PO. Hydroxy nitrate production in the OH-initiated oxidation of alkenes. Atmos Chem Phys. 2015;15(8):4297–316.

39. Waring MS, Wells JR. Volatile organic compound conversion by ozone, hydroxyl radicals, and nitrate radicals in residential indoor air: Magnitudes and impacts of oxidant sources. Atmos Environ. 2015;106:382–91.

40. Huang Y, Yang Z, Gao Z. Contributions of indoor and outdoor sources to ozone in residential buildings in Nanjing. Int J Environ Res Public Health. 2019;16(14):1–16.

41. Weschler CJ. Ozone in indoor environments: Concentration and chemistry. Indoor Air. 2000;10(4):269–88.

42. Finlayson-Pitts BJ, Pitts JN. Chapter 6 - Rates and mechanisms of gas-phase reactions in irradiated organic – NO_x – air mixtures. In: Finlayson-Pitts B.J., Pitts J.N., editors. Chemistry of the upper and

lower atmosphere. San Diego, CA: Academic Press; 2000. p. 179–263.

43. Zhou L, Ravishankara AR, Brown SS, Zarzana KJ, Idir M, Daële V, Mellouki A. Kinetics of the reactions of no_3 radical with alkanes. Phys Chem Chem Phys. 2019;21(8):4246–57.

44. Newland MJ, Mouchel-Vallon C, Valorso R, Aumont B, Vereecken L, Jenkin ME, Rickard AR. Estimation of mechanistic parameters in the gas-phase reactions of ozone with alkenes for use in automated mechanism construction. Atmos Chem Phys. 2022;22(9):6167–95.

45. Abbatt JPD, Wang C. The atmospheric chemistry of indoor environments. Environ Sci Process Impacts. 2020;22(1):25–48.

46. Nøjgaard JK. Indoor measurements of the sum of the nitrate radical, NO_3, and nitrogen pentoxide, N_2O_5 in Denmark. Chemosphere. 2010;79(8):898–904.

47. Fry J, Sackinger K. Model evaluation of no_3 secondary organic aerosol (SOA) source and heterogeneous organic aerosol (OA) sink in the western united states. Atmos Chem Phys Discuss. 2012;12:5189–223.

48. Platt U, LeBras G, Poulet G, Burrows JP, Moortgat G. Peroxy radicals from night-time reaction of no_3 with organic compounds. Nature. 1990;348(6297):147–9.

49. Wängberg I. Mechanisms and products of the reactions of NO_3 with cycloalkenes. J Atmos Chem. 1993;17(3):229–47.

50. Holme A, Sæthre LJ, Børve KJ, Thomas TD. Chemical reactivity of alkenes and alkynes as seen from activation energies, enthalpies of

protonation, and carbon 1s ionization energies. J Org Chem. 2012;77(22):10105–17.

51. Newland MJ, Nelson BS, Muñoz A, Ródenas M, Vera T, Tárrega J, Rickard AR. Trends in stabilisation of criegee intermediates from alkene ozonolysis. Phys Chem Chem Phys. 2020;22(24):13698–706.

52. Durham LJ, Greenwood FL. Ozonolysis. X. Molozonide as an intermediate in the ozonolysis of cis- and trans-alkenes. J Org Chem. 1968;33(4):1629–32.

53. Yu D-Y, Kang N, Bae W, Banks MK. Characteristics in oxidative degradation by ozone for saturated hydrocarbons in soil contaminated with diesel fuel. Chemosphere. 2007;66(5):799–807.

54. Atkinson R. Kinetics and mechanisms of the gas-phase reactions of the NO_3 radical with organic compounds. J Phys Chem Ref Data. 1991;20(3):459–507.

55. Talukdar RK, Mellouki A, Gierczak T, Barone S, Chiang S-Y, Ravishankara AR. Kinetics of the reactions of oh with alkanes. Int J Chem Kinet. 1994;26(10):973–90.

56. Weschler CJ, Shields HC. Production of the hydroxyl radical in indoor air. Environ Sci Technol. 1996;30(11):3250–8.

57. Liu Y, Misztal PK, Arata C, Weschler CJ, Nazaroff WW, Goldstein AH. Observing ozone chemistry in an occupied residence. Proc Natl Acad Sci U S A. 2021;118(6):1–8.

58. Nazaroff WW, Weschler CJ. Cleaning products and air fresheners: Exposure to primary and secondary air pollutants. Atmos Environ. 2004;38(18):2841–65.

59. National Insititutes of Health. Pubchem [Internet]. Bethesda, MD, USA: National Insititutes of Health; 2021 [cited 26.07.2021]. Available from: https://pubchem.ncbi.nlm.nih.gov/compound/6654#section=Computed-Properties.

60. Atkinson R, Aschmann SM, Goodman MA. Kinetics of the gas-phase reactions of NO_3 radicals with a series of alkynes, haloalkenes, and α,β-unsaturated aldehydes. Int J Chem Kinet. 1987;19(4):299–307.

61. Fry JL, Kiendler-Scharr A, Rollins AW, Wooldridge PJ, Brown SS, Fuchs H, Dubé W, Mensah A, dal Maso M, Tillmann R, Dorn HP, Brauers T, Cohen RC. Organic nitrate and secondary organic aerosol yield from NO_3 oxidation of β-pinene evaluated using a gas-phase kinetics/aerosol partitioning model. Atmos Chem Phys. 2009;9(4):1431–49.

62. Langer S, Ljungström E. Rates of reaction between the nitrate radical and some aliphatic alcohols. J Chem Soc, Faraday Trans. 1995;91(3):405–10.

63. Fouqueau A, Cirtog M, Cazaunau M, Pangui E, Doussin JF, Picquet-Varrault B. A comparative and experimental study of the reactivity with nitrate radical of two terpenes: α-terpinene and γ-terpinene. Atmos Chem Phys Discuss. 2020;2020:1–38.

64. Aschmann SM, Atkinson R. Rate constants for the reactions of the NO_3 radical with alkanes at 296 ± 2 k. Atmos Environ. 1995;29(17):2311–6.

65. Martínez E, Cabañas B, Aranda A, Martín P, Salgado S. Absolute rate coefficients for the gas-phase reactions of NO_3 radical with a series of monoterpenes at t = 298 to 433 k. J Atmos Chem. 1999;33(3):265–82.

66. Atkinson R, Hasegawa D, Aschmann SM. Rate constants for the gas-phase reactions of O_3 with a series of monoterpenes and related compounds at 296 ± 2 k. Int J Chem Kinet. 1990;22(8):871–87.

67. Picquet-Varrault B, Scarfogliero M, Helal WA, Doussin J-F. Reevaluation of the rate constant for the reaction propene + NO_3 by absolute rate determination. Int J Chem Kinet. 2009;41(2):73–81.

68. Geyer A, Alicke B, Konrad S, Schmitz T, Stutz J, Platt U. Chemistry and oxidation capacity of the nitrate radical in the continental boundary layer near Berlin. J Geophys Res Atmos. 2001;106(D8):8013–25.

69. Atkinson R, Arey J. Gas-phase tropospheric chemistry of biogenic volatile organic compounds: A review. Atmos Environ. 2003;37:197–219.

70. Herrington JS. Rapid determination of TO-15 volatile organic compounds (VOCs) in air [Internet]. Bellefonte, PA: Restek; 2016. [cited 08.05.2018]. Available from: http://www.restek.com/pdfs/EVAN1725B-UNV.pdf.

71. Derwent RG, Jenkin ME, Saunders SM, Pilling MJ. Photochemical ozone creation potentials for organic compounds in northwest Europe calculated with a master chemical mechanism. Atmos Environ. 1998;32(14):2429–41.

72. Bowman FM, Seinfeld JH. Ozone productivity of atmospheric organics. J Geophys Res Atmos. 1994;99(D3):5309–24.

73. Derwent RG, Jenkin ME. Hydrocarbons and the long-range transport of ozone and PAN across Europe. Atmos Environ. 1991;25(8):1661–78.

74. Carter WPL. Computer modeling of environmental chamber measurements of maximum incremental reactivities of volatile organic compounds. Atmos Environ. 1995;29(18):2513–27.

75. Kruza M, Lewis AC, Morrison GC, Carslaw N. Impact of surface ozone interactions on indoor air chemistry: A modeling study. Indoor Air. 2017;27(5):1001–11.

76. Jungkamp TPW, Smith JN, Seinfeld JH. Atmospheric oxidation mechanism of n-butane: The fate of alkoxy radicals. J Phys Chem A. 1997;101(24):4392–401.

77. Lelieveld J, Dentener FJ, Peters W, Krol MC. On the role of hydroxyl radicals in the self-cleansing capacity of the troposphere. Atmos Chem Phys. 2004;4(9/10):2337–44.

78. Bonn B, Moorgat GK. New particle formation during α- and β-pinene oxidation by O_3, OH and NO_3, and the influence of water vapour: Particle size distribution studies. Atmos Chem Phys. 2002;2(3):183–96.

79. Kanakidou M, Seinfeld JH, Pandis SN, Barnes I, Dentener FJ, Facchini MC, Van Dingenen R, Ervens B, Nenes A, Nielsen CJ, Swietlicki E, Putaud JP, Balkanski Y, Fuzzi S, Horth J, Moortgat GK, Winterhalter R, Myhre CEL, Tsigaridis K, Vignati E, Stephanou EG, Wilson J. Organic aerosol and global climate modelling: A review. Atmos Chem Phys. 2005;5(4):1053–123.

80. Ma S. Production of secondary organic aerosol from multiphase monoterpenes. In: Abdul-Razzak H., editor. Atmospheric aerosols: Regional characteristics — chemistry and physics. London: IntechOpen; 2012. p. 1–492.

81. Spittler M, Barnes I, Bejan I, Brockmann KJ, Benter T, Wirtz K. Reactions of NO_3 radicals with limonene and α-pinene: Product and soa formation. Atmos Environ. 2006;40:116–27.

82. Arata C, Zarzana KJ, Misztal PK, Liu Y, Brown SS, Nazaroff WW, Goldstein AH. Measurement of NO_3 and N_2O_5 in a residential kitchen. Environ Sci Technol Lett. 2018;5(10):595–9.

83. Grosjean D, Williams EL, Seinfeld JH. Atmospheric oxidation of selected terpenes and related carbonyls: Gas-phase carbonyl products. Environ Sci Technol. 1992;26(8):1526–33.

84. Wang CM, Barratt B, Carslaw N, Doutsi A, Dunmore RE, Ward MW, Lewis AC. Unexpectedly high concentrations of monoterpenes in a study of UK homes. Environ Sci Process Impacts. 2017;19(4):528–37.

85. Hauptmann M, Stewart PA, Lubin JH, Beane Freeman LE, Hornung RW, Herrick RF, Hoover RN, Fraumeni JF, Jr, Blair A, Hayes RB. Mortality from lymphohematopoietic malignancies and brain cancer among embalmers exposed to formaldehyde. J Natl Cancer Inst. 2009;101(24):1696–708.

86. Nielsen GD, Wolkoff P. Cancer effects of formaldehyde: A proposal for an indoor air guideline value. Arch Toxicol. 2010;84(6):423–46.

87. Alexandersson R, Kolmodin-Hedman B, Hedenstierna G. Exposure to formaldehyde: Effects on pulmonary function. Arch Environ Health. 1982;37(5):279–84.

88. Han S, Bian H, Feng Y, Liu A, Li X, Zeng F, Zhang X. Analysis of the relationship between O_3, NO and NO_2 in Tianjin, China. Aerosol Air Qual Res. 2011;11(2):128–39.

89. Song F, Young Shin J, Jusino-Atresino R, Gao Y. Relationships among the springtime ground–level NO_x, O_3 and NO_3 in the vicinity of highways in the us east coast. Atmos Pollut Res. 2011;2(3):374–83.

90. Banan N, Latif MT, Juneng L, Ahamad F. Characteristics of surface ozone concentrations at stations with different backgrounds in the Malaysian peninsula. Aerosol Air Qual Res. 2013;13(3):1090–106.

91. Dayan U, Levy I. Relationship between synoptic-scale atmospheric circulation and ozone concentrations over Israel. J Geophys Res Atmos. 2002;107(D24):ACL 31-1–ACL -12.

92. Jhun I, Coull BA, Zanobetti A, Koutrakis P. The impact of nitrogen oxides concentration decreases on ozone trends in the USA. Air Qual Atmos Health. 2015;8(3):283–92.

93. Li Y, Lau AKH, Fung JCH, Zheng J, Liu S. Importance of NO_x control for peak ozone reduction in the Pearl River Delta region. J Geophys Res Atmos. 2013;118(16):9428–43.

94. Shah V, Jacob DJ, Li K, Silvern RF, Zhai S, Liu M, Lin J, Zhang Q. Effect of changing NO_x lifetime on the seasonality and long-term trends of satellite-observed tropospheric NO_2 columns over China. Atmos Chem Phys. 2020;20(3):1483–95.

95. Khoder MI. Diurnal, seasonal and weekdays-weekends variations of ground level ozone concentrations in an urban area in greater Cairo. Environ Monit Assess. 2009;149(1–4):349–62.

96. Bauwens M, Compernolle S, Stavrakou T, Müller J-F, van Gent J, Eskes H, Levelt PF, van der A R, Veefkind JP, Vlietinck J, Yu H, Zehner C. Impact of coronavirus outbreak on NO_2 pollution assessed

using TROPOMI and OMI observations. Geophys Res Lett. 2020;47(11):1–9.

97. Lee JD, Drysdale WS, Finch DP, Wilde SE, Palmer PI. UK surface NO_2 levels dropped by 42 % during the COVID-19 lockdown: Impact on surface O_3. Atmos Chem Phys. 2020;20(24):15743–59.

98. Venter ZS, Aunan K, Chowdhury S, Lelieveld J. COVID-19 lockdowns cause global air pollution declines. Proc Natl Acad Sci U S A. 2020;117(32):18984–90.

99. Stevenson D, Derwent R, Wild O, Collins W. COVID-19 lockdown NO_x emission reductions can explain most of the coincident increase in global atmospheric methane. Atmos Chem Phys Discuss. 2021;2021:1–8.

100. Goldstein AH, Wofsy SC, Spivakovsky CM. Seasonal variations of nonmethane hydrocarbons in rural new england: Constraints on oh concentrations in northern midlatitudes. J Geophys Res Atmos. 1995;100(D10):21023–33.

101. Spivakovsky CM, Yevich R, Logan JA, Wofsy SC, McElroy MB, Prather MJ. Tropospheric oh in a three-dimensional chemical tracer model: An assessment based on observations of ch_3ccl_3. J Geophys Res Atmos. 1990;95(D11):18441–71.

102. Heard DE, Carpenter LJ, Creasey DJ, Hopkins JR, Lee JD, Lewis AC, Pilling MJ, Seakins PW, Carslaw N, Emmerson KM. High levels of the hydroxyl radical in the winter urban troposphere. Geophys Res Lett. 2004;31(18):1–5.

103. Sidra S, Ali Z, Ahmad Nasir Z, Colbeck I. Seasonal variation of fine particulate matter in residential micro–environments of Lahore, Pakistan. Atmos Pollut Res. 2015;6(5):797–804.

104. Rogula-Kozłowska W, Klejnowski K, Rogula-Kopiec P, Ośródka L, Krajny E, Błaszczak B, Mathews B. Spatial and seasonal variability of the mass concentration and chemical composition of $PM_{2.5}$ in Poland. Air Qual Atmos Health. 2014;7(1):41–58.

105. Ali Z, Shahzadi K, Sidra S, Zona Z, Zainab I, Aziz K, Ahmad M, Raza ST, Nasir ZA, Colbeck I. Seasonal variation of particulate matter in the ambient conditions of Khanspur, Pakistan. J Anim Plant Sci. 2015;25(3):700–5.

106. Chauhan A, Singh RP. Decline in $PM_{2.5}$ concentrations over major cities around the world associated with COVID-19. Environ Res. 2020;187:1–4.

107. Dobson R, Semple S. Changes in outdoor air pollution due to COVID-19 lockdowns differ by pollutant: Evidence from Scotland. Occup Environ Med. 2020;77(11):798–800.

108. Domínguez-Amarillo S, Fernández-Agüera J, Cesteros-García S, González-Lezcano RA. Bad air can also kill: Residential indoor air quality and pollutant exposure risk during the COVID-19 crisis. Int J Environ Res Public Health. 2020;17(19):1–33.

109. Uchiyama S, Tomizawa T, Tokoro A, Aoki M, Hishiki M, Yamada T, Tanaka R, Sakamoto H, Yoshida T, Bekki K, Inaba Y, Nakagome H, Kunugita N. Gaseous chemical compounds in indoor and outdoor air of 602 houses throughout Japan in winter and summer. Environ Res. 2015;137:364–72.

110. Rehwagen M, Schlink U, Herbarth O. Seasonal cycle of VOCs in apartments. Indoor Air. 2003;13(3):283–91.

111. Choi Y-H, Kim SE, Lee K-H. Changes in consumers' awareness and interest in cosmetic products during the pandemic. Fashion and Textiles. 2022;9(1):1–19.

112. Gerstell E, Marchessou S, Schmidt J, Spagnuolo E. Consumer packaged goods practice: How COVID-19 is changing the beauty world. New York City, NY: McKinsey & Company; 2020. p. 1–8.

113. Wright L, Fluharty M, Steptoe A, Fancourt D. How did people cope during the COVID-19 pandemic? A structural topic modelling analysis of free-text data from 11,000 uk adults. medRxiv. 2021:1–15.

114. Bu F, Steptoe A, Mak HW, Fancourt D. Time use and mental health in UK adults during an 11-week COVID-19 lockdown: A panel analysis. Br J Psych. 2021;219(4):551–6.

115. Giordano F, Petrolini VM, Spagnolo D, Fidente RM, Lanciotti L, Baldassarri L, Moretti FL, Brambilla E, Lonati D, Schicchi A, Locatelli CA, Draisci R. Significant variations of dangerous exposures during COVID-19 pandemic in Italy: A possible association with the containment measures implemented to reduce the virus transmission. BMC Public Health. 2022;22(1):441.

116. Koksoy Vayisoglu S, Oncu E. The use of cleaning products and its relationship with the increasing health risks during the COVID-19 pandemic. Int J Clin Pract. 2021;75(10):1–10.

117. Laltrello S, Amiri A, Lee S-H. Indoor particulate matters measured in residential homes in the southeastern United States: Effects of

pandemic lockdown and holiday cooking. Aerosol Air Qual Res. 2022;22(5):1–14.

118. Ezani E, Brimblecombe P, Hanan Asha'ari Z, Fazil AA, Syed Ismail SN, Ahmad Ramly ZT, Khan MF. Indoor and outdoor exposure to $PM_{2.5}$ during COVID-19 lockdown in suburban Malaysia. Aerosol Air Qual Res. 2021;21(3):1–12.

119. Weschler CJ, Shields HC, Naik DV. Indoor chemistry involving O_3, NO, and NO_2 as evidenced by 14 months of measurements at a site in southern California. Environ Sci Technol. 1994;28(12):2120–32.

120. Fang Y, Lakey PSJ, Riahi S, McDonald AT, Shrestha M, Tobias DJ, Shiraiwa M, Grassian VH. A molecular picture of surface interactions of organic compounds on prevalent indoor surfaces: Limonene adsorption on SiO_2. Chem Sci. 2019;10(10):2906–14.

6. Concluding Remarks

Outdoor air pollution has had the benefit of many decades of research by the scientific community. However, indoor air quality has received scarce attention until relatively recently, which is perhaps surprising given how much time people, on average, spend indoors; roughly 90%. Air pollution, in general, can lead to serious illness relating to several bodily systems, and does confer significant disease burden to populations, particularly in developing countries. This situation is likely to be exacerbated by the predicted changes to weather caused by climate change, and the further proliferation of the urban heat and pollution island effects.

Defining an indoor environment and its' air quality is impossible for anything but the broadest of generalisations, as 'indoors' encompasses a myriad of environments. Factors such as building type, age, and use need to be considered, as different buildings will have different occupancies, ventilation rates, and activities taking place there. For example, the air in a hospital is likely to have a different chemical make up to that of a university, a residence, or an office building. Even in public buildings where people spend their leisure time, chemical constituents will be different between them, such as between restaurants and gyms. However, conclusions can be drawn about these different sub-environments, and further insight will make an important contribution to this knowledge.

This thesis has provided an insight into the air quality of homes in the UK through a number of studies. First, the chamber studies in Chapter 3, performed at the University of Manchester Aerosol Chamber, allowed for the exploration of how commonly-found VOCs behave in the atmosphere. Whilst this study did not focus on indoor air specifically, it provides a general overview of how toluene, α-Pinene, and 1,3,5-trimethylbenzene oxidise and decay at concentrations pertinent to outdoor atmospheres. A variety of SOA

intermediate compounds were observed in a variety of experiments, with oxalic acid, benzaldehyde, acetaldehyde, acetic acid, and dimethylbenzaldehyde already established in the literature as known oxidation products of the parent VOCs listed above. The addition of particle number analysis provides information on particle formation in the context of oxidation. These experiments highlighted that whilst OH was an important oxidant in most circumstances, O_3 was also significant. NO_x, and the ratio of NO to NO_2, also impacted the rate to which VOCs oxidised due to its control over oxidant production. This ratio could also potentially impact the formation of highly oxygenated molecules, new particle formation, and ergo the presence of secondary organic aerosols. Exploration of the Master Chemical Mechanism provided further insight into the oxidation of these VOCs.

Regarding instrumentation, the AGC-MS provided the obvious benefit of being able to collect and analyse samples in a fast time resolution. Unfortunately, this was not fully exploited in the chamber campaigns detailed in this thesis due to instrument malfunction and operational issues, limiting the amount of usable data generated during campaigns. In addition, lockdowns implemented during the COVID-19 pandemic of 2020 prevented a third campaign from taking place. Future studies could include additional VOCs being injected into the chamber; in this study, only one monoterpene, toluene and 1,3,5-trimethylbenzene were explored extensively. Insights from the population-based study, Chapters 4 and 5, could inform of compounds that merit oxidation analysis. Making the experiments more relevant to indoor environments e.g. optimised VOC and oxidant mixing ratios would be helpful.

Secondly, the population-based study, Chapter 4, was one of the first studies in the scientific literature to take measurements of a wide variety of VOCs thought to occur commonly indoors across a relatively large cohort. This study also considered the impact of frequency of product use on indoor VOC concentrations. Whilst frequency of use did not have a statistically significant impact on concentrations, certain product types could be linked to the

emissions of certain VOCs e.g. butanes and the use of anti-perspirant deodorants. The use of two GC systems (ToF-MS and FID) clearly has potential to investigate significantly more VOCs than either system alone, and can account for a wide variety of VOCs across different functional groups. Analysis of exposure to total VOC concentrations confirmed that residents of households were exposed to higher concentrations of VOCs indoors than outdoors, especially in winter months, but rarely does this approach safe limits as defined by the European Union.

The population-based study made efforts to investigate any correlation between total VOC concentrations and property type, age, and size. Whilst no statistically significant relationships were observed in the dataset, factors such as those listed above will influence concentrations to some degree. As property type and age were taken as a proxy for ventilation, with older property assumed to be less well-insulated and therefore more ventilated, future studies would benefit from measuring air exchange rates in addition to other parameters. Assessing the air exchange rate would be challenging, even in a small cohort, requiring additional equipment and more time to make appropriate measurements.

This study benefitted from collaboration with an industry partner – who already had participants in an experimental panel from which a suitable cohort could be selected – through which samples were shipped on a weekly basis. This expedited the planning of the experimental process but having an intermediary complicated analysis in the laboratory. In the winter campaign, two sets of canister IDs were used between Givaudan and the University of York. The canister ID changed at the laboratory per usage, usually every second week, and at Givaudan for every sample replicate per household. This complex labelling system did result in recording errors in the laboratory; this was rectified as much as possible. By the summer campaign, the canister ID labelling system was simplified, so errors were significantly lower in number. Participant information was also anonymised prior to being sent

to the University of York, so participants could not be identified by their data, or attributed to their household. Again, this expedited the planning process but it meant that linking air samples to specific households was difficult when recording errors were made.

Another consideration of the population-based study is its applicability to homes located in other countries. As residential construction style and fuel type use – in both cooking and heating – tends to vary significantly between from country to country and continent to continent, the results from this study will largely be applicable only to homes in the UK, but this study provides an effective and robust methodology upon which to perform other wide-ranging indoor air studies in other locations

Thirdly, the oxidation study, Chapter 5, provided useful information of the potential oxidative capacity of indoor environments, based on data from the population study, including oxidation of VOCs via OH, O_3, and NO_3. To calculate this, two metrics were defined: the first metric is reactive potential, which is the product of the concentration of a given VOC indoors and the rate coefficient of the given VOC with a given oxidant, independent of the concentration of the oxidant indoors. The second metric is the pseudo-first order reaction rate, which extends the reactive potential metric by incorporating the indoor concentration of the oxidant. These metrics highlight the propensity of a VOC to form secondary compounds. Monoterpenes, and alkenes more generally, had the greatest reactive potential, though the reaction between n-butane and OH was the process that led to the greatest number of reactions and therefore potentially the greatest number of secondary products. Regarding median pseudo-first order reaction rates, again, monoterpenes dominated, with NO_3 contributing significantly to VOC loss.

Furthermore, this study incorporated an indoor air model that considered indoor concentrations of oxidants, particulate matter, and SPCP values using

VOC concentrations derived from the population-based study. The SPCP metric is of significant interest to the indoor air community because it provides an indoor-specific oxidation assessment and, in turn, considers the production of potentially harmful secondary products. As this study is the first to use observed VOC concentrations with the SPCP metric, it provides a valuable insight into this methodology.

The oxidation study, and further use of the indoor air model, provided an opportunity to explore the impact of the COVID-19 lockdowns on air quality indoors. Additionally, the lockdown scenario acted as a proxy for potential changes in outdoor pollutant concentrations resulting from policy changes in the UK regarding the sale of petrol and diesel vehicles. From this study, it is clear that indoor air quality will change under this future scenario, with NO_x and OH concentrations decreasing, but O_3 and SPCP increasing. Potential health outcomes from such a scenario would be an interesting addition to this work.

This thesis characterises the chemical makeup of indoor air, the methods by which oxidation occurs, and an overview of the results of these reactions taking place. Clearly, a number of mitigations can be implemented that aim to improve indoor environments, as discussed in the Introduction. Collaboration amongst international organisations and governments, as well as changes in local policy, product formulation, and education on potentially harmful pollutants are just some of the ways through which indoor air quality could be improved. Product usage needs to be assessed using different metrics to accurately identify the impact it has indoors, as the VOC load from commercially available products is increasing in urban areas outdoors. This, along with investigating oxidation mechanisms and products further, will provide a more comprehensive assessment of indoor air pollution.

Glossary of Abbreviations and Acronyms

AER	Air Exchange Rate
AGC-MS	Aircraft Gas Chromatograph-Mass Spectrometer
AURN	Automatic Urban and Rural Network
BASE	Building Assessment Survey Information
BP	Boiling Point
BREEAM	Building Research Establishment Environmental Assessment Method
BTEX	Benzene, Toluene, Ethylbenzene, and the Xylene isomers
CFC	Chlorofluorocarbon
CIMS	Chemical Ionisation Mass Spectrometry
CCN	Cloud Condensation Nuclei
DALY	Disability-adjusted Life Years
DC	Direct Current
DEFRA	Department for Environment, Food, and Rural Affairs
dl	Detection Limit
DMPS	Differential Mobility Particle Sizer
EC	European Community
ECHA	European Chemicals Agency
EEC	European Economic Community
EUPHORE	European Photoreactor
EXPOLIS	Air Pollution Exposure Distributions within Adult Urban Populations in Europe
FID	Flame Ionisation Detector
GC	Gas Chromatography
GC-FID	Gas Chromatography-Flame Ionisation Detection (or Detector)
GC-MS	Gas Chromatography-Mass Spectrometry
GC-ToF-MS	Gas Chromatography-Time-of-Flight-Mass Spectrometry
GIS	Geographical Information Systems
HEPA	High-efficiency Particulate Air (filter)
HOMEChem	House Observations of Microbial and Environmental Chemistry

HVAC	Heating, Ventilation, and Air Conditioning
INDCM	Indoor Chemical Model
IQR	Interquartile Range
IN	Ice Nuclei
LEED	Leadership in Energy and Environment Design
LoB	Limit of Blank
LoD	Limit of Detection
LOESS	Locally-estimated Scatterplot Smoothing
m/z	Expression of mass-to-charge ratio
MCM	Master Chemical Mechanism
MERV	Minimum Efficiency Reporting Value (filter)
MIR	Maximum Incremental Reactivity
MM	Miljömedicin (Swedish)
MM-RA	Miljömedicin-Residential Area
MM-S	Miljömedicin-School
MM-WP	Miljömedicin-Work Place
MS	Mass Spectrometry
MSD	Mass Selective Detector
NAEI	National Atmospheric Emissions Inventory
NCCT	United States Environmental Protection Agency National Center for Computational Toxicology
NHEXAS	National Human Exposure Assessment Survey
NIST	United States Department of Commerce National Institute of Standards and Technology
NPL	National Physical Laboratory
NPF	New Particle Formation
PAH	Polycyclic Aromatic Hydrocarbon
PEOPLE	Population Exposure to Air Pollutants in Europe
PFTBA	Perfluorotributylamine
PHYSPROP	Physical Properties (datasets)
PLOT	Porous Layer Open Tubular (column)
PM	Particulate Matter

POA	Primary Organic Aerosol
POCP	Photochemical Ozone Creation Potential
PTFE	Polytetrafluoroethylene
PTR-MS	Proton Transfer Reaction-Mass Spectrometry
QA	Quality Assurance
QC	Quality Control
REACH	Registration, Evaluation, Authorisation, and Restriction of Chemicals
RF	Response Factor
s/n	Signal-to-Noise Ratio
SA	Summer-Autumn (campaign period during population study)
SBS	Sick-Building Syndrome
SD	Standard Deviation
SDG	Sustainable Development Goals
SIM	Selective Ion Monitoring
SOA	Secondary Organic Aerosol
SPCP	Secondary Product Creation Potential
SWC	Satisfaction with Living Conditions
SWL	Satisfaction with Life
TDU	Thermal Desorption Unit
TEACH	Toxics Exposure Assessment Columbia-Harvard
TEAM	Total Exposure Assessment Methodology
TO	Toxic Organics (in reference to USEPA compendium methods)
TSCA	Toxic Substances Control Act
TVOC	Total Volatile Organic Compounds
UHI	Urban Heat Island
UK	United Kingdom
UN	United Nations
UNECE	United Nations Economic Commission for Europe
UPI	Urban Pollution Island
USA	United States of America
USEPA	United States Environmental Protection Agency
VOC	Volatile Organic Compound

VP	Vapour Pressure
WHO	World Health Organization
WS	Winter-Spring (campaign period during population study)